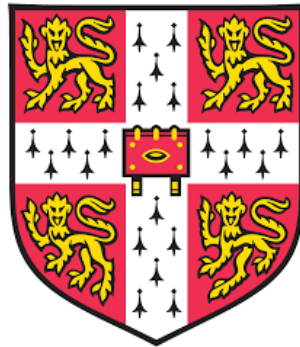


Development of *Rhodospseudomonas palustris* as a chassis for biotechnological applications

Author:
RUTH LAING
Trinity Hall

Supervisor:
PROF. CHRISTOPHER HOWE
Corpus Christi College



Department of Biochemistry
University of Cambridge

A thesis presented for the degree of
Doctor of Philosophy
September 2017

Declaration

This report is the result of work carried out in the Howe Group of the Department of Biochemistry, Cambridge, between June 2013 and September 2017, except where otherwise stated. It is the result of my own work, and includes nothing done in collaboration except where indicated in the text and acknowledgements. It is not substantially the same as any that I have submitted for a degree or diploma or other qualification at the University of Cambridge or any other university or similar institution. The total length of this dissertation does not exceed sixty thousand words.

Ruth Laing

September 2017

Acknowledgements

I thank my funding body, the BBSRC, for their contribution to this project. I am incredibly grateful to Chris Howe for the patient support he has given me over the past four years, and his ridiculous turnaround times on chapter drafts.

I am grateful to the rest of the members of the Howe lab for providing such an enjoyable environment in which to work, and for all of the advice and help they have given me over the years. There are several people in particular I must thank. Erin Butterfield possesses an inspiring level of perseverance, and I thank her for making my experience in the Howe lab approximately ten times more mischievous ($p < 0.01$). Laura Baers provided, time and again, much-needed support of the caffeinated variety in moments of crisis, and was a champion of cracking open stubborn microbes. I thank Barney Slater for providing enthusiastic conversation on a variety of Japanese fauna, and Paolo Bombelli not only for all of his help with the growth cabinet, but also for being unrelentingly cheerful. I thank Jack Hervey for being a fellow Tidy Friday enthusiast, and for commiserating in our moments of *palustris* woe. I am grateful to Isabel Nimmo and Adrian Barbrook, who both not only taught me many of the techniques I needed in the lab but also maintained a steadfast commitment to morning tea (and sometimes pre-morning tea tea!) throughout my time there.

I thank Robert Pott, Martin Chan and John Dennis for their assistance in measuring hydrogen and other advice on cultivating *R. palustris*.

I especially thank Philip Brown: turns out, I really couldn't have done this without you. I promise never to do another PhD...

I thank my whole (extended!) family for all of their support, not just during the past four years but over my whole life. I am grateful to my father for passing on a love of the natural world, ever-present curiosity and a patient approach to any problem. I thank my mother for always being there to provide a warm hug or a fierce pep talk, and for always knowing which is needed. I would not have managed this without you both.

I thank *R. palustris* for at least being a pretty colour and moderately hard to kill.

Abstract

The recent surge in biodiesel production has resulted in a huge surplus of crude glycerol, a by-product of the process to the level of 10% by weight. This in turn has caused the price of glycerol to fall dramatically, and there are now few economically viable channels for using this resource: waste glycerol is usually combusted. Therefore, much interest has arisen in the possibility of making use of glycerol with biotechnology, as this would not only be a more efficient use of resources but also make biodiesel itself more commercially viable.

The purple bacterium *Rhodospseudomonas palustris* is able to metabolize glycerol through photo-fermentation and thereby produce hydrogen, a commercially useful commodity. *R. palustris* is of particular interest for this purpose as, in contrast to many other species which have been investigated with a view to fermenting glycerol, it is highly tolerant of crude glycerol. The feedstock requires little purification or dilution to be made suitable for cultivation of *R. palustris*. Furthermore, the hydrogen gas produced by *R. palustris* when grown on glycerol is of high purity, and the organism's great metabolic diversity suggests it may be a useful strain for remediation of other waste materials.

However, much groundwork is needed to establish *R. palustris* as a viable chassis organism for biotechnological purposes. This work sets out to establish optimal conditions for cultivating *R. palustris* in the laboratory, including the design of a suitable batch photobioreactor system. It also determines optimal conditions for electroporation of *R. palustris* for the purpose of knocking out endogenous genes or introducing heterologous genes. Furthermore, the introduction of heterologous genes is attempted in order to demonstrate the possibility of producing other high-value compounds with *R. palustris*, and several deletion strains with potential benefits for hydrogen production are created. Finally, several existing deletion strains are investigated to establish their suitability as chassis strains for further genetic manipulation.

Contents

Contents	4
List of Figures	9
List of Tables	21
1 Introduction	26
1.1 Biodiesel and waste glycerol production	26
1.2 Hydrogen as a commercial product	27
1.3 The hydrogen-producing <i>Rhodopseudomonas palustris</i>	27
1.4 Hydrogen production through photofermentation and dark fermentation	31
1.5 Using <i>R. palustris</i> for photofermentation	33
1.6 <i>Rhodopseudomonas palustris</i> as a chassis organism for biotechnology	34
1.7 Glycogen- and PHB-deficient strain of <i>R. palustris</i>	36
1.8 Hydrogen production through the action of nitrogenase enzymes	37
1.9 Alternative forms of nitrogenase	39
1.10 Regulation of nitrogenases in response to fixed nitrogen	41
1.11 Production of high-value compounds from glycerol	43
1.12 Propane-1,2-diol: applications and production by heterologous organisms	44
1.13 Isoprene: applications and production by heterologous organisms	46
1.14 Aims of the project	48
2 Materials and methods	49
2.1 Reagents	49
2.2 Centrifugation	49
2.3 Growth and storage of <i>Rhodopseudomonas palustris</i>	49
2.3.1 Maintenance of <i>Rhodopseudomonas palustris</i> strains	49
2.3.2 Measurement of <i>R. palustris</i> growth	49
2.3.3 Rapid growth of and application of selection pressure to <i>R. palustris</i>	51
2.4 Spectrophotometry	51
2.4.1 Measurement of optical density as a proxy for cell concentration	51

2.4.2	Measurement of whole absorption spectrum	51
2.5	Measurement of light intensity	52
2.6	Plasmid cloning	52
2.6.1	Cultivation of <i>Escherichia coli</i>	52
2.6.2	Preparation of chemically competent cells	52
2.6.3	Transformation with and recovery of plasmid DNA	53
2.7	Extraction of DNA and RNA	55
2.7.1	Measurement of DNA and RNA concentration	55
2.7.2	Extraction of genomic DNA	55
2.7.3	Extraction of DNA for colony PCR	56
2.7.4	Extraction of RNA	57
2.8	Amplification of DNA by polymerase chain reaction	58
2.8.1	Design of primers for polymerase chain reaction	58
2.8.2	Amplification of high-fidelity DNA	58
2.8.3	Amplification of DNA for colony PCR	58
2.9	Amplification of complementary DNA from RNA	60
2.9.1	Preparation of DNA-free RNA	60
2.9.2	Synthesis of complementary DNA by reverse transcription polymerase chain reaction	61
2.10	Analysis of DNA by gel electrophoresis	61
2.11	Preparation and analysis of plasmids	62
2.11.1	Selection of restriction enzymes for plasmid construction	62
2.11.2	Creation of heterologous DNA sequences for insertion into <i>R. palustris</i>	62
2.11.3	Digestion of DNA by restriction enzyme	62
2.11.4	Purification of DNA from PCR product or agarose gel	62
2.11.5	Ligation of restriction enzyme-digested DNA	63
2.12	Sequencing of DNA fragments	64
2.13	Transformation of <i>R. palustris</i> by electroporation	64
2.13.1	Preparation of competent <i>R. palustris</i> cells	64
2.13.2	Electroporation of <i>R. palustris</i>	66
2.13.3	Generation of unmarked transformant strains of <i>R. palustris</i>	67

2.14	Assay for cellular levels of glycogen	67
2.15	Assay for cellular levels of polyhydroxybutyrate	68
2.16	Measurement of gaseous output volume	69
2.17	Genome sequences	70
2.18	Statistical analysis and figure creation	70
3	Cultivation of <i>Rhodopseudomonas palustris</i>	71
3.1	Introduction	71
3.1.1	Overview	71
3.1.2	Design of the cultivation cabinet lighting provision	72
3.1.3	Design of the cultivation cabinet mixing and support structures	73
3.1.4	Calibration of the cultivation cabinet lighting	77
3.2	Chapter Aims	78
3.3	Results	79
3.3.1	Comparison between <i>R. palustris</i> growth on cultivation cabinet and incubator	79
3.3.2	Comparison between <i>R. palustris</i> growth under anaerobic and ‘aerobic’ atmosphere	81
3.3.3	Comparison between <i>R. palustris</i> growth under different light spectra	82
3.3.4	Comparison between <i>R. palustris</i> growth under sunlight and on the cultivation cabinet	87
3.4	Discussion	89
4	Optimization of the <i>R. palustris</i> Electroporation Protocol	91
4.1	Introduction	91
4.1.1	Overview	91
4.2	Results	99
4.2.1	Testing for undirected integration of the p <i>KmobsacB</i> plasmid into <i>R. palustris</i>	99
4.2.2	The effect of pulse voltage and resistance on transformation efficiency and cell viability	100
4.2.3	The effect of culture stage on transformation efficiency	102
4.2.4	The effect of cell density on transformation efficiency	106
4.2.5	The effect of post-shock incubation on transformation efficiency	107

4.2.6	Further refinement of voltage and resistance	110
4.2.7	Assessing the reproducibility of these results	112
4.3	Discussion	114
5	Characterisation of chassis strains and introduction of heterologous pathways into <i>R. palustris</i>	115
5.1	Introduction	115
5.1.1	Introducing heterologous biosynthetic pathways into <i>R. palustris</i>	115
5.1.2	Producing valuable compounds from a glycogen- and PHB-deficient strain of <i>R. palustris</i>	118
5.1.3	Creation of the PHB, glycogen and uptake hydrogenase knockouts	119
5.1.4	Testing for loss of PHB and glycogen biosynthetic capability in the knockouts	119
5.2	Chapter Aims	122
5.3	Results	123
5.3.1	PCR verification of the <i>hupL</i> , <i>phaAB</i> and <i>glgCA</i> knockouts	123
5.3.2	Glycogen and PHB assays of the <i>hupL</i> , <i>phaAB</i> and <i>glgCA</i> knockouts	131
5.3.3	Characterization of the <i>hupL</i> , <i>phaAB</i> and <i>glgCA</i> knockouts	134
5.3.4	Identification of required heterologous genes	139
5.3.5	Identification of suitable promoter and terminator sequences	141
5.3.6	Design of the heterologous sequences	142
5.3.7	Construction of the delivery plasmids	144
5.3.8	Insertion of heterologous genes into <i>R. palustris</i>	150
5.3.9	Testing expression of heterologous genes	154
5.4	Discussion	157
5.4.1	Establishment of the <i>hupL</i> , <i>phaAB</i> and <i>glgCA</i> knockouts as chassis strains . .	157
5.4.2	Introduction of heterologous genes into <i>R. palustris</i>	160
6	Creation of potential chassis strains by manipulation of nitrogenase	163
6.1	Introduction	163
6.1.1	Regulation of the nitrogenases in the presence of fixed nitrogen	163
6.1.2	Introduction of multiple gene deletions to <i>R. palustris</i>	164
6.2	Results	165

6.2.1	Analysis of target gene co-transcription	165
6.2.2	Construction of the deletion plasmids	168
6.2.3	Introduction of deletions into <i>R. palustris</i>	169
6.2.4	Characterization of growth and the ammonium response of the $\Delta draT2\Delta glnK2$ and $\Delta nifDH$ strains	172
6.3	Discussion	176
7	Discussion and further work	178
7.1	Development of photobioreactor for cultivation of <i>R. palustris</i>	178
7.2	Optimization of electroporation protocol for transformation of <i>R. palustris</i>	180
7.3	Characterization of existing chassis strains of <i>R. palustris</i>	181
7.4	Insertion of heterologous genes into the genome of <i>R. palustris</i>	183
7.5	Creation of potential <i>R. palustris</i> chassis strains for hydrogen production	184
7.6	Conclusions	186
A	Schematic diagrams	187
B	Heterologous nucleotide sequences	191
B.1	Sequences acquired from <i>R. palustris</i> genome	191
B.2	Heterologous sequences	192
	Bibliography	194

List of Figures

- 1.1 Illustration of the distribution of purple non-sulfur bacteria and purple sulfur bacteria within the “proteobacteria”. The taxonomic groups displayed under each taxonomic level are non-exhaustive and provided as examples only, apart from the three Families represented under the Order Chromatiales, which are the only three Families of that Order. 28
- 1.2 Taken from Figure 1, Larimer *et al.*, 2004 [1]; schematic representations of the four modes of metabolism available to *R. palustris*. The multicoloured circle in each cell represents the enzymatic reactions of central metabolism. 30
- 1.3 Illustration of the general form of plasmid used to create marked knockout strains of *R. palustris*. The origin of replication (*ori*), origin of transfer (*oriT*) and *sacB* (all purple) are part of the delivery plasmid. The green and orange sequence is inserted into the multiple cloning site of the delivery plasmid. The left and right fragments (green) are sequences amplified from the *R. palustris* genome and used in overlap extension PCR to generate a recombinant product containing (a deletion and) a restriction site. The restriction site is used to introduce the resistance cassette (blue). This interrupts the gene even if no deletion is present, and allows selection of successful transformants. 35
- 1.4 Diagrammatic representation of proposed model for post-translational repression of nitrogenase in response to fixed nitrogen. A star (*) indicates an activated protein. The abbreviations + NH₄⁺ and – NH₄⁺ represent the presence and absence of this signal respectively. 42
- 1.5 Diagrammatic representation of the biosynthesis of propane-1,2-diol and the typical route for glycerol assimilation. Blue arrows indicate enzymes endogenous to *R. palustris* while red arrows indicate enzymes requiring the introduction of heterologous genes. The red box indicates the target product. 45
- 1.6 Diagrammatic representation of the biosynthesis of isoprene. Blue arrows indicate enzymes endogenous to *R. palustris* while red arrows indicate enzymes requiring the introduction of heterologous genes. The red box indicates the target product. 47
- 2.1 Photographic illustration of the gas collection apparatus. 70

3.1	Taken from Figure 3, Panel A of Brotosudarmo <i>et al.</i> 2011 [2]; the absorption spectrum of <i>Rhodospseudomonas palustris</i> in suspension under high light (continuous line) and low light (dashed line), at room temperature. The x-axis displays wavelength in nm.	72
3.2	Pictorial representation of the cultivation platform, not to scale. The Magnetic Multi-Stirrer, LED Circuit Boards, and Support Panel are shown. The surrounding cabinet is not shown.	75
3.3	Photographic illustration of the bottle caps and associated accessories.	76
3.4	Calibration curves for LEDs of each wavelength used in the cultivation cabinet.	77
3.5	Optical density measured at 660 nm of wild-type <i>R. palustris</i> cultivated in the cultivation cabinet at 34°C (blue) and an INFORS incubator at 30°C (orange): mean of three replicates each; bars show standard error.	80
3.6	Optical density measured at 660 nm of wild-type <i>R. palustris</i> cultivated in the cultivation cabinet at 34°C (blue), an INFORS incubator at 34°C (red), and an INFORS incubator at 30°C (orange): mean of three replicates each; bars show standard error.	81
3.7	Optical density measured at 660 nm of wild-type <i>R. palustris</i> cultivated under an anaerobic (blue) and under an aerobic (green) atmosphere: mean of three replicates each; bars show standard error.	82
3.8	Absorbance in culture of wild-type <i>R. palustris</i> cultivated under standard conditions in the cultivation cabinet. Mean of two culture samples; three sweeps each.	83
3.9	Optical density measured at 660 nm of wild-type <i>R. palustris</i> cultivated under standard lighting (all LEDs; blue), No Infrared (1; red), No Ultraviolet (2; purple), Visible Only (3; green): mean of three replicates each; bars show standard error.	84
3.10	Optical density measured at 660 nm of wild-type <i>R. palustris</i> cultivated in an INFORS incubator at 30°C (orange) and in the cultivation cabinet with visible light at 30°C (green): mean of three replicates each; bars show standard error. For clarity the latter data are presented only up to time 361 hours.	85
3.11	Absorbance in culture of wild-type <i>R. palustris</i> cultivated in the cultivation cabinet under the 'No Infrared' condition. Mean of three culture samples; three sweeps each.	86
3.12	Absorbance in culture of wild-type <i>R. palustris</i> cultivated in the cultivation cabinet under the 'No Ultraviolet' condition. Mean of three culture samples; three sweeps each.	86

3.13	Optical density measured at 660 nm of wild-type <i>R. palustris</i> cultivated under standard lighting (all LEDs; blue), and with no 634 nm LEDs (orange): mean of three replicates each; bars show standard error.	88
3.14	Optical density measured at 660 nm of wild-type <i>R. palustris</i> cultivated on the cultivation cabinet (blue; mean of three replicates) and under natural sunlight (red; mean of two replicates): bars show standard error.	88
4.1	Taken from Figure 1, Panel B of Schäfer <i>et al.</i> , 1994 [3]: a detailed map of the p <i>KmobsacB</i> plasmid utilized for the genetic manipulation of <i>R. palustris</i> . The kanamycin resistance cassette is indicated by 'Km ^R ' and the <i>sacB</i> gene as named: the arrows indicate the direction of transcription. The multiple cloning site, labelled 'MCS', contains the following restriction sites in order: EcoRI, SmaI, BamHI, XbaI, Sall, PstI, SphI, HindIII. Other restriction sites are labelled, as are the <i>oriV</i> (origin of replication) and <i>oriT</i> (origin of transfer).	92
4.2	Illustration of the general form of plasmid used to create unmarked knockout strains of <i>R. palustris</i> . The origin of replication (<i>ori</i>), origin of transfer (<i>oriT</i>), <i>sacB</i> and resistance cassette (blue) are all part of the delivery plasmid (otherwise purple). The left and right fragments (green), amplified from the <i>R. palustris</i> genome with appropriate restriction sites, are inserted into the multiple cloning site of the delivery plasmid in sequence. The green sequence is homologous to the target region of the genome but the sequence targeted for deletion is missing between the two fragments.	93
4.3	Illustration of the process of generating unmarked knockouts, from introducing the plasmid into the genome to testing for double recombinants.	95
4.4	Example visualisation of amplification products generated by colony PCR during creation of marked <i>R. palustris</i> knockouts. In this case the primers were designed such that the amplification product spanned the region of <i>glnK2</i> targeted for deletion (see Chapter 6). Lanes: (1) DNA ladder; (2) wild-type <i>R. palustris</i> ; (3) marked Δ <i>glnK2</i> knockout. After the first recombination event but before the second, a successful marked transformant would be identified as generating two products and therefore both bands.	96

4.5	Example visualisation of amplification products generated by colony PCR during creation of unmarked <i>R. palustris</i> knockouts. In this case the primers were designed such that the amplification product spanned the region of <i>hupL</i> targeted for deletion (see Chapter 5). Lanes: (1) DNA ladder; (2) wild-type <i>R. palustris</i> ; (3) unmarked $\Delta hupL$ knockout. After the second recombination event, a successful unmarked transformant would be identified through generating the shorter product only. . . .	96
4.6	Transformation efficiency (colonies per μg DNA) of electroporation of <i>R. palustris</i> at different pulse voltage and resistance combinations, from 0.5 to 2.5 kV, and from 200 to 1000 Ω	102
4.7	Natural logarithm of the OD ₆₆₀ (presented in Figure 3.5) of wild-type <i>R. palustris</i> grown under the same conditions as the cultures used in this Chapter. Points highlighted in orange are labelled with the corresponding OD ₆₆₀ at that time point. . . .	103
4.8	Transformation efficiency (colonies per μg DNA) of electroporation of late-log phase <i>R. palustris</i> across different pulse voltage and resistance combinations.	104
4.9	Transformation efficiency (colonies per μg DNA) of electroporation of mid-log (red) and late-log (green) <i>R. palustris</i> across different pulse voltage and resistance combinations.	105
4.10	Doubling time of wild-type <i>R. palustris</i> grown under the same conditions as the cultures used in this Chapter, from the data presented in Figure 3.5. Doubling time 't' was calculated as $t = \ln(2) / \ln(1 + \text{growth rate})$, where growth rate was calculated over the period between each time point. The doubling time is plotted against the time corresponding to the mid-point of each time period.	105
4.11	Transformation efficiency (colonies per μg DNA) of electroporation of <i>R. palustris</i> re-suspended in a final volume of 0.1% of starting culture volume (red) and re-suspended in a final volume of 0.2% of starting culture volume (turquoise) across different pulse voltage and resistance combinations.	107
4.12	Transformation efficiency (colonies per μg DNA) of electroporation of <i>R. palustris</i> across different pulse voltage and resistance combinations. Data from cells incubated post-shock at 37°C for 90 minutes (red) are contrasted with data from cells incubated on ice for 90 minutes followed by warming at 37°C for 60 minutes (blue). .	108

4.13	Transformation efficiency (colonies per μg DNA) of electroporation of <i>R. palustris</i> across different pulse voltage and resistance combinations. Top: data from cells incubated post-shock at 37°C for 90 minutes (red) are contrasted with data from cells incubated at 37°C for 150 minutes (orange). Bottom: data from cells incubated post-shock on ice for 90 minutes followed by warming at 37°C for 60 minutes (150 minutes total; blue) are contrasted with data from cells incubated on ice for 30 minutes followed by warming at 37°C for 60 minutes (90 minutes total; purple).	109
4.14	Transformation efficiency (colonies per μg DNA) of electroporation of <i>R. palustris</i> at different pulse voltage and resistance combinations, from 1.5 to 2.5 kV, and from 600 to 1000 Ω	112
4.15	Transformation efficiency (colonies per μg DNA) of electroporation of <i>R. palustris</i> at different pulse voltage and resistance combinations. Data are the average of three biological replicates; error bars indicate standard error.	113
5.1	Diagrammatic representation of the biosynthesis of propane-1,2-diol and the typical route for glycerol assimilation. Blue arrows indicate enzymes endogenous to <i>R. palustris</i> while red arrows indicate enzymes requiring the introduction of heterologous genes (see below). The red box indicates the target product.	116
5.2	Diagrammatic representation of the biosynthesis of isoprene. Blue arrows indicate enzymes endogenous to <i>R. palustris</i> while red arrows indicate enzymes requiring the introduction of heterologous genes (see below). The red box indicates the target product.	117
5.3	Diagrammatic representation of the deletions introduced by David Lea-Smith and Toby Call into (A) <i>hupL</i> , encoding a subunit of the uptake hydrogenase; (B) <i>phaA</i> and <i>phaB</i> , encoding enzymes of the PHB biosynthetic pathway; (C) <i>glgC</i> and <i>glgA</i> , encoding enzymes of the glycogen biosynthetic pathway. Genes are represented in white, areas targeted for deletion are represented in orange, and the regions amplified by PCR for verification purposes are represented by blue lines; the lengths of the expected products are shown above these.	120

- 5.4 Visualisation of amplification products generated by PCR from wild-type *R. palustris* and from the $\Delta hupL\Delta phaAB\Delta glgCA$ strain, with primers spanning the targeted deletion sites. Lanes: (1) DNA ladder; (2) wild-type / *hupL* primers; (3) knockout / *hupL* primers; (4) wild-type / *phaAB* primers; (5) knockout / *phaAB* primers; (6) wild-type / *glgCA* primers; (7) knockout / *glgCA* primers. Data provided by Dr David Lea-Smith. 123
- 5.5 Diagrammatic illustration of the different primers used to test possible *R. palustris* knockouts. Spanning primers are complementary to the regions flanking the targeted deletion sites, and generate a shorter product from the unmarked knockout than from the wild-type. Internal primers are complementary to the targeted deletion sequence, and generate no product from the unmarked knockout, but do generate a product from the wild-type. 124
- 5.6 Visualisation of amplification products generated by PCR from wild-type *R. palustris* and from the $\Delta hupL\Delta phaAB\Delta glgCA$ strain, with (A) primers spanning the targeted deletion sites in *hupL*, *phaAB* and *glgCA* and (B) primers located within the targeted deletion sites. Lanes: (1) DNA ladder; (2) wild-type / *hupL* primers; (3) knockout / *hupL* primers; (4) wild-type / *phaAB* primers; (5) knockout / *phaAB* primers; (6) wild-type / *glgCA* primers; (7) knockout / *glgCA* primers. 126
- 5.7 Visualisation of amplification products generated by PCR from wild-type *R. palustris* and from the $\Delta hupL$ strain, with (A) primers spanning the targeted deletion sites in *hupL*, *phaAB* and *glgCA* and (B) primers located within the targeted deletion sites. Lanes: (1) DNA ladder; (2) wild-type / *hupL* primers; (3) knockout / *hupL* primers; (4) wild-type / *phaAB* primers; (5) knockout / *phaAB* primers; (6) wild-type / *glgCA* primers; (7) knockout / *glgCA* primers. 127
- 5.8 Visualisation of amplification products generated by PCR from wild-type *R. palustris* and from the $\Delta hupL\Delta phaAB$ strain, with (A) primers spanning the targeted deletion sites in *hupL*, *phaAB* and *glgCA* and (B) primers located within the targeted deletion sites. Lanes: (1) DNA ladder; (2) wild-type / *hupL* primers; (3) knockout / *hupL* primers; (4) wild-type / *phaAB* primers; (5) knockout / *phaAB* primers; (6) wild-type / *glgCA* primers; (7) knockout / *glgCA* primers 128

- 5.9 Visualisation of amplification products generated by PCR from wild-type *R. palustris* and from the $\Delta phaAB$ strain. Primers (A) spanning the targeted *phaAB* deletion site. Lanes (A): (1) DNA ladder; (2) wild-type; (3) knockout. Primers (B) located within the targeted deletion sites in *hupL*, *phaAB* and *glgCA*. Lanes (B): (1) DNA ladder; (2) wild-type / *hupL* primers; (3) knockout / *hupL* primers; (4) wild-type / *phaAB* primers; (5) knockout / *phaAB* primers; (6) wild-type / *glgCA* primers; (7) knockout / *glgCA* primers. 129
- 5.10 Visualisation of amplification products generated by PCR from wild-type *R. palustris* and from the $\Delta glgCA$ strain. Primers (A) spanning the targeted *glgCA* deletion site. Lanes (A): (1) DNA ladder; (2) wild-type; (3) knockout. Primers (B) located within the targeted deletion sites in *hupL*, *phaAB* and *glgCA*. Lanes (B): (1) DNA ladder; (2) wild-type / *hupL* primers; (3) knockout / *hupL* primers; (4) wild-type / *phaAB* primers; (5) knockout / *phaAB* primers; (6) wild-type / *glgCA* primers; (7) knockout / *glgCA* primers. 129
- 5.11 Visualisation of amplification products generated by PCR from wild-type *R. palustris* and from the $\Delta phaAB\Delta glgCA$ strain. Primers (A) spanning the targeted *phaAB* and *glgCA* deletion sites. Lanes (A): (1) DNA ladder; (2) wild-type / *phaAB* primers; (3) knockout / *phaAB* primers; (4) wild-type / *glgCA* primers; (5) knockout / *glgCA* primers. Primers (B) located within the targeted deletion sites in *hupL*, *phaAB* and *glgCA*. Lanes (B): (1) DNA ladder; (2) wild-type / *hupL* primers; (3) knockout / *hupL* primers; (4) wild-type / *phaAB* primers; (5) knockout / *phaAB* primers; (6) wild-type / *glgCA* primers; (7) knockout / *glgCA* primers. 130
- 5.12 Absorbance at 635 nm of samples from *o*-toluidine glycogen assay. A sample of PBS only, containing no cells but which had been treated in the same manner, was used to blank the spectrometer. For clarity, samples from strains carrying the *glgCA* deletion are coloured in orange, while samples from strains without the deletion are coloured in blue. Mean of three replicates; bars show standard error. 131
- 5.13 Fluorescence of samples incubated with Nile Red solution, excited at 510 nm with emission measured at 590 nm. The fluorescence displayed is relative both to samples containing no Nile Red and to samples containing no cells, and is the mean of three technical replicates with bars showing error: for details see Chapter 2. For clarity, samples from strains carrying the *phaAB* deletion are coloured orange, while samples from strains without the deletion are coloured blue. 133

5.14	Optical density measured at 660 nm of <i>R. palustris</i> cultivated in the cultivation cabinet described in Chapter 3 under standard lighting and an anaerobic atmosphere: wild-type (blue); $\Delta hupL$ (orange); $\Delta phaAB$ (red); $\Delta glgCA$ (green); $\Delta phaAB\Delta glgCA$ (purple); $\Delta hupL\Delta phaAB\Delta glgCA$ (brown). Mean of three replicates each; bars show standard error.	134
5.15	(A) Volume of gas produced by <i>R. palustris</i> over four hours after 216 hours of growth and (B) volume of gas produced by <i>R. palustris</i> over four hours after 216 hours of growth normalised to the optical density of the culture: wild-type (blue); $\Delta hupL$ (orange); $\Delta phaAB$ (purple); $\Delta glgCA$ (green); $\Delta phaAB\Delta glgCA$ (red); $\Delta hupL\Delta phaAB\Delta glgCA$ (brown).	137
5.16	Taken from Figure 3, Rey <i>et al.</i> , 2006 [4]; sequence alignment of the frameshifted region of <i>hupV</i> of the CGA009 strain of <i>R. palustris</i> with the corresponding gene regions from five other <i>R. palustris</i> strains.	138
5.17	Alignment of query sequence aldehyde oxidoreductase from <i>E. coli</i> str. K-12 substr. MG1655 (AML00478.1) against the one hit obtained from <i>R. palustris</i> CGA009, for a putative L-threonine dehydrogenase (WP_011156769.1), taken from NCBI.	140
5.18	Alignment of query sequence for putative L-threonine dehydrogenase from <i>R. palustris</i> CGA009 (WP_011156769.1) against the third hit obtained from <i>E. coli</i> str. K-12 substr. MG1655, for 1,2-propanediol oxidoreductase (AAB40449.1), taken from NCBI.	140
5.19	Illustration (not to scale) of the plasmids received from GeneArt. Top: carrying sequence for propane-1,2-diol biosynthesis genes, promoter and terminator. Bottom: carrying sequence for isoprene biosynthesis genes.	143
5.20	Illustration (not to scale) of the pUC19- $\Delta hupL$ plasmid used originally in the construction of the p <i>KmobsacB</i> $\Delta hupL$ plasmid for introducing a deletion into <i>hupL</i> , and later used in this work for the construction of plasmids for inserting heterologous sequences into <i>R. palustris</i> . Features of the pUC19 plasmid are shown in purple (ori and lacZ) and blue (ampicillin resistance cassette; AmpR). The <i>hupL</i> flanking regions inserted into the multiple cloning site of pUC19, located within the lacZ sequence, are shown in green.	145

- 5.21 Illustration of the plasmids used to insert heterologous genes into *R. palustris* (not to scale). Features of the pK*mobsacB* delivery plasmid are shown in purple (*sacB*, *ori* and *oriT*) and blue (kanamycin resistance cassette; Kan^R). Sequences inserted into the multiple cloning site of pK*mobsacB* are shown in green (left and right *hupL* flanking regions; target genome insertion and introduce deletion to *hupL*) and orange (promoter, terminator and heterologous genes). The plasmid is illustrated with the heterologous genes for propane-1,2-diol biosynthesis, *mgsA* and *gldA*. The sequences present in their place in the plasmids for insertion of isoprene biosynthesis genes and insertion of *ispS* only are shown above. 147
- 5.22 Visualisation of plasmid prep digestions of (A) pK*mobsacB*Δ*hupL*::*mgsA*::*gldA*, (B) pK*mobsacB*Δ*hupL*::*ipi*::*ispS* and (C) pK*mobsacB*Δ*hupL*::*ispS*. Lanes (A): (1) DNA ladder; (2) digestion with HindIII and EcoRI; (3) digestion with BamHI and XbaI. Lanes (B and C): DNA ladder; (2) empty; (3) digestion with BamHI and XbaI.. 149
- 5.23 Visualisation of amplification products generated by PCR from wild-type *R. palustris* and from isolates potentially carrying (A) inserted *ispS* and *ipi* and (B) inserted *ispS* only, with ‘spanning’ primers complementary to regions either side of the *hupL* targeted deletion site, within which the genes were inserted. Lanes: (1) DNA ladder; (2) wild-type; (3 - 6) potential transformants. 151
- 5.24 Visualisation of amplification products generated by PCR from the Δ*phaAB*Δ*glgCA* strain and from isolates with the Δ*phaAB*Δ*glgCA* background potentially carrying (A) inserted *ispS* and *ipi* and (B) inserted *ispS* only, with ‘spanning’ primers complementary to regions either side of the *hupL* targeted deletion site, within which the genes were inserted. Lanes: (1) DNA ladder; (2) Δ*phaAB*Δ*glgCA*; (3 - 6) potential transformants. 152
- 5.25 Visualisation of amplification products generated by PCR from (A) wild-type *R. palustris* and isolates potentially carrying inserted *mgsA* and *gldA* and (B) the Δ*phaAB*Δ*glgCA* strain and isolates with the Δ*phaAB*Δ*glgCA* background potentially carrying inserted *mgsA* and *gldA*, with ‘spanning’ primers homologous to regions either side of the *hupL* targeted deletion site, within which the genes were inserted. Lanes: (1) DNA ladder; (2) wild-type; (3 - 6) potential transformants. 153

5.26	<p>Visualisation of amplification products generated by PCR from (A) the insertion plasmids and (B) genomic DNA from strains carrying the heterologous genes. Lanes (A): (1) DNA ladder; (2) <i>ispS</i> primers with the pK<i>mobsacB</i>Δ<i>hupL</i>::<i>ipi</i>::<i>ispS</i> plasmid; (3) <i>ipi</i> primers with the pK<i>mobsacB</i>Δ<i>hupL</i>::<i>ipi</i>::<i>ispS</i> plasmid; (4) <i>mgsA</i> primers with the pK<i>mobsacB</i>Δ<i>hupL</i>::<i>mgsA</i>::<i>gldA</i> plasmid; (5) <i>gldA</i> primers with the pK<i>mobsacB</i>Δ<i>hupL</i>::<i>mgsA</i>::<i>gldA</i> plasmid. Lanes (B): (1) DNA ladder; (2) <i>ispS</i> primers with a strain carrying <i>ispS</i> only; (3) <i>ispS</i> primers with a strain carrying <i>ispS</i> and <i>ipi</i>; (4) <i>ipi</i> primers with a strain carrying <i>ispS</i> and <i>ipi</i>; (5) <i>mgsA</i> primers with a strain carrying <i>mgsA</i> and <i>gldA</i>; (6) <i>gldA</i> primers with a strain carrying <i>mgsA</i> and <i>gldA</i>.</p>	155
5.27	<p>Visualisation of amplification products generated by RT-PCR from (A) a strain carrying the heterologous <i>mgsA</i> and <i>gldA</i> genes, (B) a strain carrying the heterologous <i>ispS</i> and <i>ipi</i> genes, and (c) a strain carrying the heterologous <i>ispS</i> gene only. Lanes (A): (1) DNA ladder; (2) <i>amtB2</i> primers; (3) <i>amtB2</i> primers RT-; (4) <i>mgsA</i> primers; (5) <i>mgsA</i> primers RT-; (6) <i>gldA</i> primers; (7) <i>gldA</i> primers RT-. Lanes (B and C): (1) DNA ladder; (2) <i>amtB2</i> primers; (3) <i>amtB2</i> primers RT-; (4) <i>ispS</i> primers; (5) <i>ispS</i> primers RT-; (6 – B only) <i>ipi</i> primers; (7 – B only) <i>ipi</i> primers RT-.</p>	156
6.1	<p>Diagrammatic representation of the deletion sites and flanking regions identified for construction of the deletion plasmids for (A) <i>draT2</i>, (B) <i>glnK2</i> and (C) <i>nifDH</i>, Regions targeted for deletion are represented in orange and the flanking regions used in the deletion plasmids for this purpose are represented in green.</p>	168
6.2	<p>Visualisation of amplification products generated by RT-PCR to test for co-transcription of (A) <i>draT2</i> and <i>draG</i> and (B) <i>glnK2</i> and <i>amtB2</i>. Lanes (A): (1) DNA ladder; (2) <i>draT2</i> primers; (3) <i>draT2</i> primers RT-; (4) <i>draG</i> primers; (5) <i>draG</i> primers RT-; (6) <i>draT2</i>-<i>draG</i> primers; (7) <i>draT2</i>-<i>draG</i> primers RT-. Lanes (B): (1) DNA ladder; (2) <i>glnK2</i> primers; (3) <i>glnK2</i> primers RT-; (4) <i>amtB2</i> primers; (5) <i>amtB2</i> primers RT-; (6) <i>glnK2</i>-<i>amtB2</i> primers; (7) <i>glnK2</i>-<i>amtB2</i> primers RT-.</p>	168
6.3	<p>Illustrations (not to scale) of the plasmids used to introduce deletions into <i>R. palustris</i>. Features of the pK<i>mobsacB</i> delivery plasmid are shown in purple (<i>sacB</i>, <i>ori</i> and <i>oriT</i>) and blue (kanamycin resistance cassette; Kan^R). Flanking regions inserted into the multiple cloning site of pK<i>mobsacB</i> are shown in green; the restriction sites used to do so are labelled.</p>	171

6.4	Visualisation of amplification products generated by PCR from <i>R. palustris</i> strains. Lanes: (1) DNA ladder; (2) wild-type / <i>draT2</i> spanning primers; (3) $\Delta draT2$ / <i>draT2</i> spanning primers; (4) wild-type / <i>draT2</i> internal primers; (5) $\Delta draT2$ / <i>draT2</i> internal primers; (6) wild-type / <i>glnK2</i> spanning primers; (7) $\Delta glnK2$ / <i>glnK2</i> spanning primers; (8) wild-type / <i>glnK2</i> internal primers; (9) $\Delta glnK2$ / <i>glnK2</i> internal primers.	172
6.5	Visualisation of amplification products generated by PCR from <i>R. palustris</i> strains. Lanes (A): (1) DNA ladder; (2) wild-type / <i>nifDH</i> spanning primers; (3) $\Delta nifDH$ / <i>nifDH</i> spanning primers. Lanes (B): (1) DNA ladder; (2) wild-type / <i>nifDH</i> internal primers; (3) $\Delta nifDH$ / <i>nifDH</i> internal primers.	173
6.6	Visualisation of amplification products generated by PCR from <i>R. palustris</i> strains. Lanes (A): (1) DNA ladder; (2) wild-type / <i>draT2</i> internal primers; (3) $\Delta draT2\Delta glnK2$ / <i>draT2</i> internal primers. Lanes (B): (1) DNA ladder; (2) wild-type / <i>glnK2</i> spanning primers; (3) $\Delta draT2\Delta glnK2$ / <i>glnK2</i> spanning primers. Lanes (C): (1) DNA ladder; (2) wild-type / <i>glnK2</i> internal primers; (3) $\Delta draT2\Delta glnK2$ / <i>glnK2</i> internal primers. Intervening lanes that were not relevant have been removed from (B) and (C) in the interests of clarity.	173
6.7	Optical density measured at 660 nm of <i>R. palustris</i> cultivated in the cultivation cabinet described in Chapter 3 under standard lighting and a nitrogen atmosphere: wild-type +NH ₄ ⁺ (blue); wild-type -NH ₄ ⁺ (green); $\Delta nifDH$ +NH ₄ ⁺ (red); $\Delta nifDH$ -NH ₄ ⁺ (brown).	175
6.8	Optical density measured at 660 nm of <i>R. palustris</i> cultivated in the cultivation cabinet described in Chapter 3 under standard lighting and a nitrogen atmosphere: wild-type +NH ₄ ⁺ (blue); wild-type -NH ₄ ⁺ (green); $\Delta draT2\Delta glnK2$ +NH ₄ ⁺ (orange); $\Delta draT2\Delta glnK2$ -NH ₄ ⁺ (purple).	175

A.1	Schematic diagram of the transparent PVC support panel positioned above the LED circuit board to hold up the culture flasks. Individual holes were drilled for each LED as shown (yellow) as the material was found to absorb ultraviolet light (see Chapter 1). Original design by Paolo Bombelli. Not shown: drill holes to screw each of the 6 LED circuit boards into place beneath the platform, and for 16 non-tapered screws (evenly spaced along both long edges (8), the longitudinal centre (4), and between the straight edges of the hexagons (4)) to hold the platform above the multi-stirrer without crushing the LED circuit boards.	187
A.2	Schematic diagram of the cabinet designed to surround the cultivation platform: 3-dimensional representation of the cabinet. Original design by Paolo Bombelli, adjusted for the purposes of this work by the author.	188
A.3	Schematic diagram of the cabinet designed to surround the cultivation platform: exploded 3-dimensional representation of the cabinet with detailed dimensions. Original design by Paolo Bombelli, adjusted for the purposes of this work by the author. .	189
A.4	Schematic diagram of the cabinet designed to surround the cultivation platform. (C) breakdown of parts with dimensions. Original design by Paolo Bombelli, adjusted for the purposes of this work by the author.	190

List of Tables

1.1	Summary of the advantages and disadvantages of dark fermentation compared with photofermentation. The specific advantages of photofermentation with <i>R. palustris</i> are also presented.	34
1.2	Summary of the modes of action of the nitrogenase enzyme, as determined by the presence and absence of fixed and atmospheric nitrogen.	39
1.3	Summary of the different purposes for which the dihydrogen, produced by the nitrogenase, may be used.	39
1.4	Data taken from Miller & Eady, 1988 [5] (<i>Azotobacter chroococcum</i>). Data were taken from purified protein under physiologically-likely conditions in either a 100% dinitrogen atmosphere or a 100% argon atmosphere, as indicated. Amounts represent product in nmol. per min. per mg of protein.	41
1.5	Data taken from Schneider <i>et al.</i> , 1997 [6] (<i>Rhodobacter capsulatus</i>). Data were taken from purified protein (except where indicated by 'whole cell') under physiologically-likely conditions in either a 100% dinitrogen atmosphere or a 100% argon atmosphere, as indicated. Amounts represent product in nmol. per min. per mg of protein, except where activity is measured as nmol. of N ₂ reduced per min. per mg of protein (indicated by 'N ₂ reduced').	41
2.1	Recipe for minimal medium used for cultivation of <i>R. palustris</i>	50
2.2	Recipe for TSS (Transformation and Storage Solution) Buffer used for preparation of chemically competent <i>E. coli</i> cells.	53
2.3	Reaction mix for PCR with Thermo Scientific Phusion High-Fidelity DNA Polymerase	59
2.4	Reaction conditions for PCR with Thermo Scientific Phusion High-Fidelity DNA Polymerase	59
2.5	Reaction mix for PCR with Promega GoTaq Flexi DNA Polymerase	60
2.6	Reaction conditions for PCR with Promega GoTaq Flexi DNA Polymerase.	60
2.7	Recipe for SOC (Super Optimal broth with Catabolite repression) used for electroporation of <i>R. palustris</i>	65

3.1	Technical specifications of the LEDs used in the cultivation cabinet. Target Wavelength is the approximate wavelength of the peak or region on the absorption spectrum of Figure 3.1 targeted for coverage by the relevant LED. LED Wavelength indicates the highest intensity wavelength emitted by the selected LED. Spectral Halfwidth is the width at which the spectrum emitted by the LED falls to half intensity and therefore indicates the spread of the emitted spectrum. Angle of Radiance is the angle traversed by the emitted cone of light. Model Reference is the model number of the LED.	73
3.2	Lines of best fit (Calibration Curve) and conversion equations for the LED calibration curves: V indicates the voltage (V) that should be supplied to produce photon flux P ($\mu\text{mol m}^{-2} \text{s}^{-1}$).	78
3.3	Summary of test conditions to which <i>R. palustris</i> was subjected for comparison of different light spectra. Active LEDs are indicated in green. ‘Intensity Increase’ indicates the amount the intensity of the active LEDs was increased by in order to compensate for the inactive LEDs.	83
4.1	Results of pair-wise comparisons by Tukey’s HSD on the data from Figure 4.15. Difference significant at 5% indicated by *. Difference significant at 1% indicated by **.	113
5.1	List of strains created with deletions in the biosynthetic pathways for a combination of one or more of the following: PHB; glycogen; uptake hydrogenase.	119
5.2	List of primers used to test potential $\Delta hupL$, $\Delta phaAB$ and $\Delta glgCA$ transformants.	125
5.3	ANOVA table for glycogen assay data presented in Figure 5.12.	132
5.4	Results of pair-wise comparisons by Tukey’s HSD on the glycogen assay data presented in Figure 5.12. Difference significant at 5% indicated by *. Difference significant at 1% indicated by **.	132
5.5	ANOVA table for growth assay data from timepoint $t = 216$ hours presented in Figure 5.14.	135
5.6	Results of pair-wise comparisons by Tukey’s HSD on the data from timepoint $t = 216$ hours presented in Figure 5.14. Difference significant at 5% indicated by *. Difference significant at 1% indicated by **.	135
5.7	Primers used to sequence the putative frameshifted region of <i>hupV</i> in <i>R. palustris</i> , taken from Rey <i>et al.</i> , 2006 [4].	138

5.8	Summary of restriction sites relevant to construction of delivery plasmids.	144
5.9	Product sizes (to the nearest 10 bp) expected from digestion of insertion plasmids with stated pairs of restriction enzymes.	148
5.10	Product sizes expected from PCR with DNA from wild-type <i>R. palustris</i> and strains carrying inserted heterologous genes as stated, using 'spanning' primers homologous to regions either side of the <i>hupL</i> targeted deletion site, within which the genes were inserted.	150
5.11	List of primers used to test transformants for expression of inserted heterologous genes; <i>amtB2</i> primers used as a positive control for expression; <i>ispS</i> 'Amplification' primers used to amplify <i>ispS</i> sequence from GeneArt plasmid with appropriate restriction sites and hanging nucleotides for digestion and insertion between the promoter and terminator sequences.	154
6.1	List of primers used to test for co-transcription of <i>draT2</i> and <i>draG</i> , <i>glnK2</i> and <i>amtB2</i>	167
6.2	List of primers used to amplify flanking regions for construction of deletion plasmids with associated restriction sites included to facilitate transfer into and between plasmids.	170
6.3	List of primers used to test putative $\Delta draT2$, $\Delta glnK2$ and $\Delta nifDH$ transformants.	174

Abbreviations

ADP	Adenosine Diphosphate
ANOVA	Analysis of Variance
ATP	Adenosine Triphosphate
cDNA	Complementary DNA
DHAP	Dihydroxyacetone Phosphate
DMAPP	Dimethylallylpyrophosphate
DMSO	Dimethyl Sulfoxide
DNA	Deoxyribonucleic Acid
DNase	Deoxyribonuclease
dNTP	Deoxynucleoside Triphosphate
draG	Dinitrogenase Reductase Activating Glycohydrolase
draT	Dinitrogenase Reductase ADP-Ribosyltransferase
EDTA	Ethylenediaminetetraacetic acid (disodium salt dihydrate)
Fe-nitrogenase	Iron Nitrogenase
gDNA	Genomic DNA
IPP	Isopentenyl Pyrophosphate
IPTG	Isopropyl β -D-thiogalactopyranoside
ISA	Isoamyl Alcohol
LB	Lysogeny Broth
LED	Light-Emitting Diode
LH1	Core Light-Harvesting Complex
LH2	Peripheral Light-Harvesting Complex
mRNA	Messenger RNA
Mo-nitrogenase	Molybdenum Nitrogenase
NAD	Nicotinamide Adenine Dinucleotide
NADH	NAD (reduced)
OD	Optical Density (wavelength of measurement indicated by subscript)

<i>Ori</i>	Origin of Replication
<i>OriT</i>	Origin of Transfer
PBS	Phosphate-Buffered Saline
PCR	Polymerase Chain Reaction
PHB	Poly[Hydroxybutyrate]
PNSB	Photosynthetic Non-Sulfur Bacterium
PVC	Poly[Vinyl Chloride]
RNA	Ribonucleic Acid
RNase	Ribonuclease
RT	Reverse Transcription
SOC	Super Optimal broth with Catabolite repression
TBE	Tris-Borate-EDTA
TCA	Tricarboxylic Acid
TE	Tris-EDTA
TSS	Transformation and Storage Solution
Va-nitrogenase	Vanadium Nitrogenase
X-gal	5-bromo-4-chloro-3-indolyl- β -D-galactopyranoside

1 Introduction

1.1 Biodiesel and waste glycerol production

Production of biodiesel has escalated dramatically over the past decade or so. This is due to a number of factors, including increased concern over future energy supplies, the establishment of rigorous regulatory systems for biofuels in many countries, and the emergence of new markets for biofuels beyond just road transport. Biofuels were originally promoted on the basis of a hypothetical and tenuous reduction in greenhouse gas emissions. However, their continued importance is now also due to the perceived benefits of energy security [7] and the concept of maximising outputs from a single system; specifically that biomass can and should be used to produce not only energy, but also feed and any other possible outputs [8]. In the EU alone, production of biodiesel increased from 1.9 million tonnes in 2004 to 23.1 million tonnes in 2014: a 12-fold increase in just ten years [9].

Biodiesel manufacture usually proceeds through base-catalysed transesterification of triglycerides with ethanol or methanol. Although acid-catalysis is also possible, it requires higher temperatures and the reaction times are longer [10]. The primary by-product of this process is glycerol, which constitutes around 10% of the final product by weight [11]. This by-product, termed ‘crude glycerol’, contains many impurities. Pure glycerol is a reasonably high-value commodity which is used in the manufacture of a range of products, including pharmaceuticals, cosmetics and foods. However, these demands were previously met by traditional glycerol manufacture, and the current availability of crude glycerol far exceeds them. This market saturation has caused a dramatic fall in the price of glycerol, with a ten-fold decrease from approximately \$0.55 to \$0.055 per kilogram seen in just two years between 2004 and 2006 [12]. Furthermore, the purification process required to render crude glycerol suitable for traditional uses is expensive [13]. The impurities most notably include, depending on the manufacturing process, methanol or ethanol, sodium or potassium hydroxide, and saponified fatty acids [14, 15, 16]. Selling crude glycerol to refineries is therefore not usually economically attractive to biodiesel manufacturers, as the freight costs often match or even exceed the selling price, assuming a buyer can even be found.

One possibility is to sell the glycerol for use as animal feed [17]. This, however, still requires some purification. Another option is to sell the glycerol for use as boiler fuel. Unfortunately, when used as fuel, the presence of salts causes ash production, and the presence of water reduces the heating

value. Thus neither use as feed nor use as fuel generates high levels of revenue [18]. In the absence of any economically viable use for the crude glycerol product, it must be disposed of. Even this is not a simple matter, as the methanol contamination (if present), and the high alkalinity and salinity (due to the sodium or potassium hydroxide) mean that crude glycerol is classed as an environmental hazard, making even disposal expensive [19]. Thus there is not only potential to deliver more useful products from the biodiesel manufacturing process, there is also great economic incentive to develop a robust method of revenue generation from crude glycerol.

1.2 Hydrogen as a commercial product

One possible solution is to produce hydrogen biologically from crude glycerol, using a bacterium. Hydrogen is a commercially useful commodity, used for a whole variety of processes including metallic ore reduction, hydrochloric acid production, the Haber process, and fossil fuel processing. There is also considerable interest in using hydrogen as an energy carrier in fuel cells [20]. Hydrogen is an exceptionally clean form of fuel, releasing only water as a waste product from energy generation in fuel cells [21]. Although water vapour is a strong greenhouse gas, it does not accumulate in the atmosphere, unlike carbon dioxide, instead raining out in a matter of days. The amount held in the atmosphere depends on temperature, rather than the volume introduced into the atmosphere. Another advantage of hydrogen as a manufacturing product is that the relative insolubility of hydrogen in water would make harvesting from a culture easy, and the gas would then require little purification.

1.3 The hydrogen-producing *Rhodopseudomonas palustris*

Rhodopseudomonas palustris was discovered a few years ago to be capable of producing hydrogen when grown under photofermentative conditions on crude glycerol [22]. *R. palustris* is a purple non-sulfur bacterium (PNSB); a photosynthetic “proteobacterium” (a phylum of Gram-negative bacteria) which does not use hydrogen sulfide as an electron donor for photosynthesis. This last feature distinguishes the group from the related purple sulfur bacteria, which can use hydrogen sulfide, though neither group utilizes water. Together they comprise the photosynthetic members of the “proteobacteria”, the purple bacteria. However, PNSB are members of the alpha class of “proteobacteria” and therefore more closely related to the non-photosynthetic members of this class than to the purple sulfur bacteria, which are classed as gammaproteobacteria. Within the al-

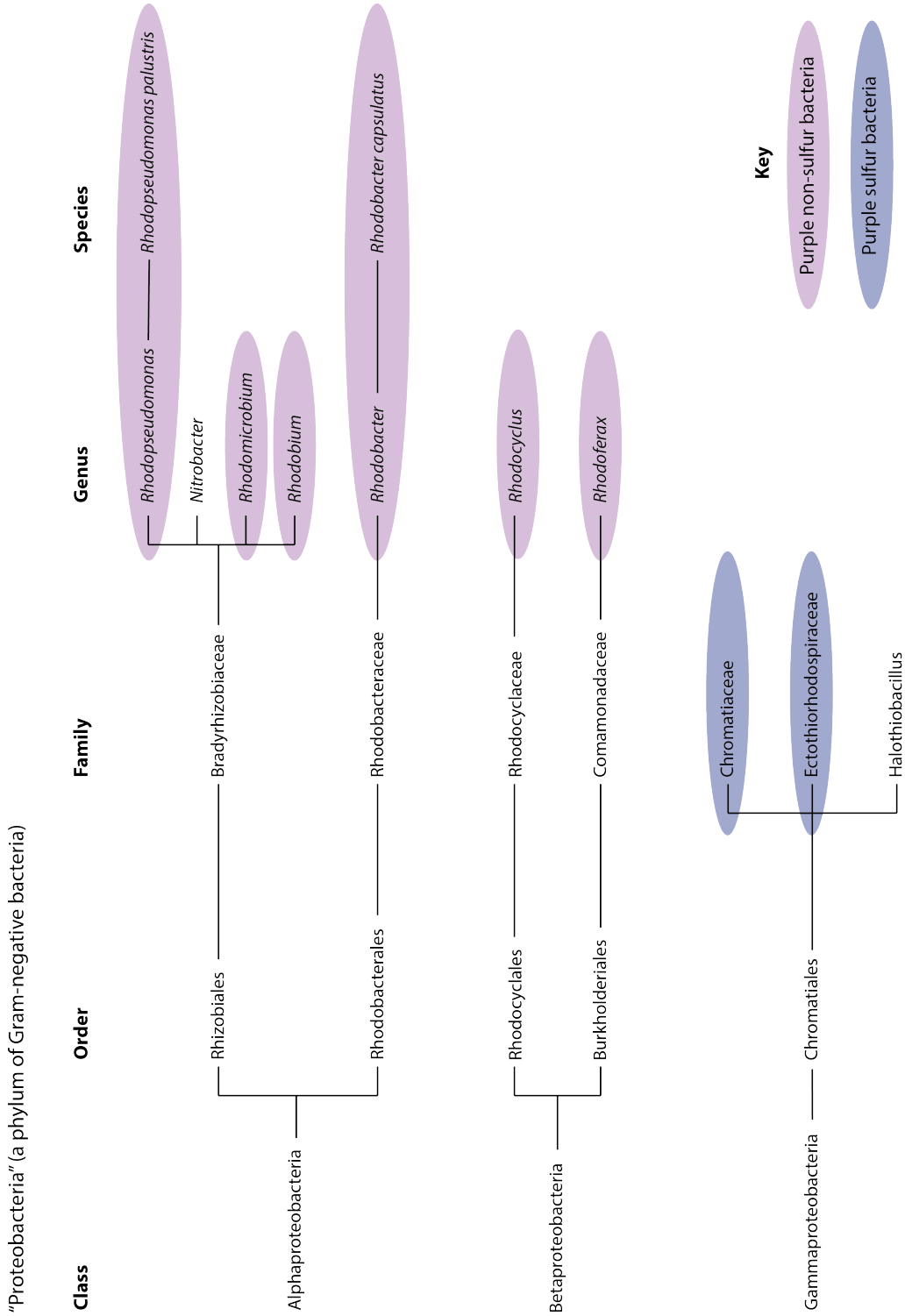


Figure 1.1: Illustration of the distribution of purple non-sulfur bacteria and purple sulfur bacteria within the "proteobacteria". The taxonomic groups displayed under each taxonomic level are non-exhaustive and provided as examples only, apart from the three Families represented under the Order Chromatiales, which are the only three Families of that Order.

phaproteobacteria class, *R. palustris* is found within the order Rhizobiales and the family Bradyrhizobiaceae. Examples of non-photosynthetic bacteria found within this family include the *Nitrobacter* genus. Other PNSB within the Rhizobiales order include the *Rhodomicrobium* genus and the *Rhodobium* genus, and more examples can be found within other orders of the alphaproteobacteria, such as the Rhodobacter family of the Rhodobacterales order, including *Rhodobacter capsulatus*. There are also some PNSB found within the betaproteobacteria, such as those of the *Rhodocyclus* genus and the *Rhodoferax* genus. In contrast, the purple sulfur bacteria are grouped exclusively within just two families, the Chromatiaceae and the Ectothiorhodospiraceae, which together with the Halothiobacillus family of non-photosynthetic bacteria make up the order Chromatiales. These relationships are illustrated in Figure 1.1.

R. palustris appears to be widely distributed globally, and has been found in a wide range of diverse habitats, from pond water and coastal sediment to earthworm droppings. Possibly as a result of this, *R. palustris* is exceptional in its level of metabolic versatility, and therefore able to grow under a wide range of conditions: this is illustrated in Figure 1.2. It has a circular 5.5 million-base-pair chromosome predicted to contain 4836 genes and an 8400-base-pair plasmid [1]. Theoretically, it can utilize four modes of metabolism: chemoautotrophy (energy acquired through oxidising inorganic or organic energy sources; carbon fixed from inorganic sources), chemoheterotrophy (energy acquired through oxidising inorganic or organic energy sources; carbon acquired from organic sources), photoautotrophy (energy acquired from photon capture; carbon fixed from inorganic sources) and photoheterotrophy (energy acquired from photon capture; carbon acquired from organic sources). The ability of *R. palustris* to grow under chemoautotrophic conditions has not been shown conclusively, however.

R. palustris can grow both aerobically and anaerobically, use a variety of inorganic electron donors, and is able to fix nitrogen. Under aerobic conditions the cells utilize the oxygen to produce ATP through respiration, but on moving to anaerobic conditions the cells start producing pigments to enable ATP production from photosynthesis [23] *R. palustris* utilizes bacteriochlorophylls *a* and *b* for photosynthesis, as well as a variety of carotenoids. These give the cells a characteristic red-pink colour [24, 25]. The photosystems of *R. palustris* contain a reaction centre surrounded by core light-harvesting complexes (LH1). There are 15 LH1 subunits surrounding a single reaction centre [26]. This core-complex consisting of the reaction centre and LH1 subunits is then surrounded by peripheral light-harvesting complexes (LH2; [27]). Unusually, *R. palustris* is able to adjust the

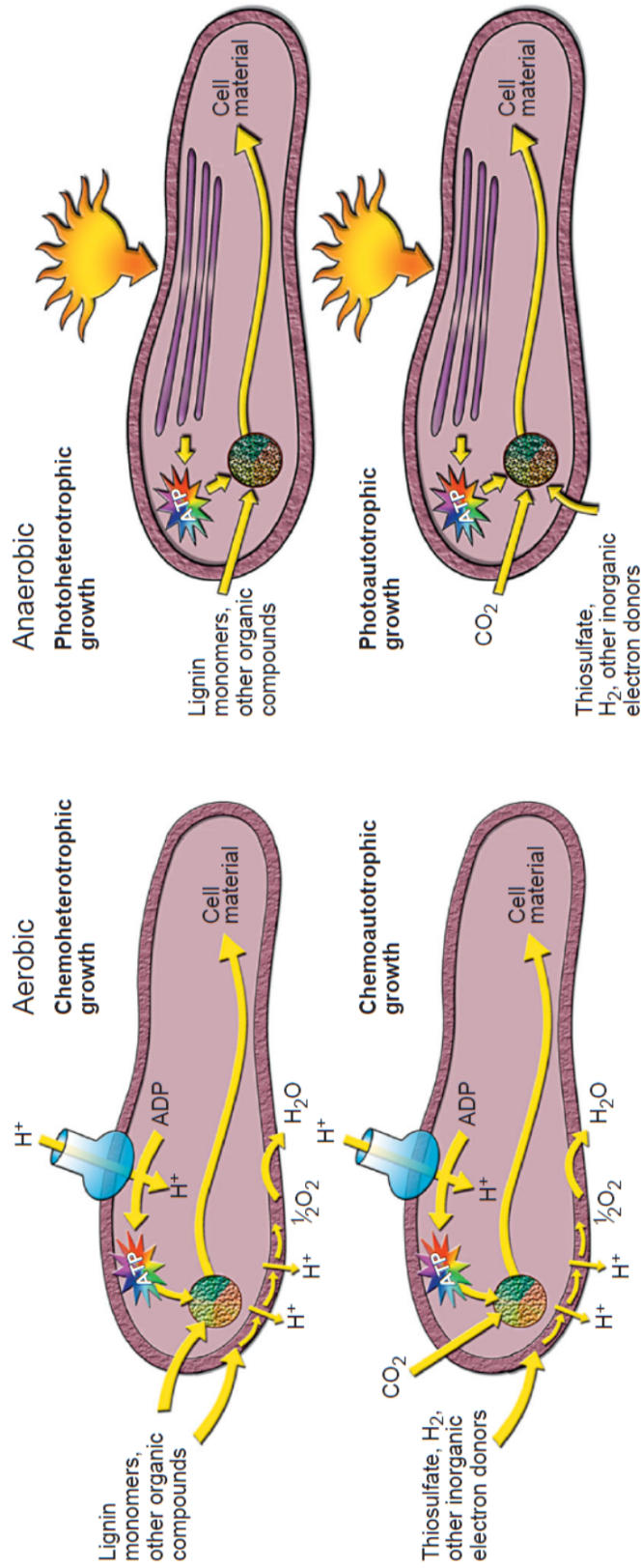


Figure 1.2: Taken from Figure 1, Larimer *et al.*, 2004 [1]; schematic representations of the four modes of metabolism available to *R. palustris*. The multicoloured circle in each cell represents the enzymatic reactions of central metabolism.

precise composition and size of its LH2 complex in response to changes in the environment. It contains genes for at least five unique pairs of LH2 polypeptides with slightly differing patterns of absorption, which are expressed differentially depending on the light intensity and spectrum of its environment [28, 29, 2].

The photosystem in purple bacteria operates cyclic electron transfer. Light energy is channelled to the reaction centre and powers the oxidation of a water-soluble cytochrome, and the reduction of quinone, forming quinol. Once the quinol has been reduced once further it diffuses through the membrane to the membrane-bound cytochrome bc_1 complex. This complex uses electrons from the reduced quinol to reduce the oxidised cytochrome, thus closing the cycle. The quinone is reduced on the cytoplasmic side of the photosynthetic membrane, while the quinol is oxidised on the periplasmic side. A proton gradient is therefore established across the membrane, which is used to power the production of ATP by an ATP-synthetase [26, 30].

1.4 Hydrogen production through photofermentation and dark fermentation

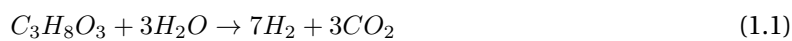
R. palustris produces hydrogen through photofermentation; that is, fermentative production of hydrogen that occurs only in the presence of light. However photofermentation, by *R. palustris* or otherwise, is not the only possible method for producing hydrogen biologically from glycerol. In fact, a considerable amount of work has been conducted on the process of dark fermentation, fermentative production of hydrogen which does not rely on light, on various substrates as well as glycerol [31, 32, 33]. Bacteria able to perform dark fermentation come from a diverse range of taxonomic groups, but two used widely in research on this process are *Enterobacter aerogenes* and various *Clostridium* species.

Dark fermentation occurs through the action of hydrogenase enzymes, and does have several advantages over photofermentation. Hydrogen production is faster by hydrogenases than by the nitrogenases responsible for hydrogen production in photofermentation, a considerable benefit for industrial processes where fast output is crucial. Furthermore, dark fermentation (clearly) does not rely on light availability. This means that, unlike photofermentation, the cultures do not require illumination, and can be mixed extremely slowly if at all. Both illumination and cell mixing may be prohibitively energy intensive and expensive for an industrial process. Compounding this disadvantage of photofermentation is the fact that the nitrogenase enzyme requires large amounts of ATP to function, conferring a particularly low photosynthetic efficiency (energy yield of product

versus solar energy absorbed) to the process as well [34].

However, if using *R. palustris* for photofermentation, the disadvantages of illumination and cell mixing may not be quite so significant. Recent work by Robert Pott and John Dennis indicates that a fairly long periodicity of the light / dark cycle can be imposed on *R. palustris* without decreasing the rate of hydrogen production significantly (unpublished data).

Furthermore, dark fermentation has its own significant disadvantages when compared with photofermentation. In particular, the conversion efficiency of substrate to product is very low. For example, in theory the maximum possible yield on a glycerol substrate is 7 moles of dihydrogen per mole of glycerol consumed: this is illustrated by equation 1.1:



Dark fermentation has only been able to reach a maximum yield of 3 moles per mole of glycerol (43%) [35], and yields of 1 – 2 moles per mole of glycerol are more usual. On any substrate the carbon source is incompletely oxidized, yielding organic acids such as acetate as waste products, for which the free energy change of further conversion is positive. Not only does this mean that much of the energy available in the feedstock remains inaccessible, the organic acids produced as waste also build up in the reaction chamber, lowering the pH and inhibiting further cell growth and hydrogen production.

In contrast, photofermentation is able to utilize light energy to overcome the positive free energy change of fully oxidising the organic acids, and can therefore use organic acids as a substrate and yield a higher conversion efficiency [36]. Although it has been suggested that photofermentation could be utilized post-dark fermentation to increase the conversion efficiency without compromising the high output of the dark fermentation stage [15, 37, 38], a two-step process is simply likely to introduce unnecessary complexity at an industrial scale.

As a comparative example to the figures given for dark fermentation of glycerol above, yields of around 87% (corresponding to about 6 moles of dihydrogen per mole of glycerol) have been achieved using *R. palustris* for photofermentation of glycerol [39]. Furthermore, an extremely high purity of 97% hydrogen was achieved in work conducted by Robert Pott, which would reduce the energy spent on purification if realised at an industrial scale [40].

A further advantage of photofermentation is that the nitrogenase-catalysed reaction is unidirectional, in contrast to that catalysed by hydrogenases for dark fermentation. Therefore, a photofer-

mentation reactor could be pressurized without favouring the reverse reaction. This would allow the hydrogen gas product to be collected under pressure. It would otherwise need to be pressurized subsequently as a gas, which is more difficult and therefore more expensive than for a liquid.

1.5 Using *R. palustris* for photofermentation

Using *R. palustris* specifically for photofermentation confers some further advantages. In particular, it is very robust to growing on crude glycerol. A study found that hydrogen production was not significantly affected by the impurities in crude glycerol diluted to 10 mM compared to pure glycerol of the same concentration [22]. More recent work conducted in this lab using 100 mM crude glycerol, without the supplemental glutamate provided in the original study, found that some growth and hydrogen production inhibition did occur [40].

Saponified fatty acids were identified to be the cause of the inhibition observed at 100 mM crude glycerol. *R. palustris* was found to be capable of withstanding methanol or ethanol at the levels found in crude glycerol, and high salt concentrations. Simple treatment of the crude glycerol prior to using it as a feedstock, with calcium chloride to precipitate the soaps followed by filtration, was found to be effective in relieving the inhibition the soaps caused. High pH was identified as another contributing factor to the inhibition, suggesting that neutralization of the glycerol prior to fermentation may also reduce inhibition.

If, however, pre-treatment of the crude glycerol feedstock is undesirable due to time, expense or energy costs, diluting the growth substrate to levels where inhibition is no longer observable should not have significant consequences. For liquid products, diluting the culture would also result in a more dilute product, requiring greater volumes of culture to be processed in order to harness the product. As the hydrogen product is gaseous, it is harvested from the headspace of the culture and will not be diluted along with the culture. The infrastructure for larger volumes of culture would still be necessary to realize the same hydrogen output, however.

Overall, the high conversion efficiency of photofermentation compared with dark fermentation, combined with the particularly high purity of hydrogen possible with *R. palustris* (see section 1.4 above) and its ability to tolerate the impurities of crude glycerol, make the possibility of employing photofermentation of crude glycerol by *R. palustris* for hydrogen production very feasible. A summary of the advantages and disadvantages of dark fermentation and photofermentation is presented in Table 1.1.

Dark Fermentation	Photofermentation
Advantages	
Hydrogenase faster than nitrogenase No reliance on light Slow / no mixing required	Can be pressurized Much higher yield
Disadvantages	
Organic acids lower pH, affecting output	Nitrogenase particularly ATP-greedy
Advantages / mitigations of <i>R. palustris</i>	
	High purity achievable Highly robust to crude glycerol Slow mixing possible

Table 1.1: Summary of the advantages and disadvantages of dark fermentation compared with photofermentation. The specific advantages of photofermentation with *R. palustris* are also presented.

1.6 *Rhodopseudomonas palustris* as a chassis organism for biotechnology

Although *R. palustris* is an attractive organism for biotechnological applications thanks to its diverse metabolic pathways, and specifically for the processing of waste glycerol as discussed above, the basic biological and genetic tools available for *R. palustris* are much more restricted than those for many other bacteria. From a pragmatic point of view, the standard photobioreactors used for oxygenic photosynthetic organisms are not well suited to cultivation of *R. palustris*, because the optimal wavelengths of light for its growth differ from many of the photosynthetic organisms typically used for these applications. This is discussed in more detail in Chapter 1. Although transformation systems are available, they are much less efficient in terms of the number of transformants per unit amount of DNA than, for example, *Escherichia coli*, and little work has been done in optimising them.

It has been possible to manipulate the genome of *R. palustris* for several decades (see, for example, [41]). A cryptic plasmid isolated from a strain of *R. palustris*, pMG101, was used to develop two shuttle cloning vectors which were maintained within the cell long-term in the absence of any selection pressure [42]. These and other broad-host-range plasmids such as pBBR1MCS [43] have been successfully used to introduce genetic material into *R. palustris* (see for example [44]).

However, for many purposes it is more desirable to integrate sequences directly into the chromosome, and direct manipulation of the genome is essential for introducing deletions. This also is possible in *R. palustris*. For example, Oda *et al.* in 2005 introduced several different deletions into

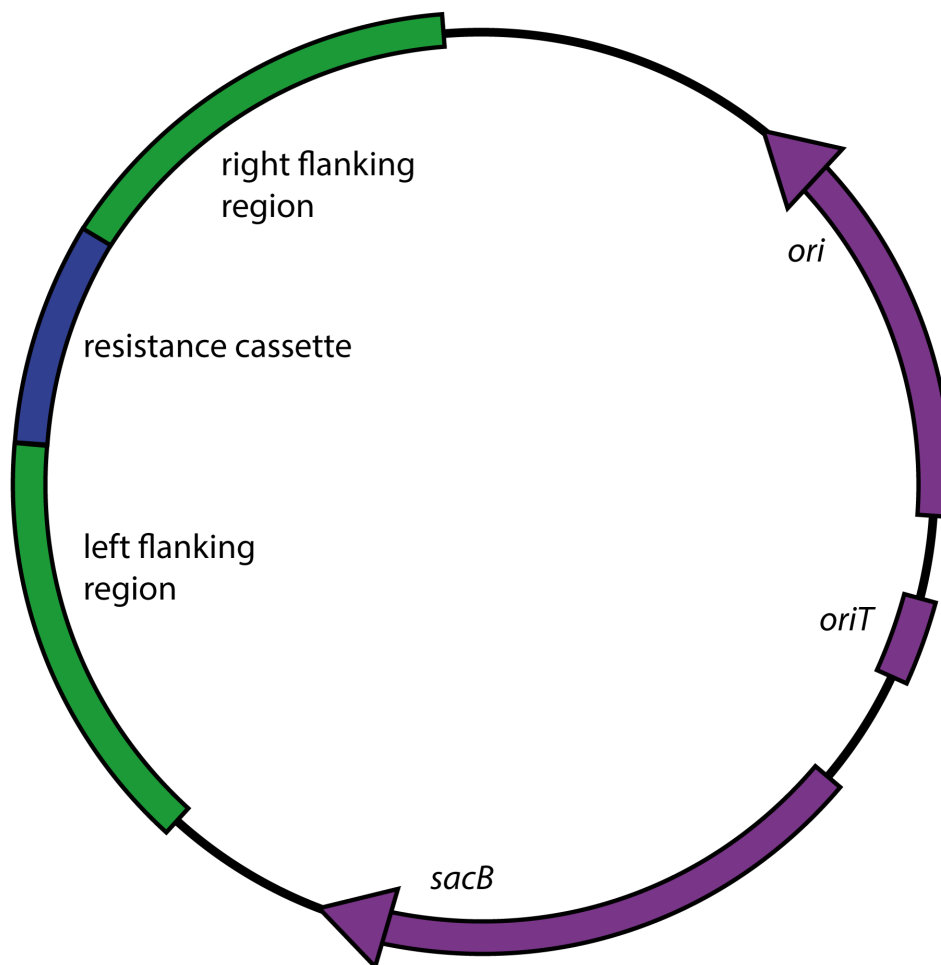


Figure 1.3: Illustration of the general form of plasmid used to create marked knockout strains of *R. palustris*. The origin of replication (*ori*), origin of transfer (*oriT*) and *sacB* (all purple) are part of the delivery plasmid. The green and orange sequence is inserted into the multiple cloning site of the delivery plasmid. The left and right fragments (green) are sequences amplified from the *R. palustris* genome and used in overlap extension PCR to generate a recombinant product containing (a deletion and) a restriction site. The restriction site is used to introduce the resistance cassette (blue). This interrupts the gene even if no deletion is present, and allows selection of successful transformants.

genes encoding nitrogenase proteins, by replacing the endogenous sequence with one created by overlap extension [45] containing both a deletion and a kanamycin-resistance cassette [46]. The delivery plasmid, illustrated in Figure 1.3, also contains the sucrose sensitivity-conferring *sacB* gene, and facilitates the selection of double recombinants with targeted gene deletions or interruptions (see also [47] [48]).

However, these transformants are ‘marked’ by their antibiotic resistance, which does confer some disadvantages. A strain containing only an interruption is at risk of reverting back to wild-type and must therefore be maintained on the appropriate antibiotic to select continuously against such reversion. This would be prohibitively expensive for industrial applications. Even in strains carrying a deletion as well, the presence of the antibiotic resistance cassette within the genome hampers the introduction of further genetic modifications. A different antibiotic must be used for each alteration, which introduces significant complexity and may require the use of less suitable antibiotics for the organism in question. Furthermore, there is always the risk of antibiotic-resistant organisms escaping into the environment. The only advantage a marked knockout may have is that maintenance on antibiotics also helps to prevent contamination by the wild-type and indeed other organisms.

A process which results in ‘unmarked’ knockouts carrying no antibiotic resistance marker would therefore be highly beneficial. Theoretically, limitless alterations could be made to the genome by this method, using the same delivery plasmid each time, containing an antibiotic appropriate to the organism. Strategies have been reported for generating unmarked strains of *R. palustris* with gene replacements (see for example [49]), and more recently a protocol was developed in-house by David Lea-Smith for the creation of unmarked strains of *R. palustris* containing targeted deletions (described in Chapter 4). However, in experiments described in Chapter 5 the transformation efficiency of the electroporation step which introduces the plasmid into *R. palustris* was found to be extremely low (approximately 200 colonies per μg DNA). Despite this, no systematic optimization of the protocol for this method had been reported, although even a modest increase in efficiency was anticipated to be beneficial for workflow.

1.7 Glycogen- and PHB-deficient strain of *R. palustris*

Previous work in this lab produced a variety of knockout strains of *R. palustris* all incapable of producing one or more of the following: uptake hydrogenase, glycogen, and poly[hydroxybutyrate]

(PHB). The plasmids used in the creation of these strains were constructed by David Lea-Smith in the manner described in Chapter 6, and the strains were created by David Lea-Smith and Toby Call.

These strains were originally created with the intention of improving hydrogen production in *R. palustris*. Glycogen and PHB are both energy storage compounds, so disrupting their biosynthetic pathways should force the cells to redirect any surplus energy toward alternative compounds, hopefully including hydrogen. The uptake hydrogenase, described in more detail in section 1.8 below, enables the cells to utilize hydrogen as a source of electrons when other supplies are low, breaking down the molecule and reducing the hydrogen yield.

These strains were also of interest to this project as potential chassis strains for further genetic manipulation. Hypothetically, the removal of pathways for storage compounds may make available more energy, reducing power and substrate molecules for use in alternative pathways introduced into the cell. This is discussed in more detail in section 1.11 below, but one of the aims of this project was therefore to introduce heterologous pathways for high-value compounds into the glycogen- and PHB-deficient strain of *R. palustris* (created by Toby Call) as well as the wild-type, to assess the feasibility and benefits of using this as a chassis strain.

However, none of these strains had been characterized: verification of both the genotypes and phenotypes had been minimal, and neither the growth nor the actual impact on hydrogen production had been measured. A slow-growing strain may well not be suitable as a chassis. Another aim of this project therefore was to characterize the growth and hydrogen production of these strains.

1.8 Hydrogen production through the action of nitrogenase enzymes

The hydrogen produced by *R. palustris* is created by the action of a nitrogenase enzyme. These naturally produce dihydrogen as a by-product of nitrogen fixation. The most common naturally-occurring form of the enzyme is termed the ‘molybdenum nitrogenase’ or Mo-nitrogenase, as it has two molybdenum-iron cofactors. It is found in all nitrogen-fixing bacteria [50], therefore including *R. palustris*. The reaction performed by this enzyme is illustrated in equation 1.2, which demonstrates the simultaneous production of hydrogen [51].

The nitrogenase enzyme consists of two proteins: a dinitrogenase, and a dinitrogenase reductase which provides reducing power to the dinitrogenase. The reductase is a homodimeric protein with a single iron-sulfur cofactor spanning the two subunits. It uses energy provided by the hydrolysis of ATP to transfer electrons from a reducing agent to the dinitrogenase protein. The dinitro-

nase is a heterotetramer with two iron-sulfur clusters and two iron-molybdenum cofactors (in the Mo-nitrogenase; see section 1.9 for details on other forms of nitrogenase). The iron-molybdenum cofactors are believed to be the site of binding and reduction of dinitrogen. The hydrolysis of ATP by the reductase causes a conformational change as well as providing energy, bringing the reductase and dinitrogenase closer for easier electron transfer [52].

The hydrogen produced within the cell via this mechanism can be oxidized to provide reducing power for carbon and further nitrogen fixation under photoautotrophic conditions. As mentioned previously, *R. palustris* encodes a nickel-containing uptake hydrogenase to facilitate use of this inorganic source of energy and reducing power [4]. Uptake hydrogenases exclusively oxidise dihydrogen, in contrast with the classical hydrogenases discussed in relation to dark fermentation, which also catalyse the reverse reaction to create dihydrogen from protons. Uptake hydrogenases containing a nickel-iron active site are one of three categories of uptake hydrogenase [53].

However, under photoheterotrophic conditions, the cell is able to use electrons liberated from organic acids in the TCA cycle to power carbon fixation. Net hydrogen production can then be possible under these conditions, if there is an excess of ATP and reducing equivalents, and the hydrogen can be used for redox balance and act as an energy store. Otherwise, the hydrogen will be recycled by the uptake hydrogenase. Even greater hydrogen production occurs when no nitrogen is available for fixation within the cell, as the Mo-nitrogenase will produce four times the amount of hydrogen when acting in the absence of dinitrogen [23]. This may be advantageous for carbon fixation, as indicated above. This reaction is illustrated in equation 1.3 and can be contrasted with equation 1.2.



The different conditions under which the nitrogenase may operate are summarized in Table 1.2. The different purposes for which the dihydrogen produced in the reaction may be used are summarized in Table 1.3.

Nitrogen availability		
Fixed nitrogen	Atmospheric dinitrogen only	No source of nitrogen
Nitrogenase is repressed	Nitrogen fixation occurs, with dihydrogen created as a by-product	No nitrogen fixation occurs, but much greater levels of dihydrogen are produced

Table 1.2: Summary of the modes of action of the nitrogenase enzyme, as determined by the presence and absence of fixed and atmospheric nitrogen.

Mode of metabolism	
Photoautotrophic conditions	Photoheterotrophic conditions
Dihydrogen is oxidized to provide reducing power for carbon and further nitrogen fixation	Dihydrogen used as an energy store and for redox balance (assuming enough ATP or reducing equivalents available from oxidation of organic acids)

Table 1.3: Summary of the different purposes for which the dihydrogen, produced by the nitrogenase, may be used.

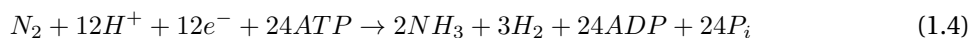
1.9 Alternative forms of nitrogenase

R. palustris is unusual in encoding two alternative nitrogenases using different cofactors as well as the Mo-nitrogenase [1]. Although many species contain one of these alternative nitrogenases, it is rare to encounter a species which contains all three forms. The first of these alternative nitrogenases contains a vanadium-iron cofactor rather than incorporating molybdenum, and is therefore termed the Va-nitrogenase. Other than *R. palustris* it has been found only in the *Azotobacter* genus (of the gammaproteobacteria class) and the cyanobacterial species *Anabaena variabilis*. The other alternative nitrogenase contains only iron in its cofactors, and is therefore termed the Fe-nitrogenase. It is found in a more diverse range of species than the Va-nitrogenase, including the alphabacterium *Rhodobacter capsulatus*.

All three forms of the nitrogenase are found to be genetically distinct from each other, rather than arising simply from different metals being substituted into the same polypeptides [51]. The Mo-nitrogenase is usually expressed preferentially over the other two alternatives. Also in contrast to other nitrogen-fixing bacteria, the expression of these alternative nitrogenases in *R. palustris* is not repressed in the presence of molybdenum. Usually, bacteria express their alternative nitrogenase when a lack of molybdenum renders them unable to express the Mo-nitrogenase. However, strains of *R. palustris* with mutations in structural genes of the Mo-nitrogenase were still able to

synthesize functional Va- and Fe-nitrogenase even when grown in concentrations of molybdenum far higher than those which repress nitrogenase expression in other bacteria. The evidence suggests that the alternative nitrogenases are expressed in response to nitrogen starvation within the cell, rather than in response to the alleviation of repression by molybdenum [46].

The reduction of dinitrogen by the Va-nitrogenase proceeds via the reaction shown in Equation 1.4, producing three times as much hydrogen as the Mo-nitrogenase per molecule of dinitrogen reduced but requiring 50% more ATP to do so [54]. This was demonstrated by experiments conducted on protein purified from *Azotobacter chroococcum*: data shown in Table 1.4 [5]. The Va-nitrogenase protein produced more nmol of hydrogen per minute per mg of protein than the Mo-nitrogenase, even though it was unable to produce as much ammonia. Furthermore, the Va-nitrogenase produced greater amounts of hydrogen in the absence of dinitrogen, though this increase (121% more) was more pronounced for the Mo-nitrogenase (256% more).



A similar experiment was carried out with the Mo- and Fe-nitrogenases of *Rhodobacter capsulatus*: data again shown in Tables 1.4 and 1.5 (nitrogenase activity here measured as dinitrogen reduced rather than ammonia produced). Again, despite a lower activity, the Fe-nitrogenase produced far greater quantities of hydrogen per minute than the Mo-nitrogenase. It also demonstrated an 85% increase in hydrogen production in the absence of dinitrogen, maintaining a greater level of production although the Mo-nitrogenase exhibited a 519% increase. However, a whole cell study comparing a strain unable to express the Mo-nitrogenase with the wild-type found that in the absence of dinitrogen, the Mo-nitrogenase produced a greater amount of hydrogen than the Fe-nitrogenase. This is likely to be due to the greater energy demands of the Fe-nitrogenase [6]. The alternative nitrogenases are strongly repressed in the presence of molybdenum, so the activity of the Fe-nitrogenase is unlikely to have been contributing to the figures obtained from the wild-type.

It is currently unclear which of these nitrogenases offers the best prospects for hydrogen production. Although the alternative nitrogenases produce more hydrogen stoichiometrically, they are slower, and their greater energy requirements seem to result in slower hydrogen production *in vivo*. In addition, this higher energy demand is likely to affect cell growth negatively to the extent that hydrogen production by the culture as a whole is lower. A study on *R. palustris* found that strains expressing only the alternative nitrogenases produced more hydrogen per mg of protein but

	100% N ₂		100% Ar
	NH ₃ produced	H ₂ produced	H ₂ produced
Va-nitrogenase	259	375	830
Mo-nitrogenase	436	296	1065

Table 1.4: Data taken from Miller & Eady, 1988 [5] (*Azotobacter chroococcum*). Data were taken from purified protein under physiologically-likely conditions in either a 100% dinitrogen atmosphere or a 100% argon atmosphere, as indicated. Amounts represent product in nmol. per min. per mg of protein.

	Whole cell			
	100% N ₂		100% Ar	100% Ar
	N ₂ reduced	H ₂ produced	H ₂ produced	H ₂ produced
Fe-nitrogenase	175	1300	2400	95
Mo-nitrogenase	235	210	1300	150

Table 1.5: Data taken from Schneider *et al.*, 1997 [6] (*Rhodobacter capsulatus*). Data were taken from purified protein (except where indicated by ‘whole cell’) under physiologically-likely conditions in either a 100% dinitrogen atmosphere or a 100% argon atmosphere, as indicated. Amounts represent product in nmol. per min. per mg of protein, except where activity is measured as nmol. of N₂ reduced per min. per mg of protein (indicated by ‘N₂ reduced’).

had much longer doubling times [46]. However, there is little data on the long-term production of hydrogen by a culture of *R. palustris* expressing either the Mo-nitrogenase or the alternative nitrogenase(s), or on the rate of hydrogen production. One aim of this project was therefore to create a strain unable to produce the Mo-nitrogenase, characterize its growth and assess its hydrogen-producing ability.

1.10 Regulation of nitrogenases in response to fixed nitrogen

The fixation of nitrogen is an energy-expensive process. The activity of the nitrogenase protein is therefore tightly regulated. In particular, the activity of nitrogenases is strongly repressed in the presence of fixed nitrogen. This is problematic for the industrial production of hydrogen from *R. palustris*, as the cells must be provided with a source of fixed nitrogen in order to facilitate growth. They cannot simply be grown in an atmosphere of dinitrogen, as this would reduce the production of hydrogen by the enzyme, and the cells would incur a great energy cost if they had to produce their own fixed nitrogen. Restricted biomass due to low nitrogen availability is not necessarily entirely disadvantageous, as more substrate can be channelled into the production of desired outputs if cell growth is not possible, and a low-density population experiences less self-shading. Most po-

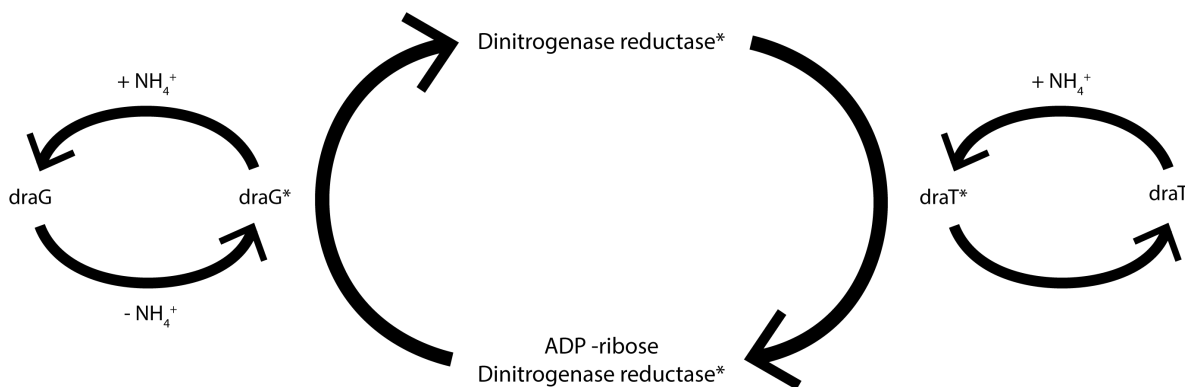


Figure 1.4: Diagrammatic representation of proposed model for post-translational repression of nitrogenase in response to fixed nitrogen. A star (*) indicates an activated protein. The abbreviations $+ \text{NH}_4^+$ and $- \text{NH}_4^+$ represent the presence and absence of this signal respectively.

tential feedstocks, including crude glycerol, have a high carbon to nitrogen ratio, so this would be a possible solution for limiting nitrogen availability [11, 55].

However, it would be preferable to be able to provide cultures with a source of fixed nitrogen without negatively affecting the activity of the nitrogenase, as higher rates of hydrogen production would be achieved with greater cell densities, even if lower yields per cell were realized. It has been suggested that a batch process could be employed, with bacteria being transferred to a low-nitrogen medium after growth to a sufficient density on a nitrogen-rich medium [22]. Batch processing adds significant complexity and expense, however. Supplemental glutamate does not repress nitrogenase synthesis or activity, but would be far too expensive for use at industrial scales. Therefore, eliminating the sensitivity of the expression of the nitrogenase enzyme to ammonium is a highly attractive prospect.

In many diazotrophs, including *Rhodospirillum rubrum* [56] and the close relative of *R. palustris*, *R. capsulatus*, [57] the Mo-nitrogenase is regulated post-translationally by a pair of enzymes, which target the reductase component of the nitrogenase enzyme (see section 1.8 above). The first is dinitrogenase reductase ADP-ribosyltransferase (encoded by *draT*), and the second is dinitrogenase reductase activating glycohydrolase (encoded by *draG*) [58]. Their mode of action is illustrated in Figure 1.4. DraT is activated transiently in the presence of ammonium, and transfers an ADP-ribosyl moiety from NAD to either of the subunits of the reductase. This disrupts the flow of electrons between the reductase and dinitrogenase, completely inactivating the nitrogenase. The DraG protein cleaves this moiety, reactivating the enzyme, but is inactivated by ammonium. It will only function to relieve the inactivation of the nitrogenase in the absence of ammonium.

R. palustris contains genes homologous to these regulatory enzymes (*draT* and *draG*), and both are expressed constitutively regardless of the levels of fixed nitrogen [46]. The nitrogenase activity of a *draT* knockout mutant was found to be relatively insensitive to ammonia in comparison to wild-type, indicating that this protein fulfils a similar role in *R. palustris* [48]. Another protein involved in the post-translational regulation of nitrogenase is GlnK, a P-II signal transduction protein which is involved in the response to fixed nitrogen in many diazotrophs, including *R. capsulatus* [59]. It is proposed to associate with DraT in the presence of ammonia, and may be responsible for the transient activation of this protein [48]. Mutations in *glnK* have been found to reduce ammonia sensitivity [60]. A homologue, *glnK2*, is found within the genome of *R. palustris*. The two protein products, DraT and GlnK2, are therefore key targets for eliminating the sensitivity of *R. palustris* to ammonium.

1.11 Production of high-value compounds from glycerol

Rather than growing *R. palustris* on crude glycerol for the purpose of producing hydrogen, it may in fact be more economically viable to produce high-value chemicals. This could be profitable even if yields are not very high, whereas a less valuable product like hydrogen must be produced in great quantities to be worthwhile. Furthermore, producing other compounds would make use of the carbon skeleton of glycerol, which is completely unutilized in hydrogen production. It may even be possible to produce multiple compounds in one strain, yielding high-value products which ensure profitability at the same time as producing hydrogen as a useful source of energy or as a chemical. Such a 'biorefinery' system would maximize the profits and utility to be made of the crude glycerol, though would introduce significant complexity at the industrial scale compared to a single-output system. Producing only hydrogen entirely wastes the carbon skeleton of the glycerol, whereas the feedstock could be more fully utilized with multiple outputs.

The introduction of a heterologous biosynthetic pathway for a high-value product is therefore an attractive prospect. Two compounds were identified as being of interest for this project: propane-1,2-diol and isoprene. Biosynthetic pathways for both of these compounds have been successfully introduced into new host organisms previously (discussed below), and in theory very few extra genes are required to allow *R. palustris* to produce either of them. There follows a discussion of the reasons for choosing each of these compounds, their biosynthetic pathways, and previous attempts to introduce these pathways into new organisms.

1.12 Propane-1,2-diol: applications and production by heterologous organisms

There is an annual global demand of around 1.4 million tonnes for propane-1,2-diol [61], with approximately half of this being used for the production of polyesters. It also has uses in various other industries as, for example, a solvent, preservative, humectant or vaporizer [62]. The rise of e-cigarettes in recent years has seen a rise in the demand for propane-1,2-diol, one of the major ingredients [63]. It is widely used as a de-icing fluid for aircraft [64], and is even used as a veterinary medicine for the treatment of ruminant hyperketonaemia [65]. Most of the current production of propane-1,2-diol ultimately stems from fossil fuel sources [62], but a rise in consumer demand for more environmentally friendly chemicals has increased the market for bio-based propane-1,2-diol.

Biologically, propane-1,2-diol is produced from dihydroxyacetone phosphate (DHAP); see Figure 1.5. After uptake, glycerol is assimilated within the cell through conversion to DHAP (by glycerol kinase and glycerol-3-phosphate dehydrogenase; encoded by *glpK* and *gpsA* respectively) which can then be isomerized into glyceraldehyde-3-phosphate (by triose phosphate isomerase; encoded by *cbbJ*) and thus enter glycolysis. However, DHAP can also feed into other biochemical pathways, such as that for propane-1,2-diol synthesis. This latter pathway occurs through the action of three enzymes: methylglyoxal synthase, aldehyde oxidoreductase, and glycerol dehydrogenase.

E. coli possesses the genes for these three enzymes and is able to produce propane-1,2-diol. Furthermore, overexpression of these genes led to increased production of propane-1,2-diol [66]. The cells were also grown on glycerol, and manipulation of the glycerol fermentation pathway to increase availability of DHAP increased propane-1,2-diol production. More significantly, introduction of methylglyoxal synthase and glycerol dehydrogenase (the two enzymes which would be required by *R. palustris*, as discussed below) into *Saccharomyces cerevisiae* led to production of propane-1,2-diol by this organism on glycerol [61].

S. cerevisiae utilizes glycerol poorly, but overexpression of genes from existing glycerol utilization pathways increased uptake 1.47-fold. Introduction of the propane-1,2-diol biosynthetic pathway increased glycerol uptake (1.86-fold compared to wild-type) even further, and overexpression of glycerol utilization pathways in this strain led to a 1.57-fold increase in propane-1,2-diol-production (from 0.62 to 0.98 g L⁻¹ over 96 hours). Although *E. coli* itself is used extensively, well-studied, and easy to culture with long-established methods, it consumes glycerol far less efficiently than *R. palustris* [22]. This makes the introduction of propane-1,2-diol biosynthesis into *R. palustris* an attractive option, especially given its tolerance of the impurities of crude glycerol.

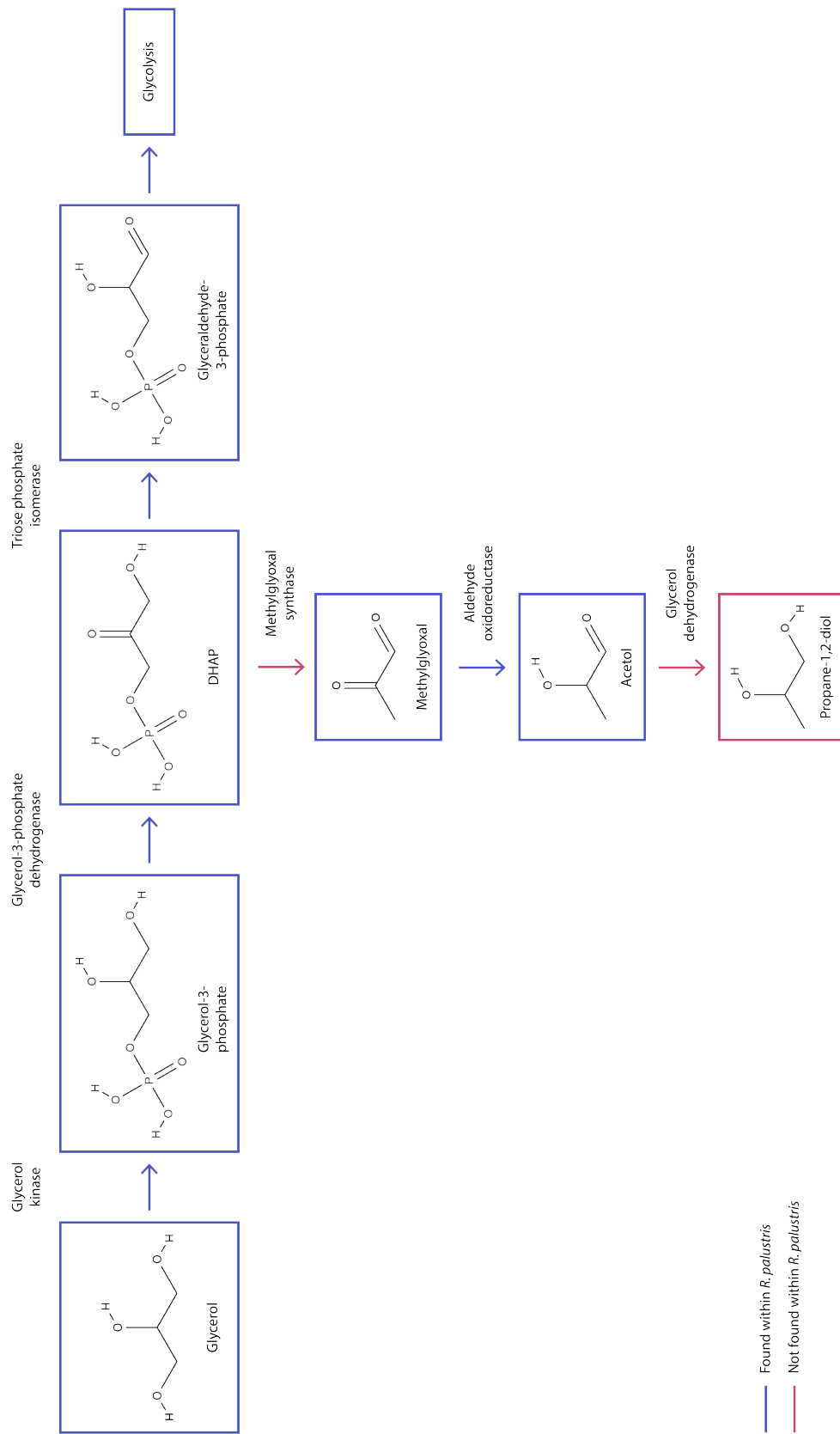


Figure 1.5: Diagrammatic representation of the biosynthesis of propane-1,2-diol and the typical route for glycerol assimilation. Blue arrows indicate enzymes endogenous to *R. palustris* while red arrows indicate enzymes requiring the introduction of heterologous genes. The red box indicates the target product.

1.13 Isoprene: applications and production by heterologous organisms

Approximately 800,000 tonnes of isoprene are produced annually, and the vast majority of this (about 70%) is used to produce a synthetic form of rubber, *cis*-1,4-polyisoprene, primarily used in the manufacture of tyres. A significant proportion of global consumption of isoprene also comes from the manufacture of adhesives. Apart from these products, the remaining isoprene consumption can be attributed to the manufacture of specialist chemicals such as vitamins and pharmaceuticals. The price is therefore heavily dependent on the fluctuating price of natural rubber. Similarly to propane-1,2-diol, most commercial isoprene is derived ultimately from crude oil. A large proportion of manufactured isoprene is sourced as a by-product from the cracking of naphtha to produce ethylene [62].

Isoprene is produced biologically from dimethylallylpyrophosphate (DMAPP) via the action of isoprene synthase; see Figure 1.6. In most bacteria, DMAPP is synthesized via the non-mevalonate pathway, by a reductase which simultaneously yields its isomer, isopentenyl pyrophosphate (IPP), as a product of the reaction. There is, however, an alternative pathway for producing these terpenoid precursors in which IPP is synthesized in isolation first, and then converted into the more reactive form, DMAPP, by the enzyme IPP isomerase. This is called the mevalonate pathway and is found in all higher eukaryotes and some bacteria. Isoprene itself is produced by many tree species, and is thought to protect against heat stress in particular, but also other abiotic stresses such as reactive oxygen species [67].

Isoprene is an attractive option to be an output from crude glycerol feedstock. It is a volatile compound, which is advantageous for biological production in two ways: harvesting the product is easy to achieve, even without destroying or disrupting the culture, and the product does not build up within the cell or culture to levels likely to inhibit its own biosynthetic pathway. The gene for isoprene synthase, *ispS*, was introduced into the cyanobacterium *Synechocystis* sp. PCC6803 from the plant *Pueraria montana*, after codon-optimization [68]. This resulted in isoprene formation, indicating that a similar approach may be successful in *R. palustris*. It is possible that introduction into *R. palustris* of the *ipi* gene for IPP isomerase along with *ispS* may increase production of isoprene by increasing flux through DMAPP (see again Figure 1.6). It may also aid the cell in maintaining its usual balance between these two precursors, as the production of isoprene may decrease the availability of DMAPP for its typical purposes within the cell.

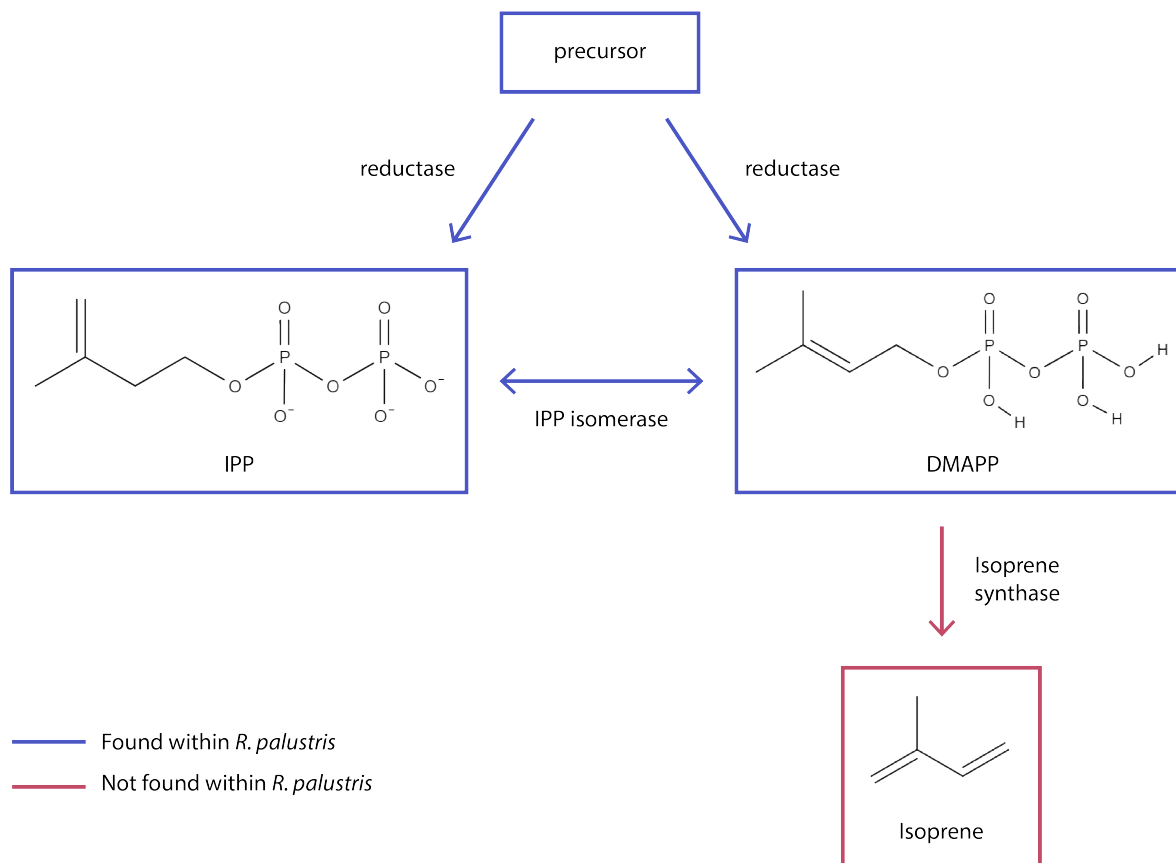


Figure 1.6: Diagrammatic representation of the biosynthesis of isoprene. Blue arrows indicate enzymes endogenous to *R. palustris* while red arrows indicate enzymes requiring the introduction of heterologous genes. The red box indicates the target product.

1.14 Aims of the project

The overall aim of the project was to develop *Rhodospseudomonas palustris* as a chassis organism for biotechnological applications, with particular reference to the use of the organism for treatment of waste glycerol, with the aim of producing hydrogen and other useful products. This required a significant investment into the development and optimization of basic systems for growth and transformation, as well as characterisation of host strains of particular interest. The specific aims of the project were therefore:

1. To develop a suitable photobioreactor system for growth of *R. palustris*, taking into account its spectral requirements.
2. To optimize the existing system of transformation by electroporation.
3. To characterize existing host strains designed to direct metabolic flux into desired products.
4. To attempt expression of heterologous genes by *R. palustris* with the aim of making high-value products.
5. To construct host strains with mutations affecting nitrogen metabolism which may enhance hydrogen yields.

2 Materials and methods

2.1 Reagents

Except where specified otherwise, all chemical reagents were supplied by Sigma-Aldrich.

2.2 Centrifugation

Where indicated that samples were centrifuged at 1800*g*, an Eppendorf Centrifuge 5810 was used with an A-4-81 rotor. Where indicated that samples were centrifuged at 14000*g*, an Eppendorf MiniSpin Plus was used with an F-45-12-11 rotor.

2.3 Growth and storage of *Rhodopseudomonas palustris*

2.3.1 Maintenance of *Rhodopseudomonas palustris* strains

Rhodopseudomonas palustris wild-type strain CGA009 (full genome sequenced by [1]), from lab stocks, and all strains deriving from this parent strain used or created during the course of this project, were cultured in minimal medium made up in Milli-Q water according to the recipe given in Table 2.1 (provided by Robert Pott and optimized further for *R. palustris* by John Hervey, Dept of Biochemistry, University of Cambridge). Strains were maintained over the short-term on agar plates: 15 g Bacto agar added per litre of medium, steam sterilized, poured and dried for at least 45 minutes under sterile conditions (stored at 4°C for up to a month unless used immediately). For long-term storage, cultures were grown to an optical density at 660 nm (OD₆₆₀; section 2.4.1) of 0.3 (log phase; see Chapter 3), harvested by centrifugation at 1800*g* for 20 minutes, and re-suspended in minimal medium, concentrated 5-fold. An equal volume of sterile 50% v/v glycerol solution was then added before snap-freezing samples in liquid nitrogen and transferring them to -80°C for storage.

2.3.2 Measurement of *R. palustris* growth

For measurement of the growth of *R. palustris* cultures over a period of time, cultures were subjected to an anaerobic argon atmosphere, stirred at 200 rpm and illuminated at 40 μmol photons m⁻² s⁻¹ in the cultivation cabinet, except where stated otherwise. For details see Chapter 3.

Base Medium	<i>Sterilize appropriate volume prior to adding further components</i>
Component	Final Concentration / mM
KH ₂ PO ₄	12.5
NaCl	6.84
MgSO ₄ •7H ₂ O	0.811
CaCl ₂ •2H ₂ O	0.340
Further Components	<i>Prepare stock solutions, sterilize and dilute into base medium</i>
Component	Final Concentration / mM
K ₂ HPO ₄	9.76
Ferric citrate	0.0167
4-aminobenzoic acid	1.458
Glycerol	50.0
Nitrogen Source	<i>Prepare, sterilize and dilute into base medium one of the following</i>
Component	Final Concentration / mM
(NH ₄) ₂ SO ₄	10.0
Sodium glutamate	20.0
Trace Elements	<i>Sterilize stock solution and dilute 1000-fold into base medium</i>
Component	Stock Concentration / mM
ZnCl ₂	0.514
MnCl ₂ •4H ₂ O	0.505
H ₃ BO ₃	0.970
CoCl ₂ •6H ₂ O	0.841
CuCl ₂ •2H ₂ O	0.117
NiCl ₂ •6H ₂ O	0.0841
NaMoO ₄ •2H ₂ O	0.165

Table 2.1: Recipe for minimal medium used for cultivation of *R. palustris*.

2.3.3 Rapid growth of and application of selection pressure to *R. palustris*

For rapid growth of cultures prior to experimentation and for all steps of the electroporation process (section 2.1.3) *R. palustris* was cultured in Yeast Peptone (YP) medium made up in Milli-Q water: 2.5 g L⁻¹ yeast extract; 2.5 g L⁻¹ peptone. Agar plates were made as previously (15 g L⁻¹ Bacto agar) where required. Kanamycin was added to a final concentration of 100 µg mL⁻¹ where required for a selectable marker. Sucrose was added to a final concentration of 10% w/v where required for a counter-selectable marker.

2.4 Spectrophotometry

2.4.1 Measurement of optical density as a proxy for cell concentration

Optical density was used as a proxy for the cell concentration of liquid cultures of both *R. palustris* and *E. coli*. The absorbance of *R. palustris* cultures was measured at a wavelength of 660 nm (OD₆₆₀). This is the standard wavelength used for *R. palustris* (see for example [69] and was shown to be an appropriate proxy for the dry cell weight of the strain of *R. palustris* used in this lab by Robert Pott [70]. The absorbance of *E. coli* cultures was measured at a wavelength of 600 nm (OD₆₀₀) as is standard. Absorbance was measured from 1 mL culture in a 1.6 mL polystyrene semi-micro cuvette (Sarstedt) by a Thermo Spectronic HeλIOS γ spectrophotometer, against a 'blank' sample of 1 mL sterile medium of the same type as the culture.

2.4.2 Measurement of whole absorption spectrum

The absorption spectrum of *R. palustris* culture was measured using a Shimadzu UV-1800 UV spectrophotometer. 1 mL culture was transferred into one compartment of a 2 mL quartz tandem cuvette. The other compartment was filled with 1 mL titanium dioxide (TiO₂) 1 mg mL⁻¹ colloidal suspension and the cuvette placed such that the light passed through the TiO₂ before passing through the culture. The 'blank' medium sample was set up in the same manner. For dense cultures, the use of TiO₂ reduces the level of noise from scattering of light by the cells: the TiO₂ suspension scatters light to a much greater extent than the culture, light scattering is accounted for by the 'blank' sample, and any scattering due to the culture is negligible in comparison. This technique (Hervey & Bombelli, manuscript in preparation) is an improvement on a previously published protocol which utilized 3M Scotch™ Magic Tape stuck to the sides of the cuvette instead [71].

Three sweeps were taken in succession, from 1000 nm to 400 nm. The average absorbance at each point of measurement was calculated; taking three sweeps helps to reduce noise in the signal.

2.5 Measurement of light intensity

Light intensity was measured with a Skye Instruments SKP 200 light meter. Measurement of LED clusters (see Chapter 3) was conducted at a point 3 cm above the centre of the cluster. A triangular platform on three supports containing a hole through which the light meter could receive light was placed in the centre of the cluster and used to support the light meter during measurement. This ensured that the distance between the LEDs and the meter was consistent between measurements.

2.6 Plasmid cloning

2.6.1 Cultivation of *Escherichia coli*

The DH5 α strain (Taylor *et al.* 1993) of *Escherichia coli* (*E. coli*), obtained from lab stocks, was cultivated for the purpose of plasmid cloning in Lysogeny Broth (LB): 25 g L⁻¹ LB powder in Milli-Q water; agar added for plates as previously where required. Ampicillin was added to a final concentration of 100 $\mu\text{g mL}^{-1}$ where required for a selectable marker. Kanamycin was added to a final concentration of 30 $\mu\text{g mL}^{-1}$ where required for a selectable marker.

2.6.2 Preparation of chemically competent cells

Chemically competent cells were prepared from fresh LB agar plates of *E. coli* (streaked from glycerol stocks one day prior) as described by the following steps:

1. One colony was selected and incubated overnight in 5 mL LB medium at 37°C with shaking.
2. This culture, 1 mL, was used to inoculate up to 99 mL pre-warmed LB medium.
3. This 100 mL culture was incubated at 37°C with shaking and monitored until OD₆₀₀ reached 0.4 – 0.6.
4. During this incubation period sterile 1.5 mL microcentrifuge tubes and TSS buffer (Transformation and Storage Solution; including DMSO (dimethyl sulfoxide) supplement; see Table 2.2) were chilled on ice.

Component	Amount / g	Final Concentration
Poly[ethylene glycol] 6000 (PEG)	10	10% w/v
MgSO ₄ •7H ₂ O	0.25	10 mM
MgCl ₂ •6H ₂ O	0.203	10 mM
LB powder	2.5	

Made up in Milli-Q water to 100 mL.

9.5 mL aliquots stored at 4°C.

*Supplemented with 0.5 mL 5% v/v DMSO solution
just before use*

Table 2.2: Recipe for TSS (Transformation and Storage Solution) Buffer used for preparation of chemically competent *E. coli* cells.

5. Post-incubation, the culture was split into two 50 mL centrifuge tubes and incubated on ice for 15 minutes.
6. The culture was harvested by centrifugation at 1800*g* for 10 minutes at 4°C All subsequent steps were carried out at 4°C with cells kept on ice wherever possible.
7. The supernatant was removed from the centrifuge tubes by pouring, followed by pipetting any remaining medium.
8. The cells were fully re-suspended in chilled TSS buffer to 10% of the original culture volume, ensuring that no clumps were present.
9. Aliquots of 100 µL were dispensed into chilled 1.5 mL microcentrifuge tubes.
10. Cells were stored at -80 °C until required.

2.6.3 Transformation with and recovery of plasmid DNA

1. A 100 µL sample of cells was taken from -80°C storage directly into ice without touching the bottom of the microcentrifuge tube.
2. The cells were left to defrost on ice for approximately 15 minutes.
3. A sample of plasmid solution (1 µL purified plasmid or 5 µL ligation solution; section 2.11.5) was added to the cells and mixed in well with gentle pipetting.
4. The cells were incubated on ice for 30 minutes.
5. The cells were subjected to heat shock at 42°C in a water bath for 30 seconds.

6. The cells were immediately transferred to ice and incubated for 2 minutes.
7. 900 μL LB medium was added to the cells.
8. The cells were incubated at 37°C with shaking for 1 hour.
9. LB agar plates, containing appropriate antibiotics if required, were treated with 40 μL X-gal solution (5-bromo-4-chloro-3-indolyl- β -D-galactopyranoside, 20 mg mL⁻¹ in DMSO; stock solution stored at -20°C wrapped in foil) and 40 μL IPTG solution (isopropyl β -D-thiogalactopyranoside, 0.1 M; stock solution filter-sterilized and stored at -20°C), spread evenly across the plate surface until absorbed.
10. Both a 50 μL and a 200 μL sample of the cells were each spread onto the prepared agar plates until absorbed.
11. The agar plates were incubated overnight at 37°C with shaking.
12. Several white colonies were then selected and each transferred to 2 mL LB medium (with antibiotics as appropriate) held within a 7 mL polystyrene bijou container.
13. These culture samples were incubated overnight at 37°C with shaking.
14. Each culture sample was transferred into a 2 mL microcentrifuge tube.
15. Cells were harvested by centrifugation at 14000*g* for 4 minutes and the supernatant discarded.
16. Plasmid was extracted from the cells using the QIAGEN MiniPrep kit, according to the manufacturer's instructions (centrifugation carried out for 45 seconds where 30 – 60 seconds advised, and the 50 μL Elution buffer added back onto the column membrane for a second incubation at the end to increase concentration of plasmid DNA acquired).

2.7 Extraction of DNA and RNA

2.7.1 Measurement of DNA and RNA concentration

The concentration of DNA or RNA in a sample was measured on a NanoDrop ND-1000 spectrophotometer using the appropriate manufacturer's setting, against a blank water sample.

2.7.2 Extraction of genomic DNA

Genomic DNA (gDNA) was extracted from *R. palustris* to provide a template for amplifying endogenous sequences (section 2.9.2), as follows:

1. Cells from 15 mL mid-log culture ($OD_{660} = 0.3$) were harvested by centrifugation at $1800g$ at $4^{\circ}C$ for 10 minutes.
2. The supernatant was removed, leaving a small amount to facilitate subsequent transfer.
3. The cells were transferred to a 1.5 mL microcentrifuge tube.
4. The cells were harvested by centrifugation at $14000g$ at $4^{\circ}C$ for 10 minutes and the supernatant discarded.
5. The cells were re-suspended in 600 μ L Tris-EDTA (TE) Buffer (10 mM Tris; 1 mM EDTA; pH 8.0 with hydrochloric acid (HCl)).
6. 600 μ L water-saturated phenol (titrated to pH 8.0) was added.
7. 100 μ L acid-washed 425 – 600 μ m glass beads were added.
8. The sample was bead-beaten for 1 minute in a BioSpec Mini-BeadBeater-16 (model: 607EUR) at 3450 oscillations per minute.
9. The sample was centrifuged at $14000g$ for 5 minutes and the supernatant retained.
10. An equal volume of phenol:chloroform:ISA (25:24:1; isoamyl alcohol) was added.
11. The sample was centrifuged at $14000g$ at $4^{\circ}C$ for 5 minutes and the supernatant retained.
12. The previous two steps were repeated until no white interface remained after centrifugation.
13. An equal volume of chloroform:ISA (24:1) was added.

14. The sample was vortexed.
15. The sample was centrifuged at 14000*g* at 4°C for 5 minutes and the supernatant retained.
16. 0.1 volume sodium acetate solution (3M; pH 5.2 with acetic acid) was added and the sample mixed.
17. 2.5 volumes ice-cold 100% ethanol were added.
18. The sample was incubated at -80°C for 1 hour.
19. The sample was removed and thawed until near melting in hand.
20. The sample was centrifuged at 14000*g* at 4°C for 30 minutes and the supernatant discarded.
21. The pellet was washed by addition of 1 mL ice-cold 70% v/v ethanol followed by vortexing.
22. The sample was centrifuged at 14000*g* at 4°C for 5 minutes and the supernatant discarded.
23. The previous two steps were repeated for a total of two washes, with as much ethanol removed as possible after the final wash.
24. The pellet was briefly dried in a fume cupboard.
25. The pellet was re-suspended in 100 µL water.

2.7.3 Extraction of DNA for colony PCR

DNA was extracted from *R. palustris* for use in colony PCR (polymerase chain reaction) to test for the presence of genomic modifications (section 2.9.3), as follows:

1. Ten to fifteen acid-washed 425 – 600 µm glass beads were added to 50 µL water in a 1.5 mL microcentrifuge tube.
2. A single colony was selected and transferred to the microcentrifuge tube.
3. The sample was vibrated for 5 minutes in an IKA VRX Vibrax shaker.
4. The sample was centrifuged at 14000*g* for 5 minutes.
5. The supernatant was sampled for use in colony PCR.

2.7.4 Extraction of RNA

RNaseZAP (Sigma-Aldrich) was used to prepare all surfaces when undertaking any work involving RNA in order to reduce the risk of RNase (ribonuclease) contamination. RNA was extracted from *R. palustris* for use in co-transcription and gene expression assays (sect), using a modified version of the protocol from [47] with the QIAGEN RNeasy Mini Kit as follows:

1. Cells from 30 mL mid-log culture ($OD_{660} = 0.3$) were harvested by centrifugation at $1800g$ at $4^{\circ}C$ for 10 minutes and the supernatant discarded.
2. The cells were re-suspended in 1 mL YP medium and transferred to a 1.5 mL microcentrifuge tube.
3. The cells were incubated overnight at $-80^{\circ}C$, without first snap-freezing.
4. The cells were left to defrost fully on ice.
5. The cells were harvested by centrifugation at $14000g$ for 5 minutes and the supernatant discarded.
6. The cells were re-suspended in 1 mL TE Buffer (Tris-EDTA; pH 8.0) with Ready-Lyse Lysozyme Solution (5000 units; Epicentre) and incubated at room temperature for 15 minutes.
7. The cells were harvested by centrifugation at $14000g$ for 5 minutes and the supernatant discarded.
8. The cells were re-suspended in $700 \mu L$ Buffer RLT (QIAGEN) containing $10 \mu L mL^{-1}$ β -mercaptoethanol and the suspension split equally into two microcentrifuge tubes.
9. Acid-washed $425 - 600 \mu m$ glass beads, $200 \mu L$, were added to each tube.
10. The samples were vortexed 5 times, each for 1 minute, with incubation on ice for 1 minute between.
11. The beads and cells were sedimented by centrifugation at $14000g$ for 5 minutes and the supernatants retained and combined using gel-loading tips.
12. 1 volume 70% v/v ethanol was added to the combined lysate and the entire sample applied to a QIAGEN spin column.

13. The manufacturer's instructions for the purification of RNA with the QIAGEN RNeasy Kit were then followed from step 3, transfer of the sample to a spin column, including the instructions for an On-Column DNase (deoxyribonuclease) Digestion (the optional 1-minute centrifugation step to dry the membrane of ethanol prior to elution of RNA was included, and the final elution performed with 30 μ L nuclease-free water which was then re-applied to the column and re-collected in order to increase the concentration of RNA obtained).

2.8 Amplification of DNA by polymerase chain reaction

2.8.1 Design of primers for polymerase chain reaction

Primer pairs were designed using Primer3 ([72, 73]; <http://bioinfo.ut.ee/primer3-0.4.0/>), and primers were synthesized by Sigma-Aldrich. Where primers were designed to check for the presence or absence of specific sequences within the genome of *R. palustris*, a BLAST search was first conducted (NCBI) to ensure there were no (other) complementary sequences present within the genome.

2.8.2 Amplification of high-fidelity DNA

DNA was amplified to a high degree of fidelity for use in plasmids for genetic manipulations and for sequencing (section 2.1.2), using Thermo Scientific Phusion High-Fidelity DNA Polymerase. The reaction mix was prepared as shown in Table 2.3. The reaction conditions are shown in Table 2.4.

2.8.3 Amplification of DNA for colony PCR

DNA was amplified from individual colonies to test for the presence of genetic modifications, using Promega GoTaq Flexi DNA Polymerase. The reaction mix was prepared as shown in Table 2.5. The reaction conditions used are shown in Table 2.6.

Component	Details	Volume / μL
5x Phusion GC Buffer		10
dNTPs	40 mM	1
Template DNA	100 ng μL^{-1}	1
Forward primer	10 mM	1
Reverse primer	10 mM	1
DMSO		3
Phusion DNA Polymerase		0.5
Water	to 50 μL	32.5

Table 2.3: Reaction mix for PCR with Thermo Scientific Phusion High-Fidelity DNA Polymerase

Cycle Step	Temperature / $^{\circ}\text{C}$	Duration / s
<i>Lid</i>	98	<i>Throughout</i>
Initial Denaturation	98	30
<i>For 35 cycles:</i>		
Denaturation	98	10
Annealing	67	30
Extension	72	30
Then for Final Extension	72	300

Table 2.4: Reaction conditions for PCR with Thermo Scientific Phusion High-Fidelity DNA Polymerase

Component	Details	Volume / μL
5x Green GoTaq Flexi Buffer		10
MgCl ₂ solution	25 mM	3
dNTPs	40	1
Forward primer	10	1
Reverse primer	10	1
Phusion DNA Polymerase		0.25
Template DNA		5
Water	to 50 μL	28.75

Table 2.5: Reaction mix for PCR with Promega GoTaq Flexi DNA Polymerase

Cycle Step	Temperature / $^{\circ}\text{C}$	Duration / s
<i>Lid</i>	98	<i>Throughout</i>
Initial Denaturation	95	120
<i>For 35 cycles:</i>		
Denaturation	95	30-60
Annealing	60	30-60
Extension	72	<i>60 per kb target sequence</i>
Then for Final Extension	72	300

Table 2.6: Reaction conditions for PCR with Promega GoTaq Flexi DNA Polymerase.

2.9 Amplification of complementary DNA from RNA

2.9.1 Preparation of DNA-free RNA

RNA extracted as described previously (section 2.7.4) was found to be still contaminated with DNA despite on-column DNase treatment, and was therefore unsuitable for use in co-transcription and gene expression assays (section 2.9.2). Prior to such use, RNA samples were treated with Promega RQ1 RNase-Free DNase according to the manufacturer's instructions, using 1 unit of RQ1 RNase-Free DNase per reaction.

To clean up this RNA and further reduce the presence of DNA before use in RT-PCR (reverse transcription polymerase chain reaction; 2.9.2), the manufacturer's instructions for RNA Cleanup with the QIAGEN RNeasy Kit were followed, including the instructions for an On-Column DNase Digestion (the optional 1-minute centrifugation to dry the membrane of ethanol prior to elution of RNA was included, and the final elution performed with 30 μL nuclease-free water which was then re-applied to the column and re-collected in order to increase the concentration of RNA obtained).

2.9.2 Synthesis of complementary DNA by reverse transcription polymerase chain reaction

Complementary DNA (cDNA) was amplified from total RNA extracted and prepared as described previously (section 2.7.4; section 2.9.1). First-strand cDNA was synthesized using the relevant gene-specific primer with the Invitrogen SuperScript IV First-Strand Synthesis System for RT-PCR (ThermoFisher Scientific) according to the manufacturer's instructions for reverse transcription with a gene-specific primer. The optional steps for removing RNA prior to PCR with RNase H were followed.

At step 1, two identical reaction mixes were set up for each sample. At step 2, preparation of RT reaction mix, a duplicate 'RT-' mix was prepared without Reverse Transcriptase enzyme (volume increased as appropriate); the RT reaction mix was added to one tube for each sample, and the 'RT-' reaction mix to the other. This allowed confirmation that any subsequent amplification by PCR was of cDNA rather than gDNA already present.

After synthesis the presence and quantity of cDNA was checked (section 2.7.1) and then amplified directly by PCR (section 2.8).

2.10 Analysis of DNA by gel electrophoresis

DNA was separated and visualized via gel electrophoresis. Gels were prepared from agarose powder to a concentration of 1% w/v, or 0.9% w/v if fragments larger than approximately 1.5 kb were to be separated, in TBE Buffer (Tris-Borate-EDTA; 5x stock solution: 54 g L⁻¹ Tris base; 27.5 g L⁻¹ boric acid; 0.01 M EDTA (to pH 8.0 with HCl); to pH 8.3 with HCl; diluted to 1x prior to use). The agarose was dissolved in an 800 W microwave for 150 seconds, allowed to cool until bubbles no longer formed on swirling, and poured into a casting tray. Ethidium bromide was then added to a concentration of 0.002% v/v. The gel was left to set for 1 hour before loading of DNA samples.

DNA samples were mixed with the appropriate volume of Bioline 5x DNA Loading Buffer before loading into wells. An appropriate Bioline DNA ladder (either HyperLadder 1kb, HyperLadder 50bp or HyperLadder 100bp) was also loaded directly to facilitate approximation of sample band sizes. A 75 V current was then applied along the gel for 45 to 90 minutes, depending on the degree of separation required. The DNA was visualized in a Syngene U:Genius3 at 302 nm. If necessary, bands were cut out using the method described in section 2.11.4.

2.11 Preparation and analysis of plasmids

2.11.1 Selection of restriction enzymes for plasmid construction

Selection of appropriate restriction enzymes for the preparation of plasmids for genetic manipulation of *R. palustris* was done with the aid of NEBcutter V2.0 ([74]; <http://nc2.neb.com/NEBcutter2/>).

2.11.2 Creation of heterologous DNA sequences for insertion into *R. palustris*

Heterologous DNA sequences for insertion into the genome of *R. palustris* were acquired as described in Chapter 5, codon-optimized manually and then synthesized by Invitrogen GeneArt (ThermoFisher Scientific).

2.11.3 Digestion of DNA by restriction enzyme

DNA was digested by restriction enzyme for insertion into plasmids intended for genetic manipulation, and to check the digestion pattern of plasmid DNA extracted from *E. coli* (section 2.6.3). The restriction enzymes were supplied by New England Biolabs (NEB) and used in conjunction with the NEB CutSmart Buffer. The reaction mix was as follows: 5 μ L template DNA; 1 μ L each restriction enzyme; 3 μ L CutSmart Buffer; to 30 μ L with water. The reaction mix was incubated at 37°C for 1 hour before separation and visualization by gel electrophoresis (section 2.10).

2.11.4 Purification of DNA from PCR product or agarose gel

DNA was purified prior to digestion by restriction enzyme (section 2.11.3) or ligation (section 2.11.5), whether from PCR reaction mix after amplification (section 2.9) or from agarose gel after separation and visualization of products (section 2.10). The MO BIO Laboratories UltraClean 15 DNA Purification Kit was used as follows:

1. If purifying PCR product directly, the reaction mix was transferred to a 1.5 mL microcentrifuge tube and 3 volumes Ultra Salt solution added.
2. If purifying from an agarose gel, the target fragment was cut out from the gel (with a minimum amount of surrounding agarose gel), transferred to a 1.5 mL microcentrifuge tube containing 300 μ L Ultra Salt solution and 30 μ L Ultra Melt solution, and then incubated at 55°C for 2 minutes (a longer incubation time was used as necessary to ensure the gel had completely melted before proceeding).

3. Glass milk (stored at 4°C and vortexed well before use) was added to the sample (5 μ L + 1 μ L per μ g DNA).
4. The tube was shaken to mix the sample, which was then incubated at room temperature for 5 minutes with occasional shaking.
5. The sample was centrifuged at 14000*g* for 1 minute and the supernatant discarded.
6. 1 mL Ultra Wash solution (including supplemental ethanol) was added to the sample.
7. The sample was vortexed to re-suspend the pellet.
8. The sample was centrifuged at 14000*g* for 1 minute and the supernatant discarded.
9. The sample was centrifuged at 14000*g* for a further 30 seconds and as much remaining supernatant as possible discarded with a fine pipette tip.
10. 15 μ L water was added to the sample, which was vortexed to re-suspend the pellet.
11. The sample was incubated for no more than 5 minutes before centrifugation at 14000*g* for 2 minutes. The supernatant was then either transferred to a new 0.5 mL microcentrifuge tube for storage or used directly.

2.11.5 Ligation of restriction enzyme-digested DNA

DNA fragments generated by restriction enzyme digestion (section 2.11.3) and purified as described (section 2.11.4) were ligated with NEB T4 DNA Ligase. The reaction mix was as follows: 12 μ L insert fragment; 5 μ L plasmid fragment; 2 μ L 10x T4 DNA Ligase Buffer; 1 μ L T4 DNA Ligase; to 20 μ L with water if required. The reaction mix was incubated at room temperature for 1 hour or, for more successful ligation, at 4°C overnight. Ligation products were then introduced into *E. coli* by transformation (section 2.6).

2.12 Sequencing of DNA fragments

All DNA sequencing was performed on an Applied Biosystems 3730xl DNA Analyser in the DNA Sequencing Facility, Department of Biochemistry, University of Cambridge. PCR products were sequenced after purification as described (section 2.11.4) using primers used in the PCR amplification. DNA purified from gels as described (section 2.11.4) was sequenced using primers used in the initial PCR amplification of the fragment being sequenced. Plasmid DNA was sequenced directly after preparation using primers used in the initial PCR amplifications used to produce one or more of the sections of interest of the plasmid.

2.13 Transformation of *R. palustris* by electroporation

R. palustris was genetically modified by electroporation with plasmid DNA based on the pKmob-sacB vector [3]. This plasmid facilitates the integration of designed nucleotide sequences into the genome of the target host, eventually resulting in an unmarked strain through a process involving two homologous recombination events; this process is described in detail in Chapter 4.

2.13.1 Preparation of competent *R. palustris* cells

Cells were prepared for electroporation (section 2.13.2) as follows (kept on ice throughout):

1. 10% v/v glycerol solution (filter sterilized) and sufficient 1 mm electroporation cuvettes were chilled on ice.
2. 50 mL fresh Super Optimal Broth with Catabolite repression (SOC) was prepared as described in Table 2.7 and warmed at 30°C.
3. 200 mL YP medium was inoculated with fresh cells and the OD₆₆₀ monitored until it reached approximately 0.3.
4. The culture was split into four 50 mL centrifuge tubes.
5. The cells were harvested by centrifugation at 1800*g* at 4°C for 10 minutes and the supernatant discarded.
6. Each pellet was re-suspended in 10 mL glycerol solution (20% starting culture volume).

Component	Stock Solution	Amount	Concentration
Tryptone	-	1 g	2% w/v
Yeast Extract	-	0.25 g	0.5% w/v
NaCl (1 M stock)	5.84 g anhydrous in 100 mL	0.5 mL	10 mM
KCl (1 M stock)	3.72 g anhydrous in 50 mL	0.125 mL	2.5 mM
MgCl ₂ (1 M stock)	20.331 g (6H ₂ O) in 100 mL	0.5 mL	10 mM
MgSO ₄ (1 M stock)	24.08 g (7H ₂ O) in 100 mL	0.5 mL	10 mM
Glucose	-	0.180 g	20 mM

Made up in Milli-Q water to 50 mL. Adjusted pH to 7.0 (6.8 – 7.0 acceptable) with NaOH. Filter sterilized; must be made fresh.

Table 2.7: Recipe for SOC (Super Optimal broth with Catabolite repression) used for electroporation of *R. palustris*.

7. The cells were harvested by centrifugation at 1800*g* at 4°C for 10 minutes and the supernatant discarded.
8. Each pellet was re-suspended in 0.5 mL glycerol solution (1% starting culture volume), and suspensions were combined into pairs and transferred to 2 mL microcentrifuge tubes for a total volume of 1 mL in each tube.
9. The cells were harvested by centrifugation at 14000*g* at 4°C for 2 minutes and the supernatant discarded.
10. Each pellet was re-suspended in 1 mL glycerol solution (1% starting culture volume).
11. The cells were harvested by centrifugation at 14000*g* at 4°C for 2 minutes and the supernatant discarded.
12. Both pellets were re-suspended together in a total volume of 0.2 mL glycerol solution (0.1% starting culture volume) and used immediately for electroporation.

2.13.2 Electroporation of *R. palustris*

Competent cells of *R. palustris* prepared as described previously (section 2.13.1) were transformed as follows (further details are given in Chapter 4):

1. 250 ng plasmid DNA was added to a 1.5 mL microcentrifuge tube.
2. 50 μ L competent cells were added and mixed gently.
3. The suspension was transferred to a chilled 1 mm electroporation cuvette, ensuring no bubbles were present.
4. A 2.0 kV, 800 Ω , 25 μ F pulse was applied to the cuvette (settings determined in Chapter 4).
5. The cells were immediately re-suspended in 1 mL SOC and then transferred to a 2 mL microcentrifuge tube.
6. The cells were incubated at 37°C with shaking for 90 minutes.
7. The suspension was spread onto YP medium agar plates containing 100 μ g mL⁻¹ kanamycin, which were then incubated at 30°C and observed over several days until colonies appeared.

8. Several colonies were selected and streaked onto fresh YP medium/kanamycin agar plates to facilitate testing by colony PCR (section 2.9.3).

2.13.3 Generation of unmarked transformant strains of *R. palustris*

After the successful generation of a marked transformant strain (section 2.13.3) of *R. palustris*, a sample of cells from the strain was used to inoculate 15 mL YP medium. This culture was then incubated at 30°C for 2 days with no selection pressure to allow a second homologous recombination event to occur, removing the selectable markers from the genome. The culture was then spread onto YP medium agar plates containing 10% w/v sucrose, which were incubated at 30°C and observed over several days until colonies appeared. Several colonies were then selected and streaked onto fresh YP medium agar plates to facilitate testing by colony PCR (section 2.9.3).

2.14 Assay for cellular levels of glycogen

Cultures of *R. palustris* were assayed to compare the levels of cellular glycogen between strains as follows. The protocol used is a modification of that described by [75]:

1. Cells from 15 mL mid-log culture ($OD_{660} = 0.3$) were harvested by centrifugation at 1800g at 4°C for 10 minutes and the supernatant discarded.
2. The cells were re-suspended in 1 mL YP medium and transferred to a 1.5 mL microcentrifuge tube.
3. The cells were incubated overnight at -80°C, without first snap-freezing.
4. The cells were left to defrost fully on ice.
5. The cells were harvested by centrifugation at 14000g for 5 minutes and the supernatant discarded.
6. The cells were re-suspended in 1 mL TE Buffer (pH 8.0) with Ready-Lyse Lysozyme Solution (2500 units; Epicentre) and incubated at room temperature for 15 minutes.
7. The cells were harvested by centrifugation at 14000g for 5 minutes and the supernatant discarded.

8. The cells were re-suspended in 400 μL phosphate-buffered saline (PBS; prepared from Sigma-Aldrich 10x concentrate by 10-fold dilution in sterile Milli-Q water).
9. 200 μL acid-washed 425 – 600 μm glass beads were added to the tube.
10. The sample was vortexed 5 times, each for 1 minute, with incubation on ice for 1 minute between.
11. The beads and cells were sedimented by centrifugation at 14000*g* for 5 minutes and 200 μL supernatant retained using a gel-loading tip.
12. 10 μL concentrated sulfuric acid was added to the sample.
13. The sample was incubated in a boiling water bath for 10 minutes.
14. 20 μL 5 M sodium hydroxide was added to halt the reaction.
15. 1 mL *ortho*-toluidine was added to the sample.
16. The sample was incubated in a boiling water bath for 10 minutes.
17. The sample was incubated on ice for 3 minutes.
18. The absorbance was measured at 635 nm against a blank sample of PBS also treated with *ortho*-toluidine in the same manner.

2.15 Assay for cellular levels of polyhydroxybutyrate

Cultures of *R. palustris* were assayed to compare the levels of cellular polyhydroxybutyrate (PHB) between strains, using a modification of the protocol described by [75]. A stock solution of Nile Red was prepared (1 mg mL⁻¹ in absolute ethanol) and stored at -4°C in the dark. A working solution was prepared by dilution in absolute ethanol to 1 $\mu\text{g mL}^{-1}$.

1. Cells from 5 mL mid-log culture (OD₆₆₀ = 0.3) were harvested by centrifugation at 1800*g* at 4°C for 10 minutes and the supernatant discarded.
2. The cells were washed with 2 mL PBS (prepared from Sigma-Aldrich 10x concentrate by 10-fold dilution in sterile Milli-Q water).

3. The cells were harvested by centrifugation at 1800*g* at 4°C for 10 minutes and the supernatant discarded.
4. The cells were re-suspended in 1 mL PBS.
5. Six 162 μ L samples were taken from each strain and transferred into sequential wells of a 96-well black polypropylene microplate (Greiner Bio-One); six samples of PBS were also included as a negative control.
6. Nile Red solution (18 μ L) was added in the dark to a final concentration of 0.1 μ g mL⁻¹ to three of the six samples for each strain, including the blank PBS samples.
7. Absolute ethanol (18 μ L) was added to the remaining three samples for each strain, including the blank PBS samples, as a negative control.
8. Samples were incubated for 30 minutes in the dark.
9. Fluorescence was measured with a Fluostar Optima microplate reader with an excitation wavelength of 510 nm and an emission wavelength of 590 nm.

The ethanol control samples were included because some fluorescence is detected even in samples without Nile Red, and even sterile PBS will increase in fluorescence on addition of Nile Red. Therefore for each set of three test samples and the PBS-only control samples, the mean fluorescence of the three equivalent ethanol control samples was subtracted from the mean measured fluorescence. The resulting value for the PBS control samples was then subtracted from the resulting values for each set of test samples. The final value is in arbitrary units.

2.16 Measurement of gaseous output volume

The volume of gas produced by cultures of *R. palustris* was measured under water: the culture bottles required are described in detail in Chapter 3. A measuring cylinder with a notch cut into the rim was submerged in a container of water. A tube was attached to the syringe filter of the gas out-port of the bottle and in turn connected to a glass tube, shape modified for the purpose, which was then inserted into the measuring cylinder. The cylinder was then carefully inverted so that it was balanced upside-down in the water, with the glass tube passing inside through the notch in the rim, while remaining full of water. Any gas produced by the culture would then displace the water, allowing the volume to be measured on the cylinder. This is illustrated in Figure 2.1.



Figure 2.1: Photographic illustration of the gas collection apparatus.

2.17 Genome sequences

Nucleotide sequences of *R. palustris* genes were obtained from NCBI (no longer available here) or CyanoBase, from which they are still available at the time of writing at the old version of the database (<http://genome.annotation.jp/cyanobase>).

2.18 Statistical analysis and figure creation

Data were recorded and managed using Microsoft Excel. Statistical analysis was carried out using the program R in conjunction with the graphical user interface R commander. Graphs were produced with MATLAB or Microsoft Excel and schematic diagrams were produced using Adobe Illustrator. Plasmid maps were created using SnapGene Viewer and BioEdit was used for sequence alignment. This document was created in LyX with the {panther} package.

3 Cultivation of *Rhodospseudomonas palustris*

3.1 Introduction

3.1.1 Overview

Several unique requirements for the effective cultivation of *R. palustris* made necessary the design of a dedicated ‘cultivation cabinet’. Firstly, *R. palustris* absorbs light for photosynthesis not only from the visible spectrum, but also from wavelengths extending into both the infrared and ultraviolet regions. This is illustrated by the absorption spectrum of *R. palustris* in suspension reported by Brotosudarmo *et al.* in 2011 ([2], Figure 3.1). Standard incubators employ fluorescent bulbs specifically optimized to convert as much energy input into visible light output as possible. They therefore emit very minimal amounts of light outside of this region (400 – 700 nm). A lighting setup better optimized to this species was therefore desirable.

Secondly, it was necessary for any proposed setup to be suitable for the measurement, collection and analysis of the gaseous output of the cells in culture, as this would be vital for any experimentation on hydrogen output or production of other gases of interest. The measurement of gas volumes takes place under water, by recording the volume of water displaced from an inverted measuring cylinder. Most incubators mix cultures by shaking, but the unstable nature of the cylinders themselves coupled with the presence of open containers of water makes this approach completely unsuitable. It was therefore proposed to design an incubator which mixed by stirring instead.

A cultivation cabinet designed to hold six 1 L cultures at a time was therefore assembled to meet these needs; the design process and specifications are described in the following pages. Subsequently, experiments were conducted to compare the growth rate of *R. palustris* in this cultivation cabinet with that in a conventional incubator, to establish whether or not the cultivation cabinet enabled more rapid growth of *R. palustris*. In addition, advantage was taken of the lighting setup in order to assess the effect of light spectrum on the growth of *R. palustris*. For research and development purposes, knowing how to achieve rapid growth is beneficial, and for industrial purposes it is vital to be able to cultivate the bacterium optimally for the desired application without any unnecessary expense. Illumination is often a prohibitive expense for biological industrial processes, so any measures which could reduce these costs are of great interest.

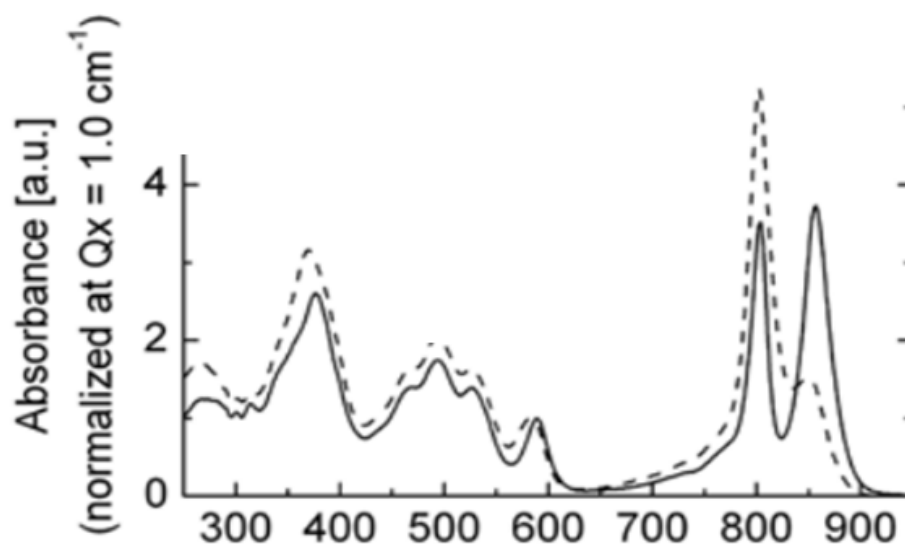


Figure 3.1: Taken from Figure 3, Panel A of Brotosudarmo *et al.* 2011 [2]; the absorption spectrum of *Rhodospseudomonas palustris* in suspension under high light (continuous line) and low light (dashed line), at room temperature. The x-axis displays wavelength in nm.

3.1.2 Design of the cultivation cabinet lighting provision

It was decided that LEDs (light-emitting diodes) would be used to provide illumination, as this would allow an entirely custom spectrum of wavelengths to be designed. The fine control provided by individual power packs would also allow the light intensity of each wavelength to be controlled independently, and the lighting would be highly consistent across cultures. Although LEDs are optimized to emit at specific wavelengths, this is impossible in practice and they actually provide a (tightly concentrated) spectrum of light around the specification wavelength, making them suitable for cultivation purposes.

LEDs of five wavelengths were therefore chosen to correspond to each of the five main peaks identifiable in the absorption spectrum shown in Figure 3.1; the targeted wavelengths are listed in Table 3.1. Where these wavelengths do not correspond exactly to the peaks visible on the spectrum, the spectral halfwidth of the LED should ensure coverage of the peak (for example the peak at approximately 800 nm is covered by the LED of wavelength 830 nm with spectral halfwidth 55 nm). This should also ensure reasonable coverage across the absorption spectrum, though the ultraviolet LED (390 nm) has a very concentrated emission spectrum. A sixth wavelength was included corresponding to the trough at approximately 650 nm, both to increase continuity across the range and also to allow experimental verification that this wavelength is unnecessary to the growth of *R.*

Target Wavelength / nm	LED Wavelength / nm	Spectral Halfwidth / nm	Angle of Radiance / °	Model Reference
380	390	5	30	UV5TZ-390-30
490	501	30	30	HLMP-CE34-Y1CDD
590	594	13	30	HLMP-EL3B-WXKDV
650	634	14	30	HLMP-EL3B-WXKDV
800	830	55	30	TSHG5510
860	860	30	30	SFH 4557

Table 3.1: Technical specifications of the LEDs used in the cultivation cabinet. Target Wavelength is the approximate wavelength of the peak or region on the absorption spectrum of Figure 3.1 targeted for coverage by the relevant LED. LED Wavelength indicates the highest intensity wavelength emitted by the selected LED. Spectral Halfwidth is the width at which the spectrum emitted by the LED falls to half intensity and therefore indicates the spread of the emitted spectrum. Angle of Radiance is the angle traversed by the emitted cone of light. Model Reference is the model number of the LED.

palustris. The technical specifications of these six LEDs can be found in Table 3.1.

Six separate circuit boards of LEDs were produced; one for each culture. All LEDs of each particular wavelength were connected to the same voltage source. This should ensure that the intensity of each wavelength will be consistent across cultures. Powering each wavelength from separate voltage sources allowed independent control of each wavelength. In practice, this required the LEDs on each circuit board to be clustered by wavelength rather than distributed evenly across the area, as the circuit board wiring would otherwise have been unmanageably complex. Fifteen LEDs of each wavelength were included on each of the six circuit boards. They were spaced so as to provide continuous coverage across the area, whilst being far enough apart to avoid overheating. The area of illumination covered the entire cross-sectional area of a 1 L culture flask. The wiring diagram for the circuit boards was designed by Paolo Bombelli, and the boards were produced by the Electronics Workshop of the School of Biological Sciences, University of Cambridge.

3.1.3 Design of the cultivation cabinet mixing and support structures

The apparatus required for the measurement of gaseous output by *R. palustris* prohibited the use of shaking for the mixing of cultures. It was therefore decided that stirring by magnetic flea would be a suitable alternative. A magnetic multi-stirrer was acquired for this purpose, chosen based on its ability to stir six solutions simultaneously, and for the strength of the magnetic field. The need to provide lighting across the whole cross-sectional area of the culture flasks required that the LED

circuit boards be positioned directly beneath the flasks. Thus, a platform to hold the flasks above the delicate LED circuit boards was also necessary. Both of these components would act to raise the culture flasks away from the multi-stirrer, and it must therefore be able to spin the magnetic fleas even at a distance of 25 mm. A Cimarec Multipoint 6 Stirrer was chosen. Continuous stirring was then achievable with a 50 x 20 mm oval magnetic flea in a flask holding 1 L of medium.

The support platform for the culture flasks was designed to maximize transmission of light. Transparent PVC (poly[vinyl chloride]) was used as the material, but on testing the absorption in a spectrophotometer it was found to absorb ultraviolet light particularly strongly. The design of the panel was therefore altered to include individual laser-cut holes corresponding to the locations of each individual LED. The LEDs were spaced such that this did not compromise the structural integrity of the platform. The schematic for the support platform was created by Paolo Bombelli and can be seen in Appendix A, and it was produced by Engineering and Design Plastics Ltd. It was subsequently drilled to allow each LED circuit board to be bolted into place beneath the platform, and to allow the addition of sixteen non-tapered screws (25mm) to hold the platform above the multi-stirrer. The overall configuration of the cultivation platform is shown in Figure 3.2.

The glass of the culture flasks was also anticipated to block ultraviolet light. The absorption of the flasks was therefore tested in a spectrophotometer and, although some ultraviolet light was absorbed, the majority was transmitted. This was deemed to be acceptable but it should be noted that the intensity of ultraviolet light experienced by the bacteria in the following experiments was reduced slightly in this way.

The entire cultivation platform was surrounded by a cabinet to reduce the effects of ambient light on growth, and situated in a room kept dark at most times. The design for the cabinet was modified from a pre-existing design supplied by Paolo Bombelli, and the cabinet was produced by Engineering and Design Plastics Ltd. The LED circuit boards, power supply and support platform were then assembled and connected within the cabinet on top of the multi-stirrer.

The spreading of the light as it travels through the culture is expected to result in a broad spectrum of light being available at most depths in the culture, but in addition the speed of mixing should ensure that individual cells at any depth are exposed to all wavelengths within a minimal period of time.

To allow the culture flasks to be sparged with gas once inoculated and sealed, and to allow samples of culture to be taken from anaerobic cultures without introducing oxygen, specific bottle caps

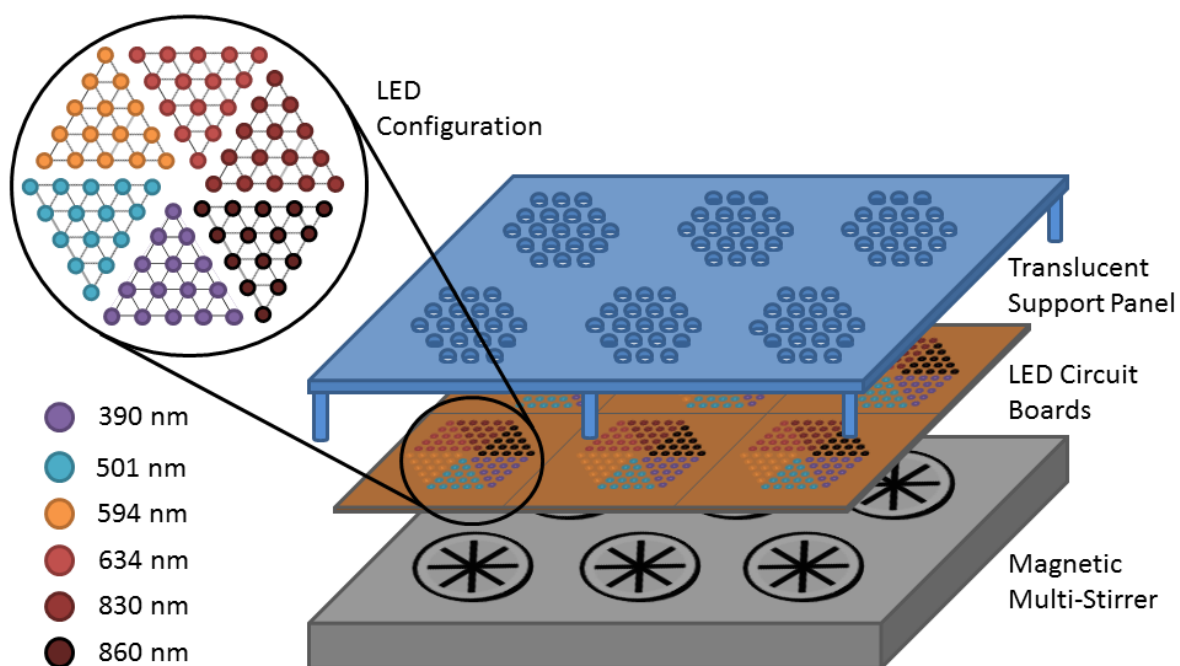


Figure 3.2: Pictorial representation of the cultivation platform, not to scale. The Magnetic Multi-Stirrer, LED Circuit Boards, and Support Panel are shown. The surrounding cabinet is not shown.

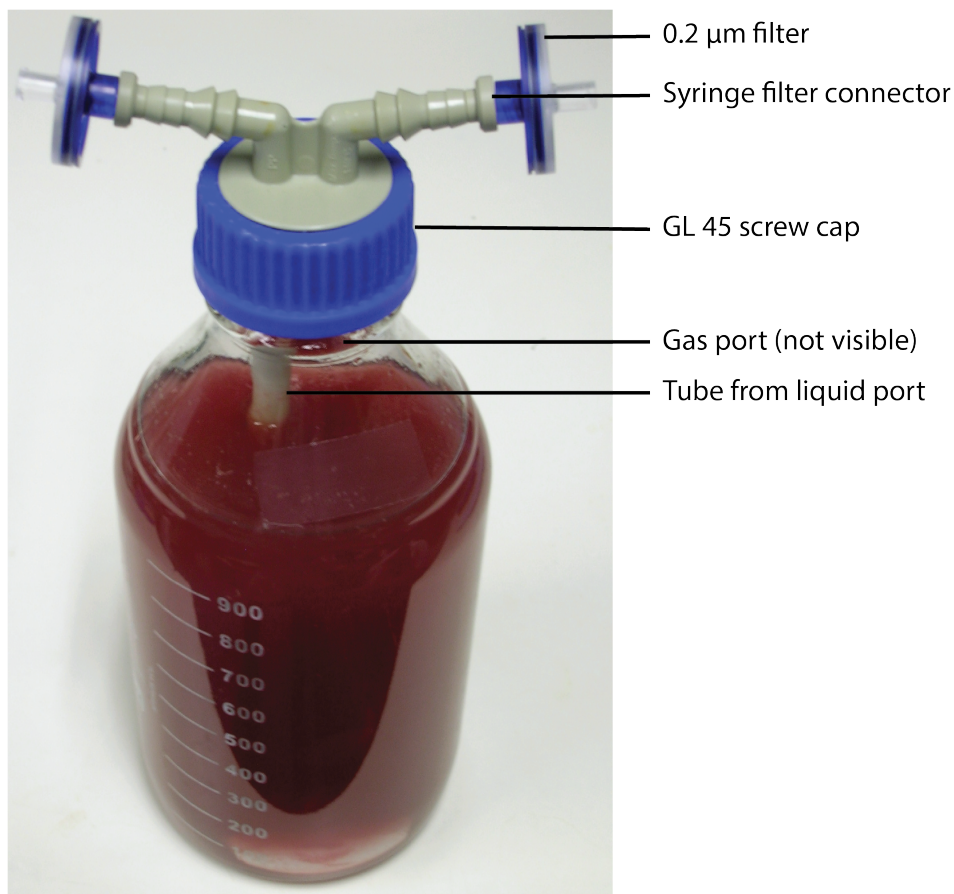


Figure 3.3: Photographic illustration of the bottle caps and associated accessories.

had to be used. A photograph is shown in Figure 3.3. The Schott-Duran GL 45 screw caps with two hose connections were used. These were then each attached to a Syringe Filter Connector (Schott-Duran, catalogue number 1129829, female Luer Slip to 5.8 mm male connector, with O-ring seal), allowing a syringe to be inserted for sample collection. When not being used for sample collection, a Minisart 0.2 µm filter was attached to both ports via the connectors, before sealing the openings with foil and electrical tape. This should ensure that the culture is not contaminated even if a small amount of air leakage is able to occur.

Inside the culture flask, one port attached to a Portex tube (internal diameter 8mm), the other end of which sat within the culture (the 'liquid port'). This is the port used to extract liquid samples with a syringe. When sparging the cultures with gas, the gas supply is connected by a Portex tube via the Minisart filter to the liquid port. Thus the gas is bubbled through the liquid, and the increased pressure forces gas from the headspace out through the other 'gas port' and filter.

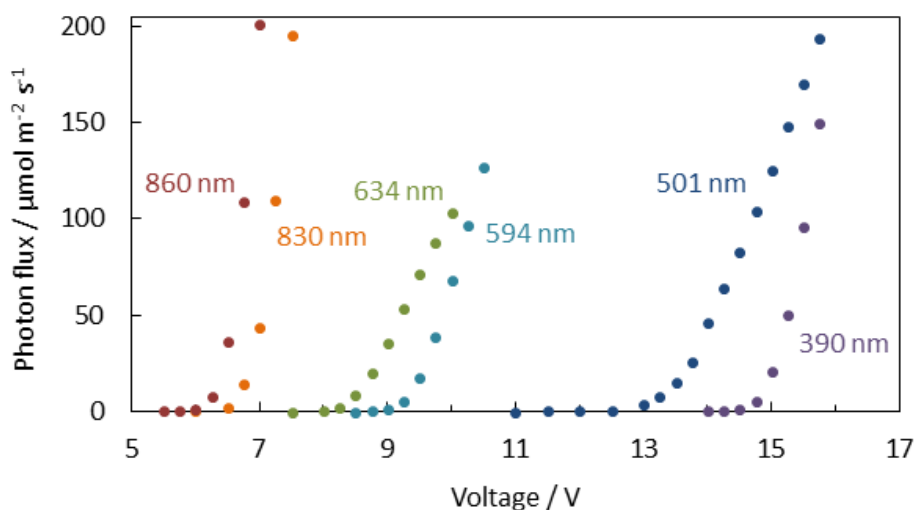


Figure 3.4: Calibration curves for LEDs of each wavelength used in the cultivation cabinet.

3.1.4 Calibration of the cultivation cabinet lighting

Finally, the LED circuit boards were calibrated after assembly of the cultivation cabinet to enable exact control of the light intensity. One circuit board was tested for the initial calibration. For each set of LEDs of particular wavelength, the voltage supplied was increased until a response was recorded on a light meter held fixed in place on a support 30 mm above the surface of the support panel. The voltage was then increased in increments of 0.25 V. For each measurement, the reading on the light meter was allowed to stabilize before recording. The voltage was increased until the light intensity stopped increasing in a linear fashion (indicating the limit of the intensity and potential for damage to the LEDs) or reached $200 \mu\text{mol photons m}^{-2} \text{s}^{-1}$. The results are shown in Figure 3.4. As expected, the smaller the wavelength, the higher the voltage required for a given intensity; LEDs of lower wavelength experience a greater voltage drop, requiring more voltage to operate at the appropriate current.

The measurements from the light meter were converted from irradiance (W cm^{-2}) into photon flux ($\mu\text{mol m}^{-2} \text{s}^{-1}$) and plotted against voltage to create calibration curves for each LED. The portions of each curve lying over the region of interest (from approximately 10 to $60 \mu\text{mol m}^{-2} \text{s}^{-1}$) were identified by eye and fitted with an appropriate line of best fit by Microsoft Excel (second-order polynomials were required for the 830 and 860 nm curves). The equations were then reversed to provide the voltage required for a particular desired light intensity. The lines of best fit and conversion equations are provided in Table 3.2. The power packs were set to provide $40 \mu\text{mol m}^{-2} \text{s}^{-1}$ from

LED Wavelength / nm	Calibration Curve	Intensity Conversion Equation
380	$y = 209.61x - 3149.7$	$V = \frac{P+3149.7}{209.61}$
490	$y = 87.529x - 1185.9$	$V = \frac{P+1185.9}{87.529}$
590	$y = 116.8x - 1100$	$V = \frac{P+1100}{116.8}$
650	$y = 67.44x - 570.33$	$V = \frac{P+570.33}{67.44}$
800	$y = 158.66x^2 - 1996.2x + 6243$	$V = \frac{2((15865P+575166)^{1/2}+9981)}{3173}$
860	$y = 261.53x^2 - 3195.9x + 9761.4$	$V = \frac{(2615300P+5452605)^{1/2}+159795}{26153}$

Table 3.2: Lines of best fit (Calibration Curve) and conversion equations for the LED calibration curves: V indicates the voltage (V) that should be supplied to produce photon flux P ($\mu\text{mol m}^{-2} \text{s}^{-1}$).

each set of LEDs. At this point, the remaining five LED circuit boards were also checked at each wavelength to ensure that their light intensities were consistent with each other.

3.2 Chapter Aims

Having designed and constructed the cultivation cabinet above, the remaining aims of this section of the work were to establish whether the cultivation cabinet allowed faster growth of *R. palustris* and optimal conditions for this by:

1. Comparing the growth of *R. palustris* on the cultivation cabinet with that in a standard commercial incubator.
2. Comparing the growth of *R. palustris* under semi-aerobic and under anaerobic conditions.
3. Comparing the growth of *R. palustris* under different lighting conditions, namely: without infrared light, without ultraviolet light, with only visible light, and with no light from the 634 nm LED.

In addition, the absorbance spectra of *R. palustris* cultures grown under the different lighting environments described under (3) were measured to assess the effects of these lighting environments on the light-harvesting complexes of *R. palustris*.

3.3 Results

For all of the following growth curves, minimal medium was inoculated to $OD_{660} = 0.06$ with log-phase *R. palustris* ($OD_{660} = 0.3$) grown under natural sunlight. The optical density was then measured until either OD_{660} was observed to surpass 1 or 28 days of observation elapsed without reaching this point. The optical density measured at this wavelength has previously been demonstrated to be a suitable proxy for the cell concentration [40]. Unless otherwise stated, cultures were sparged with argon gas post-inoculation to initiate an anaerobic atmosphere and were grown on the cultivation cabinet previously described under a light intensity of $40 \mu\text{mol m}^{-2}\text{s}^{-1}$ and stirred at 200 rpm.

3.3.1 Comparison between *R. palustris* growth on cultivation cabinet and incubator

To test whether or not the cultivation cabinet facilitates more rapid growth of *R. palustris* than a standard commercial incubator, growth of the wild-type was compared between the cultivation cabinet and an INFORS incubator. Those cultures in the incubator were shaken at 120 rpm and illuminated from above by fluorescent tube; the intensity by the top of the culture flasks was measured to be approximately $50 \mu\text{mol m}^{-2} \text{s}^{-1}$. The temperature within the incubator was kept at the standard operating temperature of 30°C , while the temperature in the cultivation cabinet was recorded directly on the support platform and found to remain at a consistent temperature of 34°C . The results taken from three replicates on each platform are shown in Figure 3.5. In contrast to the other experiments presented in this work, this experiment and the next were conducted only until the OD_{660} of the cultures on the cultivation cabinet exceeded 1, as growth in the incubator was only of interest for the purposes of comparison with the cultivation cabinet.

These results show that growth of *R. palustris* was considerably slower in the INFORS incubator than in the cultivation cabinet. A t-test comparing the final optical densities at time $t = 267$ hours returned a statistically significant difference between the two conditions ($p < 0.01$). A lag time was observed in the INFORS incubator over the first 24 hours where no increase in optical density was measured. This was possibly due to the cells adjusting their light-harvesting machinery in response to a different spectrum of light. Subsequently the growth rate in the INFORS incubator remained low; the difference in final optical density was not purely a result of the slow initial growth. This suggests that the cultivation cabinet provides a greatly superior environment for fast cultivation of *R. palustris*.

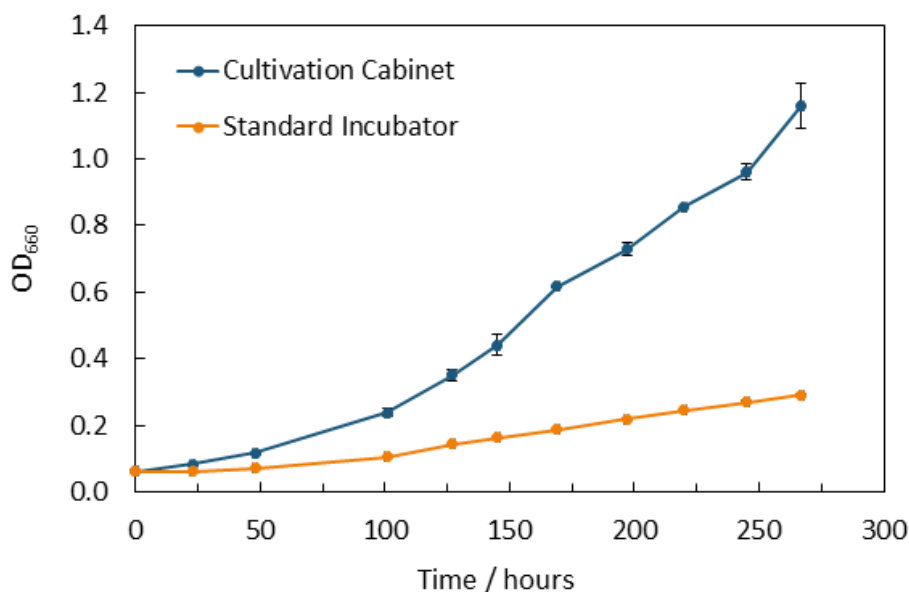


Figure 3.5: Optical density measured at 660 nm of wild-type *R. palustris* cultivated in the cultivation cabinet at 34°C (blue) and an INFORS incubator at 30°C (orange): mean of three replicates each; bars show standard error.

However, it is impossible to deduce from these results whether the increased growth rate observed was a result of the custom lighting provision or purely a result of the higher temperature, which can already be provided by standard commercial incubators. Therefore a second set of cultures were grown and measured in the INFORS incubator, under exactly the same conditions as previously but at 34°C, as the temperature at the base of the cultivation cabinet was measured to be. The results taken from three replicates are presented in Figure 3.6, contrasted with the data presented in Figure 3.5.

These results show that although the higher temperature within the INFORS incubator did confer a greater rate of growth, this was still considerably lower than the rate observed in the cultivation cabinet. A t-test comparing the final optical densities between the 30°C and 34°C conditions in the INFORS incubator returned a statistically significant difference ($p < 0.001$), as did a t-test comparing between the cultivation cabinet and the 34°C condition in the INFORS incubator ($p < 0.01$). The final measurement from the 34°C INFORS incubator was taken three hours earlier than the others, but this is unlikely to account for the difference. Furthermore, the 34°C temperature measured in the cultivation cabinet was taken from only a few centimetres away from the LEDs. Although there is limited airflow within the cabinet, it is likely that cells experience a slightly lower temperature

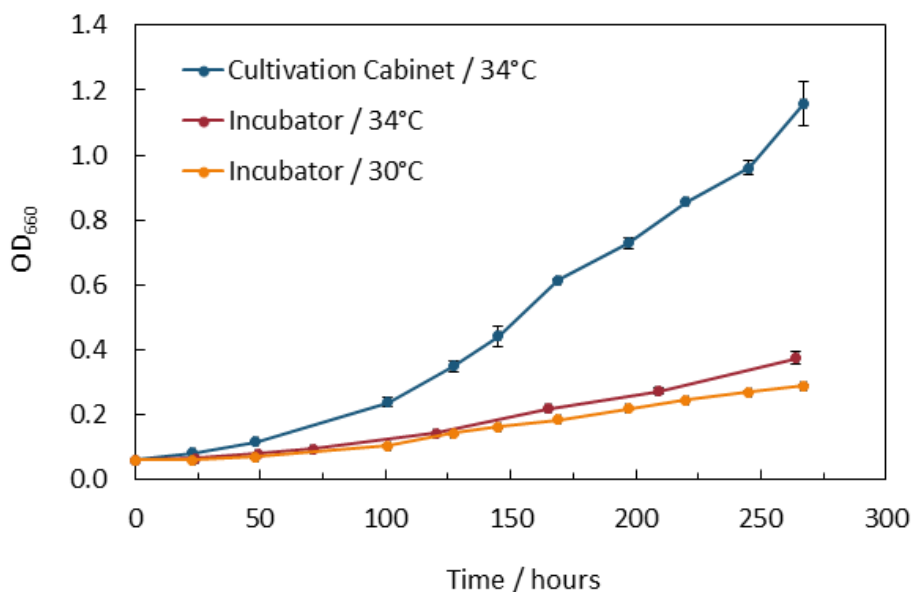


Figure 3.6: Optical density measured at 660 nm of wild-type *R. palustris* cultivated in the cultivation cabinet at 34°C (blue), an INFORS incubator at 34°C (red), and an INFORS incubator at 30°C (orange): mean of three replicates each; bars show standard error.

than this at the top of the culture flask. This indicates that temperature alone cannot account for the increased growth observed in the cultivation cabinet, and that the custom lighting provision is therefore probably responsible.

3.3.2 Comparison between *R. palustris* growth under anaerobic and ‘aerobic’ atmosphere

The growth of *R. palustris* under ‘aerobic’ and anaerobic conditions was compared on the cultivation cabinet. Although it was not possible to bubble air through cultures continuously on the cultivation cabinet, thereby maintaining a constant environment, the flasks of the cultures being subject to the ‘aerobic’ condition were opened and left to equilibrate with the atmosphere for 20 minutes every 24 hours. The pigmentation of the cultures suggested that, indeed, this was not enough to maintain a fully aerobic atmosphere [76], but cells were certainly subjected to higher levels of oxygen than otherwise. The results taken from these ‘aerobic’ cultures are presented in Figure 3.7, contrasted again with the data taken from *R. palustris* grown under anaerobic conditions presented in Figure 3.5.

These results indicate that growth was considerably slower under ‘aerobic’ than anaerobic conditions on the cultivation cabinet, taking just under twice as long to reach an OD₆₆₀ greater than 1

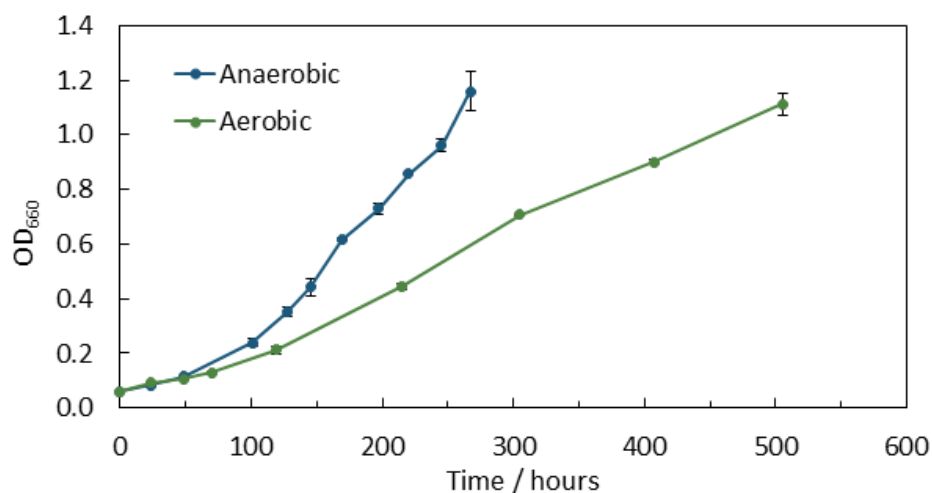


Figure 3.7: Optical density measured at 660 nm of wild-type *R. palustris* cultivated under an anaerobic (blue) and under an aerobic (green) atmosphere: mean of three replicates each; bars show standard error.

(note that this difference cannot be accounted for by a reduction in pigmentation, given the wavelength measured). This is as expected, as *R. palustris* is usually naturally found in anaerobic environments, and anaerobic growth has long been established as the faster method of cultivation for *R. palustris* [76, 77].

3.3.3 Comparison between *R. palustris* growth under different light spectra

The effects of the availability of different wavelengths of light on the growth of *R. palustris* were investigated, in order to inform our understanding of optimal conditions for *R. palustris* cultivation. Four different spectra of light, summarized in Table 3.3, were provided by different combinations of the six types of LED contained within the cultivation cabinet, and the same intensity of overall illumination was maintained by increasing the intensity of the remaining LEDs as appropriate. The spectra were chosen to investigate (a) the effects of infrared and ultraviolet light on growth and (b) whether the light provided by the 634 nm LED is necessary or beneficial to growth.

In addition, to provide further insight into the effects of wavelength availability on *R. palustris*, the absorbance spectra of the cultures were measured at the end of the cultivation period for the ‘No Infrared’ and ‘No Ultraviolet’ conditions, as well as the absorbance spectrum under standard conditions (all LEDs) for comparison. For each culture’s sample three sweeps were taken with the spectrophotometer as, particularly in the 400 nm region, interference from the cuvette itself intro-

Condition	390	501	594	634	830	860	Intensity Increase
1. No Infrared							50 %
2. No Ultraviolet							20 %
3. Visible Only							100 %
4. No 634 nm							20 %

Table 3.3: Summary of test conditions to which *R. palustris* was subjected for comparison of different light spectra. Active LEDs are indicated in green. ‘Intensity Increase’ indicates the amount the intensity of the active LEDs was increased by in order to compensate for the inactive LEDs.

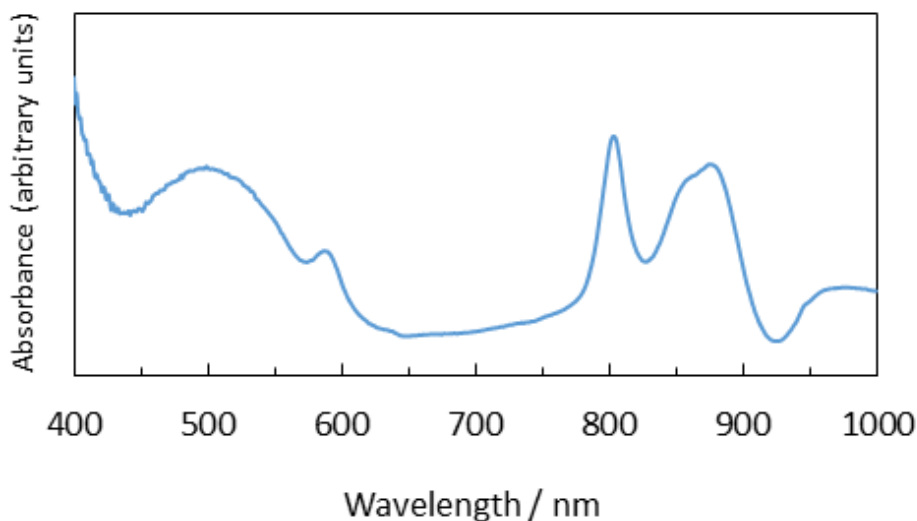


Figure 3.8: Absorbance in culture of wild-type *R. palustris* cultivated under standard conditions in the cultivation cabinet. Mean of two culture samples; three sweeps each.

duced a small amount of noise. The absorbance spectrum of *R. palustris* in culture under standard lighting (all LEDs) is shown in Figure 3.8, and can be compared with that shown in Figure 3.1 by Brotosudarmo *et al.*, in 2011 [2] (the range of wavelengths measured differs slightly). The most noticeable differences are that the three mini peaks around 500 nm are not visible in Figure 3.8, and that the peak around 860 nm seen in Figure 3.1 is much more broad in Figure 3.8, extending up towards 880 nm. Otherwise the overall distribution looks fairly similar.

The light provided by the LEDs was assumed to be the principal source of light for the cultures, as the cultivation cabinet was housed in a dark room, but it is inevitable that cells were subject to some external sources of light leaking through and around the edges of the translucent front panel when other work was being carried out in the room. However, as this light would be almost entirely from fluorescent room lighting rather than sunlight, it was assumed that very little infrared or ultraviolet light leaked into the cultivation cabinet. Cultures were again grown under anaerobic conditions.

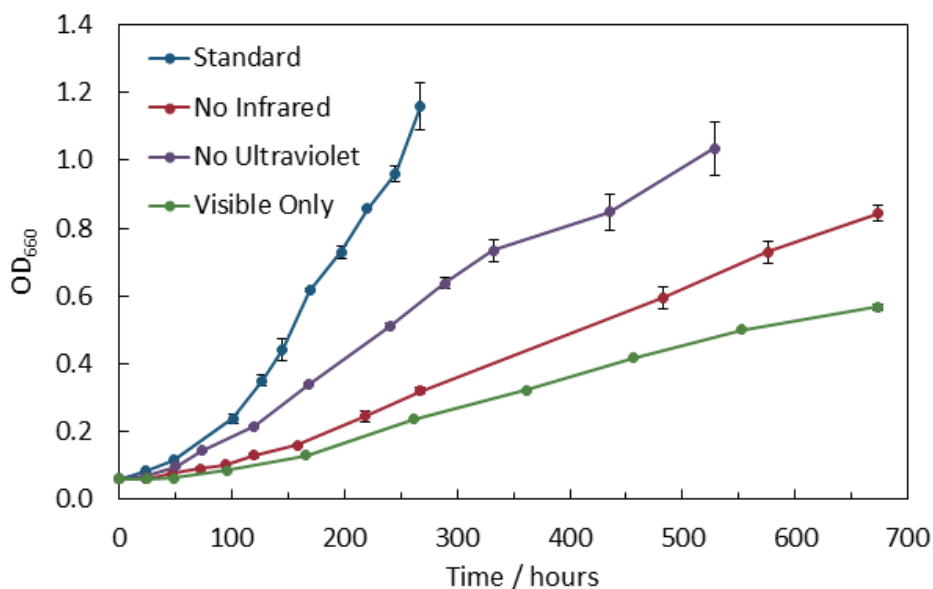


Figure 3.9: Optical density measured at 660 nm of wild-type *R. palustris* cultivated under standard lighting (all LEDs; blue), No Infrared (1; red), No Ultraviolet (2; purple), Visible Only (3; green): mean of three replicates each; bars show standard error.

The growth data from the first three spectra conditions are shown in Figure 3.9, contrasted with the data observed under standard lighting on the cultivation cabinet presented in Figure 3.5, and show that light spectrum had a considerable effect on the growth of *R. palustris*. When cultivated without infrared or without ultraviolet the growth rate was greatly reduced compared to standard conditions. In the absence of ultraviolet light, cultures took 22 days, twice as long, to exceed $OD_{660} = 1$. Measurement ceased after 28 days in the absence of infrared light, when cultures had only reached $OD_{660} = 0.843$, indicating that lack of infrared light reduced growth rate much more than a lack of ultraviolet light. The absence of both infrared and ultraviolet light had an even greater effect on the growth rate, though the effect does not appear to be additive. Cultures had reached $OD_{660} = 0.567$ after 28 days.

It should be noted that the temperature measured on the cultivation cabinet in the absence of infrared light was only 30°C, rather than 34°C as measured under all other conditions. However, the experiment conducted on temperature in the INFORS incubator (Figure 3.6) suggests that increasing the temperature to 34°C would confer only a small increase in growth rate, and that the difference observed in the absence of infrared light is therefore unlikely to be attributable only to temperature.

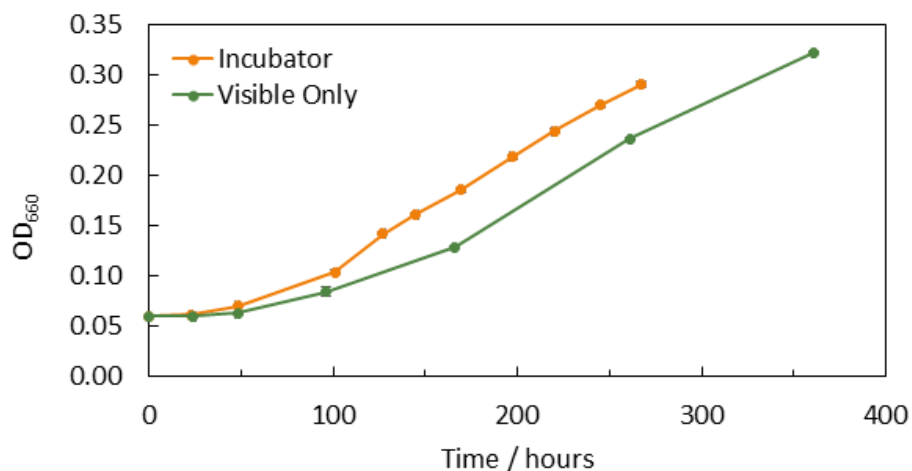


Figure 3.10: Optical density measured at 660 nm of wild-type *R. palustris* cultivated in an INFORS incubator at 30°C (orange) and in the cultivation cabinet with visible light at 30°C (green): mean of three replicates each; bars show standard error. For clarity the latter data are presented only up to time 361 hours.

Interestingly, the growth rate with visible light only was lower than that observed in the INFORS incubator (Figure 3.5). These data are presented together for clarity in Figure 3.10. This suggests that although the absence of infrared and ultraviolet light in the incubator restricted the growth of *R. palustris*, other aspects of the incubator environment compensated for the restriction somewhat in comparison with the cultivation cabinet. The average temperature experienced throughout the cultivation cabinet is likely to have been slightly lower than 30°C, which may have been one contributing factor. Another likely contributing factor is that the visible light available in the incubator covered the 400 – 600 nm part of the spectrum in a more consistent manner across wavelengths than the cultivation cabinet. This suggests that inclusion of extra wavelengths of LED covering this part of the spectrum may be beneficial to growth of *R. palustris* (say at around 450 nm). However, it is possible that this simply mitigates the effect of having no infrared or ultraviolet light, and that in the presence of these wavelengths extra provision in the visible spectrum would be of no significant benefit.

The absorbance spectra from the first two conditions (No Infrared and No Ultraviolet) are shown in Figures 3.11 and 3.12 respectively, and can be compared with Figure 3.8. When grown without infrared light, there was a marked decrease in the intensity of the 870 nm peak, and a corresponding increase in the intensity of the 810 nm peak relative to the peaks around the 500 nm region. This is similar to the effect seen under low light in Figure 3.1. There was also complete loss of the

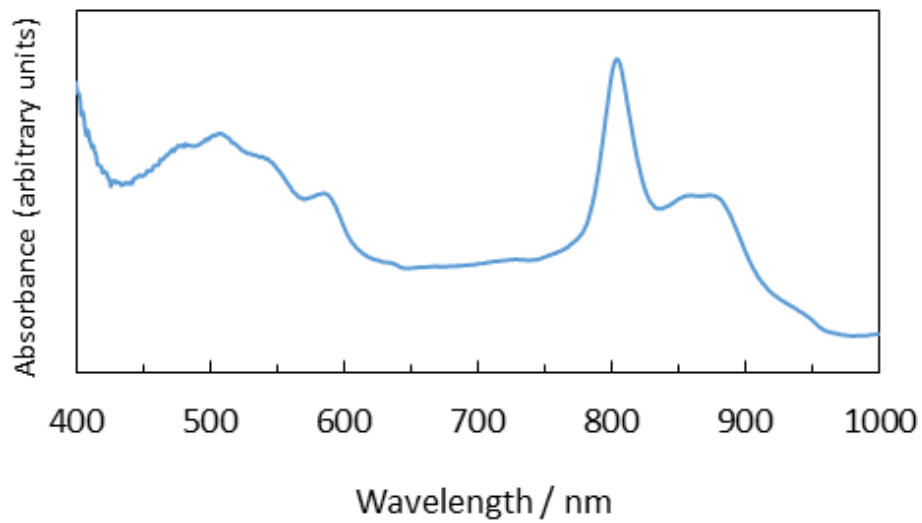


Figure 3.11: Absorbance in culture of wild-type *R. palustris* cultivated in the cultivation cabinet under the 'No Infrared' condition. Mean of three culture samples; three sweeps each.

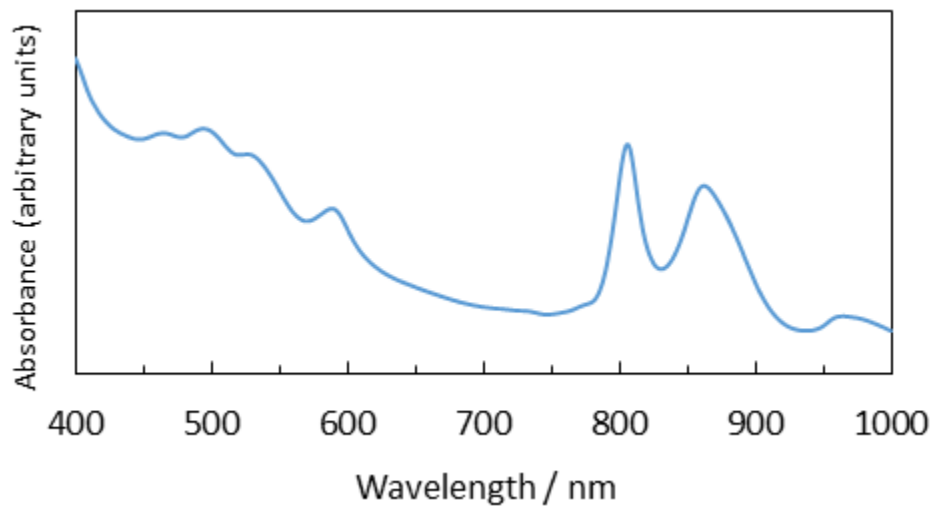


Figure 3.12: Absorbance in culture of wild-type *R. palustris* cultivated in the cultivation cabinet under the 'No Ultraviolet' condition. Mean of three culture samples; three sweeps each.

peak at 950 nm (not shown in Figure 3.1). This suggests that the cells were adjusting their light-harvesting machinery in response to the available light. When grown without ultraviolet light, on the other hand, the height of the peaks in the 400 – 600 nm region appeared to increase relative to those around the infrared region, and the trough around 430 nm all but disappeared. This possibly suggests that the cells increased their ability to absorb in this region in an effort to maximize uptake.

The growth data from condition 4, No 634 nm LEDs, are shown in Figure 3.13 contrasted with those taken under standard conditions. The absence of the 634 nm LEDs did reduce the growth rate of *R. palustris*, though to a much lesser extent than absence of the infrared or ultraviolet LEDs. The spectrum of light provided by these LEDs does overlap somewhat with the absorbance peak observed at around 590 nm (Figure 3.1), so this was not entirely surprising, although this area is already covered by the 594 nm LEDs and it was thought that the increased intensity of the other LEDs may have compensated for this minor loss of coverage. The optical density actually remained fairly similar up until about 190 hours, at which point a greater divergence between the two sets of data was observed. It would be interesting to see whether a much greater reduction in growth were observed if the intensity of the other LEDs were maintained at their standard level rather than being increased to compensate. If the reduction were still only minor, this may be a worthwhile target for reducing the costs of illumination in an industrial context, particularly if such high cell densities are not required.

3.3.4 Comparison between *R. palustris* growth under sunlight and on the cultivation cabinet

Finally, the growth of *R. palustris* under natural sunlight was also observed. Although these conditions came with considerable disadvantages to fast growth such as lower temperature, lack of agitation and periods of dark overnight, it was speculated that the broader range of wavelengths available may go some way towards mitigating these. The cultures were grown under an anaerobic atmosphere on a windowsill, where they were subject to room temperature maintained at a constant 21°C. The culture flasks contained magnetic stirrers, allowing them to be stirred for ten minute periods twice per day. The results from this experiment are shown in Figure 3.14, contrasted with those taken under standard conditions on the cultivation cabinet, and those taken under the 'No Infrared' condition. Unfortunately one culture became contaminated and had to be removed, resulting in only two replicates.

These results show that growth under natural sunlight, while considerably slower than on the

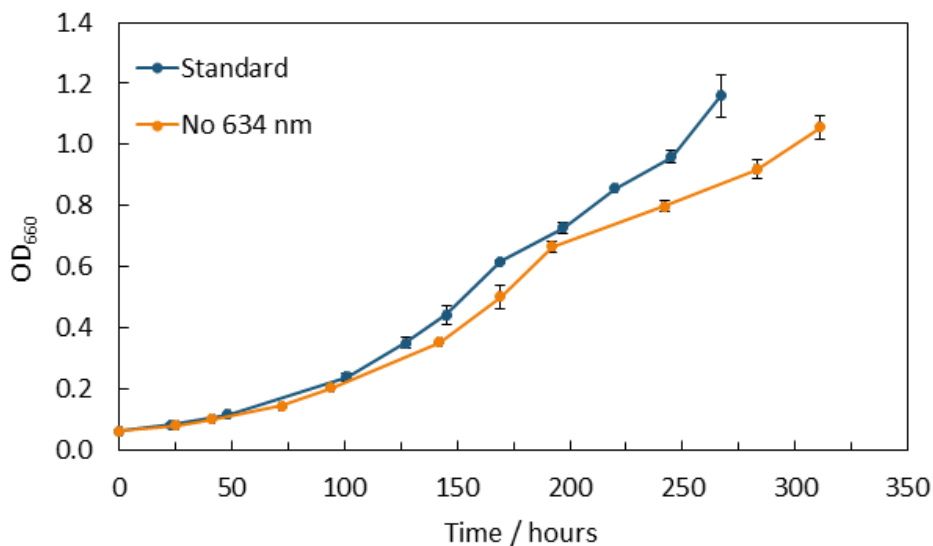


Figure 3.13: Optical density measured at 660 nm of wild-type *R. palustris* cultivated under standard lighting (all LEDs; blue), and with no 634 nm LEDs (orange): mean of three replicates each; bars show standard error.

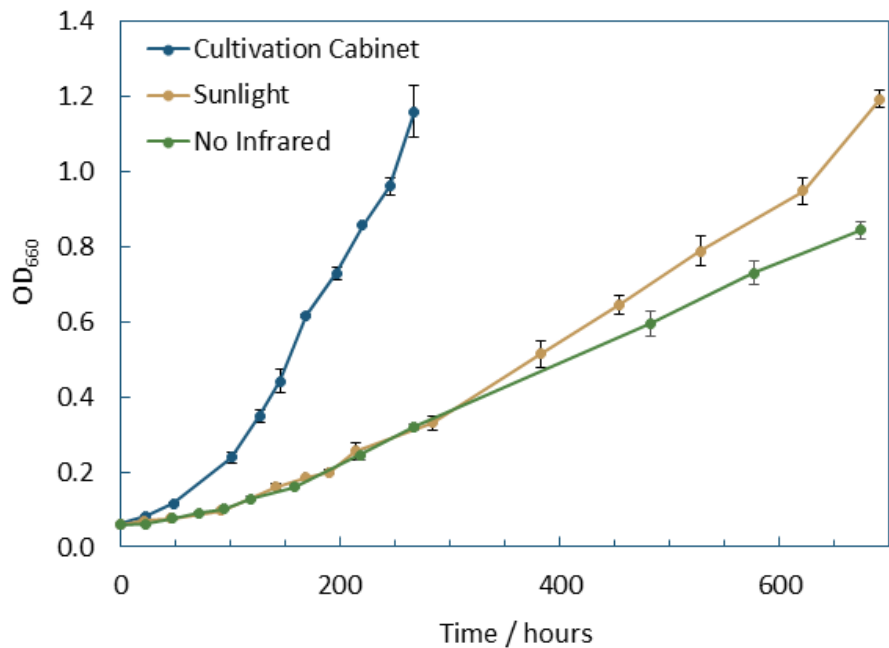


Figure 3.14: Optical density measured at 660 nm of wild-type *R. palustris* cultivated on the cultivation cabinet (blue; mean of three replicates) and under natural sunlight (red; mean of two replicates); bars show standard error.

cultivation cabinet, was still surprisingly fast given the not insubstantial disadvantages that accompanied these conditions. This gives further evidence to the suggestion that light spectrum availability is a significant limiting factor for growth of *R. palustris*. The results from the No Infrared condition highlight that loss of just these wavelengths was more detrimental to growth than the (even) lower temperature, lack of agitation and long periods of darkness experienced under sunlight. Interestingly, the cultures grown under this condition (at the same time as those under sunlight) were noticeably much more pigmented than those under sunlight, suggesting that the cultures experiencing a lack of infrared wavelengths were producing more pigment in an attempt to maximize light absorbance.

Growth on the incubator at standard temperature, though not included on this Figure for clarity's sake, was not substantially different from that under sunlight: for example at 214 hours under sunlight the OD₆₆₀ was 0.255, whilst in the incubator it was only 0.244 at the later time-point of 220 hours. This suggests that a standard commercial incubator brings no particular advantage to cultivation of *R. palustris* for experimental purposes.

3.4 Discussion

The work described in this Chapter resulted in the creation of a custom platform for cultivation of *R. palustris* which allowed the measurement of gaseous output volume and was shown to confer a significantly greater rate of growth than a standard commercial incubator operated under comparable conditions. Anaerobic conditions were shown to confer a greater rate of growth than aerobic conditions for *R. palustris*.

The spectrum of light provided for growth was found to have a considerable effect on growth rate, with absence of both infrared and ultraviolet light causing the greatest reduction in growth rate, and absence of infrared light having a greater effect than absence of ultraviolet light. The increased absorbance by *R. palustris* observed around the 450 nm region in the absence of ultraviolet light suggests that the organism may be able to make more use of this region of the spectrum if available. Furthermore, the decreased growth rate observed in the absence of coverage by the 634 nm LEDs suggests that the organism is able to utilize this light, although the effect was fairly minimal, particularly pre-190 hours.

A more thorough understanding of the light utilization of *R. palustris* could be obtained with further investigation. The altered absorbance spectrum observed in the absence of infrared light

suggests that the organism increases its ability to absorb in the near-infrared whilst decreasing its ability to absorb in the far-infrared; would growth be significantly reduced if only the 860 nm LEDs were inactivated, or would the organism be able to sufficiently compensate its light needs by absorbing more from the 830 nm and other LEDs? The increased pigmentation suggests that the organism may produce more light-harvesting machinery under these conditions, possibly at the expense of growth.

The comparatively high rate of growth observed under sunlight compared with the reduced spectrum conditions suggests the possibility that a growth setup subjecting *R. palustris* to sunlight but in a heated environment and / or with agitation may bring the growth substantially closer to that achieved on the cultivation cabinet, at a fraction of the cost and energy with no illumination requirements. Even if lighting were provided only at night it may allow comparable or even faster rates of growth, although daily weather and seasonal variation may make this untenable for industrial applications in most parts of the world.

From the point of view of improving the viability of *R. palustris* for industrial applications, it would be useful to know whether the reduced growth observed in the absence of the 634 nm LEDs is reduced further if the other LEDs are provided at their standard intensity, and conversely whether the reduction in growth can be mitigated completely by increasing the intensity of the active LEDs still further. It would also be helpful to see whether more consistent coverage over the spectrum (for example around 450 nm and 780 nm) confers even greater rates of growth, as might be suggested by the results from the sunlight experiment. Finally, it would be useful to investigate the extent to which increasing the overall light intensity affects the growth rate, if at all.

4 Optimization of the *R. palustris* Electroporation Protocol

4.1 Introduction

4.1.1 Overview

As discussed in Chapter 1, a protocol was recently developed by David Lea-Smith for the creation of unmarked rather than marked *R. palustris* knockouts (David Lea-Smith, Dept of Biochemistry, University of Cambridge, personal communication). These knockouts have targeted deletions but do not retain any antibiotic resistance marker. This is beneficial in allowing multiple genetic alterations to be made to a single strain without requiring multiple antibiotics, in allowing the resulting strains to be maintained without the need for expensive antibiotics, and in reducing the risk of antibiotic-resistant organisms being released into the environment. The protocol was based on the p*KmobsacB* delivery plasmid ([3]; Figure 4.1), which contains both the kanamycin resistance cassette and the *sacB* gene. This plasmid can be transferred into a range of Gram⁻ bacteria and even several genera of Gram⁺ bacteria. However, based on the pMB1 replicon [78], the host range for replication of the plasmid is restricted to *E. coli* and species within the *Salmonella* and *Serratia* genera [3]. It is therefore not expected to be capable of self-replication within *R. palustris*.

In contrast to the standard approach, the use of this plasmid relies unusually on single crossover rather than double crossover events. This results in an intermediate stage where successful transformants carry both the native and inserted plasmid sequence. In contrast, for example, the approach developed also by David Lea-Smith with Ravendran Vasudevan to generate unmarked knockouts in cyanobacteria relied instead on the successive use of two plasmids [79]. In the cyanobacterial system, the first double recombination results in the native sequence being swapped with a sequence carrying an antibiotic resistance cassette and the *sacB* gene within a gene deletion: the successful transformant is antibiotic resistant (and sucrose sensitive). The second double recombination, carried out with a second plasmid, swaps this sequence for one carrying only the deletion: the successful transformant is no longer sucrose sensitive (or antibiotic resistant).

The protocol for creation of unmarked *R. palustris* knockouts is as follows. The two regions flanking the target deletion site are amplified from DNA extracted from wild-type *R. palustris*, similar to the method used to create marked knockouts discussed in Chapter 1. However, rather than utilizing overlap extension, the amplification products include appropriate restriction sites at each end, which are used to introduce both products into the multiple cloning site of p*KmobsacB* in se-

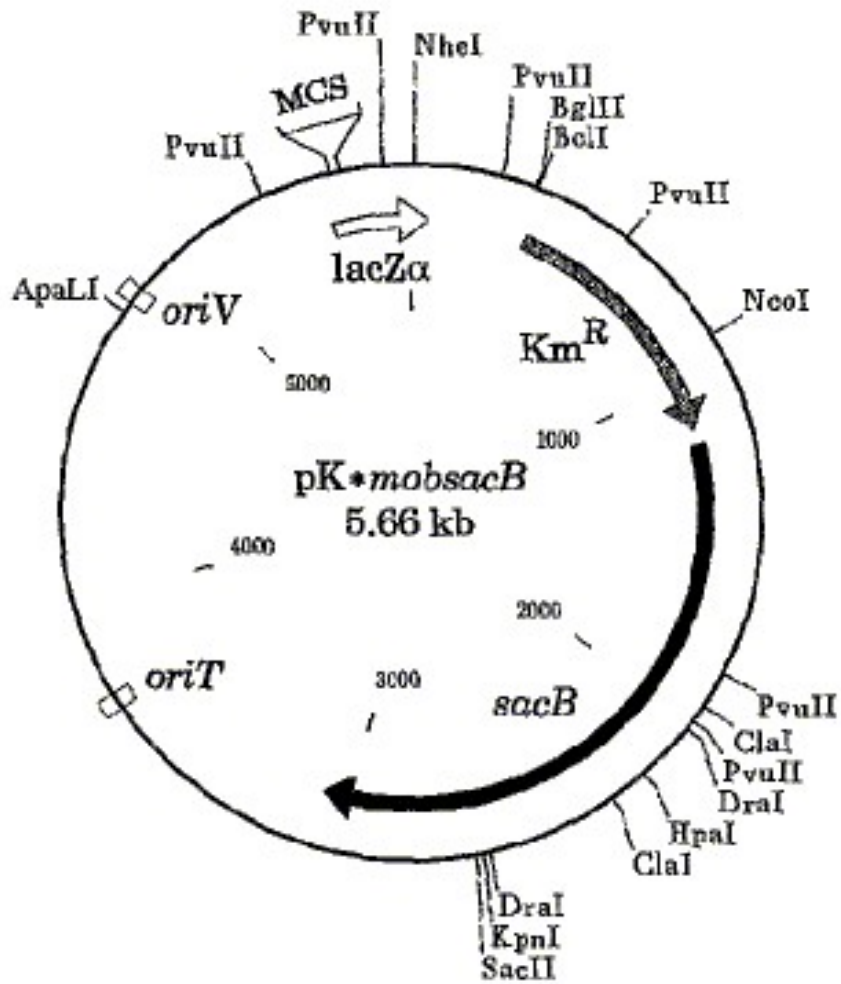


Figure 4.1: Taken from Figure 1, Panel B of Schäfer *et al.*, 1994 [3]: a detailed map of the *pK+mobsacB* plasmid utilized for the genetic manipulation of *R. palustris*. The kanamycin resistance cassette is indicated by 'Km^R' and the *sacB* gene as named: the arrows indicate the direction of transcription. The multiple cloning site, labelled 'MCS', contains the following restriction sites in order: EcoRI, SmaI, BamHI, XbaI, SalI, PstI, SphI, HindIII. Other restriction sites are labelled, as are the *oriV* (origin of replication) and *oriT* (origin of transfer).

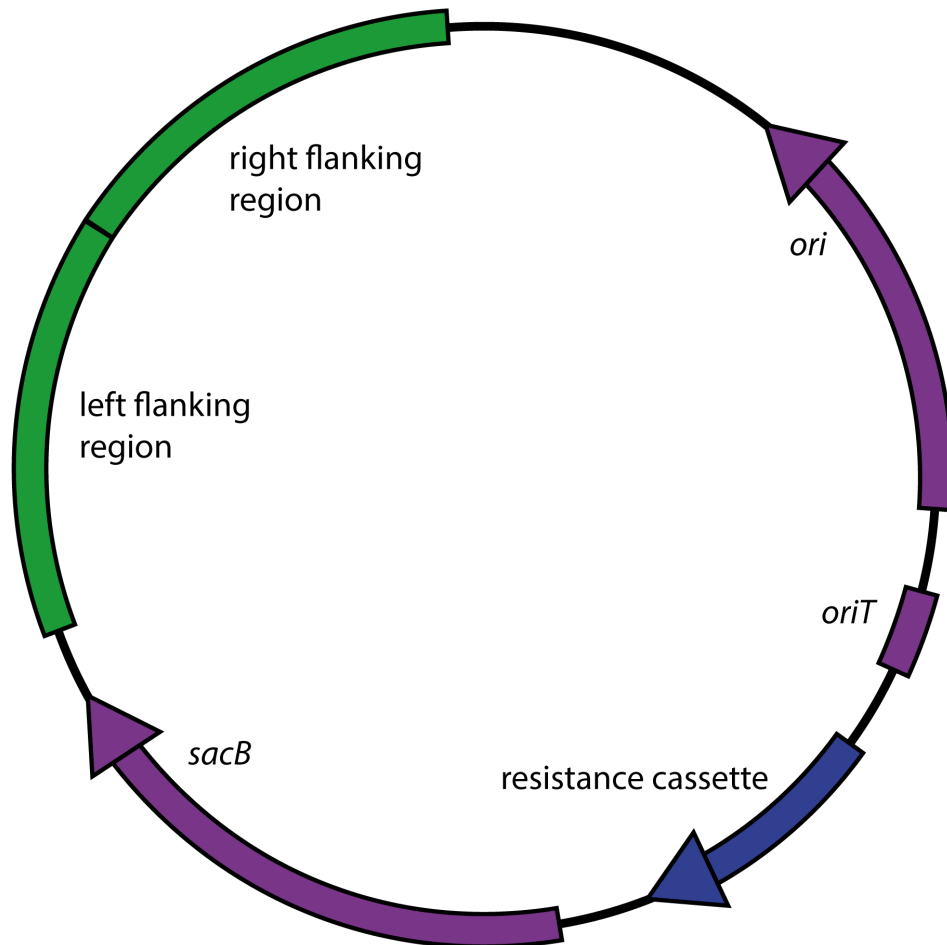


Figure 4.2: Illustration of the general form of plasmid used to create unmarked knockout strains of *R. palustris*. The origin of replication (*ori*), origin of transfer (*oriT*), *sacB* and resistance cassette (blue) are all part of the delivery plasmid (otherwise purple). The left and right fragments (green), amplified from the *R. palustris* genome with appropriate restriction sites, are inserted into the multiple cloning site of the delivery plasmid in sequence. The green sequence is homologous to the target region of the genome but the sequence targeted for deletion is missing between the two fragments.

quence. In contrast with the plasmid used to create marked knockouts, therefore, the resistance cassette is found within the backbone of the delivery plasmid rather than as an interruption of the sequence to be introduced to the genome; the plasmid is illustrated in Figure 4.2, and can be contrasted with Figure 1.3. Knocking out the gene therefore relies entirely on introducing a deletion.

The plasmid is introduced into *R. palustris* by electroporation, and incorporates into the genome via a single recombination event at the target site, illustrated in Figure 4.3. It is equally possible for the plasmid to integrate at the other end of the target sequence; only one outcome is shown for clarity. At this point, the genome contains both the endogenous sequence and the entire plasmid sequence. Cells which have successfully integrated the plasmid into their genome are selected with kanamycin, and tested by colony PCR to confirm integration of the plasmid. The primers used to test transformants by colony PCR are complementary to sequences nested within the two flanking regions. This therefore yields a product which spans the targeted deletion site in the wild-type. After the first recombination PCR therefore yields two amplification products: one generated from the endogenous sequence, and a shorter product generated from the inserted sequence. An example visualization of these amplification products is shown in Figure 4.4.

A second recombination is then selected for. However, in order to allow time for the occurrence of a second recombination event, cells of the marked knockouts are cultured for two days in the absence of any applied selection pressures, before being subjected to sucrose selection. Any cells which have failed to undergo a second recombination event will still contain the *sacB* gene within their genome. They will therefore suffer impaired viability in the presence of sucrose. This second recombination event that causes loss of the plasmid sequence can result in two different outcomes, depending on where the recombination occurs, as shown in Figure 4.3. One possible outcome is that the entire inserted sequence will be excised, including the amplified regions carrying the deletion, and the cell will revert to wild-type. The other possible outcome is that the endogenous sequence will be excised along with the pK*mobsacB* backbone sequence, leaving the cell with the targeted deletion in the genome but no selective markers [3]

Colony PCR can again be performed to test for successful creation of unmarked knockouts carrying the required deletion. The same primers, spanning the deletion site, yield only the shorter amplification product in unmarked strains, illustrated by Figure 4.3. They can be compared to the wild-type, which yields only the full-sized product. An example visualization of these amplification products is shown in Figure 4.5.

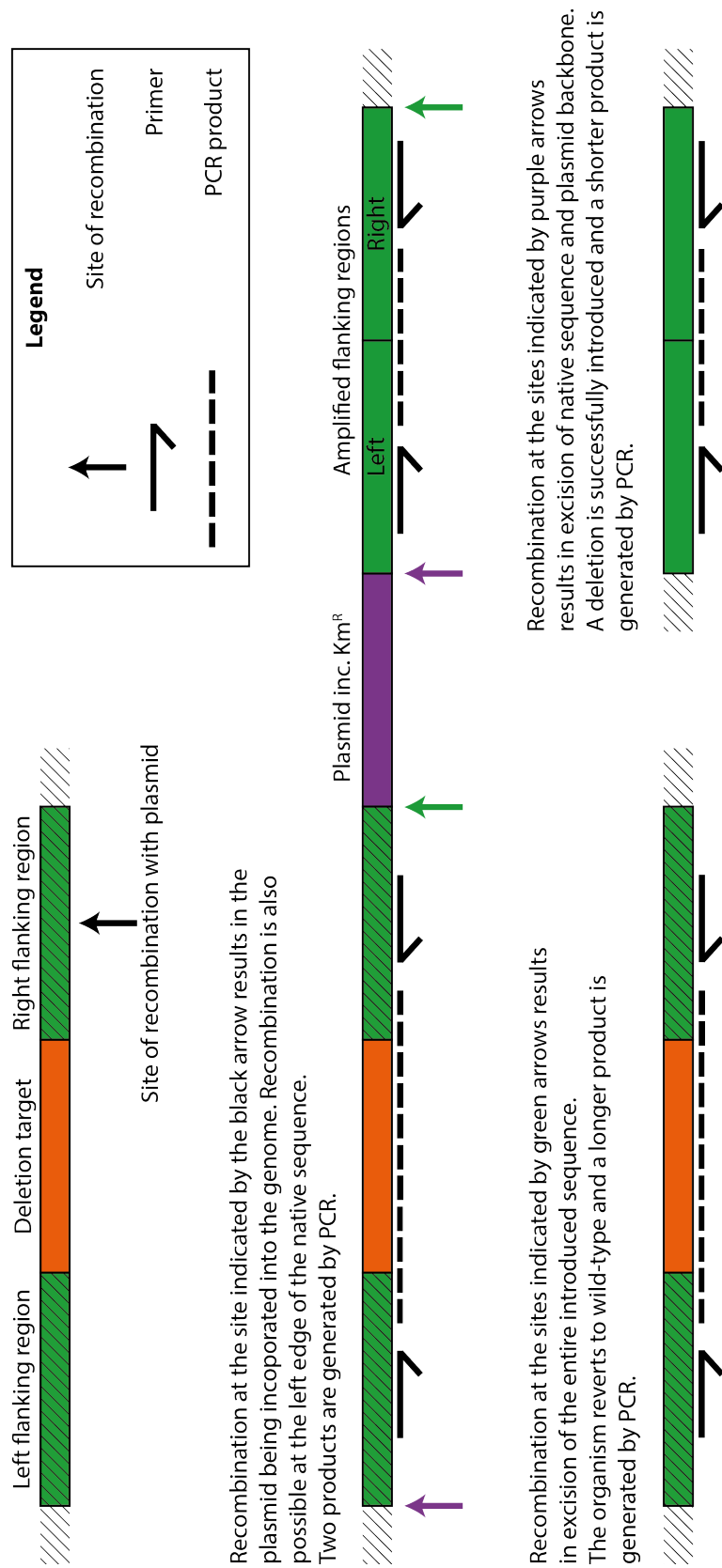


Figure 4.3: Illustration of the process of generating unmarked knockouts, from introducing the plasmid into the genome to testing for double recombinants.

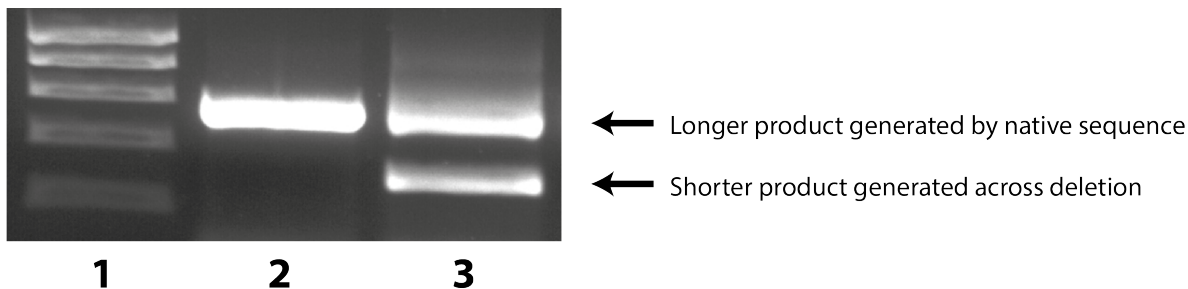


Figure 4.4: Example visualisation of amplification products generated by colony PCR during creation of marked *R. palustris* knockouts. In this case the primers were designed such that the amplification product spanned the region of *glnK2* targeted for deletion (see Chapter 6). Lanes: (1) DNA ladder; (2) wild-type *R. palustris*; (3) marked $\Delta glnK2$ knockout. After the first recombination event but before the second, a successful marked transformant would be identified as generating two products and therefore both bands.

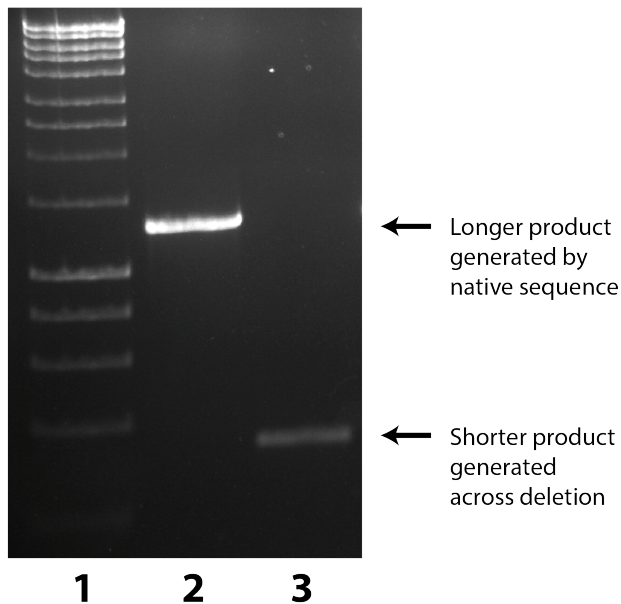


Figure 4.5: Example visualisation of amplification products generated by colony PCR during creation of unmarked *R. palustris* knockouts. In this case the primers were designed such that the amplification product spanned the region of *hupL* targeted for deletion (see Chapter 5). Lanes: (1) DNA ladder; (2) wild-type *R. palustris*; (3) unmarked $\Delta hupL$ knockout. After the second recombination event, a successful unmarked transformant would be identified through generating the shorter product only.

This method results in the successful creation of targeted deletions within the *R. palustris* genome, without also inserting permanent selectable markers. However, as discussed in Chapter 1, the transformation efficiency of the electroporation step which introduces the plasmid into *R. palustris* was extremely low for initial experiments by David Lea-Smith discussed in Chapter 5. The transformation efficiency was approximately 200 colonies per μg DNA. In contrast a transformation efficiency of typically about 10^5 colonies per μg DNA would be expected for a small plasmid inserted into *Escherichia coli* using standard procedures, for example [80]. Given that for our purposes only one successful transformant needs to be generated by this procedure, a low transformation efficiency is not apparently a problem. However, in terms of absolute numbers, this transformation efficiency results in few colonies even under ideal conditions, and over half of these may not even carry the target genetic alteration. Transformations described later in this work were carried out with larger plasmids, and on strains with reduced viability compared to the wild-type; under these conditions often only a couple of colonies, if any, were generated. Even a minor increase in efficiency was therefore anticipated to be beneficial to success rate, and so a series of experiments was carried out to enhance the efficiency of the transformation procedure.

A summary of the initial protocol follows (please see Chapter 2 for more detail):

1. Harvest cells at $\text{OD}_{660} = 0.3$.
2. Wash cells five times in 10% v/v glycerol solution.
3. Re-suspend cells in 0.1% starting culture volume of 10% v/v glycerol solution.
4. Mix 1 μL plasmid DNA with 60 μL competent cell preparation from above.
5. Transfer the cell / DNA suspension to a pre-chilled 1 mm electroporation cuvette.
6. Apply a pulse to the cuvette with the following settings: 2.5 kV; 200 Ω ; 25 μF .
7. Immediately re-suspend in 1 mL pre-warmed SOC.
8. Incubate at 37°C with shaking for 90 minutes.
9. Spread the suspension onto YP agar plates containing 100 $\mu\text{g mL}^{-1}$ kanamycin.
10. Incubate at 30°C until colonies appear.

The amount of plasmid DNA had not previously been quantified at all, so the amount present in 1 μ L of plasmid preparations used previously was measured and used to guide the setting of a standard of 250 ng in 5 μ L. From the protocol above, five key variables were identified: pulse voltage, pulse resistance, culture stage, cell density, and post-shock incubation temperature. These variables were anticipated to have a significant effect on the transformation efficiency. The capacitance of the pulse was not easily altered and therefore not investigated as part of this project. These five variables were varied individually to test their effect on transformation efficiency.

The plasmid chosen for use in these experiments was designed to insert and introduce a deletion into RPA1309, a transposase pseudogene thought to be frameshifted and incomplete. Downstream 547 base pairs is RPA1310, encoding NADH:flavin oxidoreductase, and upstream is 1247 base pairs of non-coding DNA. The plasmid was created by Jack Hervey (Department of Biochemistry, University of Cambridge) and was intended to cause minimal disruption to the functioning of the cell. It was similar to plasmids used elsewhere in this project for introducing deletions to coding genes. The backbone was p*KmobsacB*, and the flanking regions were each approximately 1 kb in length. This plasmid was chosen to be representative of typical experimental conditions while also ensuring that the resulting deletion did not negatively affect cell viability, as this could have an impact on the estimated transformation efficiency. A quantity of plasmid DNA sufficient for all optimization experiments was prepared in advance and stored as 25 μ L aliquots at -20°C, to ensure that there was as little variation in DNA quality as possible throughout the experiments.

In addition, an initial test was done to check whether significant numbers of colonies appeared after transformation with p*KmobsacB* containing no inserted *R. palustris* sequences. This would indicate either spontaneous antibiotic resistance, extrachromosomal maintenance (although the plasmid is not expected to be able to replicate autonomously in *R. palustris*), or non-homologous integration of the plasmid into the genome. If non-homologous plasmid integration were observed, the location and consistency would also be of interest.

4.2 Results

4.2.1 Testing for undirected integration of the pK*mobsacB* plasmid into *R. palustris*

Before proceeding with the optimization process, an experiment was conducted to test whether a significant number of colonies was observed after electroporation of *R. palustris* with pK*mobsacB* containing no inserted sequences, as discussed in section 4.1. If spontaneous antibiotic resistance were observed, that would indicate a background level of colonies which should be taken into account during future experiments. If non-homologous integration into the genome were observed, further tests would be undertaken to determine location and consistency.

The cells were prepared in the manner described in section 4.1 and in Chapter 2. Plasmid DNA containing no inserted sequences was diluted to $50 \text{ ng } \mu\text{L}^{-1}$ and $5 \mu\text{L}$ added to $50 \mu\text{L}$ competent cells, for a total amount of 250 ng and final concentration of $4.5 \text{ ng } \mu\text{L}^{-1}$. This concentration standard was applied to all experiments described from this point on. The sample was subjected to a pulse of 2.5 kV , 200Ω , and $25 \mu\text{F}$, as in the original protocol. After the recovery period, the entire volume of post-shock solution was spread onto YP agar plates containing $100 \mu\text{g mL}^{-1}$ kanamycin, which were subsequently incubated at 30°C and observed each day for the appearance of colonies.

Colonies would usually be visible on these plates after five days, but after ten days of observation there were still no observable colonies. This suggested that the expected background was nil, and also that pK*mobsacB* does not readily integrate into the genome of *R. palustris* other than by homologous recombination.

4.2.2 The effect of pulse voltage and resistance on transformation efficiency and cell viability

The first variables investigated were the pulse voltage and resistance. These could lie within a broad range of values, and narrowing down the probable range at an early stage reduced the number of test conditions necessary for later experiments. The resistance was adjustable in 200 Ω increments from 200 to 1000 Ω , and the voltage was adjustable in 0.01 kV increments from 0.01 to 2.5 kV. The voltage and resistance were both further refined in later experiments after testing and altering other variables. Incubator space limited the number of combinations that could be tested at a time, so the following settings were chosen for the first round of testing in order to cover the full range of possible values:

- 0.5 kV at 200, 600 and 1000 Ω
- 1.5 kV at 200, 600 and 1000 Ω
- 2.5 kV at 200, 600 and 1000 Ω

The optimal combination of field strength and rate of decay (a product of the resistance and capacitance, the latter of which was not varied) is likely to be a trade-off between higher frequencies of DNA uptake and cell viability [80]. At a higher voltage and resistance the DNA is more likely to enter any individual cell successfully, but that cell is more likely to suffer lethal damage as a result of the pulse. An understanding of the effect of voltage and resistance on the viability of competent *R. palustris* cells would inform our understanding of this trade-off for this species and therefore our choice of pulse settings. Therefore, an attempt was made to assess the viability of cells subjected to pulses with the above settings at the same time as the transformation efficiency.

The cells were prepared as previously. The DNA / competent cell mixture was prepared as a master mix and 55 μ L samples were then divided into the electroporation cuvettes, to ensure there was no variation between test samples. The cells were subjected to electroporation with pulse settings as stated above. After the recovery period, each sample of post-shock cell suspension was spread onto YP agar plates. For each set of test conditions, 500 μ L was split equally between two plates containing 100 μ g mL⁻¹ kanamycin, and 500 μ L was split equally between two plates containing no selective agent; 250 μ L per plate. Thus the cells were treated in exactly the same manner until being spread onto plates.

All plates were then incubated together, with each pair of 'identical' plates forming a stack. The top plate of each stack probably received more light: the same plate was kept at the top of the

stack throughout the observation period for consistency. The stacks were randomly redistributed throughout the incubator every 24 hours to minimize the effects of any variation in light intensity across the incubator. The number of colonies visible to the naked eye against a black background was recorded for each plate after five days. The 500 μL spread across the two plates contained 0.12 μg plasmid DNA, so the transformation efficiency was calculated as the total number of colonies on both plates divided by 0.12:

$$TE = \frac{\text{number of colonies}}{\mu\text{g of DNA}}. \quad (4.1)$$

Although each test condition was represented by two plates, these did not constitute true ‘repeats’, being one sample spread across two plates, hence the colony sum being used for these calculations. Unfortunately a lack of time and space prohibited the possibility of repeating these experiments, given the number of combinations possible, and so all results shown are from one sample only.

The transformation efficiencies of each test setting combination are shown in Figure 4.6. These results show that, broadly, increasing the voltage or resistance increases the transformation efficiency. However, at 2.5 kV and 1000 Ω the transformation efficiency (only 34 colonies per μg DNA) was drastically reduced compared to either the 2.5 kV, 600 Ω pulse (494 colonies per μg DNA) or the 1.5 kV, 1000 Ω pulse (315 colonies per μg DNA).

Unfortunately, the plates containing no selective agent were either contaminated or showed a lawn of red growth presumed to be *R. palustris*. Despite several attempts to repeat this experiment, with extra precautions taken to preserve the axenic nature of the samples, problems with contamination were always encountered, and this aspect of the experiment was ultimately abandoned.

The lack of any colonies at 0.5 kV is likely to be because the field strength was not strong enough to disrupt the cell membranes sufficiently to allow plasmid uptake. The overall trend of increasing transformation efficiency with increased field strength and resistance is likely to be a product of greatly increased DNA uptake, which more than compensates for higher levels of cell death: a greater proportion of cells’ membranes will be successfully disrupted. The large drop-off in transformation efficiency observed at 2.5 kV and 1000 Ω is probably attributable to a greatly increased frequency of cell death, which at this level overwhelms the advantage of increased DNA uptake as so few cells survive the process.

The pulse settings provisionally identified as producing the highest transformation efficiency

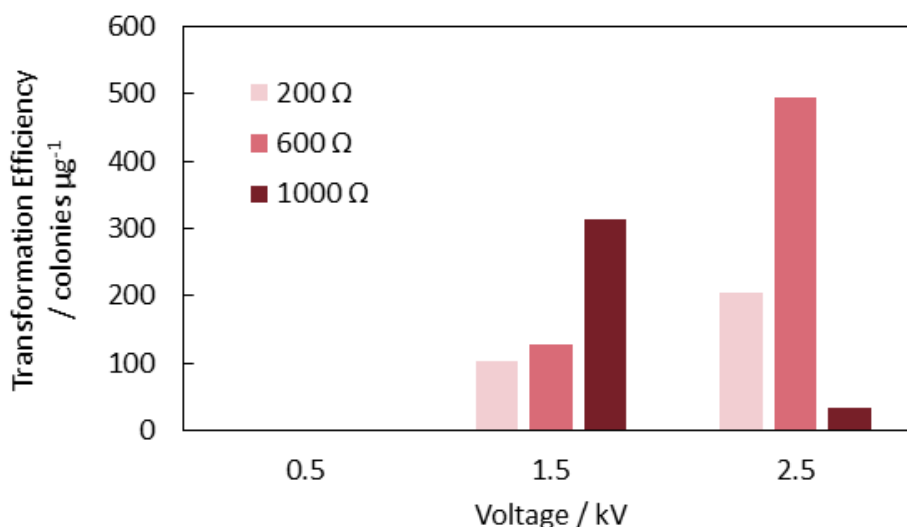


Figure 4.6: Transformation efficiency (colonies per μg DNA) of electroporation of *R. palustris* at different pulse voltage and resistance combinations, from 0.5 to 2.5 kV, and from 200 to 1000 Ω .

were therefore 2.5 kV at 600 Ω . Although not greatly different from the original protocol, which called for 2.5 kV at 200 Ω , these settings gave a more than 2-fold increase in transformation efficiency. Subsequent experiments on other variables (culture stage, cell density and post-shock recovery conditions) continued to be conducted across a range of voltage and resistance combinations, as it was possible that these variables would affect the optimal combination.

However, experiments were no longer conducted at 0.5 kV at any resistance. The absence of any colonies at this field strength indicated that the frequency of DNA uptake was too low to be useful. Even if changing other variables increased the frequency of DNA uptake at this voltage, it would be unlikely to be to such a degree that a greater transformation efficiency would be achieved than at 2.5 kV. In addition, altering the post-shock recovery conditions was predicted to affect cell viability rather than DNA uptake, which would therefore have little effect on the transformation efficiency at 0.5 kV. If the transformation efficiency at 1.5 kV and 200 Ω were later found to be greatly increased on changing another variable, the 0.5 kV settings would have been revisited.

4.2.3 The effect of culture stage on transformation efficiency

The next variable investigated was the growth stage of the cultures used. The initial protocol called for cultures at $\text{OD}_{660} = 0.3$; an experiment was conducted to determine whether use of a culture at a later stage would affect the transformation efficiency. For the experiment described in the previous

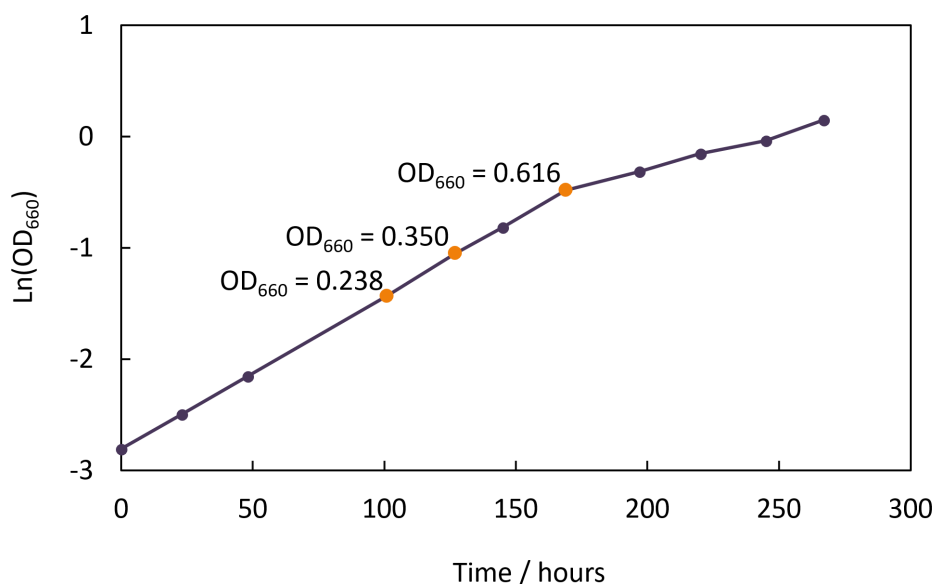


Figure 4.7: Natural logarithm of the OD₆₆₀ (presented in Figure 3.5) of wild-type *R. palustris* grown under the same conditions as the cultures used in this Chapter. Points highlighted in orange are labelled with the corresponding OD₆₆₀ at that time point.

section (4.2.2), half the volume of a culture of *R. palustris* was harvested at OD₆₆₀ = 0.3. The remaining half was maintained and harvested at OD₆₆₀ = 0.6, approximately two days later. Reference to Figure 4.7, displaying the natural logarithm of the growth data presented in Figure 3.5, reveals that these optical densities correspond roughly to mid- and late-log phase respectively. After being diluted two-fold to ensure that the cell density was consistent with that of the cells harvested earlier, these cells were treated in exactly the same manner, and subjected to each of the six combinations of pulse settings. The transformation efficiencies achieved at each combination of test settings, based on the total number of colonies across two plates as previously, are shown in Figure 4.8.

These results show that increasing the voltage from 1.5 to 2.5 kV led to an increase in transformation efficiency at 200 and 600 Ω , but a decrease at 1000 Ω . This is consistent with the pattern observed for cells harvested at OD₆₆₀ = 0.3. Unexpectedly, a greater transformation efficiency was observed at 200 Ω than at 600 Ω for 1.5 kV (68 and 43 colonies per μg DNA respectively). However, the colony counts for this experiment were very low (the most observed on one plate was 10 colonies at 2.5 kV and 600 Ω), and small variations in actual number therefore had a large impact. It is therefore likely that the higher transformation efficiency observed at 1.5 kV and 200 Ω was due to background variability across plates. It is possible that cells from later stage cultures benefitted from greatly increased cell viability at this combination of settings to an extent sufficient to coun-

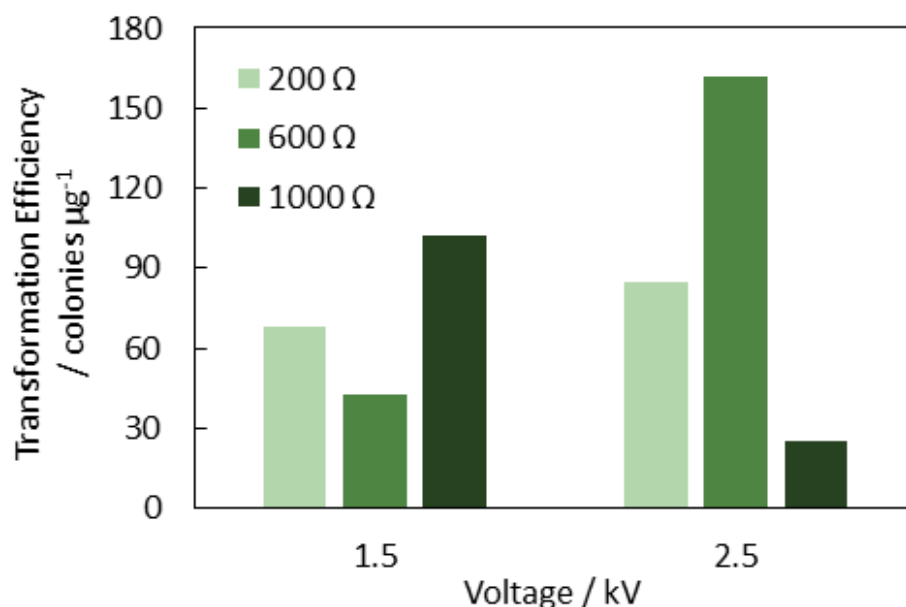


Figure 4.8: Transformation efficiency (colonies per μg DNA) of electroporation of late-log phase *R. palustris* across different pulse voltage and resistance combinations.

teract the reduced uptake of DNA, but as this combination yielded a much lower transformation efficiency than other options in any case, it was not investigated further during this project.

Figure 4.9 shows the same set of transformation efficiency data contrasted with the data from Figure 4.6, to illustrate the effect of culture stage on transformation efficiency. It can be seen that the transformation efficiency was consistently lower for late-log phase cultures at every combination of settings. The extent of the reduction was somewhat surprising, as although Figure 4.7 indicates that the cells had reached late-log phase at this point, the growth data indicate that rather than entering stationary phase, *R. palustris* continues to grow steadily in a linear fashion far beyond $\text{OD}_{660} = 0.6$. However, the doubling time of the culture, presented in Figure 4.10, suggests that the time taken for the cells to double increased greatly at around this point.

Although it is possible that a culture midway between these two values ($\text{OD}_{660} = 0.3$ and 0.6) might yield a greater transformation efficiency, this variable was not investigated further during this project, as it seemed unlikely it would have a large positive effect.

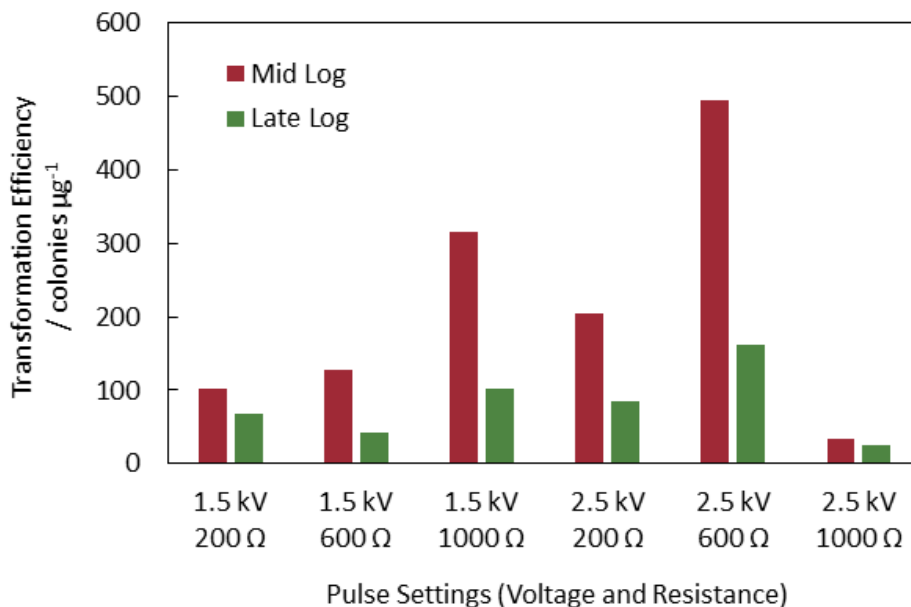


Figure 4.9: Transformation efficiency (colonies per μg DNA) of electroporation of mid-log (red) and late-log (green) *R. palustris* across different pulse voltage and resistance combinations.

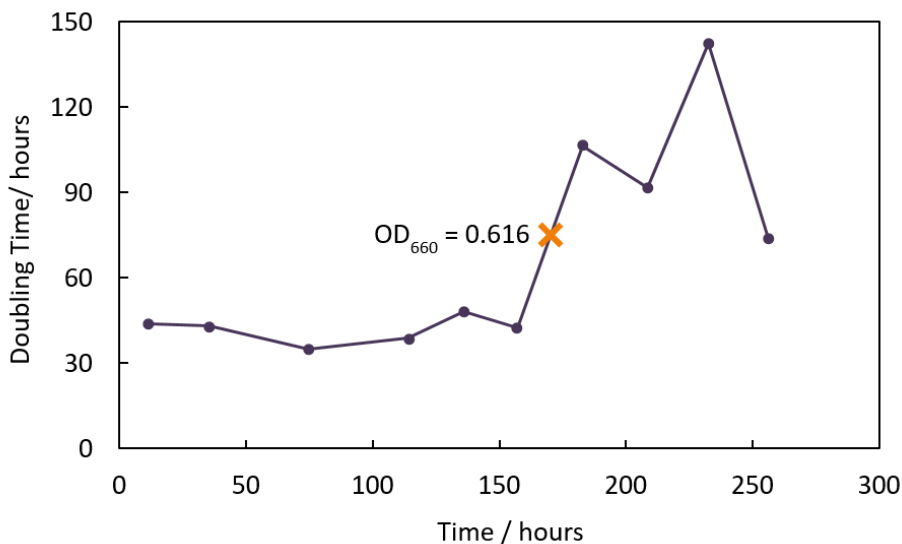


Figure 4.10: Doubling time of wild-type *R. palustris* grown under the same conditions as the cultures used in this Chapter, from the data presented in Figure 3.5. Doubling time 't' was calculated as $t = \ln(2) / \ln(1 + \text{growth rate})$, where growth rate was calculated over the period between each time point. The doubling time is plotted against the time corresponding to the mid-point of each time period.

4.2.4 The effect of cell density on transformation efficiency

The next variable investigated was the cell density in the final suspension subjected to electroporation. The initial protocol called for the cells to be re-suspended to a final volume of 0.1% of the starting culture volume. An experiment was conducted to compare the transformation efficiency achieved under these conditions with a suspension of twice the density and a suspension of half the density. The cells were prepared in the same way as previously. For the final re-suspension, one third of the cells were re-suspended in 0.05% of the equivalent starting culture volume, one third in 0.1%, and one third in 0.2%. The latter therefore had the lowest cell density.

Unfortunately, it was not possible to re-suspend the cells fully in 0.05% of the starting culture volume, and the experiment therefore proceeded without these samples. The plasmid DNA was then mixed with 60 μL volumes of these re-suspensions as before, so that only the cell density and not the volume was altered. The transformation efficiencies achieved at each combination of test settings are shown in Figure 4.11.

Under the 0.1% re-suspension condition, 2.5 kV and 600 Ω again conferred the greatest transformation efficiency, though lower than under the same conditions previously (374 compared to 494 colonies per μg DNA; Figure 4.6). The combination of 1.5 kV and 1000 Ω also conferred a lower transformation efficiency than before (204 compared to 305 colonies per μg DNA), taking it just below that of the 2.5 kV and 200 Ω combination (here 230 colonies per μg DNA). A large drop in transformation efficiency was still observed at 2.5 kV and 1000 Ω , compared to all of the other conditions, to 34 colonies per μg DNA.

Under the 0.2% re-suspension condition, a large drop was again observed at 2.5 kV and 1000 Ω , to 26 colonies per μg DNA. However, the greatest transformation efficiency observed for re-suspension in 0.2% of the starting culture volume was 204 colonies per μg DNA at 1.5 kV and 1000 Ω , and there was less variation overall in transformation efficiency between conditions. Compared to those samples re-suspended in a final volume of 0.1% of the starting culture volume, those re-suspended to 0.2% consistently gave a lower transformation efficiency at 2.5 kV, and also at 1.5 kV with 200 Ω . At 2.5 kV, this effect seemed to be greater at 600 Ω (2.2-fold lower) than at 200 Ω (1.6-fold lower).

Although the pattern was not consistent across all test conditions, a more dilute suspension of cells did not seem overall to confer a greater transformation efficiency. This is probably accounted for simply by the lower number of cells present, which means that there are fewer cells capable

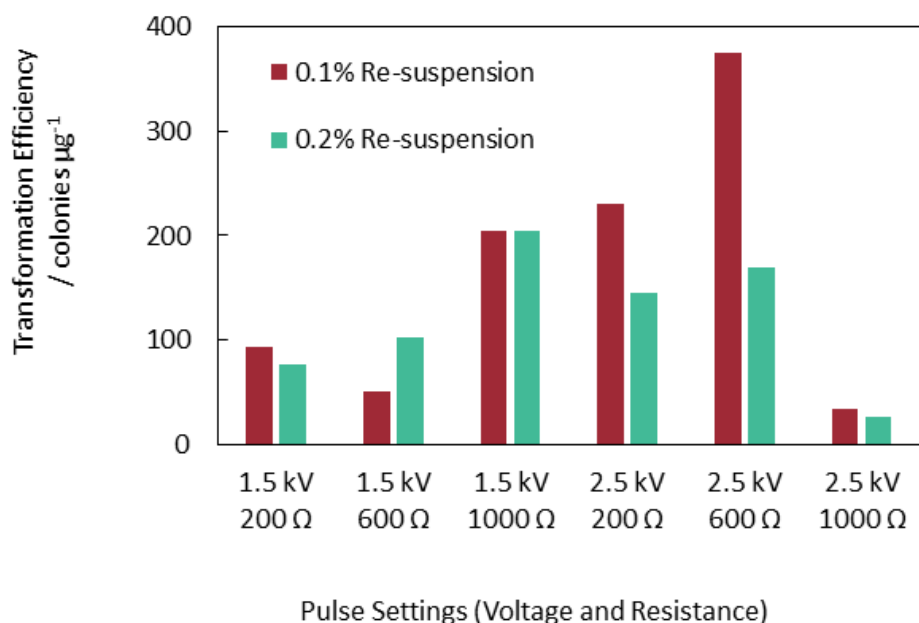


Figure 4.11: Transformation efficiency (colonies per μg DNA) of electroporation of *R. palustris* re-suspended in a final volume of 0.1% of starting culture volume (red) and re-suspended in a final volume of 0.2% of starting culture volume (turquoise) across different pulse voltage and resistance combinations.

of successfully integrating the plasmid. The highest level of transformation efficiency overall was observed for re-suspension to 0.1% of the starting culture volume, and was 1.8-fold greater than the highest transformation efficiency observed for re-suspension to 0.2%. It was therefore decided to continue using the same cell density.

4.2.5 The effect of post-shock incubation on transformation efficiency

The next variable to be investigated was the post-shock incubation temperature. Cells were treated in exactly the same manner as previously (harvested at $\text{OD}_{660} = 0.3$, final re-suspension to 0.1% of starting volume), and pairs of samples were each subjected to one of the six combinations of pulse settings. Post-shock, one sample from each pair was immediately re-suspended in SOC medium pre-warmed to 37°C and incubated for 90 minutes at the same temperature, and the other sample was immediately re-suspended in pre-chilled ice-cold SOC medium and incubated for 90 minutes on ice. The latter samples were then warmed for 60 minutes in a water bath at 37°C before being spread onto plates. The transformation efficiencies of these different treatments are shown in Figure 4.12.

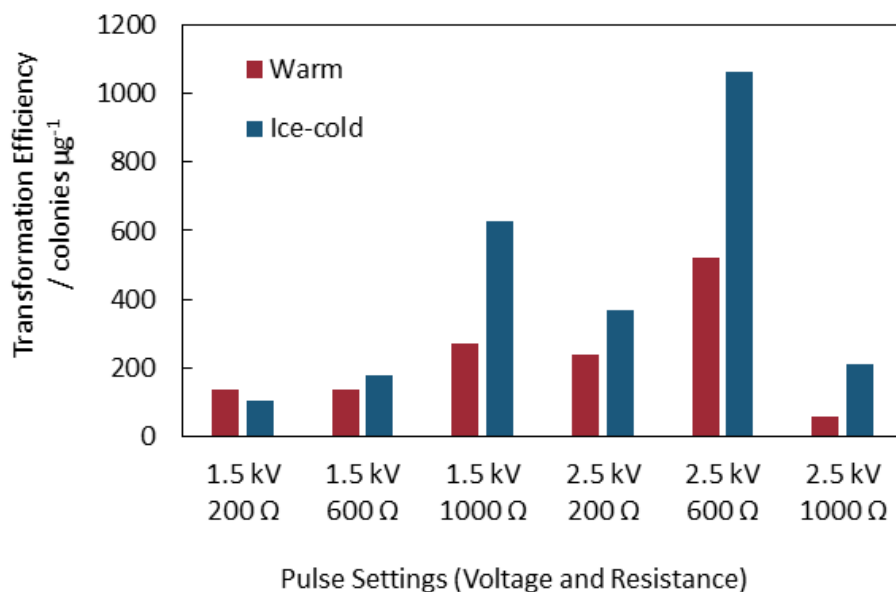


Figure 4.12: Transformation efficiency (colonies per μg DNA) of electroporation of *R. palustris* across different pulse voltage and resistance combinations. Data from cells incubated post-shock at 37°C for 90 minutes (red) are contrasted with data from cells incubated on ice for 90 minutes followed by warming at 37°C for 60 minutes (blue).

These results show that a greater transformation efficiency was achieved when samples were incubated on ice. At 2.5 kV and 600 Ω , a more than 2-fold increase in transformation efficiency was observed, from 519 colonies per μg DNA for the sample incubated at 37°C to 1064 colonies per μg DNA for the sample incubated on ice. However, this effect was much more pronounced at 2.5 kV than at 1.5 kV, and at higher resistances. At 1.5 kV and 200 Ω , there was actually a decrease in transformation efficiency from 136 to 102 colonies per μg DNA (quite possibly due to background variation; the actual colony counts were 16 and 12 respectively), whereas at 2.5 kV and 1000 Ω there was a 3.6-fold increase from 60 to 213 colonies per μg DNA. Overall, incubation on ice did not appear to affect the pattern of results across the different voltage and resistance settings, just the absolute transformation efficiencies observed at each set of conditions.

The increase in transformation efficiency observed at most combinations of settings with incubation on ice is likely to be due to increased cell viability. The electric shock received during electroporation presumably causes heating and possible cell damage, and immediate incubation on ice may help to mitigate this. The greater the field strength and resistance, the more damage may be caused by electroporation and the higher the rates of cell death would be. Incubation on ice therefore has the potential to reduce greatly the rate of cell death and thereby increase transfor-

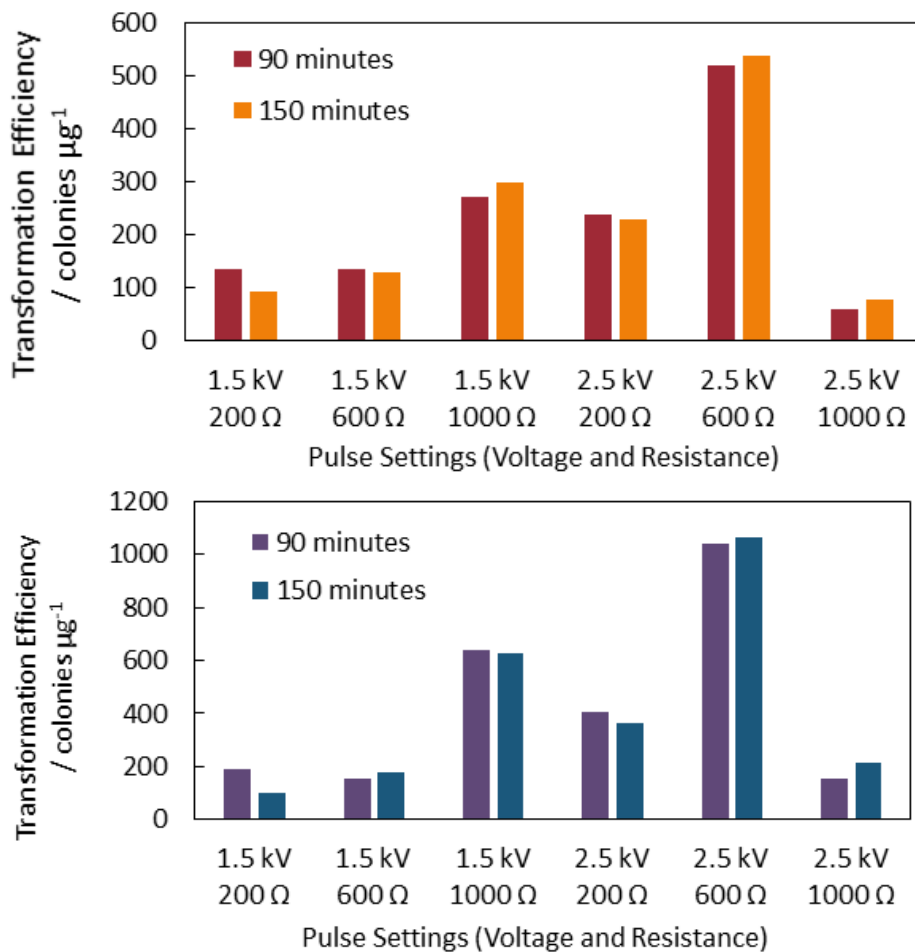


Figure 4.13: Transformation efficiency (colonies per μg DNA) of electroporation of *R. palustris* across different pulse voltage and resistance combinations. Top: data from cells incubated post-shock at 37°C for 90 minutes (red) are contrasted with data from cells incubated at 37°C for 150 minutes (orange). Bottom: data from cells incubated post-shock on ice for 90 minutes followed by warming at 37°C for 60 minutes (150 minutes total; blue) are contrasted with data from cells incubated on ice for 30 minutes followed by warming at 37°C for 60 minutes (90 minutes total; purple).

mation efficiency under these conditions. It may be that at lower field strengths, for example, the rate of cell death was not high enough for cell survival to be significantly increased by incubation on ice. Furthermore, the limiting factor to successful transformation under these conditions is the low frequency of DNA uptake; increasing cell viability further would provide diminishing returns.

The samples incubated on ice were incubated for a total of 150 minutes (90 minutes on ice and 60 minutes warming) before being spread onto plates, in contrast with the samples incubated for only 90 minutes at 37°C. In order to test whether the increased transformation efficiency was due to the incubation temperature rather than the extended incubation time, the experiment was repeated with different incubation conditions. One of these sets of samples was incubated at 37°C for a full 150 minutes; these data are compared with the samples incubated at 37°C for 90 minutes in Figure 4.13. The other set was incubated on ice for only 30 minutes before being warmed at 37°C for 60 minutes, for a total incubation time of 90 minutes; these data are compared with the samples incubated on ice for 90 minutes before warming in Figure 4.13.

These results indicate that the incubation period does not have a great effect on transformation efficiency within this range of times. Increasing the incubation period from 90 to 150 minutes at 37°C did not increase the transformation efficiency and therefore cannot account for the increased transformation efficiency observed when samples were incubated on ice for 90 minutes followed by warming. Likewise, reducing the ice incubation period from 90 to 30 minutes, followed by warming, did not decrease the transformation efficiency. This demonstrated that cells could be incubated for 90 minutes in total and still benefit from the increased transformation efficiency conferred by incubating on ice. Thus the transformation efficiency could be greatly increased without the need for a longer incubation period.

4.2.6 Further refinement of voltage and resistance

Finally, voltage and resistance were revisited, incorporating the findings of the earlier experiments. Based on these, the 1.5 - 2.5 kV range and 600 - 1000 Ω range were targeted for further investigation. Thus the following combinations were chosen:

- 1.5 kV at 600, 800 and 1000 Ω .
- 2.0 kV at 600, 800 and 1000 Ω .
- 2.5 kV at 600, 800 and 1000 Ω .

The cells were treated based on the results of the previous experiments, as follows:

1. Harvest cells at $OD_{660} = 0.3$ (mid log phase).
2. Wash cells five times in 10% v/v glycerol solution.
3. Re-suspend cells in 0.1% starting culture volume of 10% v/v glycerol solution.
4. Mix 5 μL of 50 $\text{ng}\mu\text{L}^{-1}$ plasmid DNA with 60 μL competent cell preparation from above.
5. Transfer the cell / DNA suspension to a pre-chilled 1 mm electroporation cuvette.
6. Apply a pulse to the cuvette with test settings at 25 μF .
7. Immediately re-suspend in 1 mL pre-chilled SOC.
8. Incubate on ice with shaking for 30 minutes.
9. Incubate in a water bath at 37°C for 60 minutes.
10. Spread the suspension onto YP agar plates containing 100 $\mu\text{g mL}^{-1}$ kanamycin.
11. Incubate at 30°C.

The transformation efficiencies achieved at these combinations of pulse settings are shown in Figure 4.14.

These results indicate that the optimal combination of voltage and resistance (to the nearest 0.5 kV) was 2.0 kV at 800 Ω . The difference between this combination and 2.5 kV at 600 Ω was small: the transformation efficiency increased from 1149 to 1243 colonies per μg DNA, but the actual number of colonies increased from just 135 to 146. Repeated testing may reveal that the difference is insignificant, but for the purposes of the work described here taking 2.0 kV at 800 Ω to be the optimal combination is sufficient: the long-term transformation efficiency is unlikely to be significantly lower under these conditions. Interestingly, these results also reveal that a resistance of 1000 Ω was detrimental to transformation efficiency from at least 2.0 kV. While the transformation efficiency increased with voltage at 600 Ω , it consistently decreased over this range at 1000 Ω . In contrast, the transformation efficiency at 800 Ω initially increased up to 2.0 kV, before falling at 2.5 kV.

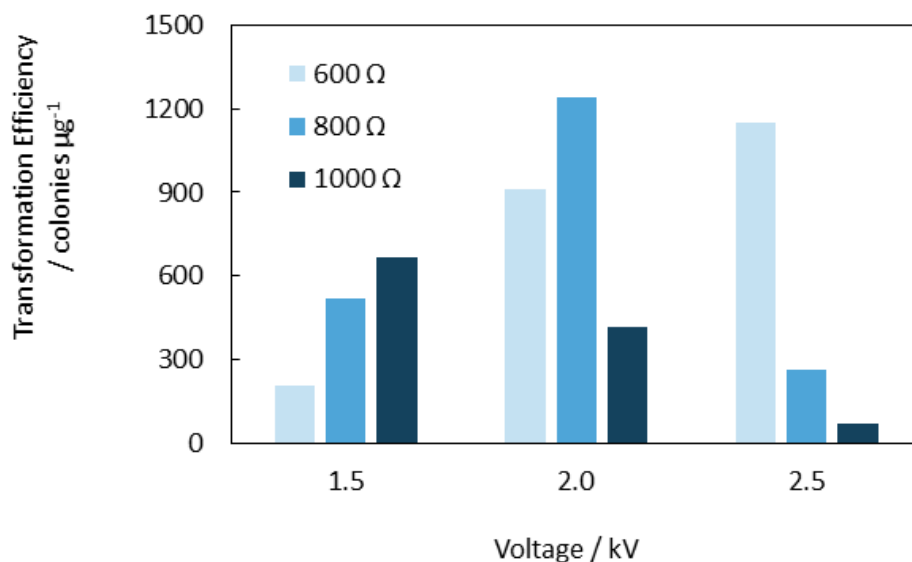


Figure 4.14: Transformation efficiency (colonies per μg DNA) of electroporation of *R. palustris* at different pulse voltage and resistance combinations, from 1.5 to 2.5 kV, and from 600 to 1000 Ω .

4.2.7 Assessing the reproducibility of these results

To assess the overall reproducibility of these results, the data from the initial set of six test conditions (section 4.2.2) were combined for statistical analysis with the data generated under the same experimental conditions shown in sections 4.2.4 and 4.2.5. The raw data of colonies observed were combined rather than transformation efficiencies, as this allows a more accurate estimation of error. The average ‘total number of colonies across two plates’ was calculated for each set of test conditions, and these values are presented in Figure 4.15.

Analysis by One-Way ANOVA generated a p-value < 0.00001 ; there is a statistically significant difference in colony number between test conditions, and there appears to be a reasonable level of reproducibility in the results. In particular, post-hoc testing with Tukey’s HSD indicated a significant difference between the 2.5 kV and 200 Ω pulse used pre-optimization and the 2.5 kV and 1000 Ω pulse initially identified as more effective ($p < 0.01$). The full set of pair-wise comparisons is shown in Table 4.1.

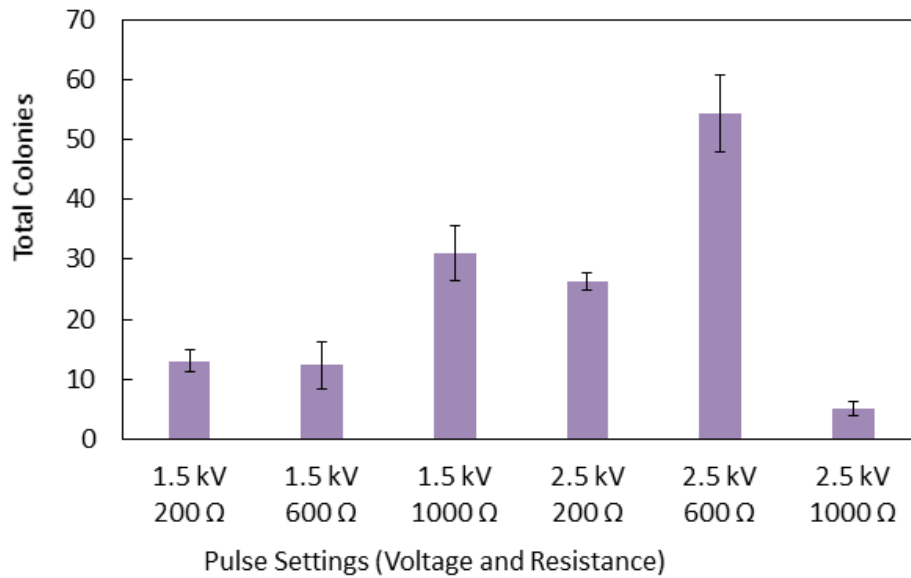


Figure 4.15: Transformation efficiency (colonies per μg DNA) of electroporation of *R. palustris* at different pulse voltage and resistance combinations. Data are the average of three biological replicates; error bars indicate standard error.

Condition 1	Condition 2	Absolute Difference	p-value
1.5 kV – 200 Ω	1.5 kV – 600 Ω	0.667	0.9999845
1.5 kV – 200 Ω	1.5 kV – 1000 Ω	18.0	0.0133567 *
1.5 kV – 200 Ω	1.5 kV – 1000 Ω	18.7	0.0103255 *
2.5 kV – 200 Ω	2.5 kV – 600 Ω	28.0	0.0003554 **
2.5 kV – 200 Ω	2.5 kV – 1000 Ω	21.3	0.0037510 **
2.5 kV – 200 Ω	2.5 kV – 1000 Ω	34.7	0.0000011 **
1.5 kV – 200 Ω	2.5 kV – 200 Ω	13.3	0.0810448
1.5 kV – 200 Ω	2.5 kV – 600 Ω	41.3	0.0000072 **
1.5 kV – 200 Ω	2.5 kV – 1000 Ω	8.00	0.4778794
1.5 kV – 600 Ω	2.5 kV – 200 Ω	14.0	0.0629095
1.5 kV – 600 Ω	2.5 kV – 600 Ω	42.0	0.0000061 **
1.5 kV – 600 Ω	2.5 kV – 1000 Ω	7.33	0.5633697
1.5 kV – 1000 Ω	2.5 kV – 200 Ω	4.67	0.8826561
1.5 kV – 1000 Ω	2.5 kV – 600 Ω	23.3	0.0017974 **
1.5 kV – 1000 Ω	2.5 kV – 1000 Ω	26.0	0.0006998 **

Table 4.1: Results of pair-wise comparisons by Tukey's HSD on the data from Figure 4.15. Difference significant at 5% indicated by *. Difference significant at 1% indicated by **.

4.3 Discussion

The experiments described here successfully refined the protocol for electroporation of component *R. palustris* cells such that a 6-fold increase in transformation efficiency, from approximately 200 (in the original protocol) to 1200 colonies per μg DNA, was achieved. Altering the voltage, resistance and post-shock incubation temperature led to an improved transformation efficiency, while alterations made here to culture stage and density either did not change the transformation efficiency or resulted in a decrease compared to the initial protocol. The optimal conditions appear to be the result of a trade-off between DNA uptake and cell viability.

The protocol established as a result of this work, and used for all subsequent attempts to manipulate *R. palustris* genetically, is as follows (changes in bold):

1. Harvest cells at $\text{OD}_{660} = 0.3$ (mid log phase).
2. Wash cells five times in 10% v/v glycerol solution.
3. Re-suspend cells in 0.1% starting culture volume of 10% v/v glycerol solution.
4. Mix **5 μL 50 ng μL^{-1}** plasmid DNA with 60 μL competent cell preparation from above.
5. Transfer the cell / DNA suspension to a pre-chilled 1 mm electroporation cuvette.
6. Apply a **2.0 kV, 800 Ω , 25 μF** pulse to the cuvette.
7. Immediately re-suspend in 1 mL **pre-chilled** SOC.
8. **Incubate on ice with shaking for 30 minutes.**
9. **Incubate in a water bath at 37°C for 60 minutes.**
10. Spread the suspension onto YP agar plates containing 100 μg mL^{-1} kanamycin.
11. Incubate at 30°C until colonies appear.

There are still areas of potential improvement to this protocol. The fact that reducing the incubation time on ice by 60 minutes did not noticeably affect the transformation efficiency suggests that it may be possible to reduce this further, saving time. It may also be that a full 60 minutes of warming after incubation on ice is unnecessary. More culture stages could be investigated, in particular those at early-log, and the voltage could be more precisely refined. Finally, the effects of plasmid DNA concentration and its interaction with cell density remain to be investigated.

5 Characterisation of chassis strains and introduction of heterologous pathways into *R. palustris*

5.1 Introduction

5.1.1 Introducing heterologous biosynthetic pathways into *R. palustris*

As discussed in Chapter 1, a long-term goal of this project was to introduce heterologous biosynthetic pathways into *R. palustris* with the aim of producing high-value compounds from glycerol biologically. This would demonstrate the feasibility of introducing heterologous genes into *R. palustris* while also creating specific strains with commercial potential. Isoprene and propane-1,2-diol were identified as target compounds for this purpose based on their global market, ease of extraction, and simplicity of their synthesis pathways for introduction into *R. palustris*.

A biosynthetic pathway for propane-1,2-diol production from glycerol has previously been introduced into *Saccharomyces cerevisiae* [81], and a later study improved the naturally low glycerol uptake rate and slow growth on glycerol of *S. cerevisiae* by overexpressing glycerol dissimilation and transporting genes [61]. The introduction of this pathway into *R. palustris* is still of great interest, however, due to the latter's naturally high rates of glycerol uptake and growth on glycerol, and its ability to withstand crude glycerol [40].

The heterologous genes introduced into *S. cerevisiae* were sourced from *Escherichia coli*. *E. coli* produces propane-1,2-diol from DHAP (dihydroxyacetone phosphate) generated during glycerol metabolism [66], as described in Chapter 1 and illustrated in Figure 5.1. This production of propane-1,2-diol occurs via the action of three enzymes: methylglyoxal synthase, aldehyde oxidoreductase, and glycerol dehydrogenase. Genes encoding methylglyoxal synthase and glycerol dehydrogenase were introduced into *S. cerevisiae*, resulting in successful production of propane-1,2-diol. The first step in introducing this pathway into *R. palustris* was therefore to determine whether all three of these genes would need to be introduced.

Likewise, a biosynthetic pathway for isoprene production has also previously been introduced into *Synechocystis* [68], though growth on glycerol was not studied. Isoprene production was achieved by introducing a codon-optimized version of the *ispS* gene for isoprene synthase, based on the sequence from *Pueraria montana*. Isoprene synthase produces isoprene from DMAPP (dimethylallylpyrophosphate), which *R. palustris* produces via the non-mevalonate pathway for isoprenoid

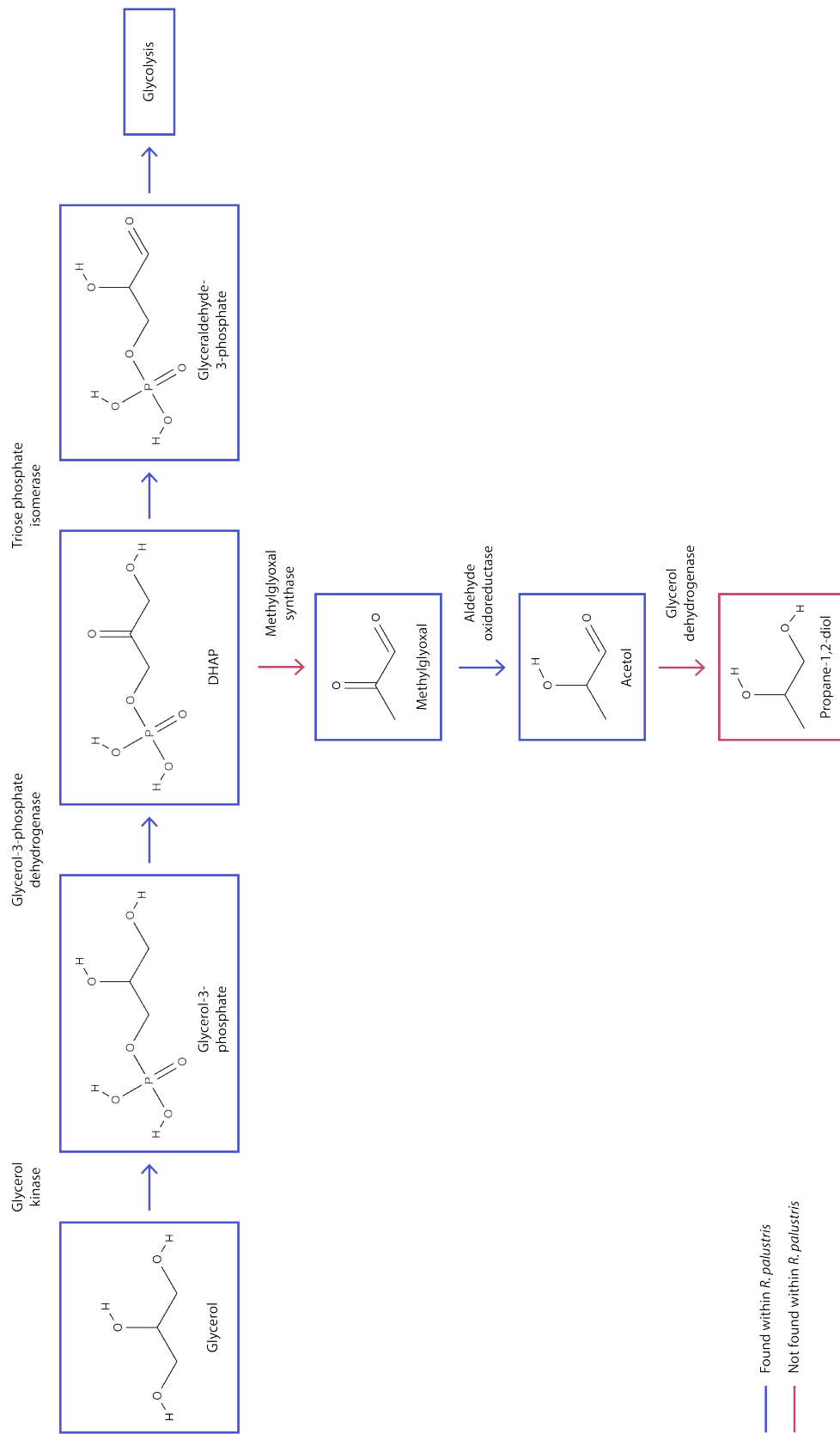


Figure 5.1: Diagrammatic representation of the biosynthesis of propane-1,2-diol and the typical route for glycerol assimilation. Blue arrows indicate enzymes endogenous to *R. palustris* while red arrows indicate enzymes requiring the introduction of heterologous genes (see below). The red box indicates the target product.

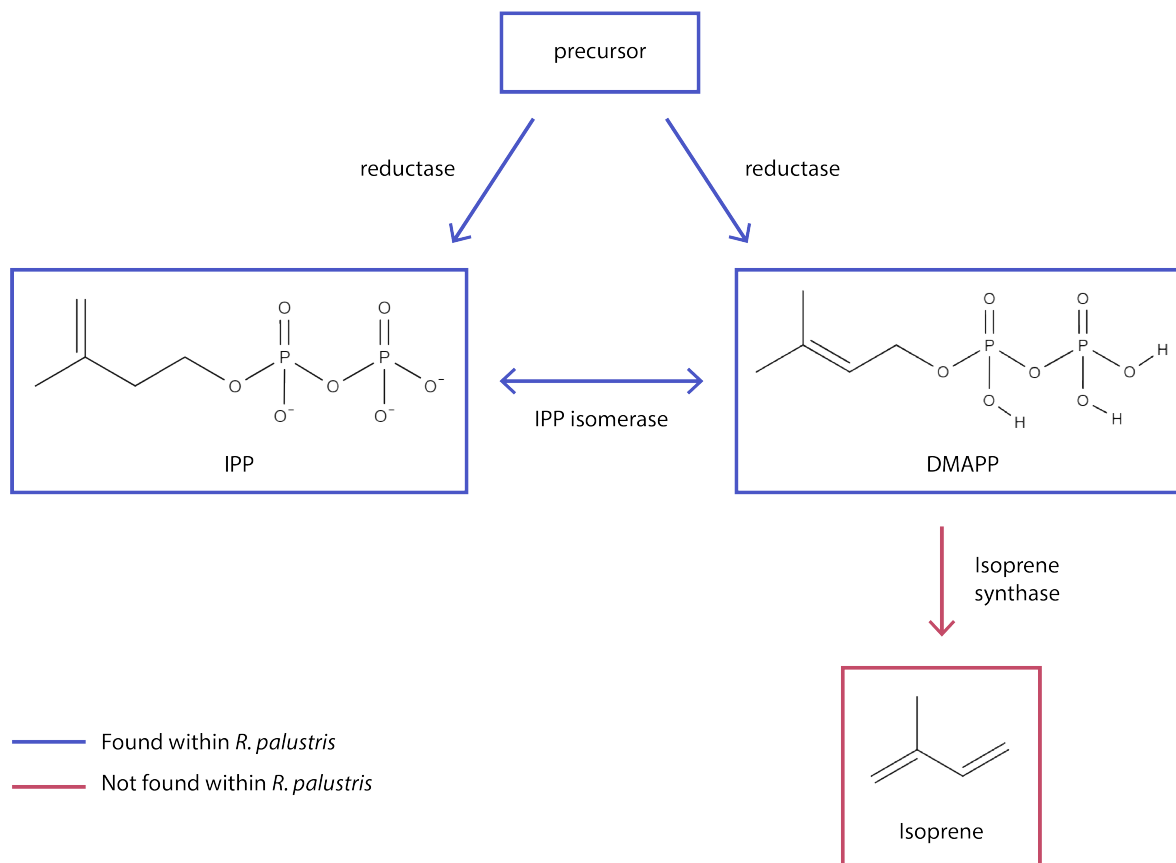


Figure 5.2: Diagrammatic representation of the biosynthesis of isoprene. Blue arrows indicate enzymes endogenous to *R. palustris* while red arrows indicate enzymes requiring the introduction of heterologous genes (see below). The red box indicates the target product.

biosynthesis, as described in Chapter 1 and illustrated in Figure 5.2. Thus introducing isoprene synthase into *R. palustris* should also result in isoprene production.

In the non-mevalonate pathway, DMAPP is created concurrently with its isomer IPP (isopentenyl pyrophosphate). It is possible for cells to interconvert between the two isomers subsequently, via the action of the IPP isomerase enzyme. In organisms employing the mevalonate pathway, such as *P. montana*, IPP is created first in the pathway and then turned into DMAPP by the action of IPP isomerase. In the event of successful isoprene production by *R. palustris*, it is possible that an extra copy of IPP isomerase, particularly one which may not be subject to the same regulatory mechanisms as the native gene and enzyme, may facilitate greater levels of isoprene production through maintaining the pool of DMAPP substrate. For comparison, it was decided to create one strain carrying both heterologous genes, *ipi* and *ispS*, and one carrying only *ispS*.

5.1.2 Producing valuable compounds from a glycogen- and PHB-deficient strain of *R. palustris*

Introducing heterologous genes into *R. palustris* requires the availability of suitable host strains, however. Before attempting to introduce heterologous genes, it was therefore important to characterise possible host strains. As mentioned in Chapter 1, previous work by David Lea-Smith (Department of Biochemistry, University of Cambridge) produced several strains of *R. palustris* with genes for one or more of the following inactivated: uptake hydrogenase, glycogen biosynthesis and poly[hydroxybutyrate] (PHB) biosynthesis. The plasmids used to create these strains were constructed in the manner described in Chapter 6. Some of the resulting strains were created by Toby Call (Department of Biochemistry, University of Cambridge) using these same plasmids. The six strains are listed alongside their creators in Table 5.1.

Glycogen and PHB are both used as storage compounds by *R. palustris*. This makes strains incapable of producing these compounds particularly interesting to this project, as they should in theory be forced to redirect any surplus energy, reducing power or substrate molecules towards alternative compounds (depending on the overall thermodynamic balance). We therefore predict that strains incapable of producing glycogen and / or PHB may be able to produce, for example, more isoprene or propane-1,2-diol than the wild-type, with the introduction of the appropriate genes. The strain with genes for production of glycogen and PHB disrupted was therefore also chosen alongside the wild-type for the introduction of the isoprene and propane-1,2-diol biosynthetic pathways. If this background strain were found to produce more of the target compound(s) than the wild-type, it would establish this as an effective strain for production of heterologous compounds.

The uptake hydrogenase is responsible for breaking down molecular hydrogen, liberating energy and electrons. The strains unable to produce the uptake hydrogenase are therefore of general interest to this work because of the enzyme's effect on hydrogen yield, but also of technical significance for this project, as the plasmid used to create the *hupL* deletion was used as the delivery plasmid for the heterologous genes. Thus all strains created here with the genes for production of isoprene or propane-1,2-diol would also carry a deletion within the uptake hydrogenase genes. It is possible that this would have a disadvantageous effect on the growth and production capability of the cells, so it was important to determine if this was in fact the case.

Targeted Pathways	Genotype	Creator
Uptake hydrogenase	$\Delta hupL$	David Lea-Smith
PHB	$\Delta phaAB$	Toby Call
Glycogen	$\Delta glgCA$	Toby Call
PHB – Glycogen	$\Delta phaAB\Delta glgCA$	Toby Call
Uptake hydrogenase – PHB	$\Delta hupL\Delta phaAB$	David Lea-Smith
Uptake hydrogenase – PHB – Glycogen	$\Delta hupL\Delta phaAB\Delta glgCA$	David Lea-Smith

Table 5.1: List of strains created with deletions in the biosynthetic pathways for a combination of one or more of the following: PHB; glycogen; uptake hydrogenase.

5.1.3 Creation of the PHB, glycogen and uptake hydrogenase knockouts

The genetic modifications made to disrupt the three processes are illustrated in Figure 5.3. To prevent the cell from being able to produce the uptake hydrogenase, a deletion was introduced into the gene encoding the large subunit of the protein, *hupL* (illustrated in Figure 5.3A).

To prevent the cell from being able to produce PHB, a deletion was introduced into two adjacent genes encoding proteins involved in the biosynthetic pathway of PHB (illustrated in Figure 5.3B). The first, *phaA*, codes for β -ketothiolase, which catalyses the formation of acetoacetyl-CoA from two acetyl-CoA molecules. The second, *phaB*, codes for an acetoacetyl-CoA reductase, which catalyses the reduction of acetoacetyl-CoA to 3-hydroxybutyryl-CoA. PHB is then produced through polymerization by PHB synthase.

To prevent the cell from being able to produce glycogen, a deletion was introduced into two adjacent genes encoding proteins involved in the biosynthetic pathway of glycogen (illustrated in Figure 5.3C). The first, *glgC*, codes for ADP-glucose pyrophosphorylase (also known as glucose-1-phosphate adenylyltransferase), which catalyses the creation of ADP-glucose from ATP and glucose-1-phosphate. The second, *glgA*, codes for glycogen synthase, which catalyses the polymerisation of glucose residues from ADP-glucose into glycogen

5.1.4 Testing for loss of PHB and glycogen biosynthetic capability in the knockouts

Although these strains had been tested by PCR at the time of construction to confirm that the intended deletions had been made, no attempt had been made to confirm the loss of glycogen or PHB biosynthetic capability. Therefore, before attempting to introduce heterologous biosynthetic pathways, further experiments were conducted to verify that these strains were indeed incapable of producing PHB and / or glycogen, as applicable.

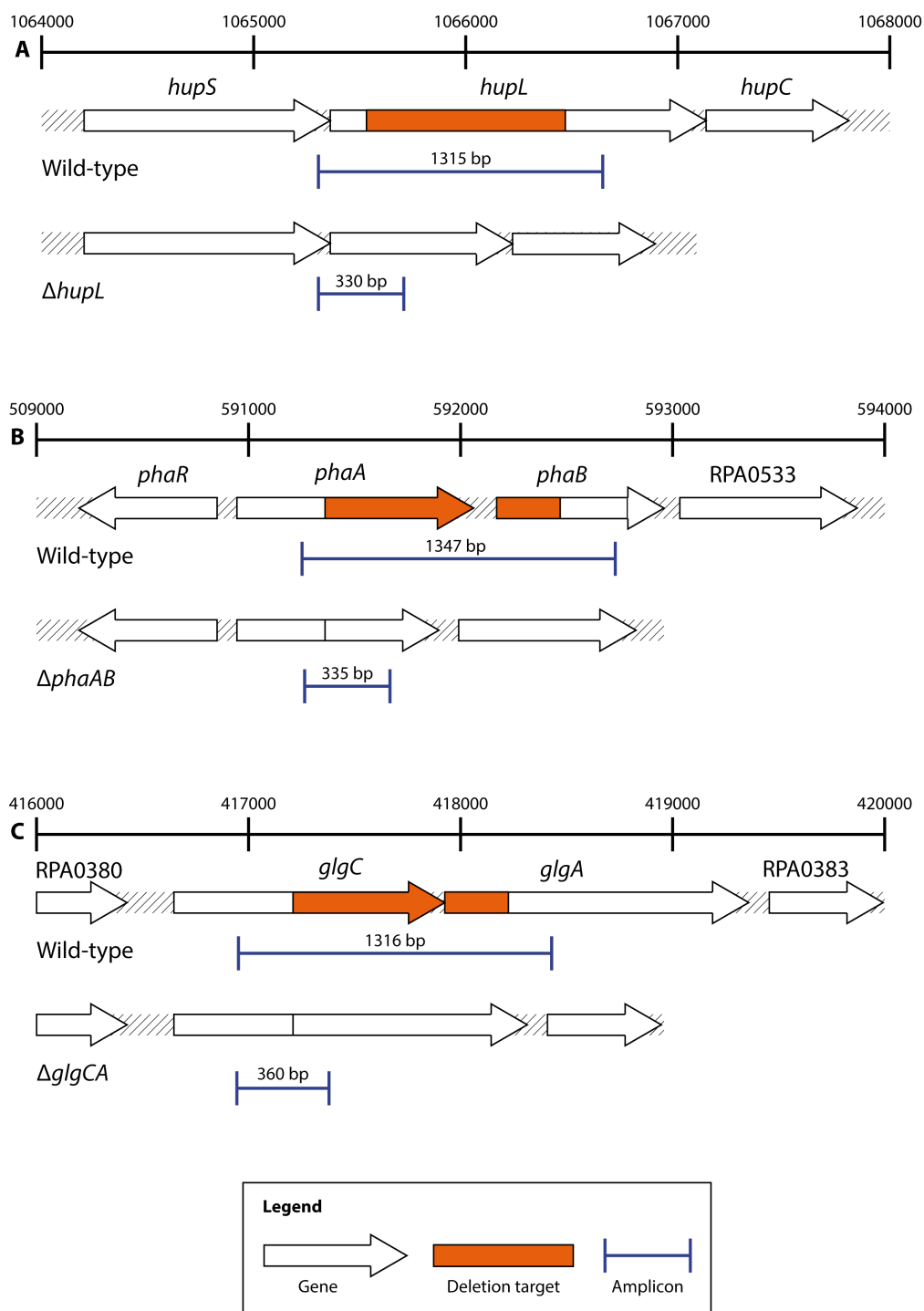


Figure 5.3: Diagrammatic representation of the deletions introduced by David Lea-Smith and Toby Call into (A) *hupL*, encoding a subunit of the uptake hydrogenase; (B) *phaA* and *phaB*, encoding enzymes of the PHB biosynthetic pathway; (C) *glgC* and *glgA*, encoding enzymes of the glycogen biosynthetic pathway. Genes are represented in white, areas targeted for deletion are represented in orange, and the regions amplified by PCR for verification purposes are represented by blue lines; the lengths of the expected products are shown above these.

Furthermore, the initial PCR verification, carried out in the manner described in Chapter 2, only tested for a deletion in the target area of the genome. It was therefore decided to carry out further analysis by PCR using primers homologous to the sequence within the targeted deletion, rather than spanning it. In the event that a copy of the target sequence had been relocated elsewhere in the genome (creating the potential for generation of a functional gene subsequently by recombination), an amplification product would be obtained.

In order to establish these as potential chassis strains for biotechnological applications with *R. palustris*, it was also important to characterize their growth. A strain capable of producing target compounds more efficiently might not be useful if growth were impaired to the detriment of overall rate of product generation. In addition, the hydrogen production of the strains was characterized. As stated earlier, it was possible that the strains carrying the *hupL* deletion would produce hydrogen more efficiently, as the uptake hydrogenase would not be able to break down and recycle molecular hydrogen, and the hydrogen production of the strains carrying the *phaAB* and *glgCA* deletions may also have been increased in response to higher levels of surplus energy and reducing power.

All six strains were tested. If the $\Delta phaAB\Delta glgCA$ strain were subsequently found to produce more target compound than the wild type, then the heterologous genes could be inserted into the $\Delta phaAB$ and $\Delta glgCA$ strains separately to assess the contribution of each deletion, thus making these single-deletion strains of interest to this project. The $\Delta hupL$ strains were of interest as the true background strains for the insertions: if growth were found to be impaired for the $\Delta hupL$ strain, it would indicate that development of a different delivery plasmid for introducing heterologous genes was vital to the successful implementation of this biotechnological application. Given its commercial value, the hydrogen-producing potential of these strains was also of interest.

5.2 Chapter Aims

The first aim of this section was therefore to verify the six knockout strains listed in Table 5.1, before introducing any heterologous gene(s). This would involve both further testing by PCR to ensure the deleted genetic material was no longer present in the genome, and glycogen and PHB assays to test whether production of these compounds had indeed been disrupted.

The next aim was to characterise growth and hydrogen production of these strains.

For introducing the heterologous pathways for isoprene and propane-1,2-diol into *R. palustris* it was necessary to identify whether any of the required enzymes were already present, which would be carried out using BLAST analyses.

Having identified which genes needed to be introduced, suitable promoter and terminator sequences would then be chosen to accompany the desired genes, and the plasmids assembled.

Finally, the heterologous genes would be introduced into both the wild-type and the $\Delta phaAB\Delta glgCA$ strain, and their presence checked by PCR. Expression of the introduced genes would be checked by RT-PCR, and in the event of expression at the RNA level strains carrying tagged versions of the heterologous genes would be tested for protein expression by Western blot. The untagged versions would then be tested, if appropriate, for isoprene or propane-1,2-diol production as relevant, via gas chromatography or high-performance liquid chromatography respectively, and production compared between the different strains.

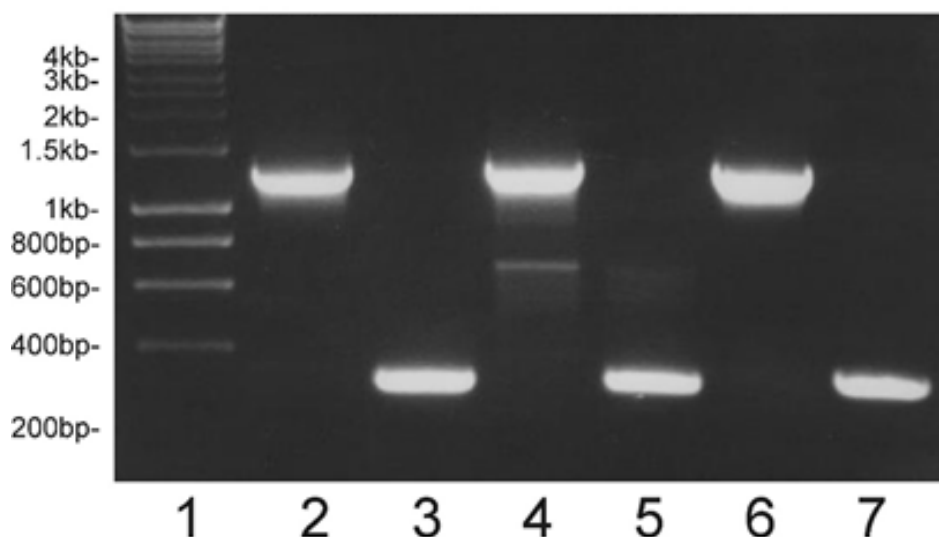


Figure 5.4: Visualisation of amplification products generated by PCR from wild-type *R. palustris* and from the $\Delta hupL\Delta phaAB\Delta glgCA$ strain, with primers spanning the targeted deletion sites. Lanes: (1) DNA ladder; (2) wild-type / *hupL* primers; (3) knockout / *hupL* primers; (4) wild-type / *phaAB* primers; (5) knockout / *phaAB* primers; (6) wild-type / *glgCA* primers; (7) knockout / *glgCA* primers. Data provided by Dr David Lea-Smith.

5.3 Results

5.3.1 PCR verification of the *hupL*, *phaAB* and *glgCA* knockouts

When the six *hupL*, *phaAB* and *glgCA* knockouts were originally created by David Lea-Smith and Toby Call, PCR analysis indicated that the targeted deletions were successful. This was undertaken with primers homologous to the genomic sequence either side of the targeted deletion sites ('spanning primers'); a shorter product is expected in a strain carrying the deletion than in the wild-type. The results of this PCR as carried out on the $\Delta hupL\Delta phaAB\Delta glgCA$ strain as an example, conducted by David Lea-Smith, are shown in Figure 5.4. This gel image demonstrates that shorter products were generated from each site in the knockout, and that no long products were generated as from the wild-type.

However, it is always possible that the supposedly deleted sequence could have been reinserted elsewhere in the genome. This might be problematic if subsequent recombination events were able to regenerate the disrupted locus. In order to test for this, primers were designed homologous to the sequence within the target deletion site. In this case no product would be expected in an unmarked strain carrying the deletion; the wild-type acts as a positive control. An illustration of these two setups is shown in Figure 5.5.

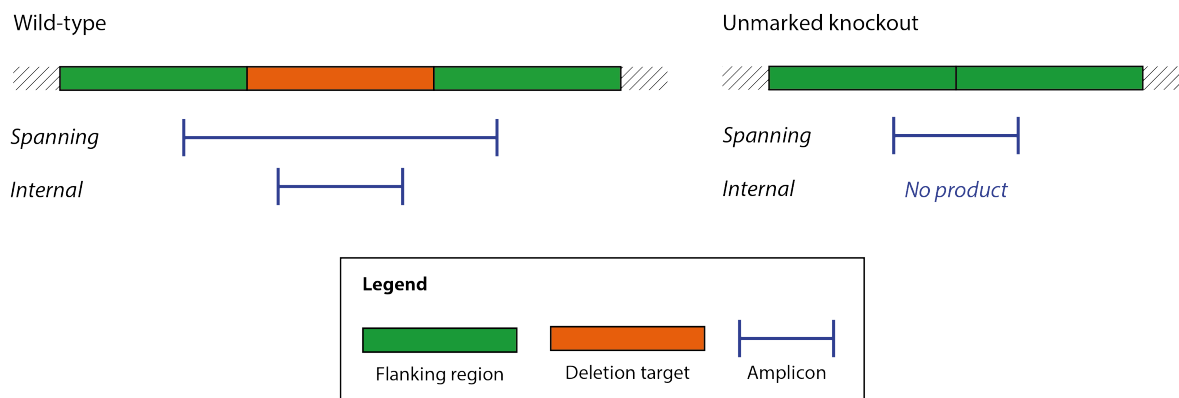


Figure 5.5: Diagrammatic illustration of the different primers used to test possible *R. palustris* knockouts. Spanning primers are complementary to the regions flanking the targeted deletion sites, and generate a shorter product from the unmarked knockout than from the wild-type. Internal primers are complementary to the targeted deletion sequence, and generate no product from the unmarked knockout, but do generate a product from the wild-type.

All six strains were subsequently tested by PCR with each of the three pairs of ‘internal primers’. The PCR was also repeated with the spanning primers on all six strains for further confirmation. The primers are listed in Table 5.2. The resulting gel images for the $\Delta hupL\Delta phaAB\Delta glgCA$ strain, carrying all three deletions, are shown in Figure 5.6. They show that shorter products only were generated from the knockout strain with the spanning primers, and that no products were visible with the internal primers. This indicates that all three deletions were successful and that the targeted material is no longer present in the genome. The resulting gel images for the other five strains are shown in Figures 5.7 - 5.11. Of particular note is the image for the $\Delta phaAB\Delta glgCA$ strain, into which the heterologous genes were later introduced, shown in Figure 5.11. Again, the image shows that the *phaAB* and *glgCA* deletions were fully successful.

Primer	Sequence	Expected product size / bp	
<i>hupL</i> Spanning Forward	TCATGACCAACGTCACGACT	Wild-type	1315
<i>hupL</i> Spanning Reverse	AGCGTCTTCAGGAGCTTTTC	Knockout	330
<i>hupL</i> Internal Forward	CAATACCATCCGCAACATCA	Wild-type	603
<i>hupL</i> Internal Reverse	CCGTAGGACATCACCGACTT	Knockout	-
<i>phaAB</i> Spanning Forward	ACTGATGAACGGCGACTCC	Wild-type	1347
<i>phaAB</i> Spanning Reverse	CTCGAGCGTCATCTTGTGAA	Knockout	335
<i>phaAB</i> Internal Forward	GGATCTCGGCTGGGATACTT	Wild-type	448
<i>phaAB</i> Internal Reverse	CTTTC AACGCCTTGCTGATT	Knockout	-
<i>glgCA</i> Spanning Forward	CGACATCATCGAGAGCTACG	Wild-type	1316
<i>glgCA</i> Spanning Reverse	AGCACATCCGGCTTGTAGTG	Knockout	360
<i>glgCA</i> Internal Forward	TTCGAGACCAAGTTCCTGCT	Wild-type	546
<i>glgCA</i> Internal Reverse	ATCTTCACCGACCACCAGAC	Knockout	-

Table 5.2: List of primers used to test potential $\Delta hupL$, $\Delta phaAB$ and $\Delta glgCA$ transformants.

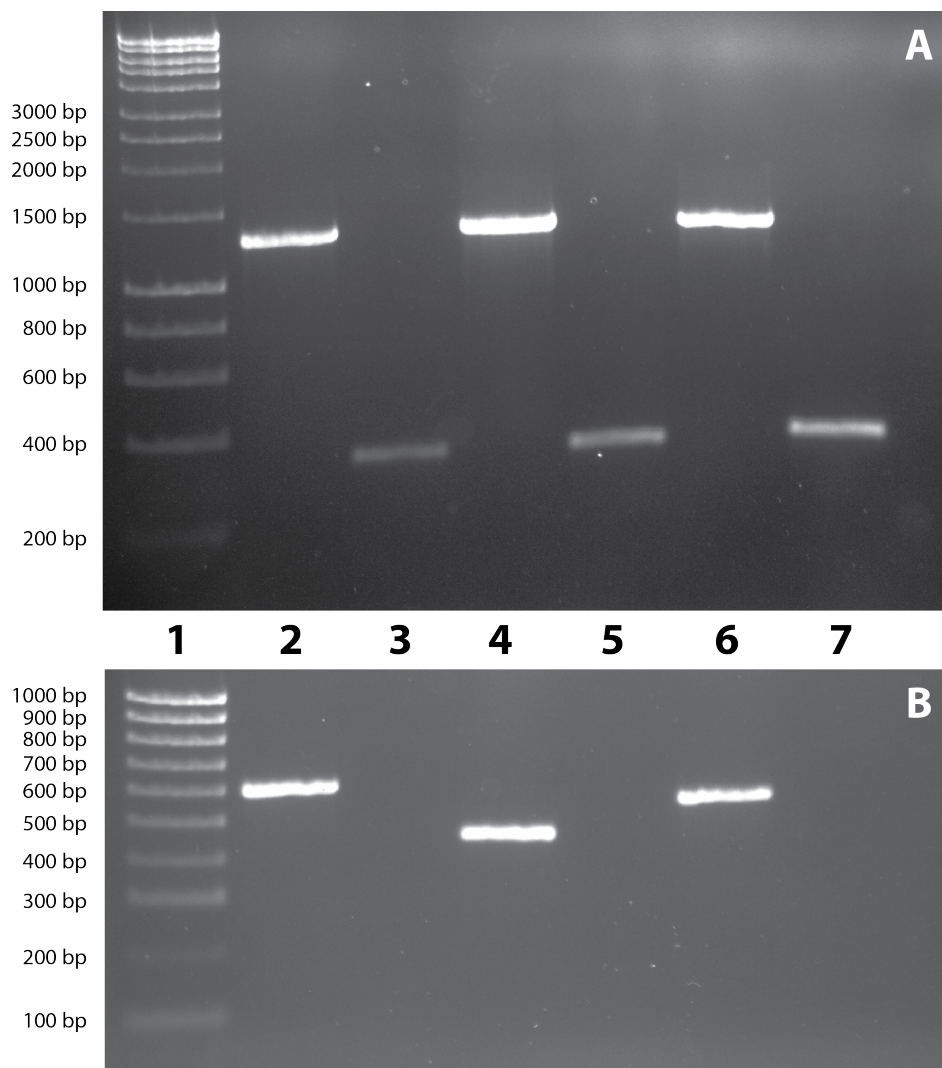


Figure 5.6: Visualisation of amplification products generated by PCR from wild-type *R. palustris* and from the $\Delta hupL\Delta phaAB\Delta glgCA$ strain, with (A) primers spanning the targeted deletion sites in *hupL*, *phaAB* and *glgCA* and (B) primers located within the targeted deletion sites. Lanes: (1) DNA ladder; (2) wild-type / *hupL* primers; (3) knockout / *hupL* primers; (4) wild-type / *phaAB* primers; (5) knockout / *phaAB* primers; (6) wild-type / *glgCA* primers; (7) knockout / *glgCA* primers.

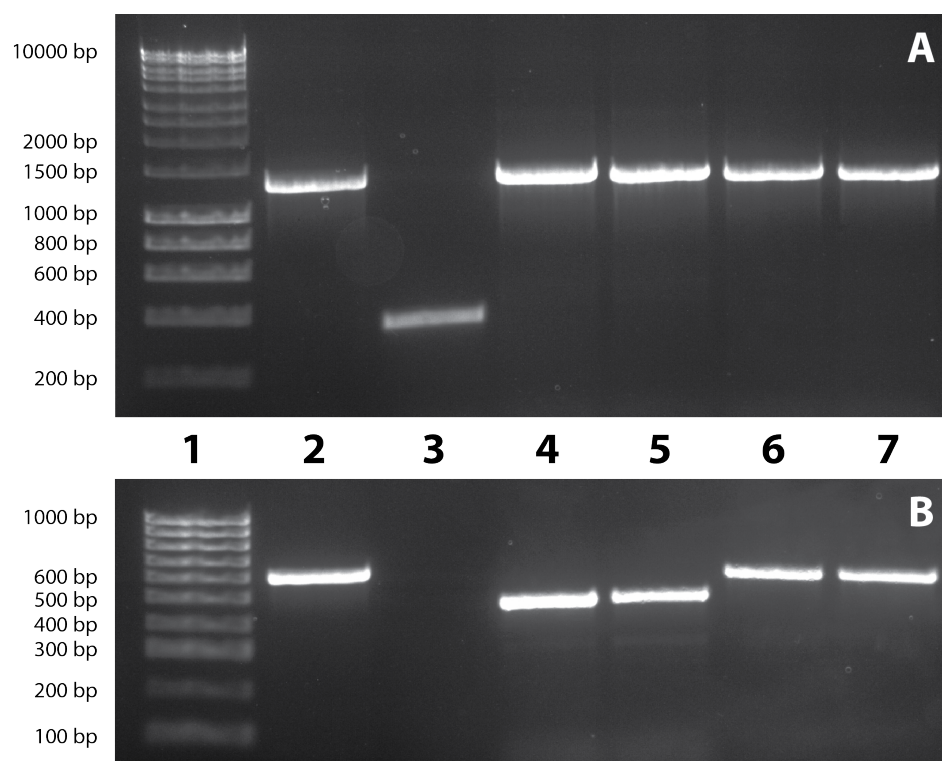


Figure 5.7: Visualisation of amplification products generated by PCR from wild-type *R. palustris* and from the $\Delta hupL$ strain, with (A) primers spanning the targeted deletion sites in *hupL*, *phaAB* and *glgCA* and (B) primers located within the targeted deletion sites. Lanes: (1) DNA ladder; (2) wild-type / *hupL* primers; (3) knockout / *hupL* primers; (4) wild-type / *phaAB* primers; (5) knockout / *phaAB* primers; (6) wild-type / *glgCA* primers; (7) knockout / *glgCA* primers.

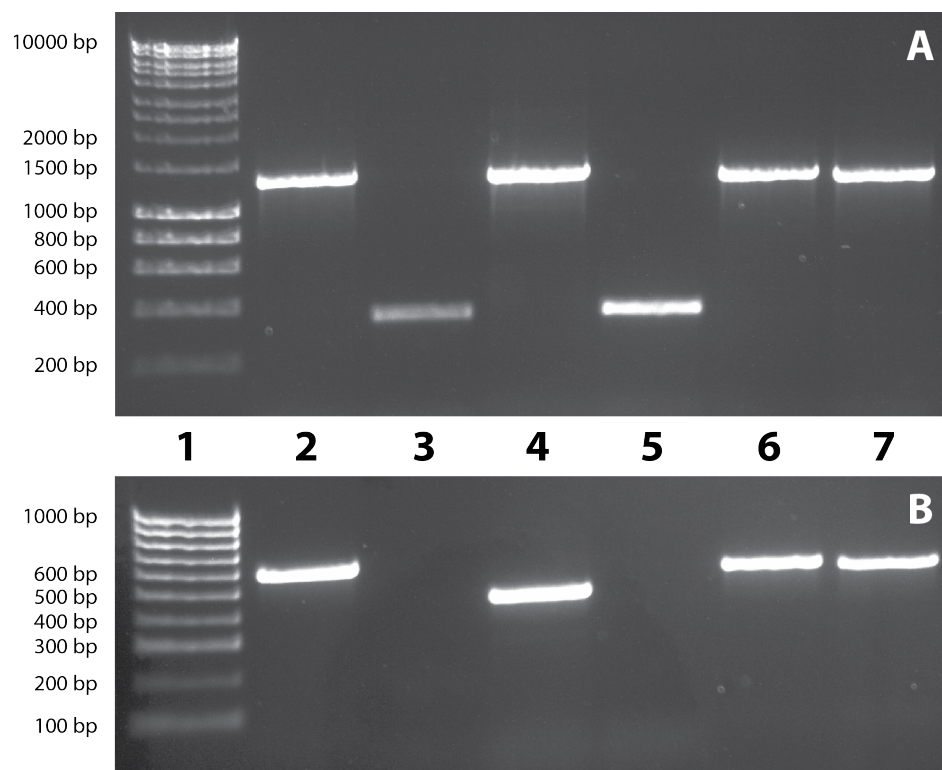


Figure 5.8: Visualisation of amplification products generated by PCR from wild-type *R. palustris* and from the $\Delta hupL\Delta phaAB$ strain, with (A) primers spanning the targeted deletion sites in *hupL*, *phaAB* and *glgCA* and (B) primers located within the targeted deletion sites. Lanes: (1) DNA ladder; (2) wild-type / *hupL* primers; (3) knockout / *hupL* primers; (4) wild-type / *phaAB* primers; (5) knockout / *phaAB* primers; (6) wild-type / *glgCA* primers; (7) knockout / *glgCA* primers

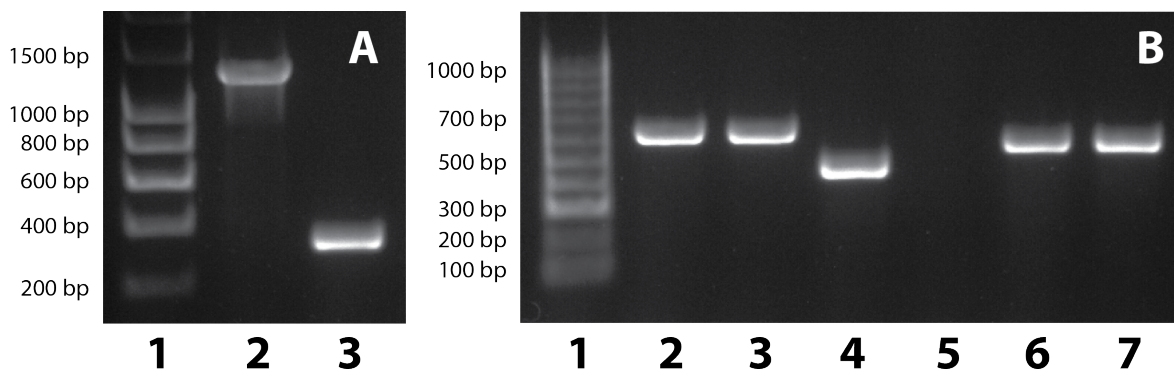


Figure 5.9: Visualisation of amplification products generated by PCR from wild-type *R. palustris* and from the $\Delta phaAB$ strain. Primers (A) spanning the targeted *phaAB* deletion site. Lanes (A): (1) DNA ladder; (2) wild-type; (3) knockout. Primers (B) located within the targeted deletion sites in *hupL*, *phaAB* and *glgCA*. Lanes (B): (1) DNA ladder; (2) wild-type / *hupL* primers; (3) knockout / *hupL* primers; (4) wild-type / *phaAB* primers; (5) knockout / *phaAB* primers; (6) wild-type / *glgCA* primers; (7) knockout / *glgCA* primers.

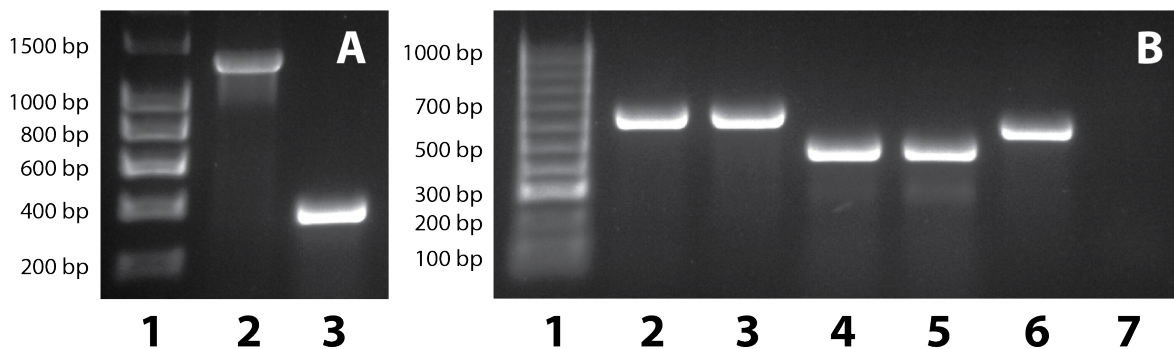


Figure 5.10: Visualisation of amplification products generated by PCR from wild-type *R. palustris* and from the $\Delta glgCA$ strain. Primers (A) spanning the targeted *glgCA* deletion site. Lanes (A): (1) DNA ladder; (2) wild-type; (3) knockout. Primers (B) located within the targeted deletion sites in *hupL*, *phaAB* and *glgCA*. Lanes (B): (1) DNA ladder; (2) wild-type / *hupL* primers; (3) knockout / *hupL* primers; (4) wild-type / *phaAB* primers; (5) knockout / *phaAB* primers; (6) wild-type / *glgCA* primers; (7) knockout / *glgCA* primers.

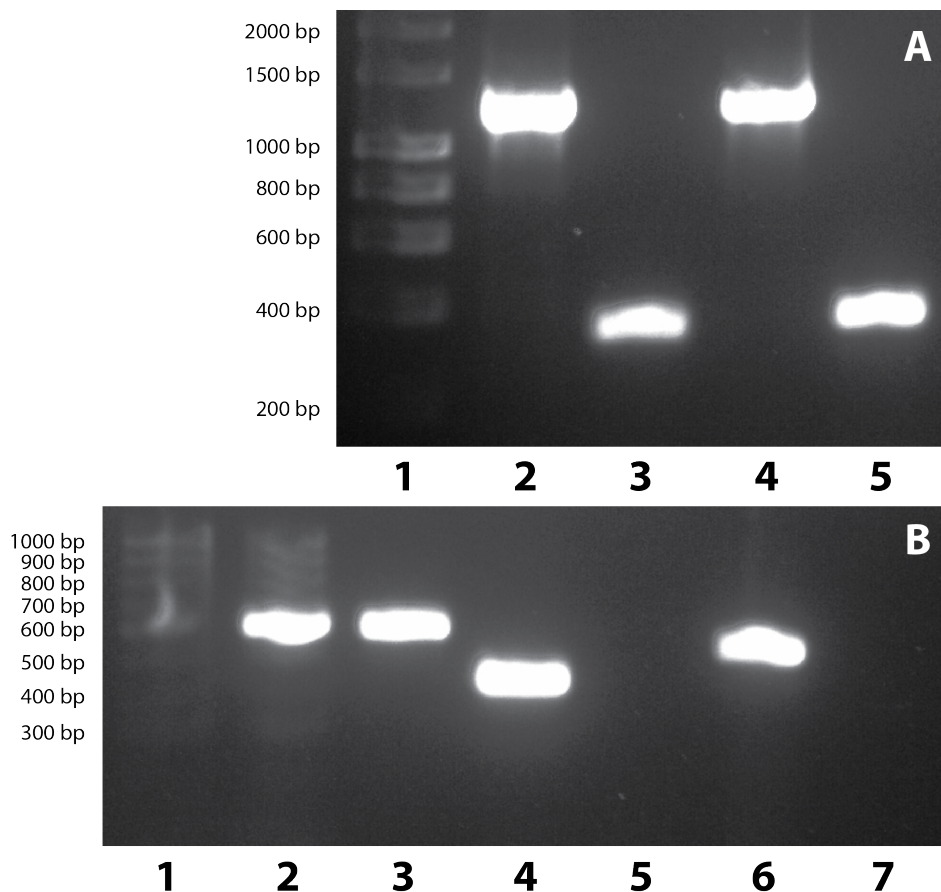


Figure 5.11: Visualisation of amplification products generated by PCR from wild-type *R. palustris* and from the $\Delta phaAB\Delta glgCA$ strain. Primers (A) spanning the targeted *phaAB* and *glgCA* deletion sites. Lanes (A): (1) DNA ladder; (2) wild-type / *phaAB* primers; (3) knockout / *phaAB* primers; (4) wild-type / *glgCA* primers; (5) knockout / *glgCA* primers. Primers (B) located within the targeted deletion sites in *hupL*, *phaAB* and *glgCA*. Lanes (B): (1) DNA ladder; (2) wild-type / *hupL* primers; (3) knockout / *hupL* primers; (4) wild-type / *phaAB* primers; (5) knockout / *phaAB* primers; (6) wild-type / *glgCA* primers; (7) knockout / *glgCA* primers.

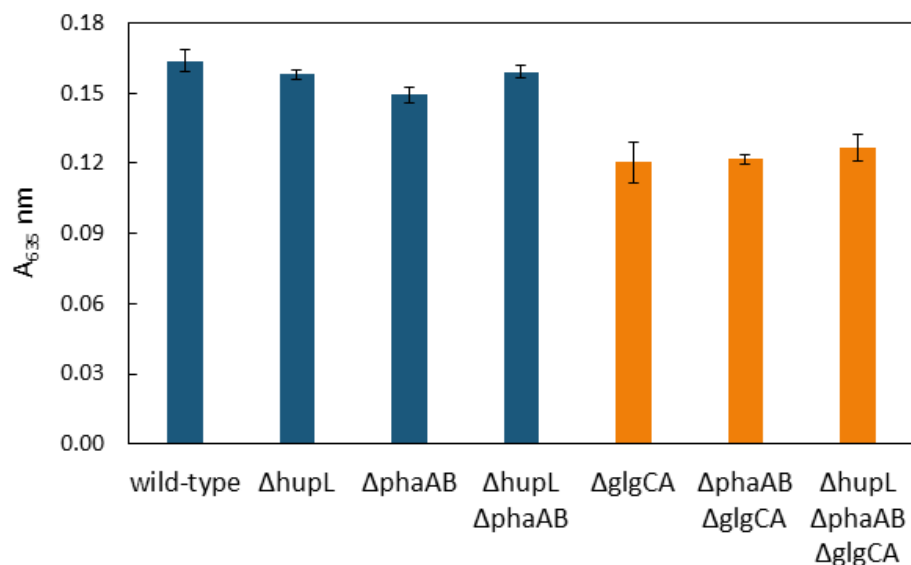


Figure 5.12: Absorbance at 635 nm of samples from *o*-toluidine glycogen assay. A sample of PBS only, containing no cells but which had been treated in the same manner, was used to blank the spectrometer. For clarity, samples from strains carrying the *glgCA* deletion are coloured in orange, while samples from strains without the deletion are coloured in blue. Mean of three replicates; bars show standard error.

5.3.2 Glycogen and PHB assays of the *hupL*, *phaAB* and *glgCA* knockouts

Following this, all six knockout strains were assayed for glycogen and PHB levels, to investigate whether or not the deletions had resulted in a loss of biosynthetic capability for these two compounds. It was important to do this as verification by PCR in the manner described previously relies entirely on a negative result, the absence of a visible band. For the spanning primers it is possible that the band representing the larger wild-type sequence was not seen simply because the PCR produced the larger molecules less efficiently (although if this were the case one might still expect the PCR reactions with primers internal to the target regions to generate products).

An *o*-toluidine assay described in Chapter 2 was used to test for glycogen levels. The samples are first subjected to sulfuric acid in order to break down any glycogen present into glucose. The *o*-toluidine, an aromatic amine, reacts with the glucose in glacial acetic acid when hot, producing a stable blue-green colour which can be measured using A_{635} , indicating the concentration of glucose within the sample [82]. Given that there is likely to be some glucose present within the cells already, some absorbance is expected from all samples.

The results of this assay are displayed in Figure 5.12, and show that all strains carrying the *glgCA*

	Degrees of Freedom	Sum of Squares	Mean Square	F Value	P(>F)
Strain	6	0.0065493	0.0010916	24.206	0.000001246
Residuals	14	0.0006313	0.0000451		

Table 5.3: ANOVA table for glycogen assay data presented in Figure 5.12.

Strain 1	Strain 2	Absolute Difference	p-value
Wild-type	$\Delta glgCA$	0.0433	0.0000258 **
Wild-type	$\Delta phaAB \Delta glgCA$	0.0420	0.0000368 **
Wild-type	$\Delta hupL \Delta phaAB \Delta glgCA$	0.0370	0.0001486 **
$\Delta phaAB$	$\Delta phaAB \Delta glgCA$	0.0277	0.0026190 **
$\Delta hupL \Delta phaAB$	$\Delta hupL \Delta phaAB \Delta glgCA$	0.0323	0.0005987 **
Wild-type	$\Delta hupL$	0.0057	0.9372403
Wild-type	$\Delta phaAB$	0.0143	0.1934566
Wild-type	$\Delta hupL \Delta phaAB$	0.0047	0.9744046
$\Delta hupL$	$\Delta phaAB$	0.0087	0.6957600
$\Delta hupL$	$\Delta glgCA$	0.0377	0.0001227 **
$\Delta hupL$	$\Delta phaAB \Delta glgCA$	0.0363	0.0001804 **
$\Delta hupL$	$\Delta hupL \Delta phaAB$	0.0010	0.9999955
$\Delta hupL$	$\Delta hupL \Delta phaAB \Delta glgCA$	0.0313	0.0008161 **
$\Delta phaAB$	$\Delta glgCA$	0.0290	0.0017050 **
$\Delta phaAB$	$\Delta hupL \Delta phaAB$	0.0097	0.5898979
$\Delta phaAB$	$\Delta hupL \Delta phaAB \Delta glgCA$	0.0227	0.0135962 *
$\Delta hupL \Delta phaAB$	$\Delta glgCA$	0.0387	0.0000923 **
$\Delta hupL \Delta phaAB$	$\Delta phaAB \Delta glgCA$	0.0373	0.0001350 **
$\Delta glgCA$	$\Delta phaAB \Delta glgCA$	0.0013	0.9999754
$\Delta glgCA$	$\Delta hupL \Delta phaAB \Delta glgCA$	0.0063	0.8995719
$\Delta phaAB \Delta glgCA$	$\Delta hupL \Delta phaAB \Delta glgCA$	0.0050	0.9644444

Table 5.4: Results of pair-wise comparisons by Tukey's HSD on the glycogen assay data presented in Figure 5.12. Difference significant at 5% indicated by *. Difference significant at 1% indicated by **.

deletion gave rise to lower absorbance, indicating lower levels of glycogen at least, and therefore presumably a reduction in glycogen biosynthesis. Analysis by One-Way ANOVA, presented in Table 5.3, generated a p-value < 0.00001 , showing there was a statistically significant difference in absorbance between strains. Post-hoc testing by Tukey's HSD indicated a significant difference between the wild-type and each of the strains carrying the *glgCA* deletion (all pair-wise tests $p < 0.001$), and a significant difference between each strain carrying the *glgCA* deletion and its equivalent background strain (i.e. $\Delta phaAB \Delta glgCA$ compared to $\Delta phaAB$, $p < 0.01$; $\Delta hupL \Delta phaAB \Delta glgCA$ compared to $\Delta hupL \Delta phaAB$, $p < 0.001$); see Table 5.4.

A Nile Red fluorescence assay, as described in Chapter 2, was used to compare PHB levels [75]. Nile Red binds to lipids, fluorescing as a result [83], which can be used as an indicator of PHB levels as PHB is stored within lipid-coated granules in the cell. However, as there are many other sources

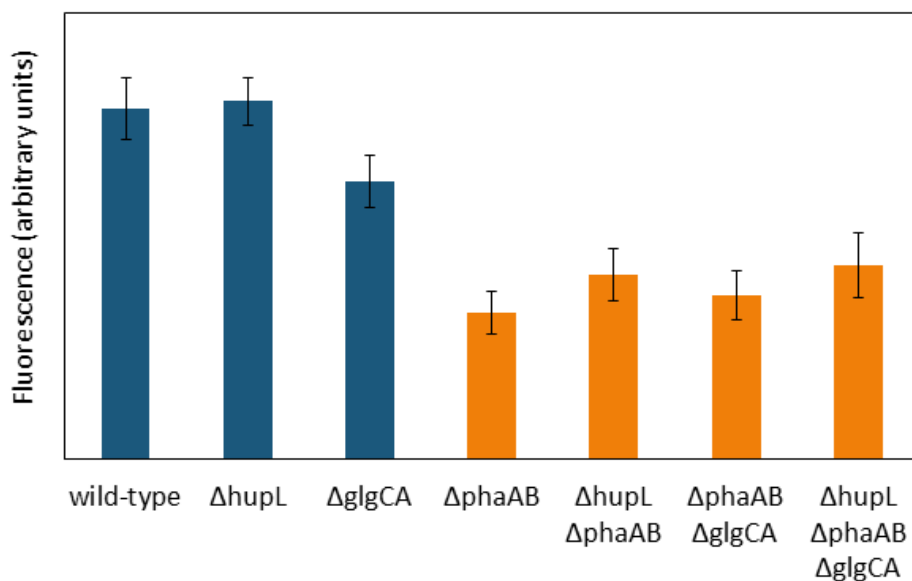


Figure 5.13: Fluorescence of samples incubated with Nile Red solution, excited at 510 nm with emission measured at 590 nm. The fluorescence displayed is relative both to samples containing no Nile Red and to samples containing no cells, and is the mean of three technical replicates with bars showing error: for details see Chapter 2. For clarity, samples from strains carrying the *phaAB* deletion are coloured orange, while samples from strains without the deletion are coloured blue.

of lipids within a cell, strains which do not contain any PHB will also fluoresce in the presence of Nile Red. Again, therefore, some fluorescence is always to be expected from all strains.

The results of this assay are displayed in Figure 5.13, and showed that all strains carrying the *phaAB* deletion gave rise to less fluorescence in the presence of Nile Red, indicating at least lower levels of PHB, and therefore presumably a reduction in PHB biosynthesis. The absolute value of fluorescence measured varied considerably between experiments, and so the data displayed is from one biological replicate only; the error bars indicate the error in three technical replicates.

If more certainty were required it may be possible to use different methods to verify that PHB and glycogen synthesis were entirely abolished. For example, PHB granules can be detected by fluorescence microscopy after staining with Nile Red [75], or cellular levels can be quantified spectrophotometrically after extraction [84]. Confirmation of a detectable reduction in PHB and glycogen synthesis was sufficient for the purposes of this work, however.

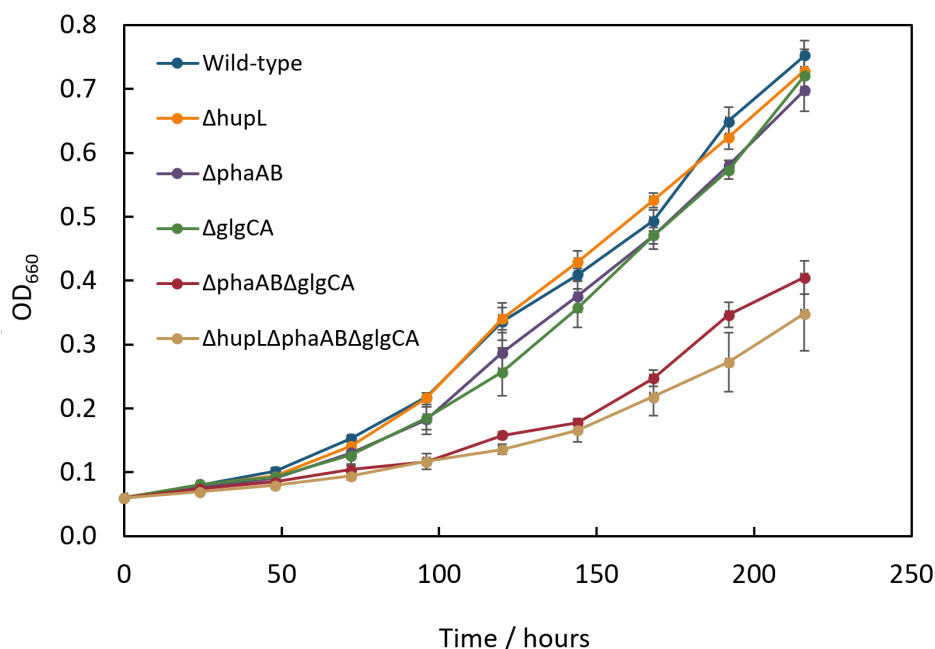


Figure 5.14: Optical density measured at 660 nm of *R. palustris* cultivated in the cultivation cabinet described in Chapter 3 under standard lighting and an anaerobic atmosphere: wild-type (blue); $\Delta hupL$ (orange); $\Delta phaAB$ (red); $\Delta glgCA$ (green); $\Delta phaAB\Delta glgCA$ (purple); $\Delta hupL\Delta phaAB\Delta glgCA$ (brown). Mean of three replicates each; bars show standard error.

5.3.3 Characterization of the *hupL*, *phaAB* and *glgCA* knockouts

Having verified the deletions and confirmed that levels of glycogen and PHB have been significantly reduced (or abolished), the growth of the knockout strains was characterized. As incubator space was limited to six samples in total for the time available, and the wild-type was included as a control, the $\Delta hupL\Delta phaAB$ strain was omitted from these experiments. The three individual knockouts were included to allow the effects of each individual deletion to be assessed. The $\Delta hupL\Delta phaAB\Delta glgCA$ strain was of interest by virtue of carrying all three deletions, and effectively being the background strain for the heterologous insertions carried out later (since the insertions would inactivate *hupL*). The $\Delta phaAB\Delta glgCA$ strain was of interest because of the possible cumulative effect of knocking out both PHB and glycogen synthesis, on both growth and potential synthesis of target compounds. The strains were cultivated as described in Chapters 2 and 3, and the results taken from three replicates are shown in Figure 5.14.

Analysis by One-Way ANOVA of the optical densities at time $t = 216$ hours, presented in Table 5.5, generated a p -value < 0.000001 , indicating a statistically significant difference between the strains. Post-hoc testing with Tukey's HSD found no significant difference between the wild-type and any

	Degrees of Freedom	Sum of Squares	Mean Square	F Value	P(>F)
Strain	5	0.49285	0.098570	37.838	0.000006102
Residuals	12	0.03126	0.002605		

Table 5.5: ANOVA table for growth assay data from timepoint t = 216 hours presented in Figure 5.14.

Strain 1	Strain 2	Absolute Difference	p-value
Wild-type	$\Delta hupL$	0.0227	0.9929488
Wild-type	$\Delta phaAB$	0.0533	0.7901849
Wild-type	$\Delta glgCA$	0.0310	0.9720042
$\Delta hupL$	$\Delta phaAB$	0.0307	0.9732541
$\Delta hupL$	$\Delta glgCA$	0.00833	0.9999425
$\Delta phaAB$	$\Delta glgCA$	0.0223	0.9934101
Wild-type	$\Delta phaAB\Delta glgCA$	0.346	0.0000293 **
$\Delta hupL$	$\Delta phaAB\Delta glgCA$	0.324	0.0000582 **
$\Delta phaAB$	$\Delta phaAB\Delta glgCA$	0.293	0.0001551 **
$\Delta glgCA$	$\Delta phaAB\Delta glgCA$	0.315	0.0000755 **
Wild-type	$\Delta hupL\Delta phaAB\Delta glgCA$	0.403	0.0000061 **
$\Delta hupL$	$\Delta hupL\Delta phaAB\Delta glgCA$	0.380	0.0000112 **
$\Delta phaAB$	$\Delta hupL\Delta phaAB\Delta glgCA$	0.349	0.0000269 **
$\Delta glgCA$	$\Delta hupL\Delta phaAB\Delta glgCA$	0.372	0.0000141 **
$\Delta phaAB\Delta glgCA$	$\Delta hupL\Delta phaAB\Delta glgCA$	0.0563	0.7528152

Table 5.6: Results of pair-wise comparisons by Tukey's HSD on the data from timepoint t = 216 hours presented in Figure 5.14. Difference significant at 5% indicated by *. Difference significant at 1% indicated by **.

of the single knockouts, nor between the double knockout $\Delta phaAB\Delta glgCA$ and triple knockout $\Delta hupL\Delta phaAB\Delta glgCA$. There was however a significant difference between the wild-type and each of these two strains ($p < 0.0001$ and $p < 0.00001$ respectively). The full set of pair-wise comparisons is shown in Table 5.6. This suggests that the combined gene deletions had an impact on growth, but that individual deletions had little effect if any by themselves. Deletion of *hupL* appears to have no significant effect on growth.

An attempt was also made to characterize the hydrogen production of the knockout strains. The volume of gas produced was measured from one set of repeats of the same cultures as above, and so the $\Delta hupL\Delta phaAB$ strain was once again not included. Immediately after the optical density was measured at the final time-point (216 hours) the cultures were set up for measurement of gas volume. The total volume produced after four hours was recorded. It was unfortunately not possible in the time available to measure the purity of hydrogen within the gas, so in interpreting these results (Figure 5.15), it must be recognised that the composition of the gas may vary between strains. However, very high levels of hydrogen purity have been reported in the past for gas production

by *R. palustris* under essentially identical growth conditions, up to 97 mol% ([40]; in the experiment described here the cells received 50 mM glycerol rather than 100 mM, but were also grown anaerobically with sodium glutamate as a source of fixed nitrogen), suggesting that changes in gas production are a reasonable indicator of changes in hydrogen production.

These results show that the $\Delta phaAB\Delta glgCA$ and $\Delta hupL\Delta phaAB\Delta glgCA$ strains had lower absolute levels of gas output, unsurprisingly given their lower cell densities. Normalising to cell density indicated that these strains had the highest levels of gas output per unit biomass, with the $\Delta phaAB\Delta glgCA$ strain producing 1.4-fold more gas than the wild-type. This suggests that removing the PHB and glycogen storage compounds creates an excess of energy or substrate, and/or a redox imbalance within the cell, resulting in greater hydrogen output. The $\Delta glgCA$ strain was also observed to produce the most gas both in absolute quantity and on a per cell basis than the wild-type or other single deletion strains, though the difference was not great in the latter case. It is therefore possible that inactivating glycogen synthesis has a more substantial effect on hydrogen output than inactivating PHB synthesis, but further investigation, especially replication, would be required to confirm this.

Interestingly, the *hupL* deletion did not appear to increase output in comparison to equivalent strains. This is consistent with the finding that the sequenced strain of *R. palustris*, CGA009, was discovered to behave like a hydrogen uptake mutant, and was subsequently found to carry a frameshift mutation in *hupV*, encoding a protein involved in regulating the uptake hydrogenase in response to hydrogen levels (Figure 5.16, [4]). Although it would remove the possibility of improving hydrogen output further through manipulation of this system if our stock of CGA009 were a natural uptake hydrogenase mutant, it would also mean that the *hupL* deletion site is potentially a suitable site for insertion of heterologous or other sequences into *R. palustris* without disrupting the normal functioning of the cell.

Given the differences between stocks of supposedly the same strain of some bacteria between different labs (see for example [85]), and the fact that this mutation was likely acquired through cultivation in the laboratory, it was not certain that the stock of CGA009 used here was also a natural uptake hydrogenase mutant. However, this issue should have been identified and verified before the $\Delta hupL$ deletion was created. In response to the growth and hydrogen production results reported here, the same primers as reported by Rey *et al* (Table 5.7) were used to amplify and then sequence a 250 bp region from the *hupV* gene of the CGA009 strain used throughout this work. The

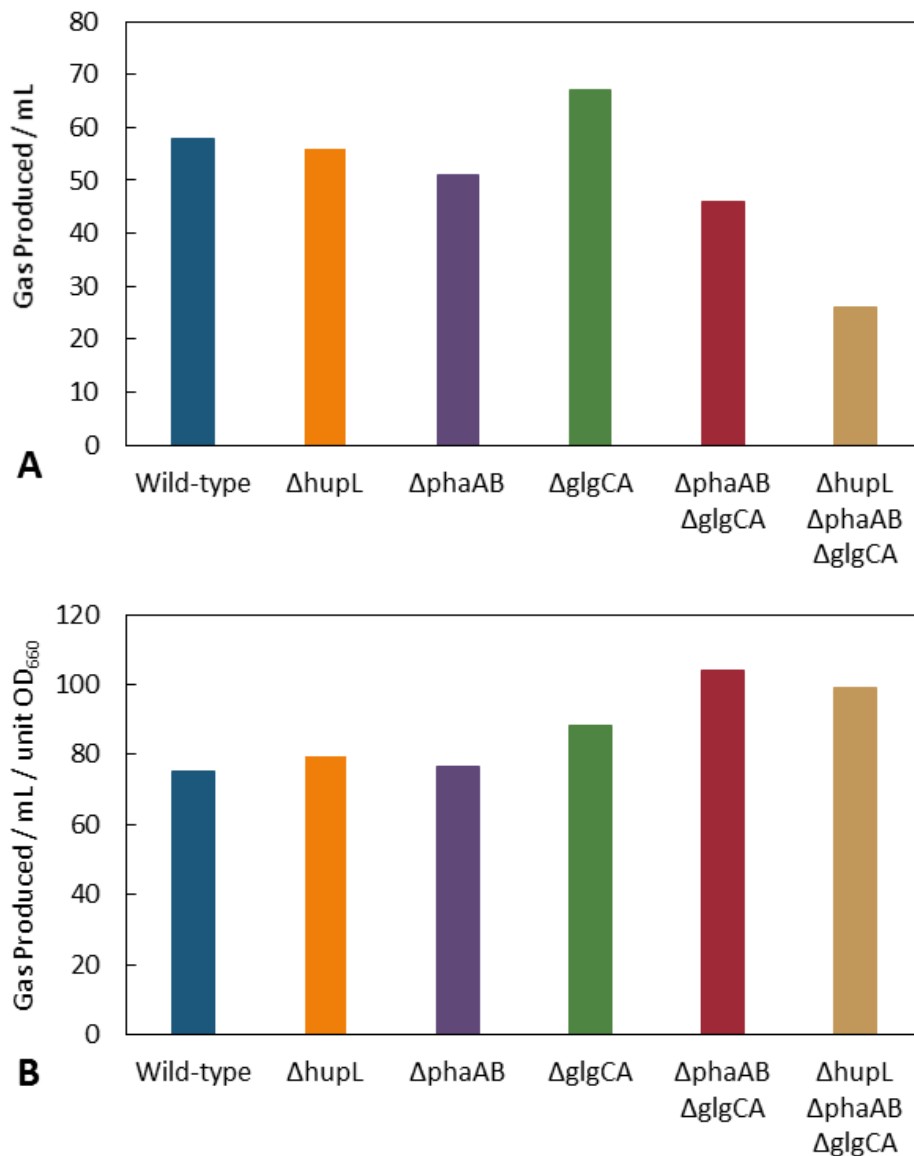


Figure 5.15: (A) Volume of gas produced by *R. palustris* over four hours after 216 hours of growth and (B) volume of gas produced by *R. palustris* over four hours after 216 hours of growth normalised to the optical density of the culture: wild-type (blue); $\Delta hupL$ (orange); $\Delta phaAB$ (purple); $\Delta glgCA$ (green); $\Delta phaAB \Delta glgCA$ (red); $\Delta hupL \Delta phaAB \Delta glgCA$ (brown).

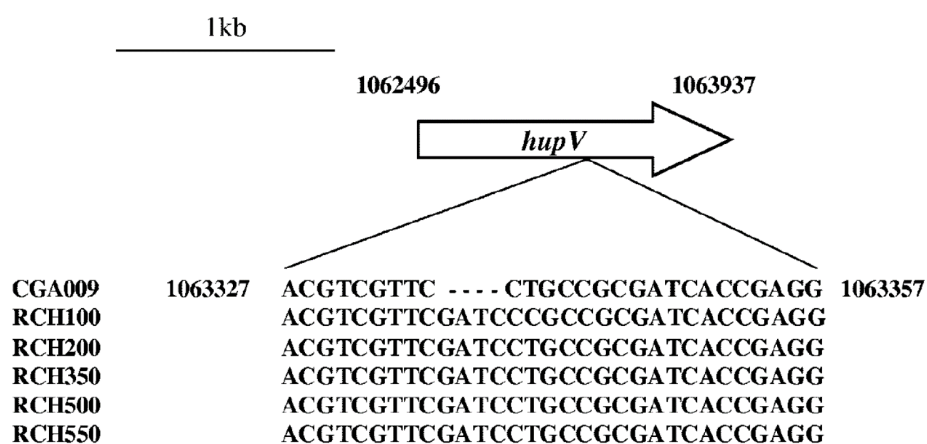


Figure 5.16: Taken from Figure 3, Rey *et al.*, 2006 [4]; sequence alignment of the frameshifted region of *hupV* of the CGA009 strain of *R. palustris* with the corresponding gene regions from five other *R. palustris* strains.

Primer	Sequence	Expected product size / bp
<i>hupV</i> Sequencing Forward	AGGATGCACCGCTGTTTGCGG	250
<i>hupV</i> Sequencing Reverse	ACAATCGCGGATCAGCGGATC	

Table 5.7: Primers used to sequence the putative frameshifted region of *hupV* in *R. palustris*, taken from Rey *et al.*, 2006 [4].

results indicate that the four nucleotide deletion apparent in Figure 5.16 is also present in the strain of CGA009 used throughout this work.

This suggested that the *hupL* locus would be suitable for insertion of heterologous genes, and that the $\Delta phaAB\Delta glgCA$ strain would be a suitable host. Inactivation of *hupL* in a natural up-take hydrogenase mutant would not be expected to have any effect on the functioning of the cell, whether in combination with other deletions or not. If the reduced growth observed in the $\Delta phaAB\Delta glgCA$ and $\Delta hupL\Delta phaAB\Delta glgCA$ strains is the result of redox imbalance, it was hoped that introduction of heterologous pathways for biosynthesis of other compounds might actually restore or at least improve the growth of this strain. The work thus proceeded with attempts to insert heterologous genes into wild-type and mutant strains of *R. palustris* as discussed in section 5.1.

5.3.4 Identification of required heterologous genes

The first step in introducing the pathway for propane-1,2-diol biosynthesis into *R. palustris* was to determine whether the genes for all three of the enzymes required to turn DHAP into propane-1,2-diol would need to be introduced. The nucleotide sequences were obtained from NCBI, *E. coli* strain K-12 substr. MG1655 (Reference Sequence NC_000913.3), and a BLAST search conducted with NCBI (<https://blast.ncbi.nlm.nih.gov/Blast.cgi>) against the *R. palustris* CGA009 genome. No hits were obtained for any of the sequences.

The associated protein sequences were then used in a BLAST search against the protein database for *R. palustris* CGA009. No hits were obtained for the methylglyoxal synthase (accession number AML02437.1). One hit was obtained for the aldehyde oxidoreductase (accession number AML00478.1), with a putative L-threonine dehydrogenase (accession number WP_011156769.1; E value 2×10^{-18} , 25% identity, score of 83.6). No hits were obtained for the glycerol dehydrogenase (accession number AMK99583.1).

The alignment of the hit for the aldehyde oxidoreductase is shown in Figure 5.17. The protein sequence for the *R. palustris* L-threonine dehydrogenase identified in this hit was then used to run a BLAST search against the protein database for *E. coli* str. K-12 substr. MG1655. Eight hits were obtained, the first of which was a generic hit for a proteobacterial alcohol dehydrogenase, and the second of which was an unnamed protein product from *E. coli* str. K-12 substr. MG1655. The third hit was for a 1,2-propanediol oxidoreductase (alt. lactaldehyde reductase; accession number AAB40449.1; E value 2×10^{-100} , 41% identity, score of 300). The alignment for this hit is shown in Figure 5.18.

It was therefore decided to proceed without introducing a heterologous sequence for this gene, although it was not certain that the identified protein would be capable of carrying out the required function for propane-1,2-diol biosynthesis. If the two introduced genes were found to be successfully transcribed and translated, but no propane-1,2-diol production were observed, the sequence for this heterologous gene would also be introduced.

For the insertion of the pathway for isoprene biosynthesis, the sequence for *ispS* was obtained from the supplementary information provided by Lindberg *et al.*, 2010 [68], based on sequence data from Sharkey *et al.*, 2005 [86]. A predicted chloroplast transit peptide had been previously removed by the authors. This sequence was also checked against that from NCBI (GenBank accession number AY31669). The sequence for *ipi* was obtained from NCBI, *P. montana* var. *lobata* (GenBank ac-

L-threonine dehydrogenase [Rhodopseudomonas palustris]

Sequence ID: [WP_011156769.1](#) Length: 383 Number of Matches: 1

Score	Expect	Method	Identities	Positives	Gaps
83.6 bits(205)	2e-18	Compositional matrix adjust.	86/343(25%)	148/343(43%)	23/343(6%)
Query 1	MNNFNLHTPTRILFGKGAIAGLREQIPHDA--RVLITYGGGSVKKTVGLDQVLDAL--KG				56
Sbjct 1	M P+ LFG G ++ + R LI G + K GV DQ+ L +				59
Query 57	MDVLEFGGIEPNPAYETLMNAVKLVREQKVTFLAVGGGSVLDGTFIAAAAANYPENIDP				116
Sbjct 60	+ + F G +PNP + + + + L++++ +++++GGGS D K IA A +I				119
Query 117	WHILQTTGGKEIKSAIPMGCVLTLPATGSESNAGAVISRKTGDKQAFHSAHVQPVFAVLD				176
Sbjct 120	+ + + + +P+ + T T SE +I+ + K A H P+ +V D				176
Query 177	PVYTYTLPPRQVANGVVDVAFVHTVEQYVTKPVDKIQDRFAEGILLTIEDGPKALKEPE				236
Sbjct 177	PV PP A +DA H +E YV+ I D A + + + E +				235
Query 237	NYDVRANVMWAATQALNGLIGAGVPQDWAT---HMLGHELTAMHGLDHAQTLAIVLPAL				292
Sbjct 236	N R + +A G + AG+ + A+ H + H+L + L H A++LP +				288
Query 293	--WNEKRDTKRAKLLQYAEVWNITEGSDDERIDAAAIAATRFN 333				
Sbjct 289	+N + R K + +A V + T +D + DAAI A +				330

Figure 5.17: Alignment of query sequence aldehyde oxidoreductase from *E. coli* str. K-12 substr. MG1655 (AML00478.1) against the one hit obtained from *R. palustris* CGA009, for a putative L-threonine dehydrogenase (WP_011156769.1), taken from NCBI.

1,2-propanediol oxidoreductase (lactaldehyde reductase [Escherichia coli str. K-12 substr. MG1655])

Sequence ID: [AAB40449.1](#) Length: 383 Number of Matches: 1

Score	Expect	Method	Identities	Positives	Gaps
300 bits(769)	2e-100	Compositional matrix adjust.	158/384(41%)	230/384(59%)	4/384(1%)
Query 1	MTATTFIFPSLNLFGAGCVSSAADHAKARGFKRALIVTDSGLHKLGVADQIASMLIERNV				60
Sbjct 1	M A + FG G V + D K RG+++ALIVTD L + GV ++ + +				60
Query 61	TSVVFPGAKPNPTIKNVEDGLALLKQENCDCVISLGGGSAHDCAKGIALTATNG--GSIK				118
Sbjct 61	++ G PNPTI V++GL + + D +I+++GGGS D K I + + N ++				120
Query 119	DYEGVDRSAHAQLPLIAINTTAGTASEMTRFCIITDEERQVKMAIVDRHTTPLLSSVNDPV				178
Sbjct 121	EG+ + +P+++AI TTAGTA+E+T +ITDEE++ K VD H P ++ D				180
Query 179	LMLGKPPALTAATGMDALTHAIEAYVSIATPITDACALKAMSIISNSLRTVVAEGQNLV				238
Sbjct 181	+M G PPAL AATG+DALTHAIE Y++ A +TDA +KA+ II+ +LR VA ++				238
Query 239	AREAMSAGFLAGMAFNASLGYVHAMAHQLGGFYDLPHGVCNAVLLPHVQAYNAQVAAG				298
Sbjct 239	A E M+ ++AGM F+N LG VH MAH LG FY+ PHGV NA+LLPHV YNA				298
Query 299	RLKDVAHALGVDTTGMTDAQGADAAIHAIQRLSADVGIPPLGLGLMKETDVPILAANAL				358
Sbjct 299	+ +D+A +GV GM+ + +AA+ A+ L+ DVGIPP L +G+++ D+P LA AL				358
Query 359	KDACGFTNPKQATQTEIETIFRAA 382				
Sbjct 359	D C NP++AT +I ++ A				382

Figure 5.18: Alignment of query sequence for putative L-threonine dehydrogenase from *R. palustris* CGA009 (WP_011156769.1) against the third hit obtained from *E. coli* str. K-12 substr. MG1655, for 1,2-propanediol oxidoreductase (AAB40449.1), taken from NCBI.

cession number AY315650; the mRNA sequence was converted into the equivalent DNA sequence, and also checked against the protein sequence). BLAST searches (both nucleotide and protein) with NCBI again revealed that *R. palustris* does not possess homologous versions of these genes, though it does encode an IPP isomerase.

All of the above sequences for heterologous genes were then manually codon-optimized for *R. palustris* using the codon table for *R. palustris* str. CGA009 from the Kazusa DNA Research Institute ([87]; www.kazusa.or.jp/codon/). The sequence was altered such that every codon encoding a particular amino acid was present at the frequency indicated by the codon table. Changes made to achieve this were done semi-randomly but with a view to distributing each codon relatively evenly throughout the sequence and while making as few changes as possible. This would be more easily achieved with software designed for the purpose.

5.3.5 Identification of suitable promoter and terminator sequences

The next step was to identify a suitable promoter sequence and a suitable terminator sequence. McKinlay *et al.* in 2013 conducted a nitrogen starvation study on *R. palustris* in which global transcript levels were monitored over the course of a period of nitrogen starvation [88]. This data was used to identify genes which were highly expressed in *R. palustris* prior to nitrogen starvation and maintained this level of expression throughout the period of nitrogen starvation. As *R. palustris* produces greater quantities of hydrogen in the absence of molecular nitrogen to fix, and strongly represses its nitrogenase in response to ammonia, a gene known to maintain high levels of expression even during nitrogen starvation was desirable for the purposes of this project. From this shortlist of genes, the candidates were narrowed down by requiring the gene to be of known function, and involved in central metabolism as it was felt that these would be more likely to maintain high levels of expression under varying conditions. There were many highly expressed genes involved in light harvesting, but these were rejected as their expression might be reduced under low light, potentially creating problems for industrial application of this approach.

The gene chosen was *aceA*, encoding isocitrate lysase (RPA4394). The sequence of *aceA* and its genomic context were obtained from CyanoBase (see Section 2.17) and also available at the BioCyc Database Collection (www.biocyc.org). Upstream of *aceA* is RPA4395, separated from *aceA* by 214 base pairs and transcribed in the opposite direction; it was therefore assumed that the two genes are not co-transcribed and that the promoter for *aceA* is located within this 214-base pair region.

Unfortunately, little is known about the location of promoters in *R. palustris*, and so it was not possible to precisely identify the promoter region of this gene. For the heterologous insertions, the 201 nucleotides upstream of the start codon of *aceA* were selected to act as the promoter region.

The final 30 nucleotides of this sequence (i.e. the 30 directly upstream of the *aceA* start codon) were selected to act as the intergenic region between each pair of heterologous genes where two were inserted together; *ispS* and *ipi*, and *mgsA* and *gldA*. Although this would result in the first gene being flanked by a direct repeat of 30 nucleotides, it was hoped this would be too short to result in recombination-mediated deletion.

Downstream of *aceA* is RPA4393, separated by only a few nucleotides. The 150 nucleotides downstream of RPA4393 (there being a gap of 264 base pairs before RPA4392) were therefore chosen to act as the terminator region for the heterologous insertions, in case *aceA* and RPA4394 are co-transcribed.

5.3.6 Design of the heterologous sequences

Having identified the component parts of the sequences to be introduced into *R. palustris*, the final sequences were assembled. The plasmid for inserting only *ispS* was created at a later point from the plasmid for inserting both *ispS* and *ipi*, so two sequences only were designed to be ordered from GeneArt, one containing the genes for propane-1,2-diol biosynthesis (*mgsA* and *gldA*) and the other containing the genes for isoprene biosynthesis (*ispS* and *ipi*).

In order to reduce the cost of the ordered sequences, the promoter and terminator regions were included only with the sequence for *mgsA* and *gldA* (the shorter pair of genes) with the intention of later substituting out the gene sequences for those for isoprene biosynthesis. The promoter and terminator sequences were therefore designed with restriction sites (NcoI and StuI) to allow the intervening gene sequence to be swapped out, although this was considered a useful feature anyway, should the promoter or terminator sequences ever need to be changed themselves.

The p*KmobsacB*-based plasmid for introducing a deletion into *hupL* was chosen as the delivery plasmid for these insertions. The heterologous sequences were designed to be inserted between the left and right flanking regions used to create the *hupL* deletion, in the opposite sense to the *hupL* sequence. This required that they include the appropriate restriction sites, the promoter sequence commencing with a BamHI site and the terminator sequence capped by an XbaI site.

The full sequences for each pair of heterologous genes are provided in Appendix B, which also

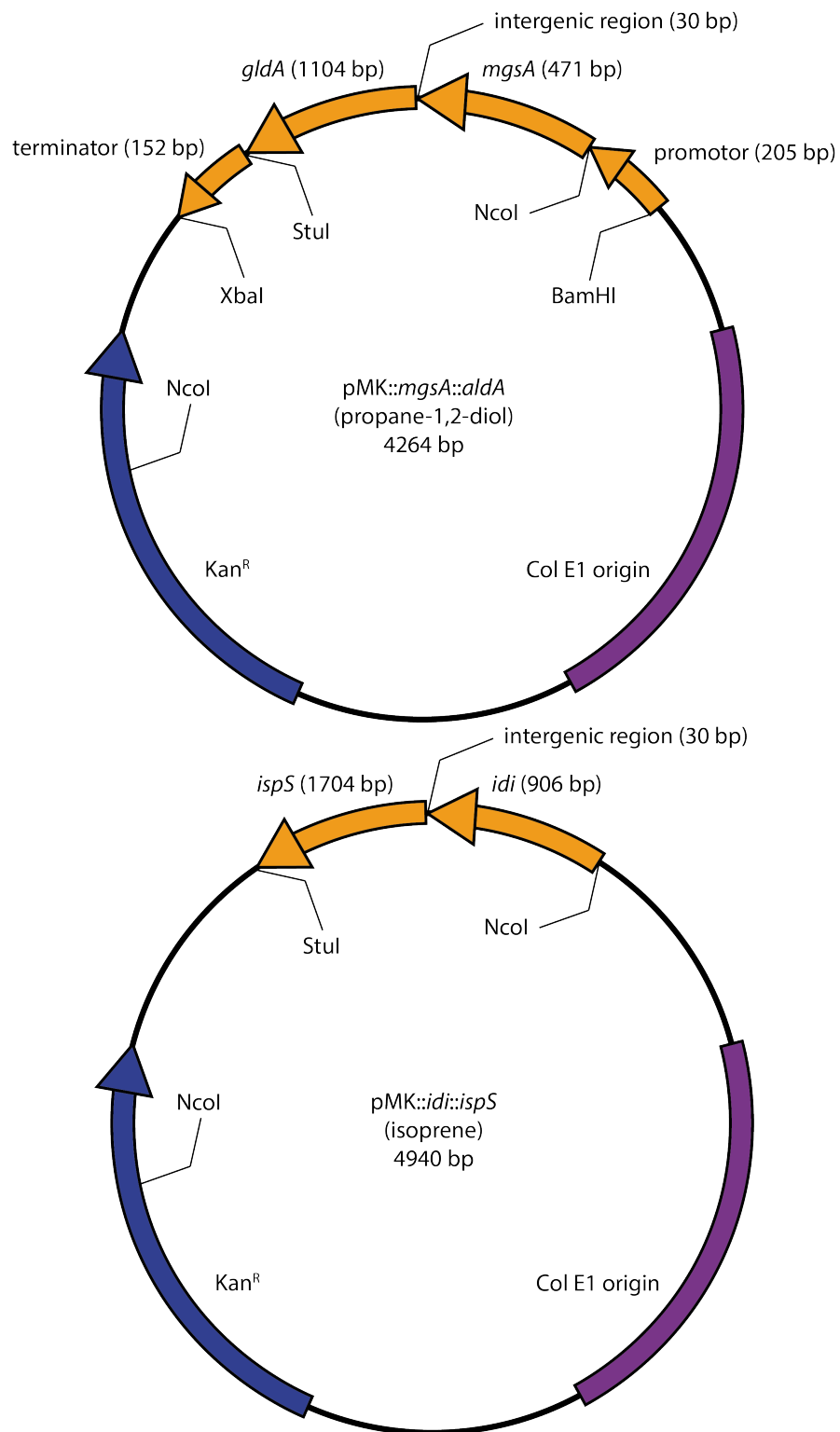


Figure 5.19: Illustration (not to scale) of the plasmids received from GeneArt. Top: carrying sequence for propane-1,2-diol biosynthesis genes, promoter and terminator. Bottom: carrying sequence for isoprene biosynthesis genes.

Position	Restriction Enzyme	Site of Recognition
End of right flanking region	EcoRI	G [^] AATTC
Start of promoter	BamHI	G [^] GATCC
End of promoter	NcoI	C [^] CATG _G
Start of terminator	StuI	AGG [^] CCT
End of terminator	XbaI	T [^] CTAGA
Start of left flanking region	HindIII	A [^] AGCTT

Table 5.8: Summary of restriction sites relevant to construction of delivery plasmids.

details specific nucleotide alterations made, for example, to introduce restriction sites. These two sequences were ordered from Invitrogen GeneArt and were delivered in the plasmid pMK. The plasmids are illustrated in Figure 5.19.

5.3.7 Construction of the delivery plasmids

The pK*mobsacB*-based *hupL* deletion plasmid provided by David Lea-Smith to act as the delivery plasmid was found to contain an additional unexpected BamHI site. To avoid the need to use BamHI digestion of pK*mobsacB*-based Δ *hupL* the propane-1,2-diol sequence (including promoter and terminator) was therefore first excised from the GeneArt plasmid with BamHI and XbaI and inserted between the *hupL* flanking regions within the pUC19- Δ *hupL* plasmid used in the construction of the pK*mobsacB* Δ *hupL* plasmid, illustrated in Figure 5.20 [89]. The entire sequence, including *hupL* flanking regions, propane-1,2-diol biosynthesis genes, promoter and terminator, was then transferred into pK*mobsacB* with an EcoRI / HindIII digest to generate the final plasmid, pK*mobsacB* Δ *hupL*::*mgsA*::*gldA*.

To construct the *ipi*::*ispS* isoprene insertion plasmid the promoter-*mgsA*::*gldA*-terminator sequence was first excised from its GeneArt plasmid with BamHI and XbaI and inserted into the MCS of pUC19, digested with the same enzymes. The *mgsA*::*gldA* sequence was then excised with NcoI and StuI (leaving the promoter and terminator) and replaced with the *ipi*::*ispS* sequence excised from the second GeneArt plasmid with the same enzymes (the two-step process was necessary as the kanamycin resistance cassette includes both StuI and NcoI restriction sites). The entire expression cassette was then excised using BamHI and XbaI and used to replace the propane-1,2-diol biosynthesis cassette from pK*mobsacB* Δ *hupL*::*mgsA*::*gldA* to generate pK*mobsacB* Δ *hupL*::*ipi*::*ispS*.

To construct the *ispS* insertion plasmid, the coding sequence was amplified from the GeneArt plasmid with primers with appropriate restriction sites, digested with NcoI and StuI and used in the

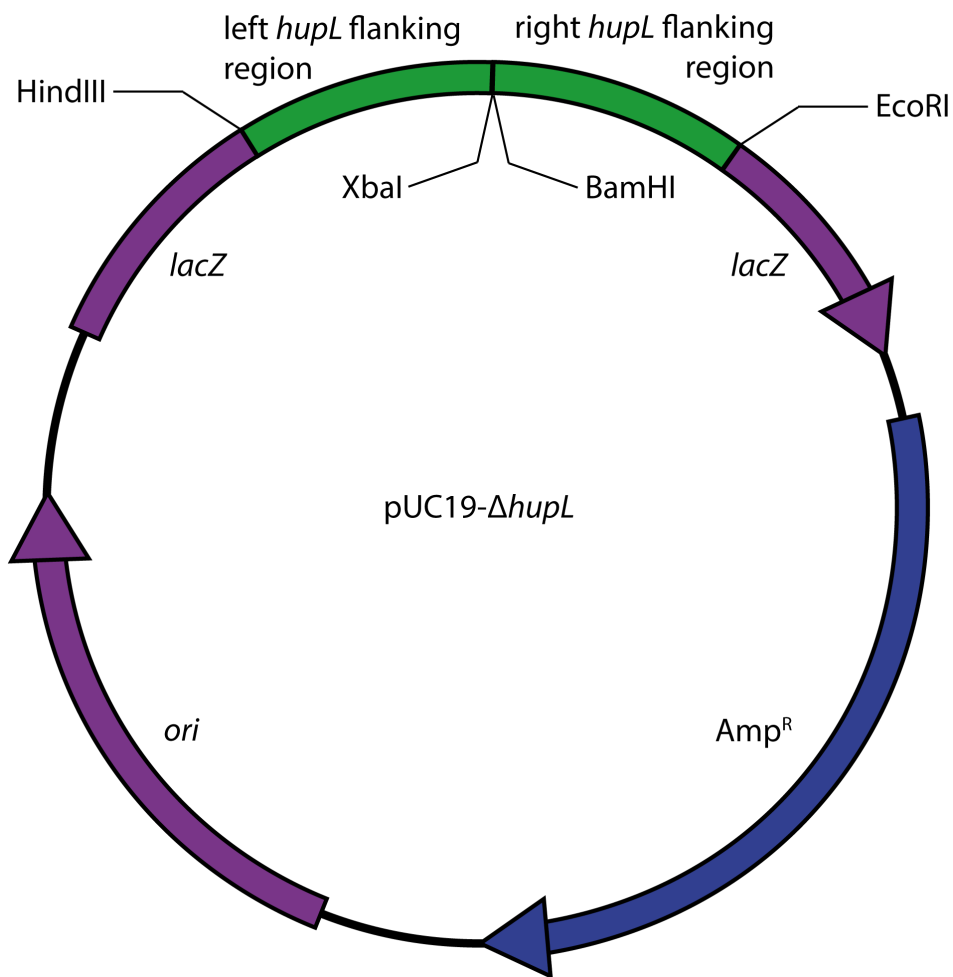


Figure 5.20: Illustration (not to scale) of the pUC19- $\Delta hupL$ plasmid used originally in the construction of the p*KmobsacB* $\Delta hupL$ plasmid for introducing a deletion into *hupL*, and later used in this work for the construction of plasmids for inserting heterologous sequences into *R. palustris*. Features of the pUC19 plasmid are shown in purple (ori and lacZ) and blue (ampicillin resistance cassette; Amp^R). The *hupL* flanking regions inserted into the multiple cloning site of pUC19, located within the lacZ sequence, are shown in green.

same way as the *ipi::ispS* sequence in the preceding paragraph to generate pK*mobsacB*Δ*hupL::ispS*. The restriction sites are summarized in Table 5.8, and a plasmid map illustrating the three versions of delivery plasmid is shown in Figure 5.21.

To summarize, the steps taken to create the pK*mobsacB*Δ*hupL::mgsA::gldA* plasmid were:

1. Digest the GeneArt propane-1,2-diol plasmid with BamHI and XbaI and extract the heterologous sequence including promoter and terminator.
2. Insert this sequence between the left and right flanking regions of the pUC19-Δ*hupL* plasmid, also digested with BamHI and XbaI.
3. Also insert this sequence into the MCS of pUC19, also digested with BamHI and XbaI, to facilitate the later creation of the isoprene insertion plasmid.
4. Digest the pUC19Δ*hupL::mgsA::gldA* plasmid with EcoRI and HindIII and extract the sequence including *hupL* flanking regions, promoter, terminator and heterologous genes.
5. Insert this sequence into the MCS of pK*mobsacB*, also digested with EcoRI and HindIII.

The steps taken to create the pK*mobsacB*Δ*hupL::ipi::ispS* plasmid were:

1. Digest the GeneArt isoprene plasmid with NcoI and StuI and extract the heterologous genes sequence; a long period of electrophoresis was required to adequately separate out the heterologous sequence from the two fragments created from the backbone.
2. Digest the pUC19::*mgsA::gldA* plasmid with NcoI and StuI and extract the fragment consisting of the pUC19 backbone, promoter and terminator.
3. Insert the heterologous sequence from (1) into the plasmid from (2).
4. Digest the pUC19::*ipi::ispS* plasmid with BamHI and XbaI and extract the heterologous sequence including promoter and terminator.
5. Digest the pK*mobsacB*Δ*hupL::mgsA::gldA* plasmid with BamHI and XbaI and extract the fragment consisting of the pK*mobsacB* backbone and *hupL* flanking regions.
6. Insert the heterologous sequence from (4) into the plasmid from (5).

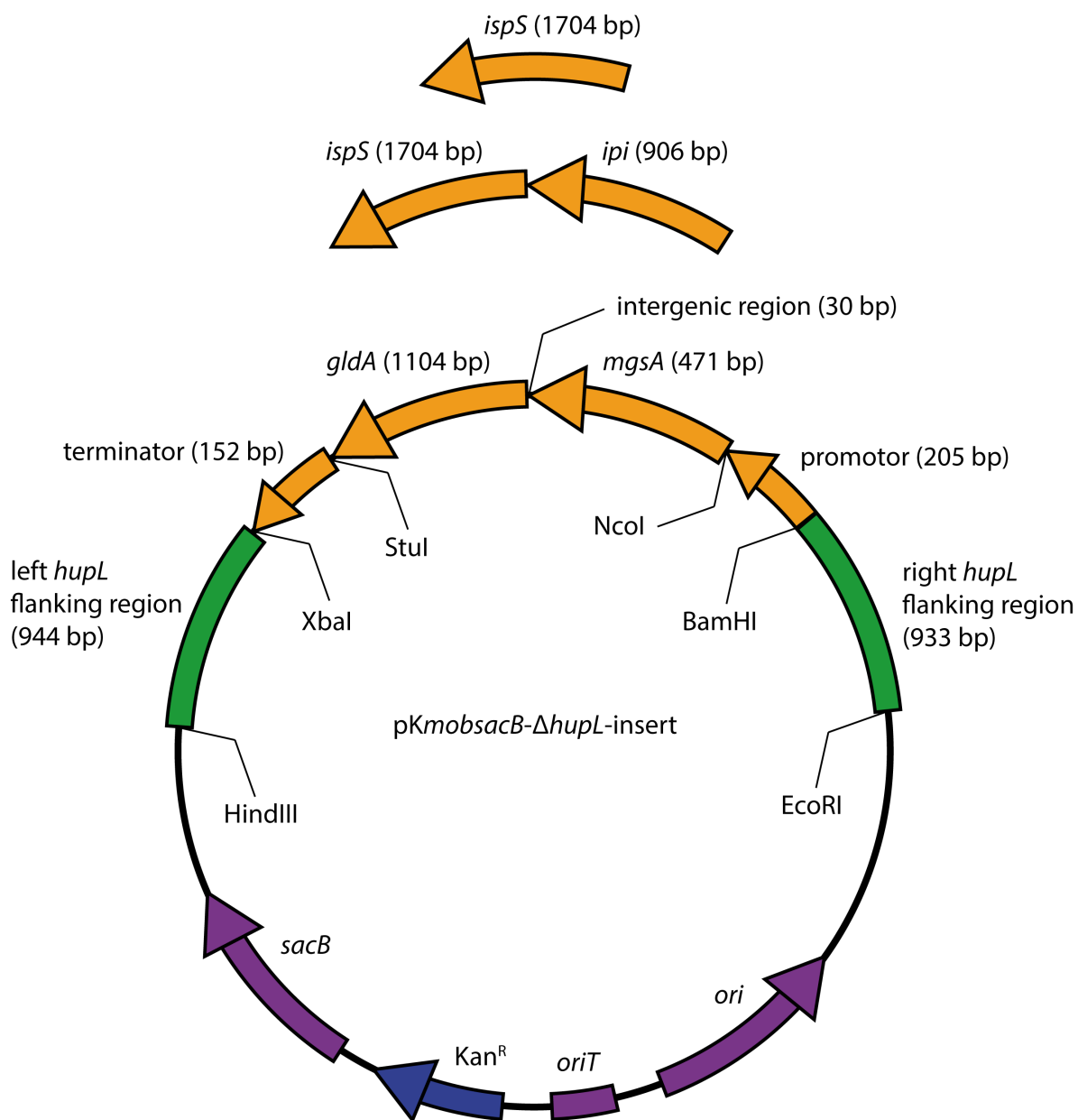


Figure 5.21: Illustration of the plasmids used to insert heterologous genes into *R. palustris* (not to scale). Features of the pKmobsacB delivery plasmid are shown in purple (*sacB*, *ori* and *oriT*) and blue (kanamycin resistance cassette; Kan^R). Sequences inserted into the multiple cloning site of pKmobsacB are shown in green (left and right *hupL* flanking regions; target genome insertion and introduce deletion to *hupL*) and orange (promoter, terminator and heterologous genes). The plasmid is illustrated with the heterologous genes for propane-1,2-diol biosynthesis, *mgsA* and *gldA*. The sequences present in their place in the plasmids for insertion of isoprene biosynthesis genes and insertion of *ispS* only are shown above.

Plasmid	Restriction Enzyme	Expected product sizes / bp
pK <i>mobsacB</i> Δ <i>hupL</i> :: <i>mgsA</i> :: <i>gldA</i>	HindIII / EcoRI	5660 & 3840
pK <i>mobsacB</i> Δ <i>hupL</i> :: <i>mgsA</i> :: <i>gldA</i>	BamHI / XbaI	7540 & 1970
pK <i>mobsacB</i> Δ <i>hupL</i> :: <i>ipi</i> :: <i>ispS</i>	BamHI / XbaI	7540 & 3000
pK <i>mobsacB</i> Δ <i>hupL</i> :: <i>ispS</i>	BamHI / XbaI	7540 & 2070

Table 5.9: Product sizes (to the nearest 10 bp) expected from digestion of insertion plasmids with stated pairs of restriction enzymes.

The steps taken to create the pK*mobsacB*Δ*hupL*::*ispS* plasmid were:

1. Amplify the *ispS* sequence from the GeneArt isoprene plasmid with primers designed to add an NcoI site to the start of the gene; see Table 5.11 for primer sequences.
2. Digest this product with NcoI and StuI.
3. Digest the pUC19::*mgsA*::*gldA* plasmid with NcoI and StuI and extract the fragment consisting of the pUC19 backbone, promoter and terminator.
4. Insert the sequence from (2) into the plasmid from (3).
5. Digest the pUC19::*ispS* plasmid with BamHI and XbaI and extract the heterologous sequence including promoter and terminator.
6. Digest the pK*mobsacB*Δ*hupL*::*mgsA*::*gldA* plasmid with BamHI and XbaI and extract the fragment consisting of the pK*mobsacB* backbone and *hupL* flanking regions.
7. Insert the heterologous sequence from (5) into the plasmid from (6).

These plasmids were confirmed by restriction digest at each stage of the construction process. The results of this verification step for the final stage of construction are shown in Figure 5.22. The expected product sizes for each of the digestions presented are shown in Table 5.9, and can be seen to be consistent with the results observed.

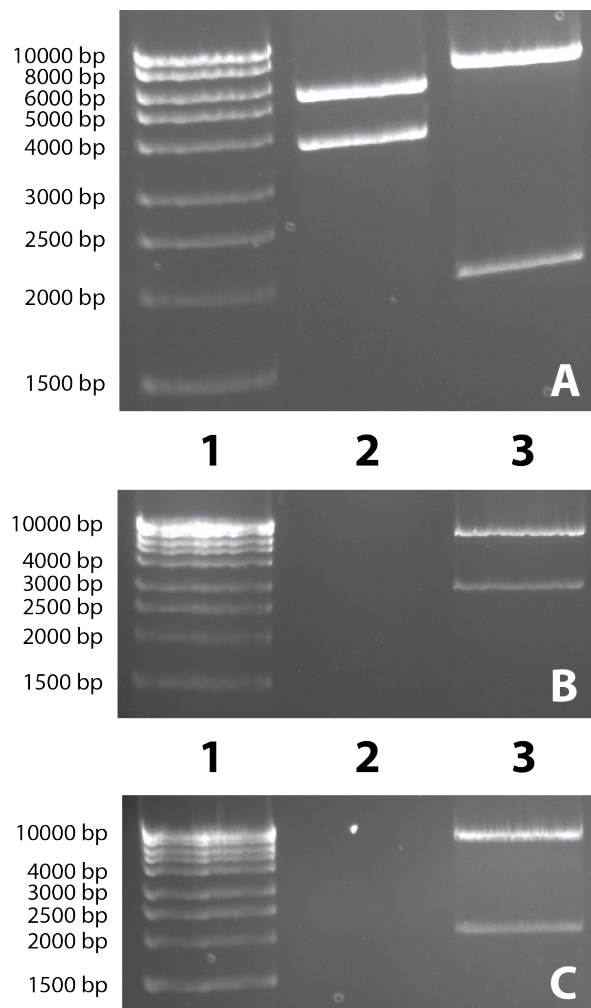


Figure 5.22: Visualisation of plasmid prep digestions of (A) *pKmobsacBΔhupL::mgsA::gldA*, (B) *pKmobsacBΔhupL::ipi::ispS* and (C) *pKmobsacBΔhupL::ispS*. Lanes (A): (1) DNA ladder; (2) digestion with HindIII and EcoRI; (3) digestion with BamHI and XbaI. Lanes (B and C): DNA ladder; (2) empty; (3) digestion with BamHI and XbaI..

Strain	Expected phenotype	Expected product size / bp
Wild-type	Wild-type	1315
<i>hupL::ispS</i>	Isoprene production	2397
<i>hupL::ispSipi</i>	Isoprene production	3330
<i>hupL::mgsAglDA</i>	Propane-1,2-diol production	2295

Table 5.10: Product sizes expected from PCR with DNA from wild-type *R. palustris* and strains carrying inserted heterologous genes as stated, using ‘spanning’ primers homologous to regions either side of the *hupL* targeted deletion site, within which the genes were inserted.

5.3.8 Insertion of heterologous genes into *R. palustris*

The delivery plasmids described above were introduced into both wild-type *R. palustris* and the $\Delta phaAB\Delta glgCA$ strain in the manner described in Chapters 2 and 4. Four colonies each were initially picked for testing after transformation. PCR was used to test for successful insertion of the heterologous genes into the genome. As they were expected to be inserted between the flanking regions of the targeted *hupL* deletion site, the spanning primers used to verify this deletion were also used to verify the insertion of the heterologous genes. The presence of the heterologous genes between the two flanking regions of the *hupL* deletion should result in a longer product if the insertion had been successful than from the wild-type. The product sizes expected from each strain are displayed in Table 5.10. The results of the PCRs are shown in Figures 5.23 - 5.25; note that these strains have not been selected for excision of the delivery plasmid backbone, and therefore the ‘wild-type band’ at 1315 bp appeared for all strains.

These results suggest that the heterologous genes have successfully been inserted into the genome of *R. palustris*, both the wild-type and $\Delta phaAB\Delta glgCA$ strain. For the wild-type host, one of the four putative *ispS::ipi* transformants, and three of the putative *ispS* transformants showed the expected pattern. For the $\Delta phaAB\Delta glgCA$ host the numbers were two and four respectively. Interestingly, in both cases the frequency of colonies displaying a positive result was lower for the strain transformed with the considerably larger $pKmobsacB\Delta hupL::ipi::ispS$ plasmid. This may indicate more reliable gene insertion with smaller sequences, although the amount of data is too low to allow robust conclusions to be drawn. In each case the strain corresponding to the first lane displaying a positive result was chosen for further experimentation.

From the putative *mgsA::glDA* transformants, three of the four putative transformants with the wild-type background showed the expected pattern, as did three of the four putative transformants with the $\Delta phaAB\Delta glgCA$ background. An unexpected pattern was observed from the first putative

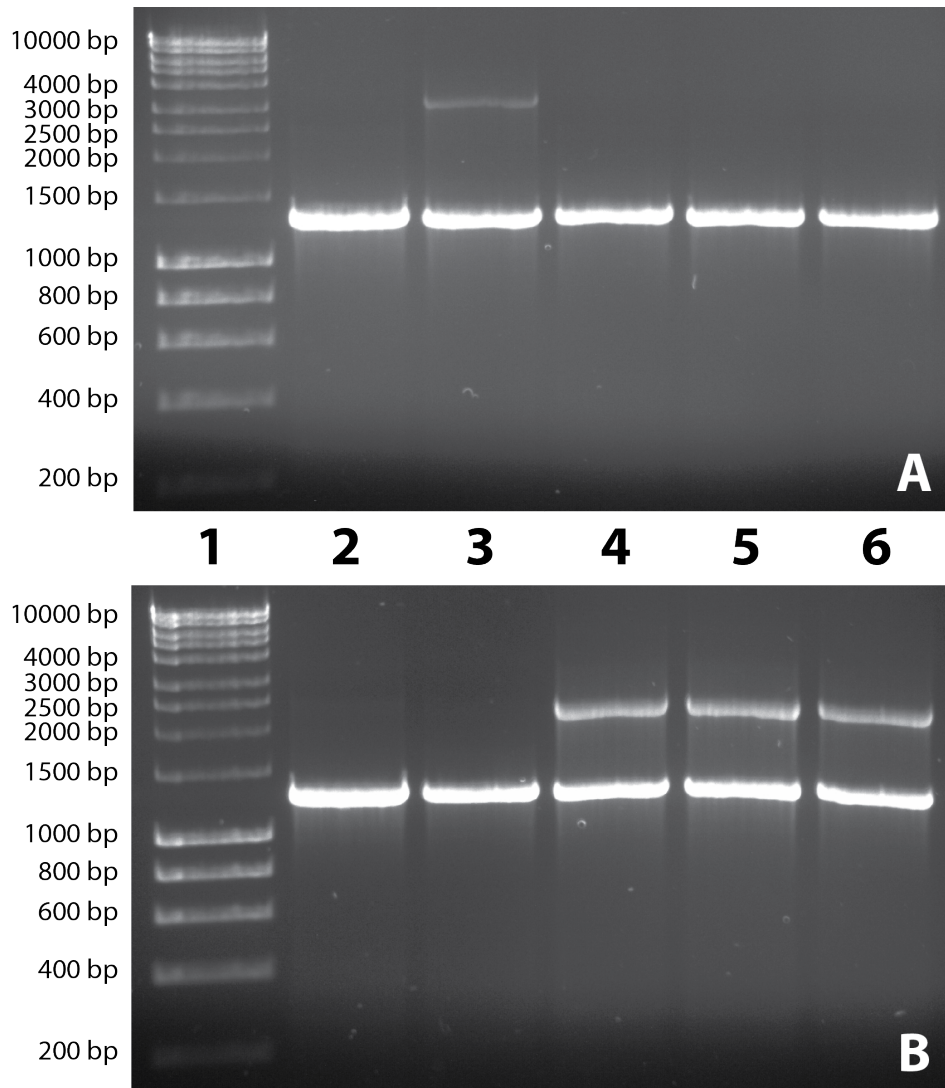


Figure 5.23: Visualisation of amplification products generated by PCR from wild-type *R. palustris* and from isolates potentially carrying (A) inserted *ispS* and *ipi* and (B) inserted *ispS* only, with 'spanning' primers complementary to regions either side of the *hupL* targeted deletion site, within which the genes were inserted. Lanes: (1) DNA ladder; (2) wild-type; (3 - 6) potential transformants.

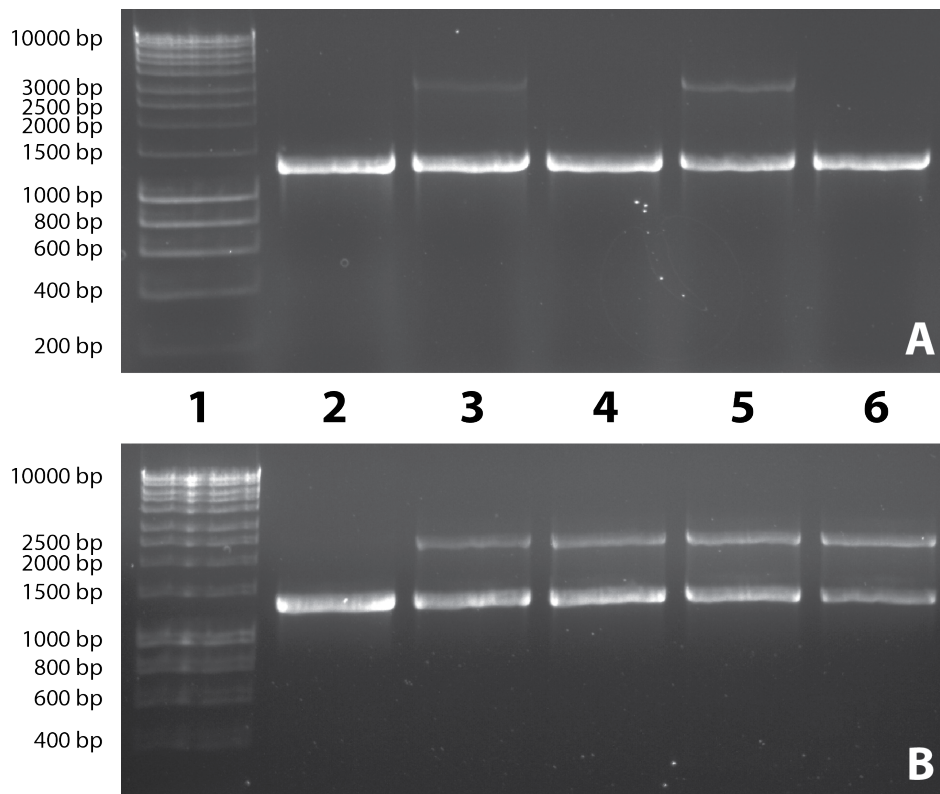


Figure 5.24: Visualisation of amplification products generated by PCR from the $\Delta phaAB\Delta glgCA$ strain and from isolates with the $\Delta phaAB\Delta glgCA$ background potentially carrying (A) inserted *ispS* and *ipi* and (B) inserted *ispS* only, with ‘spanning’ primers complementary to regions either side of the *hupL* targeted deletion site, within which the genes were inserted. Lanes: (1) DNA ladder; (2) $\Delta phaAB\Delta glgCA$; (3 - 6) potential transformants.

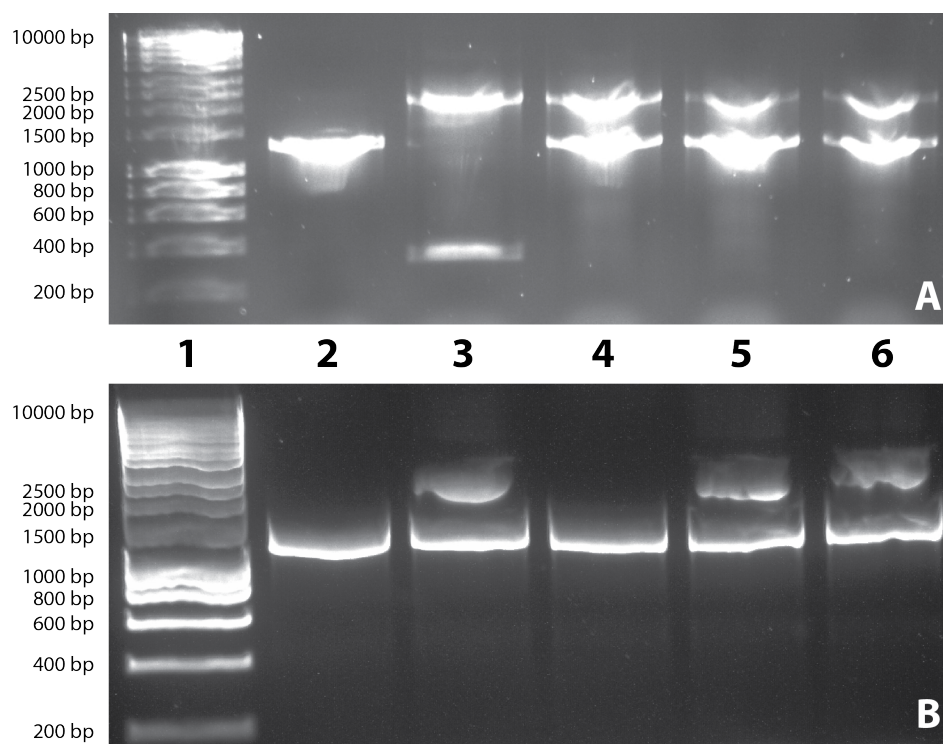


Figure 5.25: Visualisation of amplification products generated by PCR from (A) wild-type *R. palustris* and isolates potentially carrying inserted *mgsA* and *gldA* and (B) the $\Delta phaAB\Delta glgCA$ strain and isolates with the $\Delta phaAB\Delta glgCA$ background potentially carrying inserted *mgsA* and *gldA*, with 'spanning' primers homologous to regions either side of the *hupL* targeted deletion site, within which the genes were inserted. Lanes: (1) DNA ladder; (2) wild-type; (3 - 6) potential transformants.

Primer	Sequence	Product size / bp
<i>ispS</i> Forward	GCTTCTCGGGTGAAGTGAAG	586
<i>ispS</i> Reverse	GTGTTGATGGCATTACGTC	-
<i>ipi</i> Forward	CCATGGCGCAGTCGTCGATC	910
<i>ipi</i> Reverse	TCACGTGAGCTTGTGAATGG	-
<i>mgsA</i> Forward	GAAGCATATCGCCCTGGTC	385
<i>mgsA</i> Reverse	CAAGATGTCCACTGCATCGT	-
<i>gldA</i> Forward	TAAATTCGTGCTGGGTTTCG	309
<i>gldA</i> Reverse	GGCATGTTGTGGATCGTTTC	-
<i>amtB2</i> Forward	GTGCTGGTGCTGTTGATGAC	516
<i>amtB2</i> Reverse	GTTGACTTCGTCGAGCTTGG	-
<i>ispS</i> Amplification Forward	CTAGCCATGGTACCGTGGATTTGCGCC	1720
<i>ispS</i> Amplification Reverse	GTACAGGCCTCACACGTACATCAG	-

Table 5.11: List of primers used to test transformants for expression of inserted heterologous genes; *amtB2* primers used as a positive control for expression; *ispS* ‘Amplification’ primers used to amplify *ispS* sequence from GeneArt plasmid with appropriate restriction sites and hanging nucleotides for digestion and insertion between the promoter and terminator sequences.

transformant in the wild-type background. The expected product from the inserted sequence was observed, but instead of the expected product from the native sequence, a much smaller product was observed. This looked to be about the size expected for the *hupL* deletion sequence. This suggests that the targeted deletion sequence has been excised, but that the native copy of at least one of the flanking regions remained (otherwise only the larger of the two products ought to be generated). It is unknown whether this has also resulted in excision of the plasmid backbone. The strain corresponding to lane 2 was chosen for further experimentation in this case, and the strain corresponding to lane 1 in Figure 5.25B as the $\Delta phaAB\Delta glgCA$ background strain.

5.3.9 Testing expression of heterologous genes

An RT-PCR was carried out on the strains carrying copies of the heterologous genes in the wild-type background, to verify whether or not the genes were being expressed. RNA was extracted from each of the three strains, and RT-PCR was conducted using gene-specific primers complementary to the inserted gene sequences, listed in Table 5.11. These primers were used to amplify the expected products from the delivery plasmids in standard PCR to verify that the primers behaved as expected, and to amplify the inserted sequences from genomic DNA extracted from the same strains, to verify that the inserted sequences were definitely present in the genome (Figure 5.26). Finally, as well as primers complementary to the inserted sequences, primers complementary to *amtB2*, known to be expressed in *R. palustris* under the conditions used here (see Chapter 6), were used to verify

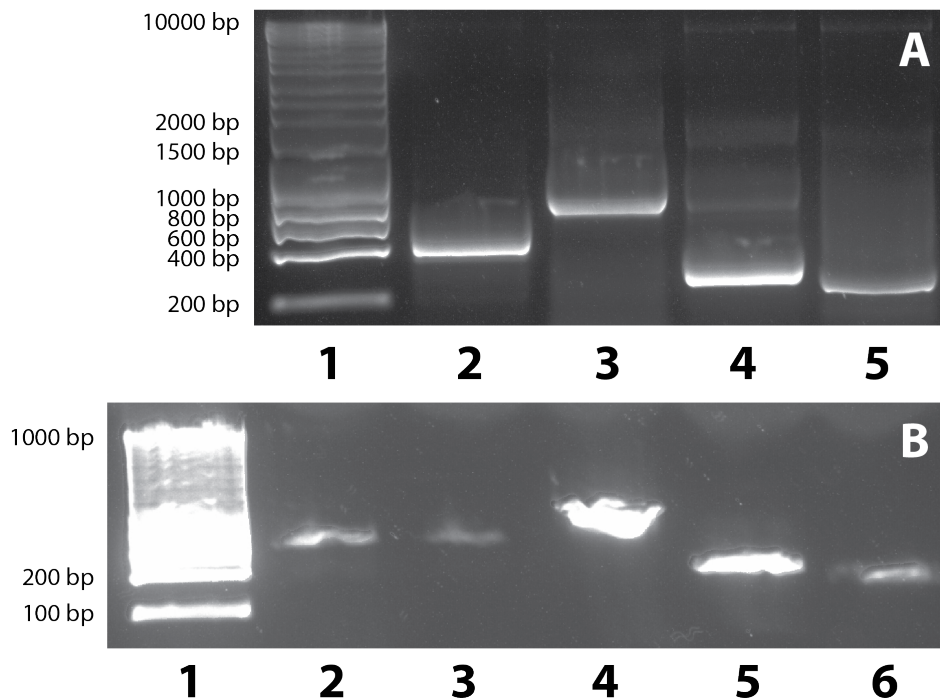


Figure 5.26: Visualisation of amplification products generated by PCR from (A) the insertion plasmids and (B) genomic DNA from strains carrying the heterologous genes. Lanes (A): (1) DNA ladder; (2) *ispS* primers with the p*KmobsacB* Δ *hupL::ipi::ispS* plasmid; (3) *ipi* primers with the p*KmobsacB* Δ *hupL::ipi::ispS* plasmid; (4) *mgsA* primers with the p*KmobsacB* Δ *hupL::mgsA::gldA* plasmid; (5) *gldA* primers with the p*KmobsacB* Δ *hupL::mgsA::gldA* plasmid. Lanes (B): (1) DNA ladder; (2) *ispS* primers with a strain carrying *ispS* only; (3) *ispS* primers with a strain carrying *ispS* and *ipi*; (4) *ipi* primers with a strain carrying *ispS* and *ipi*; (5) *mgsA* primers with a strain carrying *mgsA* and *gldA*; (6) *gldA* primers with a strain carrying *mgsA* and *gldA*.

that the RNA was in suitable condition for reverse transcription. An ‘RT-’ sample was included for each RT-PCR reaction, as a control to check that any product seen was the result of RNA rather than contaminating genomic DNA (see Chapter 2). The results of this RT-PCR are shown in Figure 5.27.

The positive controls shown in Figure 5.26 confirmed that the primers amplified a product of the expected size from the plasmids, and confirmed the presence of the inserted sequences in all three strains tested (wild-type background). It was therefore assumed that a reverse transcription assay would be viable with these primers and strains.

These results were unfortunately slightly ambiguous. Despite conducting three DNase treatments in an effort to remove all DNA contamination from the RNA prep used for the reverse transcription assay, there was still presumed gDNA contamination in most if not all of the RT- lanes. This is a common problem with RT-PCR and *R. palustris* (Jack Hervey, University of Cambridge, personal communication). However, a more intense product was consistently observed from the RT+ lanes

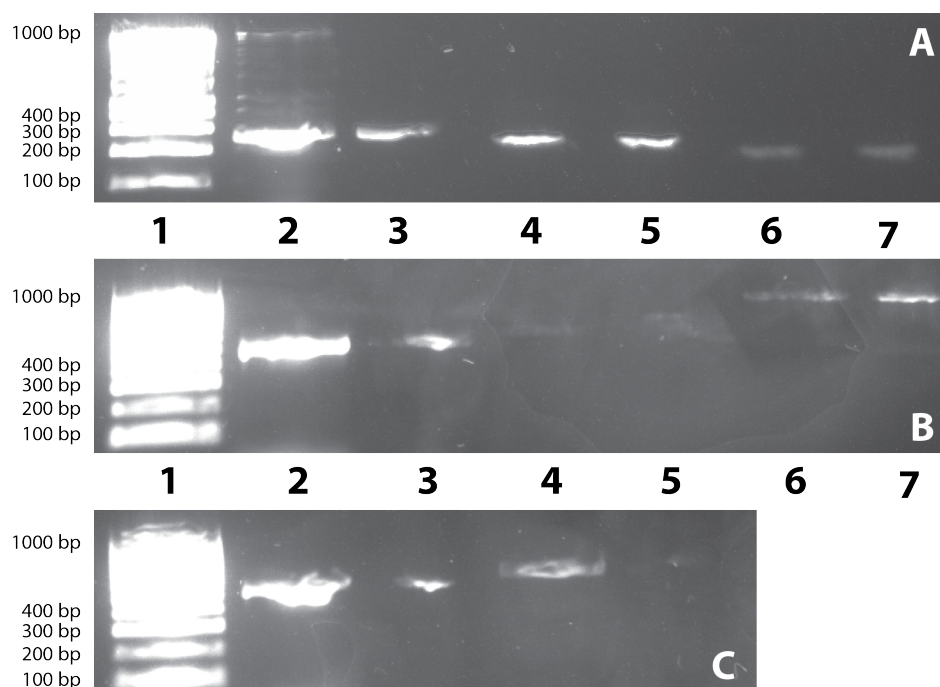


Figure 5.27: Visualisation of amplification products generated by RT-PCR from (A) a strain carrying the heterologous *mgsA* and *gldA* genes, (B) a strain carrying the heterologous *ispS* and *ipi* genes, and (c) a strain carrying the heterologous *ispS* gene only. Lanes (A): (1) DNA ladder; (2) *amtB2* primers; (3) *amtB2* primers RT-; (4) *mgsA* primers; (5) *mgsA* primers RT-; (6) *gldA* primers; (7) *gldA* primers RT-. Lanes (B and C): (1) DNA ladder; (2) *amtB2* primers; (3) *amtB2* primers RT-; (4) *ispS* primers; (5) *ispS* primers RT-; (6 – B only) *ipi* primers; (7 – B only) *ipi* primers RT-.

of the positive control *amtB2* primers with all three strains (compare lanes 2 and 3 in panels A, B and C of Figure 5.27). This suggested that RNA was present and suitable for reverse transcription, and that if a more intense band were seen in the RT+ lane for a given assay it would indicate that transcripts were present. On that basis, it seems likely that transcripts for the inserted heterologous genes were not present at a significant level in either of the strains carrying two heterologous genes. The RT+ lane for *ispS* in the *ispS*-only transformants showed a more intense band than the RT- lane (panel C, lanes 4 and 5), suggesting that *ispS* transcripts were present in the strain carrying only this heterologous gene. If so, that would suggest that the two-gene construct model is not suitable for expressing heterologous genes in *R. palustris*.

5.4 Discussion

5.4.1 Establishment of the *hupL*, *phaAB* and *glgCA* knockouts as chassis strains

This work demonstrated that the material targeted for deletion in the knockout strains of *R. palustris* created by David Lea-Smith and Toby Call was completely eliminated from the genome in all cases, and that the levels of glycogen and PHB were reduced if not abolished in those strains with disruptions to the relevant biosynthetic pathways.

There is a chance that the shorter products observed on amplification with the spanning primers were amplified from the plasmid, and that the longer products were not visible on the gel due to lower amplification frequency resulting in less product, but the pK*mobsacB* plasmid is not expected to be capable of replication within the cell [3]. A PCR with one primer homologous to a region of the chromosome upstream of the flanking regions contained within the plasmid and the other downstream of the point of deletion would confirm this.

The growth and hydrogen production of these strains was then characterized. After finding that the Δ *hupL* genotype had no significant effect on growth and no discernible effect on hydrogen production, sequencing the *hupV* gene region of the wild-type subsequently demonstrated that the CGA009 strain used throughout this work is a natural uptake hydrogenase mutant, in agreement with the findings of Rey *et al.* in 2006 [4]. In light of this, it is not surprising that the Δ *hupL* strain was not observed to grow at a different rate from the wild-type, nor the Δ *hupL* Δ *phaAB* Δ *glgCA* strain in comparison with Δ *phaAB* Δ *glgCA*; they might otherwise have been expected to grow more slowly with no ability to recycle hydrogen. Although this negates the possibility of increasing hydrogen production through manipulation of the uptake hydrogenase, the lack of growth impairment re-

sulting from the *hupL* deletion is important in demonstrating that this locus is in principle suitable for insertion of heterologous genes.

The $\Delta phaAB\Delta glgCA$ (and $\Delta hupL\Delta phaAB\Delta glgCA$) strain was found to have reduced growth in comparison to the wild-type, while none of the strains carrying single deletions had significantly different growth rates to the wild-type. This indicates that cells may be capable of compensating for the loss of either PHB or glycogen biosynthetic capability, but that loss of both is detrimental to growth. This might suggest that resources are being redirected from glycogen to PHB and vice versa where one pathway is removed, but the $\Delta phaAB$ strain did not show increased glycogen production, nor did the $\Delta glgCA$ strain show increased PHB production (if anything this strain exhibited a lower level of fluorescence than the wild-type in the PHB assay). Nor does it seem that loss of these pathways causes *R. palustris* to channel more resources into growth rather than storage, as no increase in growth was observed.

It is possible that loss of these pathways has a detrimental effect on the osmotic balance of the cells, as well as affecting their ability to utilise stored carbon when external sources become depleted. Both glycogen and PHB act as osmotically-neutral carbon stores, and the loss of both pathways may render the cells largely unable to respond to osmotic stress, through either synthesis or hydrolysis of these compounds. Indeed, beyond the relevance of carbon storage to handling osmotic stress, glycogen and PHB usually make up a significant proportion of cell mass and their loss is likely to affect the physical properties of the cell. Furthermore, PHB granules were recently discovered in *Cupriavidus necator* to actually support the integrity of the cell membrane and prevent leakage of the cytoplasm [90]. Thus it may be that loss of the ability to dynamically synthesise and hydrolyse either these compounds is the main reason for impaired growth rather than simply carbon storage capacity.

Although the slower growth of the $\Delta phaAB\Delta glgCA$ and $\Delta hupL\Delta phaAB\Delta glgCA$ strains is not ideal for industrial applications, growth may nevertheless be adequate, especially if there is a need to generate product rather than general biomass. The fact that the combinations of mutations are not lethal is important in this regard.

Conversely, the $\Delta phaAB\Delta glgCA$ and ($\Delta hupL\Delta phaAB\Delta glgCA$) strain was observed to produce more gas (presumed to be mostly hydrogen) per unit biomass than the wild-type or strains carrying single deletions. This suggests that loss of the PHB and glycogen biosynthetic pathways causes more resources to be channelled into hydrogen production, possibly as a means of addressing redox

imbalance within the cell. This is supported by a study from McKinlay and Harwood in 2010 [91] which found that hydrogen production plays a role in cofactor recycling in *R. palustris*, and by various studies which have taken advantage of the redox imbalance *R. palustris* suffers when grown on reduced substrates such as acetate under photoheterotrophic conditions to drive greater levels of hydrogen production (see for example [92]). Indeed, it might be expected that introduction of heterologous pathways for other compounds into these strains may actually improve or even restore their growth rate. Jung *et al.* in 2011 [61] found that introducing the ability to produce propane-1,2-diol into *S. cerevisiae* increased the growth rate and rate of glycerol consumption in that organism, for example. This suggests that these multiple knockouts may be particularly effective chassis strains for industrial production of high-value compounds.

These strains produced less hydrogen in absolute amount over the same period of time as the wild-type as a result of their reduced growth. The balance between growth rate and rate of hydrogen production would need to be addressed at an industrial level, but if a batch process were employed it could also be worthwhile to use the $\Delta phaAB\Delta glgCA$ strain for hydrogen production. More replicates would enable a more detailed analysis of the balance between these two factors. Furthermore, much insight could be gained from analysing hydrogen production from cells re-suspended in fresh growth medium. Although the data presented here were adjusted for optical density, this does not account for the presumably differing compositions of the growth media between cultures at this point. Were the cells to be re-suspended to the same optical density in fresh growth medium, it might be that greater hydrogen production would be observed from the wild-type, for example, as this culture had presumably consumed more of the available glycerol and other resources available in the medium than the slower-growing strains.

Although the $\Delta hupL$ strain brings no particular advantage as a chassis for hydrogen production compared with CGA009, the *hupL* site and indeed other genes associated with the uptake hydrogenase, such as those for the other predicted subunits HupS and HupC and regulatory proteins HupU and HupV, may be useful sites for introduction of heterologous genes. If the strain were not already a natural uptake hydrogenase mutant, removal of this protein would actually be expected to be detrimental to production of other compounds, as the cell would have no ability to recycle hydrogen. Production of propane-1,2-diol from glycerol, for example, is a net electron-sink, and Clomburg & Gonzalez found that concurrent fermentative pathways were necessary in *E. coli* for high rates of propane-1,2-diol production, in order to provide redox equivalents and ATP [66]. It

would in fact potentially be worth utilizing a different strain of *R. palustris* able to recycle hydrogen for introduction of redox-consuming pathways, or restoring the functionality of *hupV* in CGA009 if using the sequenced strain is more desirable.

Given the reduced growth rates observed for two of the strains, it will be important in future to determine whether complementation restores the phenotype of these knockouts. It should be possible to restore the wild-type genotype via the same method used to generate the deletions; the entire wild-type sequence including flanking regions could be amplified from wild-type gDNA and introduced into the knockout strains, and transformants would simply be selected for generating the longer wild-type product rather than the shorter deletion product by PCR. It was however not possible to undertake creating these plasmids, strains and growth assays within the time available.

5.4.2 Introduction of heterologous genes into *R. palustris*

After the initial characterisation of the chassis strains, the work attempted to introduce heterologous pathways for isoprene and propane-1,2-diol production into these strains of *R. palustris*. Gene sequences from organisms which naturally produce these compounds were codon-optimized for *R. palustris* and introduced into the cell with a promoter sequence from the isocitrate lyase gene *aceA*, and a terminator sequence from the downstream gene RPA4393. These sequences were successfully integrated into the genome of both wild-type *R. palustris* and the $\Delta phaAB\Delta glgCA$ strain at the site targeted for deletion of *hupL*, as demonstrated by PCR showing the longer product expected from successful transformants with the *hupL* spanning primers, and by PCR showing the presence of the inserted heterologous sequences. Again, ideally this would be further confirmed with primer pairs designed to be complementary to both the chromosome sequence upstream or downstream of the *hupL* flanking regions and the inserted heterologous sequences, but as the pK*mobsacB* plasmid is not expected to be capable of replication with the cell [3], it is unlikely that the observed products were amplified from anywhere but the genome, and off-target integration has not been observed at all thus far in other experiments. This part of the project demonstrates novel proof-of-principle that the *hupL* locus can be used for the insertion of heterologous genes.

The largest plasmid used for insertion of heterologous genes, pK*mobsacB* $\Delta hupL::ipi::ispS$, was observed to result in a lower percentage of tested colonies displaying the inserted sequence, although the sample size was small. Furthermore, fewer colonies were observed on the plates after transformation with this plasmid (estimated by eye only). This suggests that inserting a shorter

sequence into the genome may yield a greater frequency of successful transformants, as might be expected, though further investigation would be necessary before drawing any firm conclusions.

A reverse transcription assay was then carried out to assess whether these heterologous genes were successfully being transcribed. The difficulty of fully eliminating any gDNA within the RNA preps made these results somewhat difficult to interpret, but in strains with two heterologous genes, the latter did not give rise to transcripts at clearly detectable levels. However, a transcript may have been present for the strain carrying *ispS* only. If so, this suggests that the promoter region used is suitable for driving expression of heterologous genes, but that inserting a sequence of two sequential genes does not result in transcript accumulation, for reasons that are unclear. This would be particularly problematic for the introduction of the propane-1,2-diol pathway, as both genes are expected to be necessary for any production to occur. Possible solutions include re-designing the sequence to contain a separate promoter and terminator for each gene, or inserting the two genes separately into different loci. Other possible target locations include the putative 'neutral site' targeted by the plasmid used in Chapter 4 and other *hup* genes as discussed previously.

However, to be able to select for a second insertion event, the plasmid background carrying the kanamycin resistance cassette would need to be fully excised following the first insertion event. It was found to be very difficult to create an unmarked insertion mutant; several rounds of sucrose selection were attempted, but in every case all colonies tested persisted in carrying the wild-type sequence as well as the inserted sequence. At the time this was not considered too problematic, as the aim was not to delete a sequence of the genome fully, but the persistence of the plasmid backbone would prevent any further manipulations being carried out unless a different antibiotic resistance cassette is used.

Given the lack of conclusive evidence for the successful transcription of the inserted gene sequences, further investigation of these strains was not attempted at this time. However, with more time it would certainly be worthwhile revisiting at least the strain carrying *ispS*. Putative myc-tagged strains were also generated (data not shown) but not characterised because of lack of time. Western analysis would indicate whether or not protein expression had been achieved.

If isoprene production were observed from the mutant strain, it would be very interesting to see whether a greater level of production were achieved from the $\Delta phaAB\Delta glgCA$ background than from the wild-type background. Not only would this be valuable for industrial application directly, it would also provide the possibility of using the *phaAB* and *glgCA* deletion sites as targets for het-

erologous insertions. Introducing the heterologous genes into the $\Delta phaAB\Delta glgCA$ strain directly was found to have a low rate of success, as often no colonies would appear after electroporation, possibly because of reduced viability in this strain. Targeting the *glgCA* site in the $\Delta phaAB$ background or vice versa may therefore provide a greater rate of successful insertion while also creating the $\Delta phaAB\Delta glgCA$ background in the process. This would also remove the need to disrupt other parts of the genome, which always carries the risk of unintended side-effects even if the site is assumed to be neutral. However, it would then be essential to resolve the problem of fully excising the wild-type and plasmid backbone sequence from the genome.

Finally, if isoprene production were observed in the insertion strain, it would be necessary to conduct growth assays to determine whether this has any effect on the growth of the insertion strain, and whether the growth of the $\Delta hupL\Delta phaAB\Delta glgCA$ strain is improved by introduction of this pathway; if the impaired growth is largely a result of being unable to respond dynamically to osmotic stress it may be that introduction of a synthesis pathway alone (and unregulated by the cell) does little to compensate.

6 Creation of potential chassis strains by manipulation of nitrogenase

6.1 Introduction

As previously discussed, *R. palustris* is able to fix nitrogen through the action of a nitrogenase enzyme, of which it has three genetically distinct forms [1]. As well as comprising different polypeptide chains [51], each of these three forms also contains a different co-factor: one a molybdenum-iron cofactor, one a vanadium-iron cofactor, and one an iron-only cofactor ('Mo-nitrogenase', 'Va-nitrogenase' and 'Fe-nitrogenase', respectively).

The nitrogenase containing a molybdenum-iron cofactor is expressed and used preferentially over the other two 'alternative nitrogenases', as in all diazotrophs [50]. Experiments conducted on other species which encode the Va-nitrogenase (*Azotobacter chroococcum*; [5]) or the Fe-nitrogenase (*Rhodobacter capsulatus*; [6]) demonstrate that, *in vitro*, these enzymes produce more hydrogen both stoichiometrically and per minute than the Mo-nitrogenase. All three nitrogenases produce more hydrogen stoichiometrically in the absence of dinitrogen to fix [23]. However, data from *A. chroococcum* suggest that this increase is more substantial for the Mo-nitrogenase than for the Va-nitrogenase, such that the Mo-nitrogenase actually produces more hydrogen per minute in a 100% argon atmosphere [5]. The Va-nitrogenase however is more active at lower temperatures.

Furthermore, *in vivo* studies have been less conclusive. Experiments conducted on *R. palustris* itself found that strains expressing only the alternative nitrogenases produced more hydrogen per mg of enzyme, but had longer doubling times [46]. The alternative nitrogenases have much greater energy demands than the Mo-nitrogenase and produce ammonia more slowly, which is likely to reduce the rate of cell growth significantly. It is therefore unclear whether a culture of *R. palustris* expressing only one or both of the alternative nitrogenases would produce more hydrogen than a wild-type culture over the long-term.

6.1.1 Regulation of the nitrogenases in the presence of fixed nitrogen

As stated above, all three forms of nitrogenase produce more hydrogen stoichiometrically in the absence of atmospheric dinitrogen. Thus the ideal conditions for maximal hydrogen production from *R. palustris* would be a nitrogen-free atmosphere with supplemental ammonia to aid growth.

However, nitrogenase activity is strongly repressed in the presence of fixed nitrogen: fixation of nitrogen is an extremely energy-expensive process and thus tightly controlled. In many diazotrophs, the Mo-nitrogenase is inactivated post-translationally in the presence of fixed nitrogen by the enzyme dinitrogenase reductase ADP-ribosyltransferase (DraT; [58]). *R. palustris* encodes two DraT homologues, Dra T1 and DraT2. A strain unable to produce the latter was found to be relatively insensitive to ammonia [48], suggesting that this protein performs a similar if not identical function in *R. palustris*. Little has been reported on the putative ADP-ribosyltransferase DraT1, and its function is unknown; one copy of *draT* only is usually reported in bacteria possessing this nitrogenase switch-off mechanism.

An *R. palustris* homologue of a P-II signal transduction protein, GlnK2, is also suspected to be involved in the post-translational regulation of Mo-nitrogenase in response to fixed nitrogen, as other bacteria such as *R. capsulatus* possess similar sets of genes responsible for regulation of nitrogen fixation [93]. The Va- and Fe-nitrogenases of *R. palustris* have been reported to be subject to post-translational inactivation in the presence of ammonium as well as the Mo-nitrogenase [94], which has otherwise never been reported for the Va-nitrogenase, but it is not yet certain whether the DraT2 protein is responsible for this.

6.1.2 Introduction of multiple gene deletions to *R. palustris*

As discussed in Chapters 2 and 5, David Lea-Smith developed a protocol in-house for the creation of 'unmarked' *R. palustris* knockouts prior to the start of this project. This protocol is based on the delivery plasmid p*KmobsacB* [3], and allows the creation of targeted deletions without leaving any selective marker within the genome. The resulting strains therefore do not need to be maintained on antibiotics.

Three loci were identified as deletion targets for this project: *draT2* and *glnK2*, described above, and *nifDH*, encoding multiple structural units of the Mo-nitrogenase. The aim in creating these strains was to develop potential chassis strains for the industrial production of hydrogen, as well as providing a means of investigating features of the nitrogenases and associated regulatory systems of *R. palustris*. This Chapter describes the creation of *R. palustris* strains with deletions in the *nifDH*, *draT2* and *glnK2* genes, and combinations thereof. Growth assays were also conducted on these strains to assess whether the deletions had affected growth rate, which might affect their suitability as chassis strains.

6.2 Results

6.2.1 Analysis of target gene co-transcription

The genomic contexts of the three genes / gene pairs targeted for deletion is illustrated in Figure 6.1, which shows that each of these was found to be very close to another gene downstream and in the same orientation. This was significant because of the potential for the deletions to disrupt the transcription of these downstream genes as well as the target if co-transcription were occurring. In the case of *nifDH*, the presence of *nifK* downstream was not considered problematic. The *nif* genes are found together in an operon, and as the intention was to prevent the cell from being able to produce Mo-nitrogenase, it should make no difference to the outcome if other structural genes such as *nifK* were disrupted as well as *nifD* and *nifH*.

In the case of *draT2*, the gene downstream was *draG*. As discussed in Chapter 1, the DraG protein is anticipated to be responsible for re-activation of the Mo-nitrogenase in the absence of ammonium, by removal of the ADP-ribosyl moiety transferred to the nitrogenase by DraT2. This suggests that even if this gene were to be disrupted, it should have little if any effect on the cell, as it should not be possible for the Mo-nitrogenase to be inactivated by DraT2 in the first place. It has been reported that disruption of DraT1 has no effect on the ammonium-mediated inhibition of the Mo-nitrogenase, indicating that this protein does not act to inactivate the Mo-nitrogenase [48].

In the case of *glnK2*, the gene downstream was *amtB2*, which encodes an ammonium transporter. This was potentially concerning as the overall intention was to feed *R. palustris* ammonium in a nitrogen-free atmosphere to maximize hydrogen output. This would be unviable if the protein plays an essential role in ammonium uptake or metabolism, as the cell would become unable to take up or metabolize external fixed nitrogen. However, a homologue of this protein, *amtB*, is also present in *R. capsulatus*, which possesses the same DraT / DraG system responsible for nitrogenase inactivation in *R. palustris*, as well as the same regulatory proteins GlnK and GlnB [57]. In *R. capsulatus*, an *amtB* knockout strain did not exhibit any growth defect and was capable of taking up ammonium at close to the rate of the wild-type. In addition, the strain was unable to carry out ADP-ribosylation of the Fe-nitrogenase possessed by *R. capsulatus* and the activity of the nitrogenase was unaffected by the presence of ammonium [95]. This suggested that rather than being problematic, disruption of the *amtB2* gene in addition to *glnK2* may in fact contribute to inactivation of the regulatory system for the Mo-nitrogenases (and possibly the alternatives), or at least be redundant.

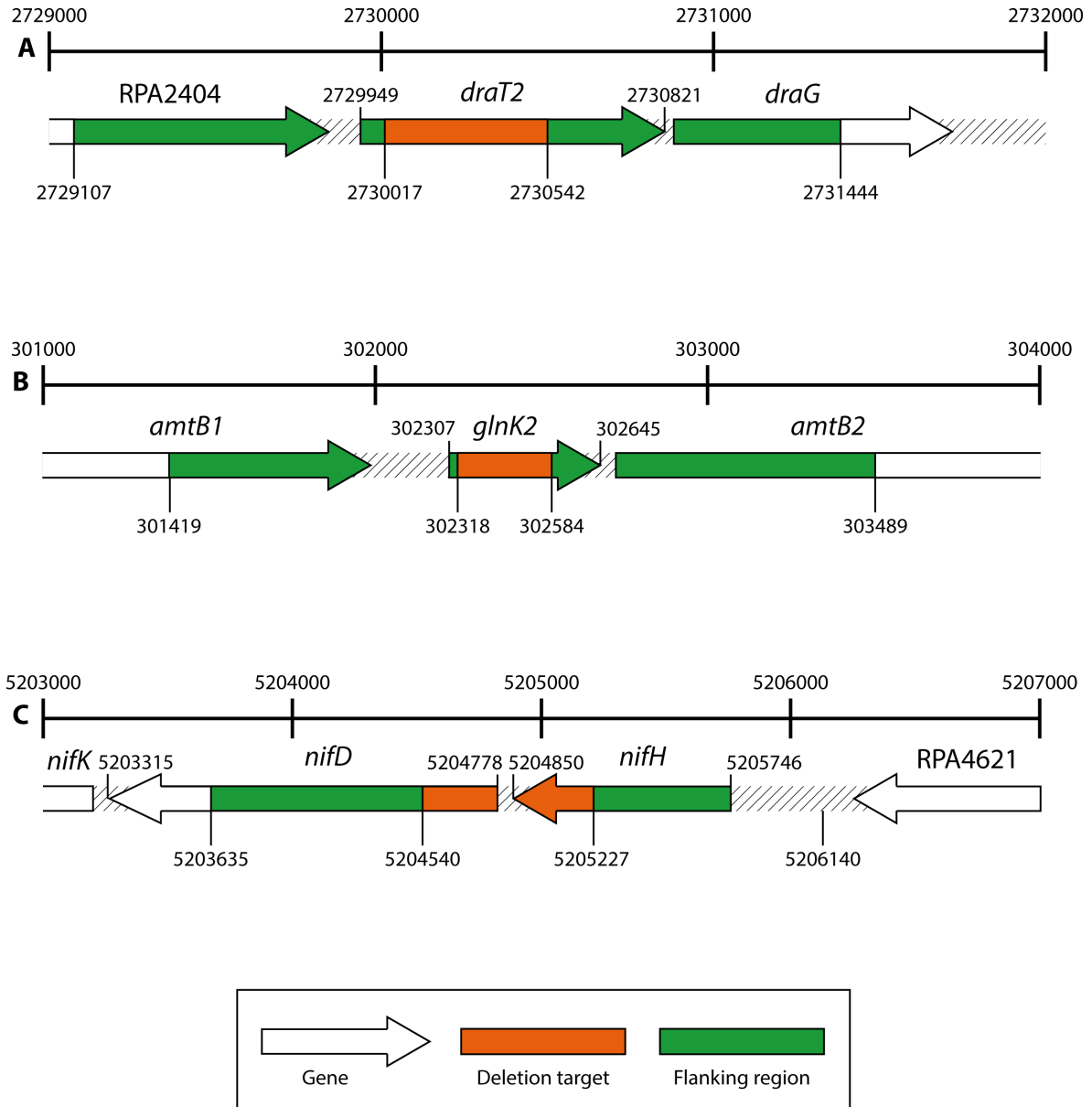


Figure 6.1: Diagrammatic representation of the deletion sites and flanking regions identified for construction of the deletion plasmids for (A) *draT2*, (B) *glnK2* and (C) *nifDH*, Regions targeted for deletion are represented in orange and the flanking regions used in the deletion plasmids for this purpose are represented in green.

Primer	Sequence	Expected product size / bp
<i>draT2</i> Forward	ACGCACATTACGCTGTATCG	204
<i>draT2</i> Reverse	AGCCAGCAGCTTGTTGAAAA	-
<i>draG</i> Forward	GCGATGCAGGGAAGCTATT	195
<i>draG</i> Reverse	CAACAGCACCTGCAACATCT	-
<i>draT2-draG</i> Forward	GAGGGCGAGTATCTGGTGAT	200
<i>draT2-draG</i> Reverse	GTCCTTGTGCACGCCGTAG	-
<i>glnK2</i> Forward	TGGCGATCATTAAAGCCATTC	205
<i>glnK2</i> Reverse	GTCTTCTCGACCTGCTCGTT	-
<i>amtB2</i> Forward	CTACGGCAAGGAGTTGATGG	203
<i>amtB2</i> Reverse	GACCCTTGAAGATCCACTCG	-
<i>glnK2-amtB2</i> Forward	GTCATCGGCCTCGACCAC	204
<i>glnK2-amtB2</i> Reverse	TTGTCGCCCTTGTTGACC	-

Table 6.1: List of primers used to test for co-transcription of *draT2* and *draG*, *glnK2* and *amtB2*.

However, in the latter two cases it was not certain what the effect of disrupting *draG* and *amtB2* would be, and so a co-transcription assay was carried to verify whether or not these genes were co-transcribed with their upstream neighbours. This would at least inform interpretation of any data generated from these knockout strains in the future. In order to carry out the co-transcription assays, primers were designed complementary to three regions: the upstream gene, the downstream gene, and the region of overlap. They were designed such that the expected product in each case was as close to 200 bp as possible, so that differences in amplification efficiency would not be a confounding factor in determining the presence or absence of transcripts. The primers are listed in Table 6.1.

To carry out the co-transcription assay, total RNA was extracted from wild-type *R. palustris* and cDNA created by first-strand synthesis with the appropriate gene-specific primers, as described in Chapter 2 with both RT+ and RT- samples to control for the presence of contaminating gDNA. This was then used in a PCR reaction with the appropriate primer pairs, the results of which are shown in Figure 6.2.

Although multiple attempts were made to extract RNA without genomic DNA contamination, and the samples used in the above experiment were treated three times with DNase, there was still some apparent gDNA contamination (see also Chapter 5). However, the bands appear at consistently higher intensity in the RT+ lanes of the single gene amplicons (for which we would expect stable transcripts to be present) than in the RT- lanes, suggesting that RNA was present and suitable for reverse transcription, and that a more intense band in the RT+ lane would indicate the presence of transcripts (compare lanes 2 and 3, 4 and 5 in both Figures 6.2A and 6.2B). For both amplicons

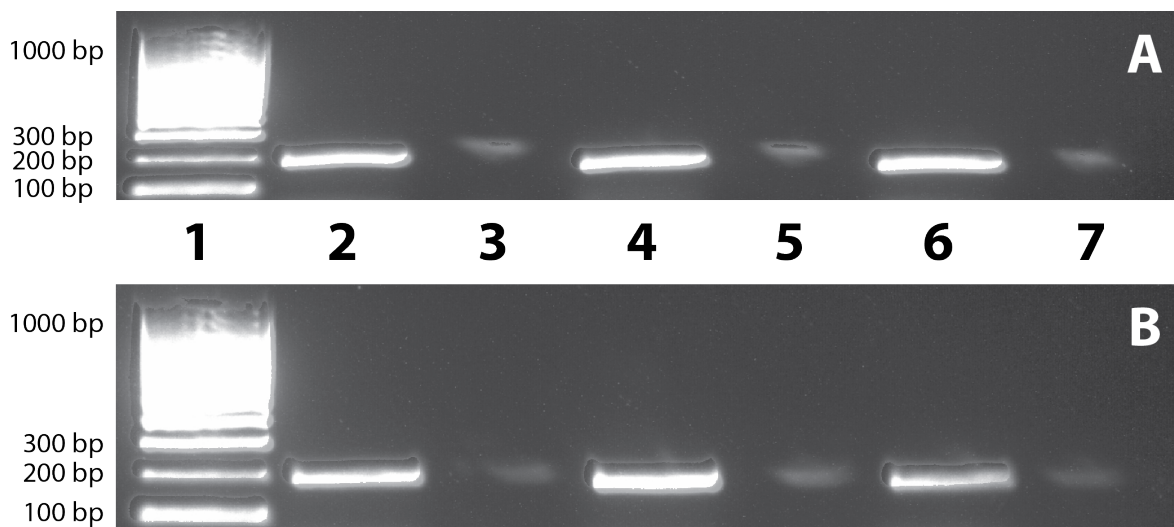


Figure 6.2: Visualisation of amplification products generated by RT-PCR to test for co-transcription of (A) *draT2* and *draG* and (B) *glnK2* and *amtB2*. Lanes (A): (1) DNA ladder; (2) *draT2* primers; (3) *draT2* primers RT-; (4) *draG* primers; (5) *draG* primers RT-; (6) *draT2-draG* primers; (7) *draT2-draG* primers RT-. Lanes (B): (1) DNA ladder; (2) *glnK2* primers; (3) *glnK2* primers RT-; (4) *amtB2* primers; (5) *amtB2* primers RT-; (6) *glnK2-amtB2* primers; (7) *glnK2-amtB2* primers RT-.

spanning the pairs of putatively co-transcribed genes, more intense bands were seen in the RT+ than in the RT- lanes (compare lanes 6 and 7 in both Figures 6.2A and 6.2B). On that basis, it seems likely that transcripts spanning each of the two pairs of genes investigated were present, indicating that both pairs of genes (*draT2* and *draG*; *glnK2* and *amtB2*) were co-transcribed. This must therefore be taken into account when drawing any conclusions about strains created with deletions within *draT2* or *glnK2*.

6.2.2 Construction of the deletion plasmids

The plasmids designed to introduce deletions into *glnK2*, *draT2* and *nifDH* were constructed by first identifying suitable flanking regions for the targeted deletion sites. Ideally the region deleted would be approximately 1000 bp in length, and the two flanking regions 900 bp each, based on successful experience with other gene disruptions (David Lea-Smith, personal communication; see also Chapter 5). In practice the former requirement was not often possible, either because the gene targeted for deletion was less than 1000 bp in length itself, or because restriction sites present in the genomic sequence upstream or downstream of the flanking regions constrained the possible positions of the flanking regions. It was considered more important that the flanking regions should be long enough to confer a high rate of recombination with the genome. Figure 6.1 illustrates flanking

regions identified for construction of the deletion plasmids.

In order to construct a deletion plasmid, the two flanking regions were first amplified separately from wild-type gDNA by PCR with primers including appropriate restriction sites. The left flanking region was then digested and inserted into pUC19 digested with the same restriction enzymes. The resulting plasmid was then digested with the appropriate restriction enzymes and the right flanking region inserted into this plasmid adjacent to the left. The full sequence of left and right flanking regions were then removed by digestion and inserted into pK*mobsacB* digested by the same enzymes. The primers used for amplification of each set of flanking regions, the associated restriction sites and expected lengths are listed in Table 6.2, and the final plasmids are illustrated in Figure 6.3.

6.2.3 Introduction of deletions into *R. palustris*

These plasmids were then introduced into wild-type *R. palustris* by electroporation in the manner described in Chapters 2 and 4. Again, PCR with ‘spanning primers’ was used to test for this as described for the deletion mutants in Chapter 5; a shorter product only is expected from an unmarked knockout, compared to a longer product from the wild-type. Both products are expected from marked knockouts.

After selection on kanamycin for transformants, 4 putative Δ *draT2* colonies, 5 putative Δ *glnK2* colonies and 6 putative Δ *nifDH* colonies were picked and PCR was used to test for successful insertion of the plasmid into the genome. Of these, 4, 4 and 2 for the *draT2*, *glnK2* and *nifDH* knockouts respectively gave the expected products (data not shown), and one transformant line for each targeted deletion was chosen to carry forward.

These were then selected on sucrose medium for successful excision of the plasmid and native sequence from the genome, leaving only the shortened deletion sequence introduced by the plasmid. Of 9 putative Δ *draT2* colonies, 10 putative Δ *glnK2* colonies and 8 colonies putative Δ *nifDH* picked for testing by PCR, 6, 3 and 5 respectively gave the expected products (data not shown), and one transformant line for each targeted deletion was chosen to carry forward.

To further verify that the sequences targeted for deletion had been completely removed from the genome, PCR was also conducted using primers complementary to the sequences targeted for deletion, ‘internal’ primers. In this case a product is not expected from an unmarked knockout, in contrast with the wild-type. The spanning primers and internal primers used to verify the putative knockout strains are listed in Table 6.3.

Primer	Sequence	Restriction site	Product size / bp
<i>draT2</i> Left Forward	GTACTCTAGAGAGTTCGACGAGACCGAATT	XbaI	911
<i>draT2</i> Left Reverse	GTACGTCGACTCACCTTGGCCGGTTCT	Sall	-
<i>draT2</i> Right Forward	GTACGTCGACGCACGCACATTACGCTGTAT	Sall	903
<i>draT2</i> Right Reverse	GTACAAAGCTTGGCGTGAAGCCGAAAATG	HindIII	-
<i>glnK2</i> Left Forward	GTACGAAATCTGGTTCGGATTCAAATGG	EcoRI	900
<i>glnK2</i> Left Reverse	GTACGGATCCACAATTTTCATGGTCTATCC	BamHI	-
<i>glnK2</i> Right Forward	GTACGGATCCGTCATCGGCCTCGACCAC	BamHI	906
<i>glnK2</i> Right Reverse	GTACTCTAGATGGTTCATGGTCAGCGAGT	XbaI	-
<i>nifDH</i> Left Forward	GTACGAAATCCACCCTTCCATGCCGAGAT	EcoRI	906
<i>nifDH</i> Left Reverse	GTACGGATCCAAAGGACATGTCCACATCA	BamHI	-
<i>nifDH</i> Right Forward	GTACGGATCCGACGAGGCGTACTTCAGAAATG	BamHI	941
<i>nifDH</i> Right Reverse	GTACGCAATGCTTGGATTGCCGTCGCTTC	SphI	-

Table 6.2: List of primers used to amplify flanking regions for construction of deletion plasmids with associated restriction sites included to facilitate transfer into and between plasmids.

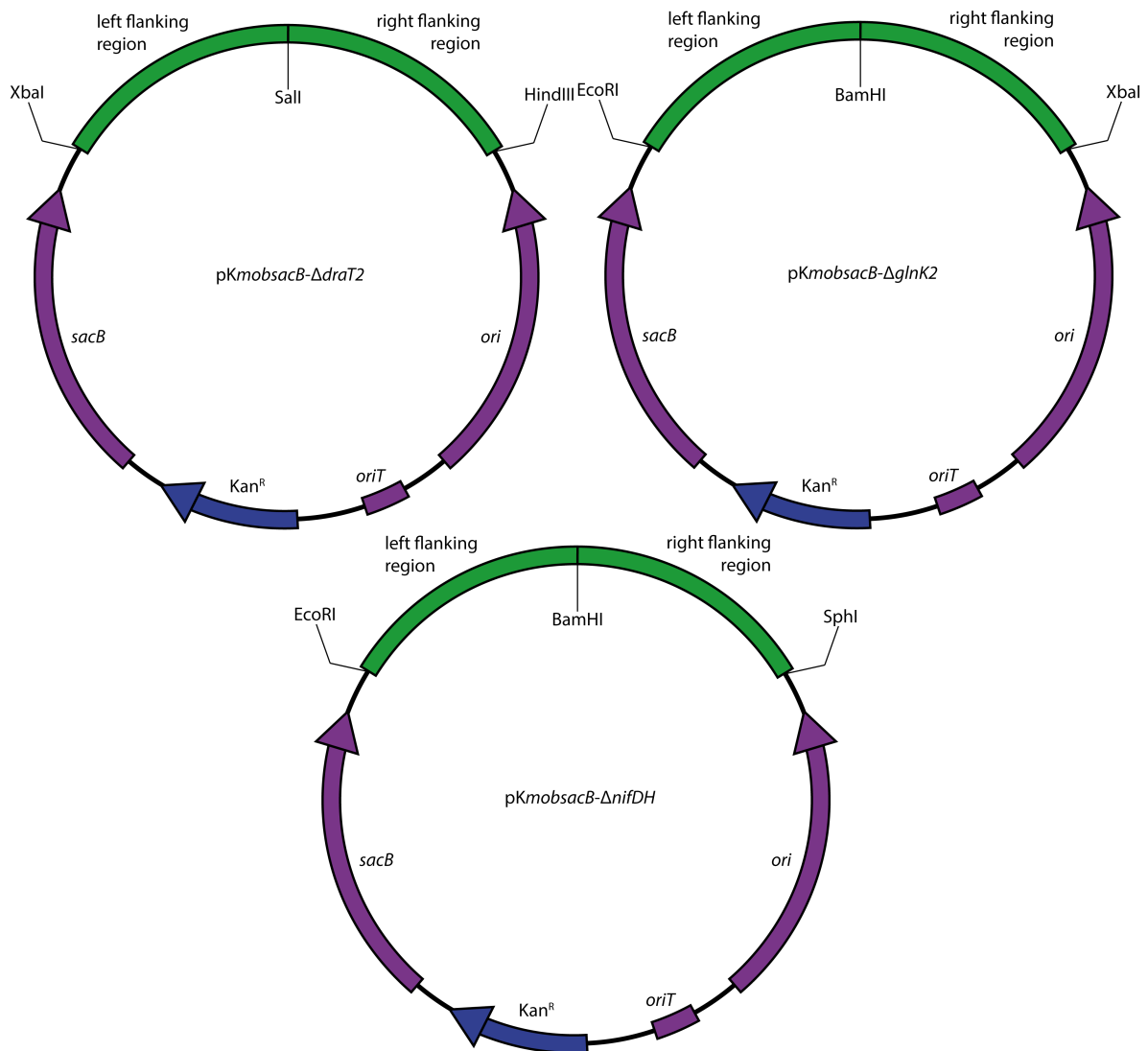


Figure 6.3: Illustrations (not to scale) of the plasmids used to introduce deletions into *R. palustris*. Features of the pKmobsacB delivery plasmid are shown in purple (*sacB*, *ori* and *oriT*) and blue (kanamycin resistance cassette; Kan^R). Flanking regions inserted into the multiple cloning site of pKmobsacB are shown in green; the restriction sites used to do so are labelled.

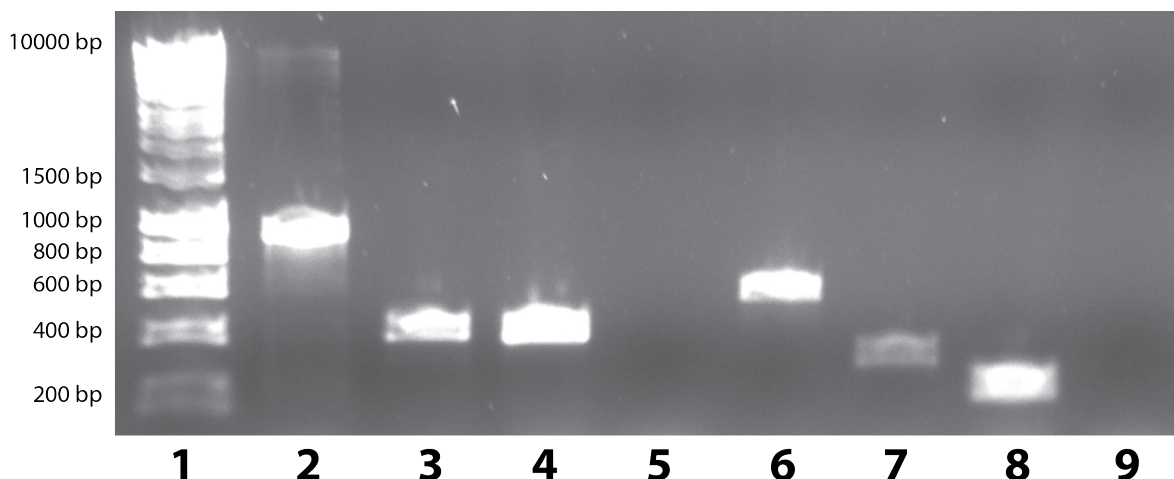


Figure 6.4: Visualisation of amplification products generated by PCR from *R. palustris* strains. Lanes: (1) DNA ladder; (2) wild-type / *draT2* spanning primers; (3) $\Delta draT2$ / *draT2* spanning primers; (4) wild-type / *draT2* internal primers; (5) $\Delta draT2$ / *draT2* internal primers; (6) wild-type / *glnK2* spanning primers; (7) $\Delta glnK2$ / *glnK2* spanning primers; (8) wild-type / *glnK2* internal primers; (9) $\Delta glnK2$ / *glnK2* internal primers.

Having created three single knockout lines ($\Delta draT2$, $\Delta glnK2$, $\Delta nifDH$), the *glnK2* and *nifDH* deletions were also introduced separately into the $\Delta draT2$ strain with the aim of creating both a $\Delta draT2\Delta glnK2$ strain and a $\Delta draT2\Delta nifDH$ strain. Representative results of PCRs conducted to verify these strains are presented in Figures 6.4 to 6.6.

6.2.4 Characterization of growth and the ammonium response of the $\Delta draT2\Delta glnK2$ and $\Delta nifDH$ strains

Having created the strains described above, it was desirable to characterize not only their growth (an important feature of any potential chassis strains) but also potential effects of the deletions on the inactivation of the Mo-nitrogenase by ammonium. The available space on the cultivation cabinet restricted the number of strains which could be cultivated simultaneously, and as the effect of fixed nitrogen was also of interest only two strains could be compared with the wild-type. Thus the $\Delta nifDH$ strain was chosen to assess the growth of *R. palustris* when the Mo-nitrogenase is unavailable and the $\Delta draT2\Delta glnK2$ strain was chosen to assess whether these deletions had had an effect on the ammonium inactivation response. It was reasoned that if either the *draT2* or the *glnK2* deletion had an effect it would be apparent from this strain, and follow-up work with the individual knockouts would reveal the separate contributions to this effect of each gene deletion.

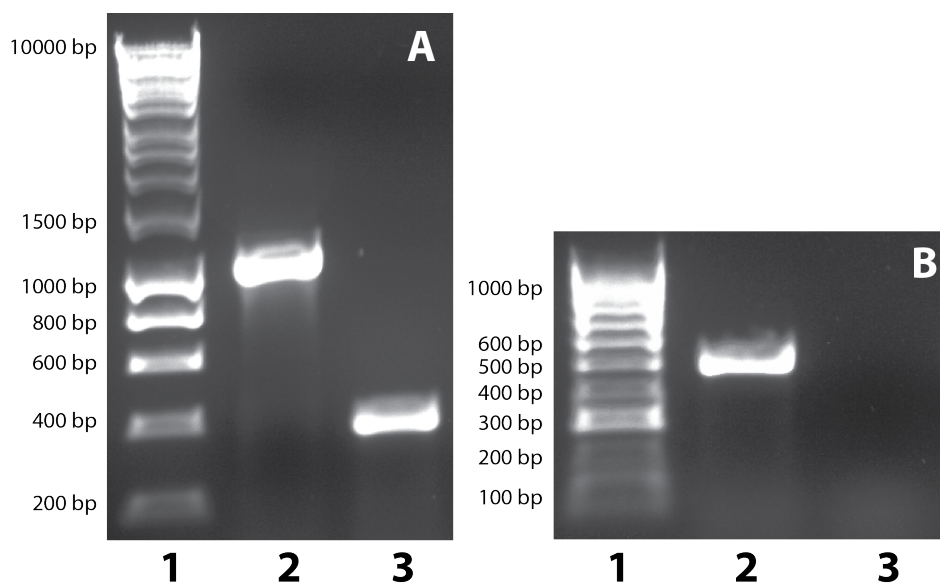


Figure 6.5: Visualisation of amplification products generated by PCR from *R. palustris* strains. Lanes (A): (1) DNA ladder; (2) wild-type / *nifDH* spanning primers; (3) $\Delta nifDH$ / *nifDH* spanning primers. Lanes (B): (1) DNA ladder; (2) wild-type / *nifDH* internal primers; (3) $\Delta nifDH$ / *nifDH* internal primers.

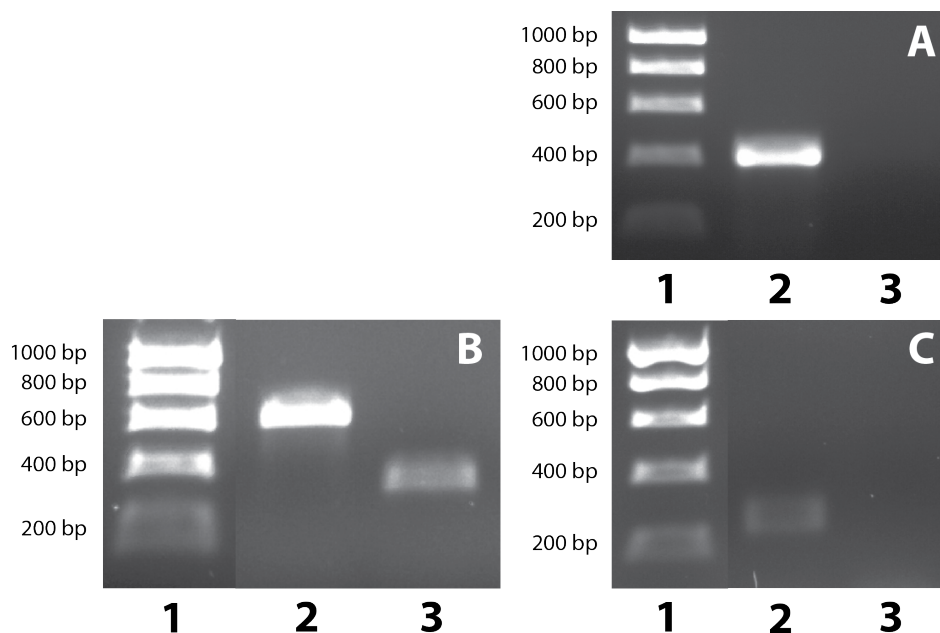


Figure 6.6: Visualisation of amplification products generated by PCR from *R. palustris* strains. Lanes (A): (1) DNA ladder; (2) wild-type / *draT2* internal primers; (3) $\Delta draT2\Delta glnK2$ / *draT2* internal primers. Lanes (B): (1) DNA ladder; (2) wild-type / *glnK2* spanning primers; (3) $\Delta draT2\Delta glnK2$ / *glnK2* spanning primers. Lanes (C): (1) DNA ladder; (2) wild-type / *glnK2* internal primers; (3) $\Delta draT2\Delta glnK2$ / *glnK2* internal primers. Intervening lanes that were not relevant have been removed from (B) and (C) in the interests of clarity.

Primer	Sequence	Expected product size / bp	
<i>draT2</i> Spanning Forward	CCATTTGCGCCAACGACTATC	Wild-type	929
<i>draT2</i> Spanning Reverse	TGTTGAAAAACAGGACCTTCG	Knockout	403
<i>draT2</i> Internal Forward	GCATTCCAGCAACCTCGT	Wild-type	403
<i>draT2</i> Internal Reverse	TTCGACGTACACCGTCCATA	Knockout	-
<i>glnK2</i> Spanning Forward	CGCTGATTCCGAAATGATTC	Wild-type	555
<i>glnK2</i> Spanning Reverse	GCCGTAGGGACGTTTGAA	Knockout	288
<i>glnK2</i> Internal Forward	TGGCGATCATTAAGCCATTC	Wild-type	205
<i>glnK2</i> Internal Reverse	GTCTTCTCGACCTGCTCGTT	Knockout	-
<i>nifDH</i> Spanning Forward	GATCTTGCCGAGCTTCTTGT	Wild-type	1077
<i>nifDH</i> Spanning Reverse	CATCACCGCGATCAACTTC	Knockout	389
<i>nifDH</i> Internal Forward	GCGTTCGTACGTATTGAGGT	Wild-type	491
<i>nifDH</i> Internal Reverse	AACTCGCAGCTGATCCACTT	Knockout	-

Table 6.3: List of primers used to test putative $\Delta draT2$, $\Delta glnK2$ and $\Delta nifDH$ transformants.

Cultures were grown as described in Chapters 2 and 3, on the cultivation cabinet under $40 \mu\text{mol photons m}^{-2} \text{ s}^{-1}$ and stirred at 200 rpm. The growth media were supplemented with either ammonium sulfate to a final concentration of 10 mM or an equivalent volume of water. Cultures were grown under a nitrogen atmosphere; this would allow the cells to survive through nitrogen fixation in the absence of supplemental fixed nitrogen, and the same atmosphere was provided to cultures supplemented with fixed nitrogen in order to keep the conditions otherwise the same. The results of this growth assay are presented in Figures 6.7 and 6.8.

These results show that growth of both the wild-type and $\Delta nifDH$ strains was lower under nitrogen-fixing conditions. The growth of the $\Delta nifDH$ strain was comparable to that of the wild-type when grown with supplemental ammonium. This was as expected; the Mo-nitrogenase is strongly repressed in the presence of ammonium, and so the wild-type would not be expected to be utilizing the Mo-nitrogenase under these conditions. The $\Delta nifDH$ strain however suffered a greater reduction in growth rate under nitrogen-fixing conditions, such that its growth was substantially slower than the wild-type under the same conditions. This suggests that strains unable to utilize the Mo-nitrogenases experience a slower rate of growth, in agreement with previous findings by for example [46].

As the growth medium used for these experiments does not contain any vanadium, the $\Delta nifDH$ strain is presumably only able to utilize the Fe-nitrogenase under these conditions. Although it is possible that the cells are recycling existing vanadium in order to synthesise the Va-nitrogenase, it would be interesting to see whether supplementing the growth medium with vanadium affected the growth rate, as utilizing the Fe-nitrogenase alone is expected to confer the lowest rate of growth

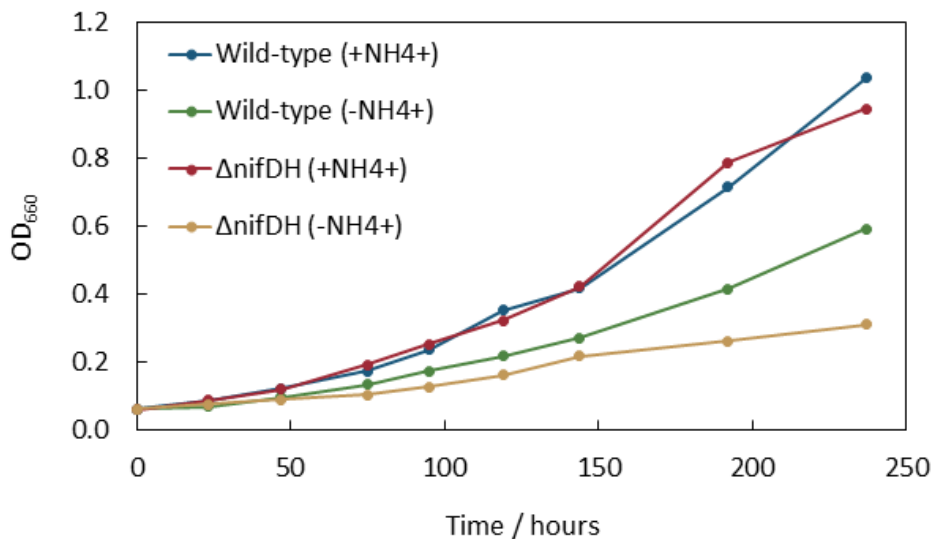


Figure 6.7: Optical density measured at 660 nm of *R. palustris* cultivated in the cultivation cabinet described in Chapter 3 under standard lighting and a nitrogen atmosphere: wild-type +NH₄⁺ (blue); wild-type -NH₄⁺ (green); $\Delta nifDH$ +NH₄⁺ (red); $\Delta nifDH$ -NH₄⁺ (brown).

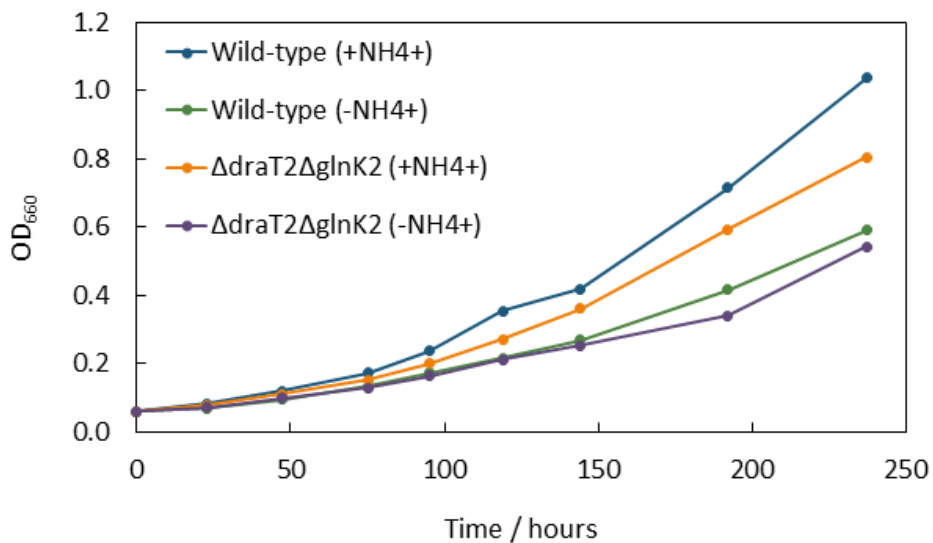


Figure 6.8: Optical density measured at 660 nm of *R. palustris* cultivated in the cultivation cabinet described in Chapter 3 under standard lighting and a nitrogen atmosphere: wild-type +NH₄⁺ (blue); wild-type -NH₄⁺ (green); $\Delta draT2\Delta glnK2$ +NH₄⁺ (orange); $\Delta draT2\Delta glnK2$ -NH₄⁺ (purple).

[46].

In contrast, the results for the $\Delta draT2\Delta glnK2$ strain show that growth of this strain was comparable to that of the wild-type under nitrogen-fixing conditions. Again, this might be expected, as these proteins are thought to act in response to fixed nitrogen to regulate the nitrogenases. This strain was found to have a slightly lower rate of growth than the wild-type in the presence of fixed nitrogen. Assuming that the loss of the DraT / DraG and possibly other nitrogenase regulatory systems in this strain prevented the cells from inactivating the Mo-nitrogenase, this reduced growth is likely to have been a result of the significant energy cost associated with nitrogen fixation, an unnecessary expense in the presence of external fixed nitrogen.

6.3 Discussion

This work resulted in the creation of several strains believed to be promising candidates as chassis strains for hydrogen production, and for investigation into the nitrogenase regulatory system of *R. palustris*. Single knockouts of *draT2*, *glnK2* and *nifDH* were created, as were two double knockouts, $\Delta draT2\Delta glnK2$ and $\Delta draT2\Delta nifDH$. As discussed in section 5.4.1, these would ideally be further verified by PCR with one primer homologous to part of the chromosome not present within the delivery plasmid, but persistence of the plasmid within the cells is highly unlikely [3]. A Mo-nitrogenase knockout has been previously created in *R. palustris* [46], but not in conjunction with a disruption of *draT2*. Preliminary findings with these strains show that the growth of $\Delta nifDH$ was impaired in comparison with the wild-type under nitrogen-fixing conditions, presumably as a result of the higher energy demands of the Fe-nitrogenase (or possibly Va-nitrogenase) on which it must rely for its nitrogen fixation requirements under these circumstances. With the addition of supplemental ammonium the growth of this mutant did not differ notably from that of the wild-type, as might be expected.

The $\Delta draT2\Delta glnK2$ strain was found to have a lower growth rate than the wild-type during growth on supplemental ammonium. If the ability of the cell to inactivate nitrogenase activity in response to fixed nitrogen has been disrupted in this strain, these results are as one would expect; the high energy costs associated with nitrogen fixation come at a cost to the growth of the cell. The reduction in growth rate was not so large as to suggest that this strain would make an unsuitable candidate for industrial production of hydrogen, however.

Clearly there is much potential work that could be carried out in future with these strains. Repli-

cates of the growth assays would allow more robust conclusions to be drawn from these data, and concurrent measurement of hydrogen output would provide much more insight into the factors driving any differences in growth rate. Supplementation of the growth medium with vanadium would allow for comparison between the Va- and Fe-nitrogenases. Complementation analyses could be used to confirm the effects are due to the intended deletions, rather than additional ones introduced during the manipulations. Although growth and hydrogen production data already exists for a Mo-nitrogenase knockout [46], no data have yet been reported on the long-term overall output of a Mo-nitrogenase knockout compared with wild-type *R. palustris*, which might provide some insights into the balance between growth rate and the higher rates of hydrogen production by the alternative nitrogenases.

This balance should also be assessed for the $\Delta draT2\Delta glnK2$ strain, and furthermore the contributions to any changes in hydrogen output by *draT2* and *glnK2* separately could be investigated. The $\Delta draT2\Delta nifDH$ strain is also of interest as it could provide insight into the mechanisms by which post-translational regulation of the alternative nitrogenases occurs; this is believed to be mediated by ADP-ribosylation as for the Mo-nitrogenase, but the DraT2 protein has not been definitively shown to be responsible [94]. The DraT proteins of other bacteria have been reported to post-translationally regulate Fe-nitrogenases (see for example [96]), but this has never been reported for a Va-nitrogenase.

Finally, there are further possible targets for gene deletion in *R. palustris* for the purpose of improving hydrogen production by this organism. Although increasing the hypothetical maximum rate of a culture is an important avenue to pursue, consideration should also be given to the more practical aspects of cultivating bacteria on a large scale for industrial purposes. Light penetration and surface photoinhibition have been identified as both key barriers to successful implementation of photofermentative technologies (although purple bacteria are much less sensitive to photoinhibition than oxygenic organisms [97]) and also therefore as key targets for further research and potential genetic manipulation [36, 34]. Reducing the size of antenna complexes in *R. palustris* could improve penetration of light through dense or deep cultures and allow cultivation under higher light intensities, though the effects of such manipulation have been variable in other species (for example see [98]). If this did result in greater productivity in *R. palustris*, however, the combination of such alterations with those described here to *draT2* and / or *glnK2* could result in a highly effective strain for large-scale hydrogen production.

7 Discussion and further work

7.1 Development of photobioreactor for cultivation of *R. palustris*

One of the first aims of this work was to develop a suitable platform for cultivating *R. palustris* for research purposes, while also informing our understanding of the growth requirements of the organism with a view to potential industrial application in the future. A ‘cultivation cabinet’ was constructed to meet two particular needs for this purpose: the specific spectral requirements of *R. palustris* [2], and the ability to collect and measure hydrogen and other outputs. This cultivation cabinet was shown to allow a greatly higher rate of growth than a standard laboratory incubator, and was successfully used to measure the rate of hydrogen production by *R. palustris*.

Investigation into the effects of light wavelength spectrum on growth revealed that infrared light in particular and also ultraviolet light had a significant impact on growth rate. It can be assumed that the provision of these wavelengths by the cultivation cabinet is a large contributing factor to the higher growth rate observed on the cabinet than in a standard laboratory incubator; the only other major differences were the higher temperature, shown to confer only a minimal increase in growth rate, and the method of agitation by stirring rather than shaking, which seems unlikely to be responsible.

Growth under sunlight was also observed and found to confer a surprisingly high rate of growth given the low temperature, relative lack of agitation, and long periods of darkness. As a result, cultures of *R. palustris* being prepared for experiments were grown up under sunlight rather than in an incubator, except where the cultivation cabinet was available for this purpose. As costs of illumination can be prohibitive for industrial applications, these results suggest that for industrial purposes pursuing growth under sunlight may well be the most efficient approach in terms of energy and cost, even if higher absolute rates of growth can be achieved with custom lighting.

Light penetration has been identified as one of the key barriers to successful implementation of photofermentative hydrogen production at an industrial level [36, 34], and for most organisms studied increasing the light intensity in an effort to combat this simply results in greater photoinhibition at the surface layers (see for example [99]). However, simulations of growth in a shallow pond setup suggest that *R. palustris* is able to withstand high irradiances of light without overall levels of photosynthesis suffering as a result of photoinhibition [27]. Similarly, it has been found that the photosystems of *R. palustris* grown in an outdoor tubular photobioreactor remained active

throughout the day without suffering impairment from high irradiance [100].

Addessi et al. also reported a relatively high rate of hydrogen production (27.2 mL per L culture per hour), but found that hydrogen yield was negatively affected during periods of darkness [100]. This was presumably due to hydrogen recycling by *R. palustris*, though the cause was not investigated. In this case the strain used was not CGA009, which is thought to be a natural hydrogen uptake mutant [4]. The latter observation supports the use of CGA009 for industrial hydrogen production, though loss of hydrogen overnight could also be mitigated by provision of artificial light during this time. This evidence all points towards *R. palustris* being an excellent candidate for outdoor biotechnological applications.

The preference of *R. palustris* for anaerobic growth should mean that stirring need only provide enough agitation to ensure cells receive sufficient exposure to light, and to mix in fresh feedstock in the case of continuous reactors. Indeed, recent work by Robert Pott and John Dennis indicates that the rate of hydrogen production by *R. palustris* is maintained even under a fairly long light / dark cycle (unpublished data). The results presented in this work also suggest that a high rate of growth and presumably hydrogen production could be obtained by provision of artificial light overnight and / or greater levels of agitation and temperature. Furthermore, glycerol is not the only potential feedstock for production of hydrogen by *R. palustris*; there are many potential waste streams which could be effectively utilized via photofermentation (see for example [69, 101]).

Reduction in yield because of photoinhibition could also be tackled through manipulation of the light-harvesting complexes of photofermentative bacteria; these complexes are usually optimized for low light intensities and thus absorb more energy than the cell can cope with under high intensities [34]. Reduction of the antennae complexes has therefore been identified as a key target of research for improving photofermentative hydrogen production [36, 102]. However, thus far conflicting results have been achieved through this approach (see for example the study on *Synechocystis* sp. PCC 6803 [98], and studies on *Rhodobacter sphaeroides* [103, 104]). A key area of investigation for *R. palustris* is therefore to determine the effects of similar manipulations on this organism's hydrogen output, which could be achieved through deletion mutants created as described here. If hydrogen production were successfully increased by reduction of antenna size, there would be great potential for combining these modifications with those for *phaAB*, *glgCA* or *draT2*, for example, for potentially even greater hydrogen yields.

The key questions in this area which could be addressed with further work are:

- How does the intensity of light on the cultivation cabinet affect the growth rate of *R. palustris*?
- Can the rate of growth under sunlight be increased to a level approaching or exceeding that achieved on the cultivation cabinet by providing heating, agitation and / or artificial light overnight?

It would also be interesting to see whether greater rates of growth could be achieved with the general cultivation cabinet setup by providing extra wavelengths of light (for example around 450 nm, 780 nm and 275 nm), particularly if the number and intensity of LEDs were not increased in doing so (or if the number were increased but individual intensity decreased). It would be interesting to compare this to growth under sunlight, which is presumably benefitted by a greater range of wavelengths. It would however require the construction of an entirely new cultivation cabinet to conduct this investigation.

7.2 Optimization of electroporation protocol for transformation of *R. palustris*

Another key aim of this work was to improve the low transformation efficiency previously achieved with electroporation of *R. palustris*. Although for our purposes the procedure only needed to generate one transformant successfully, in terms of absolute number of colonies the low efficiency was particularly problematic when an inherently inefficient transformation was being attempted. For example, attempts to introduce further deletions into the $\Delta hupL\Delta phaAB\Delta glgCA$ strain were entirely unsuccessful (data not shown), and as mentioned in Chapter 5, electroporation of the $\Delta phaAB\Delta glgCA$ strain resulted in very few or no colonies; possibly because of the lower viability of these strains. Likewise, introduction of the large pKmobsacB $\Delta hupL::ipi::ispS$ plasmid also resulted in very few colonies and a high percentage of colonies showing reversion to wild-type. It was therefore highly desirable to improve the efficiency of this process to increase the chances of successfully generating transformants. Furthermore, future work may require generation of multiple strains of the same genotype, in which case a higher number of colonies would be very beneficial.

The optimization strategy followed resulted in a 6-fold increase in transformation efficiency to approximately 1200 colonies per μg DNA with the neutral plasmid used in those experiments. This was achieved through adjusting the voltage and resistance of the pulse applied to *R. palustris* cells, and through incubation of the cells post-shock on ice rather than in warm medium. Use of cells at a

later culture stage resulted in a reduced transformation efficiency, and a lower density of cells either had no effect or decreased the transformation efficiency, depending on the pulse strength. Compared with other model organisms such as *Escherichia coli*, for which a transformation efficiency of about 10^5 colonies per μg DNA for a small plasmid would be expected [80], this still represents a very low transformation efficiency. However, it represents a significant improvement to the process which is anticipated to improve the rate at which mutant strains can be created.

The key questions in this area which could be addressed with further work are:

- Can the incubation period be further reduced? This applies both to the 30-minute period on ice, and the subsequent 60-minute period of warming.
- Is a higher rate of transformation efficiency achievable with an earlier culture stage, or even a culture stage between the two investigated?
- What effect does DNA concentration have on transformation efficiency, and how does this interact with cell density?
- Does the efficiency depend on the plasmid itself; for example the extent of homology with the bacterial chromosome?

7.3 Characterization of existing chassis strains of *R. palustris*

The growth and hydrogen production of several genetically altered strains of *R. palustris* were characterized. These strains carried deletions in genes for an uptake hydrogenase, for biosynthesis of PHB, and for biosynthesis of glycogen, and were of interest as potential chassis strains. None of the single knockout strains were found to have significantly different growth rates from the wild-type, nor observed to produce more or less hydrogen.

The fact that the $\Delta hupL$ strain was not found to produce greater quantities of gas than the wild-type prompted the discovery that the CGA009 strain used throughout this work is a natural uptake hydrogenase mutant due to a frameshift mutation in the gene for the regulatory protein HupV, consistent with the findings of Rey *et al.* [4]. Greater overall production of hydrogen might otherwise have been expected from the $\Delta hupL$ strain, given the loss of the hydrogen-recycling capability provided by the uptake hydrogenase. This also explained the lack of growth impairment observed from

the *hupL* deletion. Altogether this established that *hupL* and indeed other genes associated with the uptake hydrogenase are suitable sites for insertion of transgenes.

The $\Delta phaAB\Delta glgCA$ (and $\Delta hupL\Delta phaAB\Delta glgCA$) strain was found to have a significantly lower rate of growth than the wild-type, but the rates observed suggest that this strain may nevertheless be suitable for industrial applications, especially where production of specific high-value compounds, rather than biomass, is the goal. The fact that the combined loss of PHB and glycogen biosynthetic capability resulted in reduced growth but the growth of neither of the equivalent single knockouts was markedly affected suggests that *R. palustris* may redirect resources from one to the other when needed, though this was not supported by evidence from the glycogen and PHB assays conducted to verify the mutant strains. Another possibility is that loss of both pathways impairs the ability of the cells to respond dynamically to osmotic stress [90], while compensation is possible in the strains still able to produce either glycogen or PHB.

These two multiple knockout strains were also both found to produce more gas (assumed to be mostly hydrogen, based on other studies [40]) per unit biomass than the other strains, suggesting that *R. palustris* redirects resources into hydrogen production if other routes are unavailable (supported by [91]), and presenting these strains as good candidates for industrial hydrogen production. This could possibly work better as a batch process to overcome their slower growth, though it is suggested that continuous processes are in general likely to result in higher rates of hydrogen production [105]. The greater hydrogen output of these strains is likely to be due to an excess of reducing equivalents [92]: PHB has been identified as a major sink of reducing equivalents in purple non-sulfur bacteria [106], and creation of PHB-deficient mutants in species such as *Rhodobacter sphaeroides* has successfully resulted in increased hydrogen production, though this was sometimes reported to be dependent on the carbon source [107, 108].

It is possible that introduction of heterologous electron-consuming pathways for production of alternative compounds may actually improve or even restore the growth of these strains, positioning them as excellent candidate chassis strains for industrial of other compounds as well. Insertion of heterologous genes for redox-consuming pathways has been reported to increase growth rate in *Saccharomyces cerevisiae*, for example [61]. However, the effect may be limited if the growth impairment observed is at least partially due to reduced robustness to osmotic stress, as discussed above.

The key questions in this area which should be addressed with further work are:

- How does hydrogen production compare between strains when cells are re-suspended in fresh medium before measurement? Do replicates, under these conditions, support the current findings, particularly the increased gas output of the multiple knockout strains?
- Does complementation of these strains restore the wild-type phenotype, in particular the growth rate of the multiple knockout strains? This would confirm that it is the known mutations that are responsible for the effects observed.
- Can uptake hydrogenase activity be restored through genetic manipulation, and does this improve the growth rate of the CGA009 strain?
- Do the multiple knockout strains exhibit greater vulnerability to osmotic stress than the wild-type? If so, are the single knockout strains wholly able to compensate for this?

7.4 Insertion of heterologous genes into the genome of *R. palustris*

Heterologous gene sequences were introduced into *R. palustris* with the aim of conferring the ability to produce isoprene and propane-1,2-diol, into the site targeted for deletion of *hupL*, with a promoter sequence derived from *aceA* and a terminator sequence obtained from downstream of RPA4393. This successfully resulted in integration of heterologous sequences into the *R. palustris* genome, and is a novel demonstration of insertion of heterologous genes into the *hupL* locus. RT-PCR carried out to confirm the presence of transcripts in the transformants gave inconclusive results, and suggested that transcripts were not present at detectable levels in strains carrying two heterologous genes. However, transcripts were potentially detected in the strain carrying *ispS* only, suggesting that the promoter sequence used was suitable. The lack of conclusive evidence for the presence of stable transcripts of the heterologous genes meant that further investigation of these strains was not carried out at this time.

The key questions in this area which should be addressed with further work are:

- Does PCR with primer pairs complementary to the native chromosome sequence and to the inserted sequences confirm the integration of these sequences into the genome?
- Does insertion of longer sequences suffer from a lower rate of successful integration?
- Can translated protein be detected by Western blot in the strains carrying tagged versions of the genes, particularly that carrying the *ispS* gene only?
- Does this strain (or these strains) produce the target compound, and if so is the rate or yield greater in the $\Delta phaAB\Delta glgCA$ background, and is the growth rate affected?

More broadly, it will be desirable to characterise more closely the expression signals used by *R. palustris* CGA009 for transcription and translation as has been done for more widely-used photo-synthetic bacteria, such as the cyanobacteria (see for example [109]). For example, the *R. palustris* promoter for *pckA*, encoding phosphoenolpyruvate carboxykinase, has been shown to drive expression consistently for growth on a variety of carbon sources [42], but a more recent study on GFP-expressing strains found this promoter to be ineffective at driving expression, and that of the three promoters tested the codon-optimized *E. coli*-derived *lac* promoter was the most effective [44]. This indicates that much more work is needed to inform our understanding of these systems in *R. palustris*.

7.5 Creation of potential *R. palustris* chassis strains for hydrogen production

As well as characterization of existing candidate chassis strains, this work produced several new candidates for hydrogen production with deletions in *draT2*, *glnK2* and *nifDH*. The $\Delta nifDH$ strain was found to suffer from impaired growth under nitrogen-fixing conditions, as has been reported previously [46]. However, no analysis has yet been undertaken to determine the trade-off between growth rate and hydrogen production per unit biomass, for which this strain could be used. The fairly substantial reduction in growth suggests that the Mo-nitrogenase may indeed be the better candidate for industrial production of hydrogen, but the lack of supplemental vanadium in the growth medium means that the cells may have been utilizing only Fe-nitrogenase. It is possible that under conditions where the Va-nitrogenase can be utilized the growth rate would be improved, and there may also be other advantages to the alternative nitrogenases. The Va-nitrogenase for ex-

ample is more active at lower temperatures than the Mo-nitrogenase [5], which might make strains utilizing this nitrogenase better candidates for outdoor growth as discussed previously.

The $\Delta draT2\Delta glnK2$ strain was found to grow more slowly than the wild-type in the presence of supplemental ammonium. It has previously been reported that a *draT2* knockout was relatively insensitive to ammonium [48], which suggests that this growth reduction is due to energy-expensive nitrogenase activity in this strain even in the presence of fixed nitrogen. Some inhibition still occurred, however, suggesting that either other proteins are able to carry out at least partial post-translational regulation of the Mo-nitrogenase, or that inhibition at the transcriptional or translational level was also occurring. It would therefore be interesting to see whether the $\Delta draT2\Delta glnK2$ strain exhibits complete abolishment of the ammonium response. The reduction in growth was not substantial enough to definitely preclude the use of this strain for industrial purposes were it found to confer a greater rate of hydrogen production.

The key questions in this area which should be addressed with further work are:

- Does supplementation with vanadium affect the growth rate of the $\Delta nifDH$ strain under nitrogen-fixing conditions?
- Does the $\Delta draT2\Delta glnK2$ strain show a more complete abolishment of the ammonium response than has previously been reported for *draT2* knockouts, and does this result in an even greater hydrogen yield?
- Does long-term cultivation of the $\Delta draT2\Delta glnK2$ and $\Delta nifDH$ strains result in a greater yield of hydrogen, or is the lower rate of growth of these strains substantial enough to cancel out greater rates of production per unit biomass?
- Is DraT2 involved in the post-translational regulation of the alternative nitrogenases, and does disruption of *draT2* in the $\Delta nifDH$ strain also abolish the ammonium response of the alternative nitrogenases?

7.6 Conclusions

In conclusion, *R. palustris* continues to present a promising prospect for biotechnological applications, not only for hydrogen production from glycerol, but potentially also from other feedstocks and for the production of other, higher-value compounds. There is an increasing appreciation of the importance of waste remediation by microorganisms, and it will be essential to find ways to use our resources more efficiently in the future as land usage becomes more congested with the increasing food and fuel requirements of a growing and developing global population.

This work has resulted in the development of a platform for cultivation of *R. palustris* superior to standard laboratory incubators, the improvement of the transformation efficiency of electroporation of *R. palustris*, the characterization of several potential chassis strains and the creation of several more, and the successful insertion of heterologous gene sequences into the *R. palustris* genome. With further development of the process for production of novel compounds by *R. palustris* in particular, and more investigation into the prospects for improving hydrogen production by the nitrogenase(s) of *R. palustris*, this organism has the potential to become a highly attractive system for industrial production of a wide variety of commercial compounds, and the bioremediation of a range of waste streams.

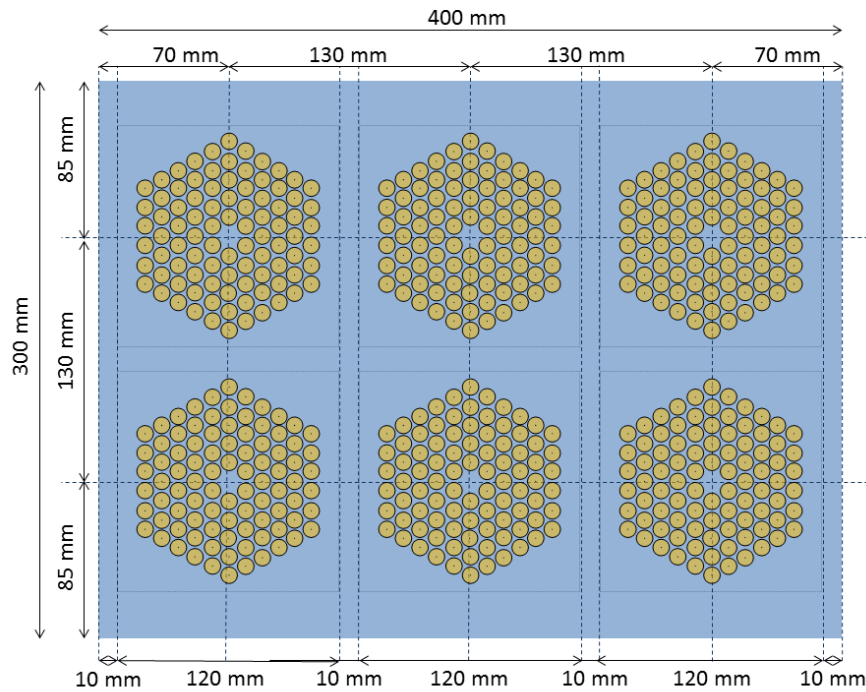


Figure A.1: Schematic diagram of the transparent PVC support panel positioned above the LED circuit board to hold up the culture flasks. Individual holes were drilled for each LED as shown (yellow) as the material was found to absorb ultraviolet light (see Chapter 1). Original design by Paolo Bombelli. Not shown: drill holes to screw each of the 6 LED circuit boards into place beneath the platform, and for 16 non-tapered screws (evenly spaced along both long edges (8), the longitudinal centre (4), and between the straight edges of the hexagons (4)) to hold the platform above the multi-stirrer without crushing the LED circuit boards.

A Schematic diagrams

This appendix provides schematic diagrams for the cabinet designed to enclose the cultivation platform constructed for cultivation of *R. palustris* and the support panel positioned over the LEDs to support the weight of the culture flasks. Both were created by Engineering and Design Plastics Ltd from original designs by Paolo Bombelli; the dimensions and associated figures for the cabinet itself were adjusted for the purposes of this work by the author.

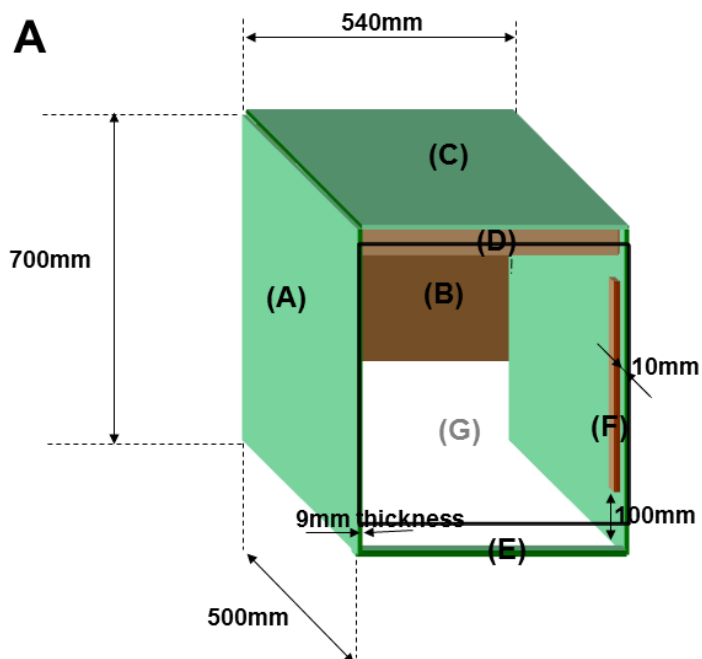


Figure A.2: Schematic diagram of the cabinet designed to surround the cultivation platform: 3-dimensional representation of the cabinet. Original design by Paolo Bombelli, adjusted for the purposes of this work by the author.

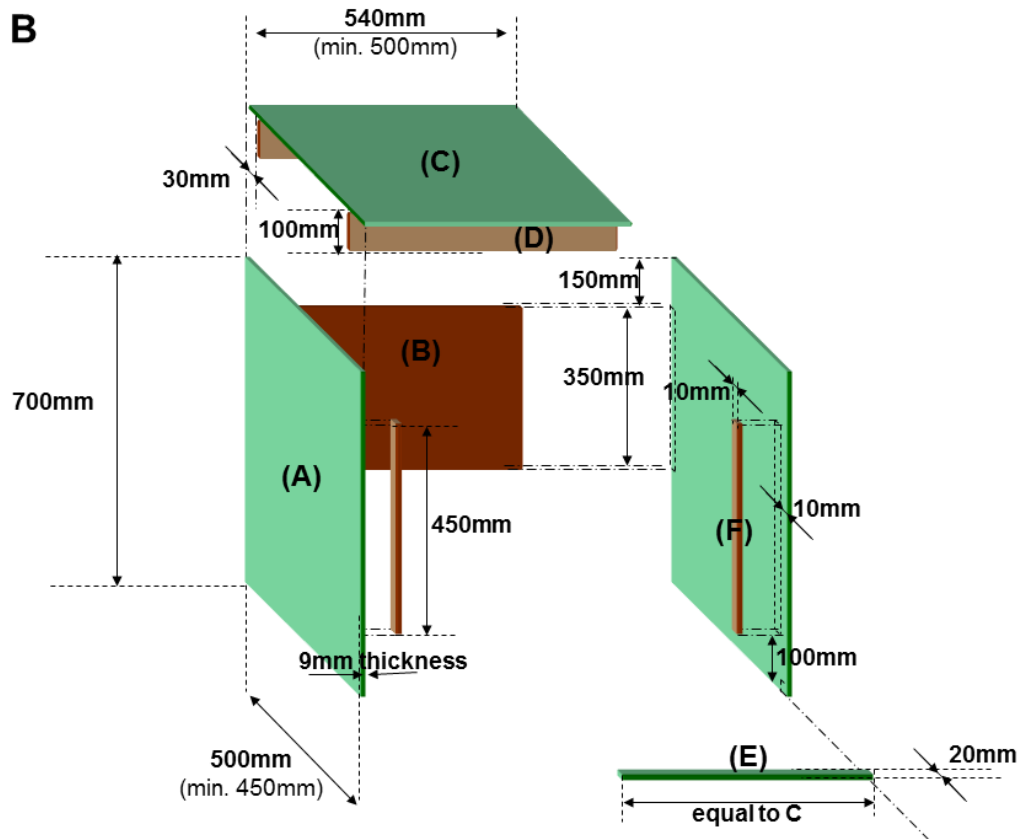


Figure A.3: Schematic diagram of the cabinet designed to surround the cultivation platform: exploded 3-dimensional representation of the cabinet with detailed dimensions. Original design by Paolo Bombelli, adjusted for the purposes of this work by the author.

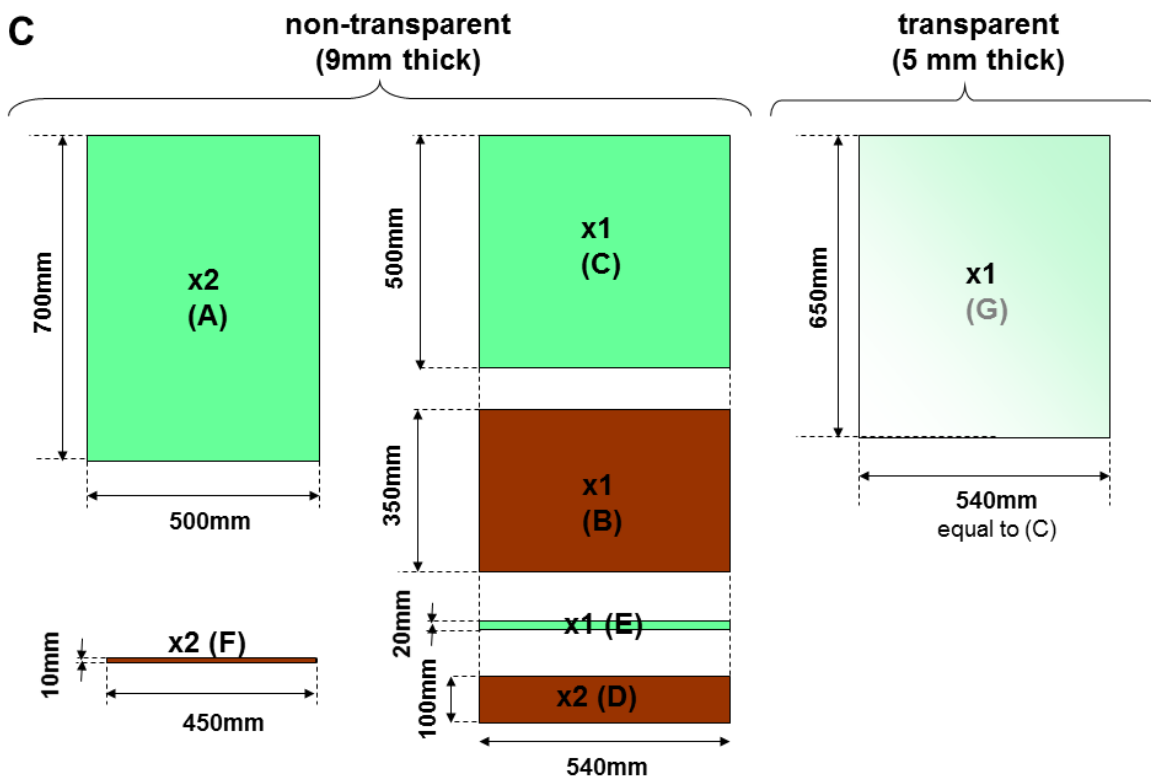


Figure A.4: Schematic diagram of the cabinet designed to surround the cultivation platform. (C) breakdown of parts with dimensions. Original design by Paolo Bombelli, adjusted for the purposes of this work by the author.

B Heterologous nucleotide sequences

This appendix details the sequences used for insertion of heterologous genes into *R. palustris* and nucleotide alterations made to these prior to ordering from GeneArt.

B.1 Sequences acquired from *R. palustris* genome

Taken from reference genome for strain CGA009 on NCBI (GenBank number: BX572607.1).

The 201 nucleotides selected to act as the promoter region:

```
TCAGATTCCGCCCCAGATATCGCGTTTTACAAAATTTACAAAATAACAATTGTTACATGTACTGAAGT
TACATGACATCACCATTCGTTTCGCAAGAGGTCTGTACGTCTTCTGTCATCTCGCGTTTATCTCTCGGC
ACGTTTTCACGGCGCGATTGTCACGAATGTCGCGCTGCGAATTATTCGTACCGAAGGGATCATGTC
```

Chromosome position: 4947990 - 4948190

Upstream of *aceA* (RPA4394; encoding isocitrate lyase)

Translation of the *aceA* nucleotide sequence and comparison with the isocitrate lyase protein sequence (NCBI) confirmed that the ATG highlighted in green above was out of frame and not the true start codon of *aceA*.

The 150 nucleotides selected to act as the terminator region:

```
TGCGCTCCTGAGCCGAGGCGGGCCACGCGCCGCCCGGGGAGCTGACGAGATAGAAGACGTCCAAGGAC
TTTGCGGCTCCTGTCGGGGCAACCCGTCAGGGCCGCCATCGTCGTTTCGGGGGCCCTTAGGCCGGAT
GGGGAACGTCCT
```

Chromosome position: 4945964 – 4946114

Downstream of RPA4393

B.2 Heterologous sequences

Full sequence designed for insertion of *mgsA* and *gldA*, propane-1,2-diol biosynthesis genes, including and ordered with promoter and terminator sequences:

```

GGATCC TCAGATTCGGCCCCAGATATCGCGTTTTACAAAATTTACAAAATAACAATTGTTACATGTAC
TGAAGTTACATGACATCACCATTCGTTTCGCAAGAGGTCTGTACGTCTTCTGTATCTCGCGTTTATCT
CTCGGCACGTTTACGGCGGATTTGTCACGAATGTGCGCTGCGAATTATTCGTACCGAAGGGATCAT
CCCATGGTA TATATCATGGAAGTACTACCCGACGTTGCCGGCGCGGAAGCATATCGCCCTGGTCCG
GCACGACCATTCGAAGCAGATGCTCATGAGCTGGGTGGAGCGCCACCAGCCCCGCTGGAACAACATG
TCCTGTACGCTACCGGGACCACGGGCAACCTCATCTCGCGTGGCACCAGGATGAATGTGAACGCCATG
CTGAGCGGTCCGATGGGCGCGATCAGCAGGTGCGGCGCGTGATCTCGGAGGGCAAAATTGACGTGCT
CATCTTCTTCTGGGACCCGCTTAACGCCGTCGCCGACGATCCGGACGTGAAGGCGCTGCTGCGCCTAG
CCACGGTCTGGAATATCCCCGTGGCCACCAACGTTGCCACCGCGGACTTTATCATCCAGTCCCCGCAC
TTCAACGATGACAGTGGACATCTTGATCCCGGATTATCAGCGGTACCTCGCGGACCGCCTGAAGTGC
GAATTATTCGTACCGAAGGGATCATCTCATGACCGCATCATCCAGTCCCCGGCAAGTACATCCAGG
GCGCCGACGTGATCAACCGGCTGGGCGAGTATCTCAAGCCGCTGGCTGAGCGCTGGTTGGTGGTGGG
GATAAATTCTGTGCTGGGTTTCGCCCAGTGCACCGTGGAAAAGTCATTCAAGGACGCGGGGCTCGTGGT
CGAGATTGCCCCGTTTCGGCGGAGAGTGCTCGCAAAATGAAATCGACCGTCTGCGCGGCATCGCGGAGA
CCGCCAGTGGGGGCGATCCTGGGTATCGGCGGCGCAAGACGCTTGATACCGCTAAGGCCCTCGCC
CACTTCATGGGCGTTCGCCGTCGCCATCGCGCCGACAAATCGCCAGCACGGACGCGCCGTGTTGGCGTT
GAGCGTGATTTACACCGACGAGGGCGAATTTGATCGGTATCTGTGCTCCCCAACAAATCCGAACATGG
TAATCGTCGACACCAAGATCGTGGCCGGAGCGCCTGCGAGACTGCTGGCAGCCGGCATCGGCGACCG
CTGGCCACGTGGTTTCGAGGCGGAGCGTGCTCCCGCTCGGGCGCCACCACGATGGCGGGCGGCAAGTG
CACCCAGGCCGACTCGCCCTGGCGGAGCTGTGCTACAATACTCTGCTCGAAGAGGGTGAAGAAAGCCA
TGCTTGCTGCGGAACAGCATGTCGTGACCCCGGCCCTGGAGCGGGTTCATCGAGGCGAACACGTATCTG
AGTGGCGTGGGCTTCGAATCGGGGGGCTCGCCGACGCGCACGCCGTGCATAACGGCCTGACCGCGAT
CCCAGATGCCACCACTACTATCACGGCGAGAAGGTGCGGTTCCGGCACCCCTAACGCAGTTGGTTCTCG
AGAACGCGCCGCTCGAAGAGATCGAGACCGTGGCCGCTCTGAGCCATGCCGTCGGTCTGCCCATCACC
CTGGCCCAGCTCGACATCAAGGAAGACGTGCCGGCGAAGATGCGCATTGTCCGCGAGGGCGGCTGCGC
GGAGGGCGAAACGATCCACAACATGCCGGGCGGGCAACCCGGATCAGGTGTACGCCGCGCTGCTCG
TCGCGGACCACTACGGCAACGCTTCTGCAGGAATGGGAAATGAGGCCCTGCGCTCCTGAGCCGAGGCG
GCGCACGCCGCCCGGCGAGCTGACGAGATAGAAGACGTCCAAGGACTTTGGCGGTCTGTGCGGGC
AACCCGTGAGGGCCGCATCGTCGTTTCGGGGGCCCTTAGGCCGATGGGGAAACGTCCTGCTAGGA

```

Additions in purple, substitutions in blue, start codons in green, stop codons in red.

Six nucleotides were added at the start of the sequence to create the BamHI site, and five were added at the end of the sequence to create the XbaI site. To avoid any possible frameshift errors as a result of the out-of-frame ATG in the promoter sequence, and create the NcoI site needed at the end of the promoter, the three nucleotides at the end of the promoter sequence were altered from GTC to CCC and three extra nucleotides were introduced directly after the start codon of *mgsA*, the first gene in the sequence. A similar change was made to the intergenic sequence, without introducing the NcoI site, by changing the final three nucleotides from GTC to CTC. Four nucleotides were also added at the beginning of the terminator sequence to create the StuI site.

Full sequence ordered for insertion of *ipi* and *ispS*, isoprene biosynthetic genes, ordered without promoter and terminator sequences:

```

CCATCGCGCAGTCGTCGATCGTCGTC AACCTCAGCCAGCACCTGTTTAAGCGGAACCTTACCTCGCTG
AGTGTGATCGCGCACTCTAGCTATTTCCGGCTCGCGGAGCCTGTGTCGCTCGCTCTCCTTCAGCCAGCGTCG
CAGAGGCCCTCACACGCCGCTCACCCCTCACCGCCTCCTTCTCGAGCCACACCGCGATGGGCGAGACCT
CCGCGCCCGCAGCTGATCGCGGCATGGACGCAGTCCAGCGACGCTCATGTTTGAAGACGAATGCATC
CTCGTGGACGAGAATGACCGTGTGGTTGGCCATGATTCCAAGTACAACCTGCCACTTGATGGAAAAGAT
CGAAGCGGAAAATCTCCTGCATCGCGCCTTCTCGGTCTTCTGTTCAACTCGAAGTATGAGCTCCTGTC
TGCAGCAACGCTCGGCCACCAAGTACAGTTCCCGCTGGTGTGGACGAACACCTGTTGCAGCCATCCG
CTGTACCGCGAAAAGCGAGCTGATCGAGGAGAACGCCCTGGGAGTCCGCAATGCGGCGCAGCGGAAGCT
GCTCGACGAGCTTGGTATCGTGGCCGAAGATGTCCCAGTTCGACAGTTCACCCCATGGGCCGATCC
TGTACAAGGCCCGCTCGGATGGCAAGTGGGCGAGCAGCAACTGGACTACCTGCTGTTTCATCGTCCGG
GACGTTAACGTGAACCCGAATCCGGATGAAGTGGCCGACATCAAATATGTGAACCGCGATCAGCTCAA
GGAGCTGTTGCGGAAGGCGGATGCGGGTGAGGAGGGCCTGAAGCTGTCCCGTGGTTCCGCCTAGTGG
TGGACAACCTCCTGTTCAAATGGTGGGACCATCTGGAGCAAGGCAGCTGGGGGAGGTCACTGACATG
AAGACCATTACAAGCTCAGTGA GCGAATTATTTCGTACCGAAGGGATCATCTCATCGCTGGATTTG
CGCCACGAGCTCTCAGTTACCCAAATCACCGAACATAACTCGCGGCGGTAGGCCAATTACCAGCCGA
ACCTCTGGAACTTTGAATTCCTGCAGTCGCTGGAGAATGACCTGAAGGTGGAAAAGCTGGAAGAGAAG
GCACCAAGCTGGAGGAGGAGTCCGCTGCATGATCAACCGCTCGACACACAGCCACTCAGCCTGCT
AGAATTGATCGACGATGTCCAGCGTCTGGGCCCTACCTACAAGTTCGAGAAGGACATCATCAAGGCC
TTGAGAACATTGTCTCCTGGACGAGAATAAGAAAAACAAGAGTGACCTCCACGCTACGGCCCTCAGC
TTCCGGCTGTGCGCCAGCATGGCTTCGAGGTGTCCCAGGATGTGTTTCGAGCGCTTTAAGGACAAGGA
GGGAGGCTTCTCGGGTGAAGTGAAGGGCGATGTGCAAGGGTGTGAGTCTGTACGAAGCGTCTATC
TGGGCTTCGAGGGCGAAAATCTCCTCGAGGAGGCACGGACCTTCTCAATCACCCACCTCAAGAACAC
CTGAAAGAAGGCATCAACACCAAGGTGGCGGAACAGGTCTCGCATGCACTGGAACCTCCCTATCACCA
GCGCCTCCATCGCCTGGAAGCGCGCTGGTTCTTGGACAAGTATGAACCGAAGGAACCCACCACCAGC
TGCTACTCGAGCTGGCGAAGCTGGATTTCAACATGGTGCAGACCTTGCACCAGAAAGAGCTGCAAGAC
CTGAGCAGGTGGTGGACGGAGATGGGGCTGGCGAGCAAGCTGGACTTTCGTCGCGACCGCCTGATGGA
AGTGTACTTCTGGGCGCTCGGCATGGCGCCGACCCGAGTTCGGTGAATGTGTAAGGCCGTCACTA
AGATGTTTGGCTTGGTCAACATCATCGATGATGTCTATGACGTTTATGGCACGCTCGATGAGCTGCAG
CTCTTACGGATGCCGTCGAGCGCTGGGACGTGAATGCCATCAACACCCCTGCCGACTACATGAAGCT
CTGCTTCTTGGCGCTTTATAACACCGTCAACGACACGTCGTATAGCATCCTGAAAGAAAAGGGCCACA
ACAACCTGTCCATTTGACCAAGTCGTGGCGGGAGCTGTGCAAAGCATTCTTCAGGAGGCGAAGTGG
TCGAAACAAGATCATTCGGCGTTTCAGCAAGTACCTGGAAAATGCGTGGTGTCTCCTCCTCCGGTGT
GGCTCTCCTGGCCCTTCTACTTCTCGGTGTGCCAACAGCAGGAAGACATCAGCGACCATGCCCTGC
GTTTCGCTGACTGATTTCCACGGCCTGGTGGCTCGTGTGCGTCATCTTCCGCCTCTGCAACGATCTC
GCCACCAGCGCGCCGAGCTGGAGCGGGCGAGACGACCAATAGCATCATCTCGTACATGCACGAGAA
CGACGGCAGCTCGGAAGAGCAGGCGCGGGAGGAGTTGCGCAAATCATCGATGCGGAGTGGAAAGA
TGAACCGGAGCGCGTGAAGCATTCGACCTGCTCCCGACGGCCTTTATGGAGATCGCCGTCAACATG
GCCCGAGTTTCGATTGCACCTACCAGTATGGCGACGGCCTGGGCCGGCGGACTACGCCACCAGAGAA
TCGCATCAAGCTCCTGCTGATCGACCCCTTCCCGATCAATCAGCTGATGTACGTG TGAGGCCCT

```

Additions in purple, substitutions in blue, start codons in green, stop codons in red.

Note that there was no need to add an extra three nucleotides at the beginning of the first gene in this case as the sequence already contains the needed NcoI site.

Bibliography

- [1] Frank W. Larimer, Patrick Chain, Loren Hauser, Jane Lamerdin, Stephanie Malfatti, Long Do, Miriam L. Land, Dale A. Pelletier, J. Thomas Beatty, Andrew S. Lang, F. Robert Tabita, Janet L. Gibson, Thomas E. Hanson, Cedric Bobst, Janelle L. Torres y Torres, Caroline Peres, Faith H. Harrison, Jane Gibson, and Caroline S. Harwood. Complete genome sequence of the metabolically versatile photosynthetic bacterium *Rhodospseudomonas palustris*. *Nature Biotechnology*, 22(1):55–61, January 2004.
- [2] Tatas H. P. Brotosudarmo, Aaron M. Collins, Andrew Gall, Aleksander W. Roszak, Alastair T. Gardiner, Robert E. Blankenship, and Richard J. Cogdell. The light intensity under which cells are grown controls the type of peripheral light-harvesting complexes that are assembled in a purple photosynthetic bacterium. *Biochemical Journal*, 440(1):51–61, November 2011.
- [3] Andreas Schäfer, Andreas Tauch, Wolfgang Jäger, Jörn Kalinowski, Georg Thierbach, and Alfred Pühler. Small mobilizable multi-purpose cloning vectors derived from the *Escherichia coli* plasmids pK18 and pK19: selection of defined deletions in the chromosome of *Corynebacterium glutamicum*. *Gene*, 145(1):69–73, July 1994.
- [4] Federico E. Rey, Yasuhiro Oda, and Caroline S. Harwood. Regulation of Uptake Hydrogenase and Effects of Hydrogen Utilization on Gene Expression in *Rhodospseudomonas palustris*. *Journal of Bacteriology*, 188(17):6143–6152, September 2006.
- [5] R W Miller and R R Eady. Molybdenum and vanadium nitrogenases of *Azotobacter chroococcum*. Low temperature favours N₂ reduction by vanadium nitrogenase. *Biochemical Journal*, 256(2):429–432, December 1988.
- [6] Klaus Schneider, Ute Gollan, Melanie Dröttboom, Sabine Selsemeier-Voigt, and Achim Müller. Comparative Biochemical Characterization of the Iron-Only Nitrogenase and the Molybdenum Nitrogenase from *Rhodobacter Capsulatus*. *European Journal of Biochemistry*, 244(3):789–800, March 1997.
- [7] Paul B. Weisz. Basic Choices and Constraints on Long-Term Energy Supplies. *Physics Today*, 57(7):47–52, July 2004.

- [8] United Nations Conference. *The State of the Biofuels Market: Regulatory, Trade and Development Perspectives*. 2013.
- [9] European Biodiesel Board. European Biodiesel Board.
- [10] George Anastopoulos, Ypatia Zannikou, Stamoulis Stournas, and Stamatis Kalligeros. Trans-esterification of Vegetable Oils with Ethanol and Characterization of the Key Fuel Properties of Ethyl Esters. *Energies*, 2(2):362–376, June 2009.
- [11] J. C. Thompson and B. B. He. Characterization of crude glycerol from biodiesel production from multiple feedstocks. *Applied Engineering in Agriculture*, 22(2):261–265, 2006.
- [12] Syed Shams Yazdani and Ramon Gonzalez. Anaerobic fermentation of glycerol: a path to economic viability for the biofuels industry. *Current Opinion in Biotechnology*, 18(3):213–219, June 2007.
- [13] D. Hedtke. *Wiley: Bailey's Industrial Oil and Fat Products, 6 Volume Set, 6th Edition - Fereidoon Shahidi*. 2005.
- [14] Denver J. Pyle, Rafael A. Garcia, and Zhiyou Wen. Producing Docosahexaenoic Acid (DHA)-Rich Algae from Biodiesel-Derived Crude Glycerol: Effects of Impurities on DHA Production and Algal Biomass Composition. *Journal of Agricultural and Food Chemistry*, 56(11):3933–3939, June 2008.
- [15] Saurabh Jyoti Sarma, Satinder Kaur Brar, Eduardo Bittencourt Sydney, Yann Le Bihan, Gerardo Buelna, and Carlos Ricardo Soccol. Microbial hydrogen production by bioconversion of crude glycerol: A review. *International Journal of Hydrogen Energy*, 37(8):6473–6490, April 2012.
- [16] Zhanyou Chi, Denver Pyle, Zhiyou Wen, Craig Frear, and Shulin Chen. A laboratory study of producing docosahexaenoic acid from biodiesel-waste glycerol by microalgal fermentation. *Process Biochemistry*, 42(11):1537–1545, November 2007.
- [17] P. J. Lammers, B. J. Kerr, T. E. Weber, W. A. Dozier, M. T. Kidd, K. Bregendahl, and M. S. Honeyman. Digestible and metabolizable energy of crude glycerol for growing pigs. *Journal of Animal Science*, 86(3):602–608, March 2008.

- [18] Duane T. Johnson and Katherine A. Taconi. The glycerin glut: Options for the value-added conversion of crude glycerol resulting from biodiesel production. *Environmental Progress*, 26(4):338–348, December 2007.
- [19] Takeshi Ito, Yutaka Nakashimada, Koichiro Senba, Tomoaki Matsui, and Naomichi Nishio. Hydrogen and ethanol production from glycerol-containing wastes discharged after biodiesel manufacturing process. *Journal of Bioscience and Bioengineering*, 100(3):260–265, September 2005.
- [20] George W. Crabtree, Mildred S. Dresselhaus, and Michelle V. Buchanan. The hydrogen economy. *Physics Today*, 57(12):39–44, December 2004.
- [21] Joan M. Ogden. Hydrogen: The fuel of the future? *Physics Today*, 55(4):69–75, April 2002.
- [22] Guillaume Sabourin-Provost and Patrick C. Hallenbeck. High yield conversion of a crude glycerol fraction from biodiesel production to hydrogen by photofermentation. *Bioresource Technology*, 100(14):3513–3517, July 2009.
- [23] Dominic Deo Androga, Ebru Özgür, Inci Eroglu, Ufuk Gündüz, and Meral Yücel. Amelioration of photofermentative hydrogen production from molasses dark fermenter effluent by zeolite-based removal of ammonium ion. *International Journal of Hydrogen Energy*, 37(21):16421–16429, November 2012.
- [24] A R Varga and L A Staehelin. Pigment-protein complexes from *Rhodospseudomonas palustris*: isolation, characterization, and reconstitution into liposomes. *Journal of Bacteriology*, 161(3):921–927, March 1985.
- [25] Tadashi Mizoguchi, Megumi Isaji, Jiro Harada, and Hitoshi Tamiaki. Isolation and pigment composition of the reaction centers from purple photosynthetic bacterium *Rhodospseudomonas palustris* species. *Biochimica et Biophysica Acta (BBA) - Bioenergetics*, 1817(3):395–400, March 2012.
- [26] Simon Scheuring, Rui Pedro Gonçalves, Valérie Prima, and James N. Sturgis. The Photosynthetic Apparatus of *Rhodospseudomonas palustris*: Structures and Organization. *Journal of Molecular Biology*, 358(1):83–96, April 2006.

- [27] Raymond J. Ritchie. The Use of Solar Radiation by the Photosynthetic Bacterium, *Rhodospseudomonas palustris*: Model Simulation of Conditions Found in a Shallow Pond or a Flatbed Reactor. *Photochemistry and Photobiology*, 89(5):1143–1162, September 2013.
- [28] Andrew Gall and Bruno Robert. Characterization of the Different Peripheral Light-Harvesting Complexes from High- and Low-Light Grown Cells from *Rhodospseudomonas palustris*. *Biochemistry*, 38(16):5185–5190, April 1999.
- [29] Katie Evans, Anthony P. Fordham-Skelton, Hiten Mistry, Colin D. Reynolds, Anna M. Lawless, and Miroslav Z. Papiz. A bacteriophytochrome regulates the synthesis of LH4 complexes in *Rhodospseudomonas palustris*. *Photosynthesis Research*, 85(2):169–180, August 2005.
- [30] Michael R. Jones. The petite purple photosynthetic powerpack. *Biochemical Society Transactions*, 37(2):400–407, April 2009.
- [31] Rujira Jitrwung and Viviane Yargeau. Optimization of media composition for the production of biohydrogen from waste glycerol. *International Journal of Hydrogen Energy*, 36(16):9602–9611, August 2011.
- [32] Anniina Kivistö, Ville Santala, and Matti Karp. Closing the 1,3-propanediol route enhances hydrogen production from glycerol by *Halanaerobium saccharolyticum* subsp. *saccharolyticum*. *International Journal of Hydrogen Energy*, 36(12):7074–7080, June 2011.
- [33] Ken-Jer Wu, Yeuh-Hui Lin, Yung-Chung Lo, Chun-Yen Chen, Wen-Ming Chen, and Jo-Shu Chang. Converting glycerol into hydrogen, ethanol, and diols with a *Klebsiella* sp. HE1 strain via anaerobic fermentation. *Journal of the Taiwan Institute of Chemical Engineers*, 42(1):20–25, January 2011.
- [34] Patrick C. Hallenbeck and Dipankar Ghosh. Improvements in fermentative biological hydrogen production through metabolic engineering. *Journal of Environmental Management*, 95, Supplement:S360–S364, March 2012.
- [35] Priscilla A. Selembo, Joe M. Perez, Wallis A. Lloyd, and Bruce E. Logan. High hydrogen production from glycerol or glucose by electrohydrogenesis using microbial electrolysis cells. *International Journal of Hydrogen Energy*, 34(13):5373–5381, July 2009.

- [36] Nitai Basak and Debabrata Das. The Prospect of Purple Non-Sulfur (PNS) Photosynthetic Bacteria for Hydrogen Production: The Present State of the Art. *World Journal of Microbiology and Biotechnology*, 23(1):31–42, June 2006.
- [37] Patrick C. Hallenbeck and Dipankar Ghosh. Advances in fermentative biohydrogen production: the way forward? *Trends in Biotechnology*, 27(5):287–297, May 2009.
- [38] Kaushik Nath, Anish Kumar, and Debabrata Das. Hydrogen production by *Rhodobacter sphaeroides* strain O.U.001 using spent media of *Enterobacter cloacae* strain DM11. *Applied Microbiology and Biotechnology*, 68(4):533–541, January 2005.
- [39] Dipankar Ghosh, Alexandre Tourigny, and Patrick C. Hallenbeck. Near stoichiometric reforming of biodiesel derived crude glycerol to hydrogen by photofermentation. *International Journal of Hydrogen Energy*, 37(3):2273–2277, February 2012.
- [40] Robert W. M. Pott, Christopher J. Howe, and John S. Dennis. Photofermentation of crude glycerol from biodiesel using *Rhodospseudomonas palustris*: Comparison with organic acids and the identification of inhibitory compounds. *Bioresource Technology*, 130:725–730, February 2013.
- [41] Paul G. Egland and Caroline S. Harwood. BadR, a New MarR Family Member, Regulates Anaerobic Benzoate Degradation by *Rhodospseudomonas palustris* in Concert with AadR, an Fnr Family Member. *Journal of Bacteriology*, 181(7):2102–2109, April 1999.
- [42] Masayuki Inui, Kaori Nakata, Jung Hyeob Roh, Kenneth Zahn, and Hideaki Yukawa. Molecular and Functional Characterization of the *Rhodospseudomonas palustris* No. 7 Phosphoenolpyruvate Carboxykinase Gene. *Journal of Bacteriology*, 181(9):2689–2696, May 1999.
- [43] Michael E. Kovach, Philip H. Elzer, D. Steven Hill, Gregory T. Robertson, Michael A. Farris, R. Martin Roop II, and Kenneth M. Peterson. Four new derivatives of the broad-host-range cloning vector pBBR1mcs, carrying different antibiotic-resistance cassettes. *Gene*, 166(1):175–176, December 1995.
- [44] Devin F. R. Doud, Eric C. Holmes, Hanno Richter, Bastian Molitor, Georg Jander, and Largus T. Angenent. Metabolic engineering of *Rhodospseudomonas palustris* for the obligate reduction of n-butyrate to n-butanol. *Biotechnology for Biofuels*, 10:178, July 2017.

- [45] R. M. Horton, S. N. Ho, J. K. Pullen, H. D. Hunt, Z. Cai, and L. R. Pease. Gene splicing by overlap extension. *Methods in Enzymology*, 217:270–279, 1993.
- [46] Yasuhiro Oda, Sudip K. Samanta, Federico E. Rey, Liyou Wu, Xiudan Liu, Tingfen Yan, Jizhong Zhou, and Caroline S. Harwood. Functional Genomic Analysis of Three Nitrogenase Isozymes in the Photosynthetic Bacterium *Rhodospseudomonas palustris*. *Journal of Bacteriology*, 187(22):7784–7794, November 2005.
- [47] Faith H. Harrison and Caroline S. Harwood. The *pimFABCDE* operon from *Rhodospseudomonas palustris* mediates dicarboxylic acid degradation and participates in anaerobic benzoate degradation. *Microbiology*, 151(3):727–736, 2005.
- [48] Erin K. Heiniger, Yasuhiro Oda, Sudip K. Samanta, and Caroline S. Harwood. How Post-translational Modification of Nitrogenase Is Circumvented in *Rhodospseudomonas palustris* Strains That Produce Hydrogen Gas Constitutively. *Applied and Environmental Microbiology*, 78(4):1023–1032, February 2012.
- [49] Federico E. Rey, Erin K. Heiniger, and Caroline S. Harwood. Redirection of Metabolism for Biological Hydrogen Production. *Applied and Environmental Microbiology*, 73(5):1665–1671, March 2007.
- [50] Ray Dixon and Daniel Kahn. Genetic regulation of biological nitrogen fixation. *Nature Reviews Microbiology*, 2(8):621–631, August 2004.
- [51] Robert R. Eady. Structure-Function Relationships of Alternative Nitrogenases. *Chemical Reviews*, 96(7):3013–3030, January 1996.
- [52] Hermann Schindelin, Caroline Kisker, Jamie L. Schlessman, James B. Howard, and Douglas C. Rees. Structure of ADP·AIF₄ --stabilized nitrogenase complex and its implications for signal transduction. *Nature*, 387(6631):370–376, May 1997.
- [53] Bat-Erdene Jugder, Jeffrey Welch, Kondo-Francois Aguey-Zinsou, and Christopher P. Marquis. Fundamentals and electrochemical applications of [Ni-Fe]-uptake hydrogenases. *RSC Advances*, 3(22):8142–8159, May 2013.
- [54] Dieter Rehder. Vanadium nitrogenase. *Journal of Inorganic Biochemistry*, 80(1–2):133–136, May 2000.

- [55] T. Keskin, M. Abo-Hashesh, and P. C. Hallenbeck. Photofermentative hydrogen production from wastes. *Bioresource technology*, 102(18):8557–8568, September 2011.
- [56] J H Liang, G M Nielsen, D P Lies, R H Burris, G P Roberts, and P W Ludden. Mutations in the *draT* and *draG* genes of *Rhodospirillum rubrum* result in loss of regulation of nitrogenase by reversible ADP-ribosylation. *Journal of Bacteriology*, 173(21):6903–6909, November 1991.
- [57] Bernd Masepohl, Thomas Drepper, Annette Paschen, Silke Gross, Alice Pawlowski, Karsten Raabe, Kai-Uwe Riedel, and Werner Klipp. Regulation of nitrogen fixation in the phototrophic purple bacterium *Rhodobacter capsulatus*. *Journal of Molecular Microbiology and Biotechnology*, 4(3):243–248, May 2002.
- [58] H Fu, R H Burris, and G P Roberts. Reversible ADP-ribosylation is demonstrated to be a regulatory mechanism in prokaryotes by heterologous expression. *Proceedings of the National Academy of Sciences of the United States of America*, 87(5):1720–1724, March 1990.
- [59] Thomas Drepper, Silke Groß, Alexander F. Yakunin, Patrick C. Hallenbeck, Bernd Masepohl, and Werner Klipp. Role of GlnB and GlnK in ammonium control of both nitrogenase systems in the phototrophic bacterium *Rhodobacter capsulatus*. *Microbiology*, 149(8):2203–2212, 2003.
- [60] Nathalie Michel-Reydellet and P. Alexandre Kaminski. Azorhizobium caulinodans PII and GlnK Proteins Control Nitrogen Fixation and Ammonia Assimilation. *Journal of Bacteriology*, 181(8):2655–2658, April 1999.
- [61] Joon-Young Jung, Hyun Shik Yun, Jinwon Lee, and Min-Kyu Oh. Production of 1,2-propanediol from glycerol in *Saccharomyces cerevisiae*. *Journal of Microbiology and Biotechnology*, 21(8):846–853, August 2011.
- [62] Hans Martin Weitz and Eckhard Loser. Isoprene. In *Ullmann's Encyclopedia of Industrial Chemistry*. Wiley-VCH Verlag GmbH & Co. KGaA, June 2000.
- [63] Constantine I. Vardavas, Nektarios Anagnostopoulos, Marios Kougias, Vassiliki Evangelopoulou, Gregory N. Connolly, and Panagiotis K. Behrakis. Short-term pulmonary effects of using an electronic cigarette: Impact on respiratory flow resistance, impedance, and exhaled nitric oxide. *Chest*, 141(6):1400–1406, June 2012.

- [64] David S. Bausmith and Ronald D. Neufeld. Soil Biodegradation of Propylene Glycol Based Aircraft Deicing Fluids. *Water Environment Research*, 71(4):459–464, 1999.
- [65] N. I. Nielsen and K. L. Ingvarsten. Propylene glycol for dairy cows. *Animal Feed Science and Technology*, 115(3):191–213, August 2004.
- [66] James M. Clomburg and Ramon Gonzalez. Metabolic engineering of *Escherichia coli* for the production of 1,2-propanediol from glycerol. *Biotechnology and Bioengineering*, 108(4):867–879, April 2011.
- [67] Thomas D. Sharkey, Amy E. Wiberley, and Autumn R. Donohue. Isoprene Emission from Plants: Why and How. *Annals of Botany*, 101(1):5–18, January 2008.
- [68] Pia Lindberg, Sungsoo Park, and Anastasios Melis. Engineering a platform for photosynthetic isoprene production in cyanobacteria, using *Synechocystis* as the model organism. *Metabolic Engineering*, 12(1):70–79, January 2010.
- [69] Shaliza Ibrahim, S. Vikineswary, Sujjat Al-Azad, and L. L. Chong. The effects of light intensity, inoculum size, and cell immobilisation on the treatment of sago effluent with *Rhodospseudomonas palustris* strain B1. *Biotechnology and Bioprocess Engineering*, 11(5):377–381, October 2006.
- [70] Robert William McClelland Pott. *The bioconversion of waste glycerol into hydrogen by Rhodospseudomonas palustris*. PhD thesis, Robert William McClelland Pott, Cambridge, 2014.
- [71] Simon A. Jackson, John R.D. Hervey, Asher J. Dale, and Julian J. Eaton-Rye. Removal of both Ycf48 and Psb27 in *Synechocystis* sp. PCC 6803 disrupts Photosystem II assembly and alters QA- oxidation in the mature complex. *FEBS Letters*, 588(20):3751–3760, October 2014.
- [72] Triinu Koressaar and Mairo Remm. Enhancements and modifications of primer design program Primer3. *Bioinformatics*, 23(10):1289–1291, May 2007.
- [73] Andreas Untergasser, Ioana Cutcutache, Triinu Koressaar, Jian Ye, Brant C. Faircloth, Mairo Remm, and Steven G. Rozen. Primer3—new capabilities and interfaces. *Nucleic Acids Research*, 40(15):e115–e115, August 2012.
- [74] Tamas Vincze, Janos Posfai, and Richard J. Roberts. NEBcutter: a program to cleave DNA with restriction enzymes. *Nucleic Acids Research*, 31(13):3688–3691, July 2003.

- [75] Maximilian Schlebusch and Karl Forchhammer. Requirement of the Nitrogen Starvation-Induced Protein Sll0783 for Polyhydroxybutyrate Accumulation in *Synechocystis* sp. Strain PCC 6803. *Applied and Environmental Microbiology*, 76(18):6101–6107, September 2010.
- [76] C. B. van Niel. The culture, general physiology, morphology, and classification of the non-sulfur purple and brown bacteria. *Bacteriological Reviews*, 8(1):1–118, March 1944.
- [77] Takashi Uemura, Kohichi Suzuki, Kei Nagano, and Shigehiro Morita. Comparative Studies on Growth, Respiration, Photosynthesis and Pigment Content in *Rhodospseudomonas Palustris*. *Plant and Cell Physiology*, 2(4):451–461, November 1961.
- [78] J. G. Sutcliffe. Complete nucleotide sequence of the *Escherichia coli* plasmid pBR322. *Cold Spring Harbor Symposia on Quantitative Biology*, 43 Pt 1:77–90, 1979.
- [79] David Lea-Smith, Ravendranv Vasudevan, and Christopher Howe. Generation of Marked and Markerless Mutants in Model Cyanobacterial Species. *Journal of Visualized Experiments*, 2016, May 2016.
- [80] Christopher Howe. *Gene Cloning and Manipulation*. Cambridge University Press, second edition, 2007.
- [81] Joon-Young Jung, Eun-Sil Choi, and Min-Kyu Oh. Enhanced production of 1,2-propanediol by *tpi1* deletion in *Saccharomyces cerevisiae*. *Journal of Microbiology and Biotechnology*, 18(11):1797–1802, November 2008.
- [82] Kurt M. Dubowski. An o-Toluidine Method for Body-Fluid Glucose Determination. *Clinical Chemistry*, 8(3):215–235, June 1962.
- [83] P. Greenspan, E. P. Mayer, and S. D. Fowler. Nile red: a selective fluorescent stain for intracellular lipid droplets. *The Journal of Cell Biology*, 100(3):965–973, March 1985.
- [84] O. P. Peoples and A. J. Sinskey. Poly-beta-hydroxybutyrate (PHB) biosynthesis in *Alcaligenes eutrophus* H16. Identification and characterization of the PHB polymerase gene (*phbC*). *Journal of Biological Chemistry*, 264(26):15298–15303, September 1989.
- [85] J. N. Morris, J. J. Eaton-Rye, and T. C. Summerfield. Phenotypic variation in wild-type substrains of the model cyanobacterium *Synechocystis* sp. PCC 6803. *New Zealand Journal of Botany*, 55(1):25–35, January 2017.

- [86] Thomas D. Sharkey, Sansun Yeh, Amy E. Wiberley, Tanya G. Falbel, Deming Gong, and Donna E. Fernandez. Evolution of the Isoprene Biosynthetic Pathway in Kudzu. *Plant Physiology*, 137(2):700–712, February 2005.
- [87] Y. Nakamura, T. Gojobori, and T. Ikemura. Codon usage tabulated from international DNA sequence databases: status for the year 2000. *Nucleic Acids Research*, 28(1):292, January 2000.
- [88] James B. McKinlay, Yasuhiro Oda, Martin Rühl, Amanda L. Posto, Uwe Sauer, and Caroline S. Harwood. Non-growing *Rhodospseudomonas palustris* Increases the Hydrogen Gas Yield from Acetate by Shifting from the Glyoxylate Shunt to the Tricarboxylic Acid Cycle. *The Journal of Biological Chemistry*, 289(4):1960–1970, January 2014.
- [89] Celeste Yanisch-Perron, Jeffrey Vieira, and Joachim Messing. Improved M13 phage cloning vectors and host strains: nucleotide sequences of the M13mpl8 and pUC19 vectors. *Gene*, 33(1):103–119, 1985.
- [90] Stanislav Obruca, Petr Sedlacek, Filip Mravec, Vladislav Krzyzanek, Jana Nebesarova, Ota Samek, Dan Kucera, Pavla Benesova, Kamila Hrubanova, Miluse Milerova, and Ivana Marova. The presence of phb granules in cytoplasm protects non-halophilic bacterial cells against the harmful impact of hypertonic environments. *New Biotechnology*, 39:68 – 80, 2017.
- [91] James B. McKinlay and Caroline S. Harwood. Carbon dioxide fixation as a central redox co-factor recycling mechanism in bacteria. *Proceedings of the National Academy of Sciences*, 107(26):11669–11675, June 2010.
- [92] Maria J Barbosa, Jorge M. S Rocha, Johannes Tramper, and René H Wijffels. Acetate as a carbon source for hydrogen production by photosynthetic bacteria. *Journal of Biotechnology*, 85(1):25–33, January 2001.
- [93] Bernd Masepohl, Thomas Drepper, Annette Paschen, Silke Gross, Alice Pawlowski, Karsten Raabe, Kai-Uwe Riedel, and Werner Klipp. Regulation of nitrogen fixation in the phototrophic purple bacterium *Rhodobacter capsulatus*. *Journal of Molecular Microbiology and Biotechnology*, 4(3):243–248, May 2002.
- [94] Erin K. Heiniger and Caroline S. Harwood. Posttranslational modification of a vanadium nitrogenase. *MicrobiologyOpen*, 4(4):597–603, August 2015.

- [95] Alexander F. Yakunin and Patrick C. Hallenbeck. AmtB Is Necessary for NH₄⁺-Induced Nitrogenase Switch-Off and ADP-Ribosylation in *Rhodobacter capsulatus*. *Journal of Bacteriology*, 184(15):4081–4088, August 2002.
- [96] B. Masepohl, R. Krey, and W. Klipp. The draTG gene region of *Rhodobacter capsulatus* is required for post-translational regulation of both the molybdenum and the alternative nitrogenase. *Journal of General Microbiology*, 139(11):2667–2675, November 1993.
- [97] J. Tandori, E. Hideg, L. Nagy, P. Maróti, and I. Vass. Photoinhibition of carotenoidless reaction centers from *Rhodobacter sphaeroides* by visible light. Effects on protein structure and electron transport. *Photosynthesis Research*, 70(2):175–184, 2001.
- [98] David J. Lea-Smith, Paolo Bombelli, John S. Dennis, Stuart A. Scott, Alison G. Smith, and Christopher J. Howe. Phycobilisome-Deficient Strains of *Synechocystis* sp. PCC 6803 Have Reduced Size and Require Carbon-Limiting Conditions to Exhibit Enhanced Productivity. *Plant Physiology*, 165(2):705–714, June 2014.
- [99] J. Miyake and S. Kawamura. Efficiency of light energy conversion to hydrogen by the photosynthetic bacterium *Rhodobacter sphaeroides*. *International Journal of Hydrogen Energy*, 12(3):147–149, January 1987.
- [100] Alessandra Adessi, Giuseppe Torzillo, Enrico Baccetti, and Roberto De Philippis. Sustained outdoor H₂ production with *Rhodospseudomonas palustris* cultures in a 50l tubular photobioreactor. *International Journal of Hydrogen Energy*, 37(10):8840–8849, May 2012.
- [101] F. Ben Rebah, F. Frikha, W. Kamoun, L. Belbahri, Y. Gargouri, and N. Miled. Culture of *Staphylococcus xylosum* in fish processing by-product-based media for lipase production. *Letters in Applied Microbiology*, 47(6):549–554, December 2008.
- [102] Gökhan Kars, Ufuk Gündüz, Gabor Rakhely, Meral Yücel, İnci Eroğlu, and Kornel L. Kovacs. Improved hydrogen production by uptake hydrogenase deficient mutant strain of *Rhodobacter sphaeroides* O.U.001. *International Journal of Hydrogen Energy*, 33(12):3056–3060, June 2008.
- [103] Lyudmila Vasilyeva, Masato Miyake, Emir Khatipov, Tatsuki Wakayama, Makoto Sekine, Masayuki Hara, Eiju Nakada, Yasuo Asada, and Jun Miyake. Enhanced hydrogen production

- by a mutant of *Rhodobacter sphaeroides* having an altered light-harvesting system. *Journal of Bioscience and Bioengineering*, 87(5):619–624, January 1999.
- [104] Toshihiko Kondo, Masayasu Arakawa, Toshiro Hirai, Tatsuki Wakayama, Masayuki Hara, and Jun Miyake. Enhancement of hydrogen production by a photosynthetic bacterium mutant with reduced pigment. *Journal of Bioscience and Bioengineering*, 93(2):145–150, February 2002.
- [105] Nitai Basak, Asim Kumar Jana, Debabrata Das, and Dipankar Saikia. Photofermentative molecular biohydrogen production by purple-non-sulfur (PNS) bacteria in various modes: The present progress and future perspective. *International Journal of Hydrogen Energy*, 39(13):6853–6871, April 2014.
- [106] Gökhan Kars and Ufuk Gündüz. Towards a super H₂ producer: Improvements in photofermentative biohydrogen production by genetic manipulations. *International Journal of Hydrogen Energy*, 35(13):6646–6656, July 2010.
- [107] Eilert Hustede, Alexander Steinbüchel, and Hans G. Schlegel. Relationship between the photoproduction of hydrogen and the accumulation of PHB in non-sulphur purple bacteria. *Applied Microbiology and Biotechnology*, 39(1):87–93, April 1993.
- [108] Elisabetta Franchi, Claudio Tosi, Giuseppe Scolla, Gino Della Penna, Francesco Rodriguez, and Paola Maria Pedroni. Metabolically engineered *Rhodobacter sphaeroides* RV strains for improved biohydrogen photoproduction combined with disposal of food wastes. *Marine Biotechnology (New York, N.Y.)*, 6(6):552–565, December 2004.
- [109] Elias Englund, Feiyan Liang, and Pia Lindberg. Evaluation of promoters and ribosome binding sites for biotechnological applications in the unicellular cyanobacterium *Synechocystis* sp. PCC 6803. *Scientific Reports*, 6:srep36640, November 2016.